

**Development and *in vitro* biological studies of polymer-based
wound dressings with high haemostatic capability for the
management of bleeding wounds**

by

Xhamla Nqoro



University of Fort Hare
Together in Excellence

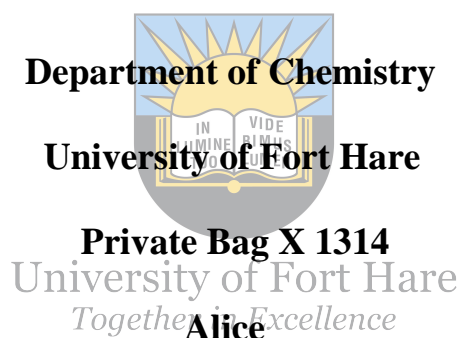


University of Fort Hare
Together in Excellence

Development and *in vitro* biological studies of polymer-based wound dressings with a high haemostatic ability for the management of wounds

Xhamla Nqoro (201300305)

**A thesis submitted to the Faculty of Science and Agriculture,
University of Fort Hare, in fulfilment of the requirements for the degree
Doctor of Philosophy in Chemistry**



5700

South Africa

Supervisor: Prof Blessing A. Aderibigbe

2022

Declaration

“I Nqoro Xhamla declare that this thesis submitted for the degree of PhD in Chemistry Department, University of Fort Hare, Alice Campus is my own original work. It has not been previously submitted for any degree or examination in any other institution of higher learning. I further declare that all sources cited or quoted are indicated and acknowledged in a comprehensive list of references.”

__2022/09/28__
Date

Signature



University of Fort Hare
Together in Excellence

Dedication

I dedicate this work to my nephews and cousins, Ukhonaye Nqoro, Lunje-uthando Gwala, Chwayita Nqoro, Iminathi Nqoro, and Lakhanya Jona. “Work willingly at whatever you do, as though you were working for the Lord rather than for people” --Colossians 3 verse 23. “My son, if you accept my words and store up my commands within you, turning your ear to wisdom and applying your heart to understanding.....Then you will understand the fear of the Lord and find the knowledge of God.” Proverbs 2 verse 1-5.



University of Fort Hare
Together in Excellence

Abstract

Wounds are usually accompanied by complications such as excessive bleeding and bacteria invasion. The design of wound dressings that rapidly stop excessive bleeding and inhibit bacterial invasion is crucial to promoting accelerated wound healing. To meet the abovementioned requirements in wound dressings, topical gels were prepared from sodium alginate (SA) and carboxymethylcellulose (CMC). The wound dressings were loaded with an antifibrinolytic agent, tranexamic acid (TA), essential oils, and a variety of metal-based nanoparticles, and carbon-based biomaterials. The scanning electron microscopy (SEM) and X-ray diffraction (XRD) confirmed the successful formation of the nanoparticles. The prepared formulations exhibited *in vitro* drug release kinetics that best fitted with the Korsmeyer-Peppas model. These gels exhibited good spreadability and viscosity, showing a shear-thinning behaviour with pH between 6.7 and 7.3, signifying suitability for skin application and ease of application. The prepared topical gels exhibited significant antibacterial effects against gram-negative and gram-positive strains of bacteria. SA/EO-based formulations showed high antibacterial activity across all bacterial strains, followed by SA-based formulations compared to CMC-based formulations, which exhibited moderate antibacterial activity. Moreover, the prepared gels showed good cytocompatibility, promoted cell proliferation, and exhibited >80% wound closure on day 3 compared to the untreated group, which showed a 38% wound reduction *in vitro*. Excellent blood clotting properties were observed with CMC-based gels compared to other formulations. However, all the prepared formulations exhibited outstanding blood clotting ability compared to the control, showing that they can promote rapid blood coagulation. The features presented by the prepared gels reveal that they are suitable for rapid wound healing.

Keywords: Haemostasis; tranexamic acid; nanoparticles; topical gels; wound dressings; essential oils; antibacterial activity

Acknowledgements

My gratitude goes first to the Lord God for the gift of life, for giving me the strength to finish my work, and for being a light on my path to the future.

The author would also like to express his sincere gratitude to the following people and organizations for their involvement in the completion of this thesis:

Prof. B.A. Aderibigbe, my supervisor, for her tireless and persistent guidance and support, not only regarding my work but also regarding my life as a whole. “I appreciate your kindness Prof.; you have helped me in many ways and paid attention to me every time I needed it.”

Department of Chemistry, University of Fort Hare, Alice Campus, from the HOD and all other staff members.

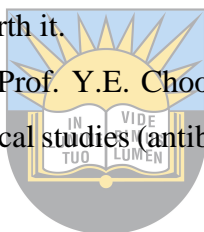
Mr. T. Mcaiko for assistance with FTIR and UV-Vis spectroscopy (University of Fort Hare, Department of Chemistry).

Organic chemistry group (Buhle Buyana, Zintle Mbese, Tobeka Naki, Sindi Ndlovu, Vuyolwethu Khwaza, Sibusiso Alven, Sijongesonke Peter, and Zizo Feketshane) for every moment we shared together, it was worth it.

Dr. S.A. Adeyemi, Dr. P. Ubanako¹, Prof. Y.E. Choonara, and Prof. D.T. Ndinteh for their external assistance with *in vitro* biological studies (antibacterial, cytotoxicity, Haemostasis, and wound healing).

My family and friends.

Financial support from the National Research Foundation (NRF), Sasol Inzalo Foundation (SIF), and Medical Research Council (MRC).



University of Fort Hare

Conference and Publications

Refereed Journal Articles

1. Nqoro X, Tobeka N, Aderibigbe BA. Quinoline-based hybrid compounds with antimalarial activity. *Molecules*. 2017(12):22. doi:10.3390/molecules22122268
2. Nqoro X, Aderibigbe BA. 4-Aminoquinoline-ferrocene Hybrids as Potential Antimalarials. *Recent Patents on Anti-Infective Drug Discovery*. 2020;15(2):157-72.
3. Alven S, Nqoro X, Buyana B, Aderibigbe BA. Polymer-Drug Conjugate, a Potential Therapeutic to Combat Breast and Lung Cancer. *Pharmaceutics*. 2020 May;12(5):406.
4. Nqoro X, Jama S, Morifi E, Aderibigbe BA. 4-Aminosalicylic Acid-based Hybrid Compounds: Synthesis and *in vitro* Antiplasmodial Evaluation. *Letters in Drug Design & Discovery*. 2021 Mar 1;18(3):284-98.
5. Alven S, Nqoro X, Aderibigbe BA. Polymer-Based Materials Loaded with Curcumin for wound healing applications. *Polymers*. 2020;12(10):2286.

Manuscripts submitted for publication

1. X. Nqoro¹, S. A. Adeyemi², P. Ubanako², D.T. Ndinteh³, P. Kumar², Y.E. Choonara², B. A. Aderibigbe¹ “A Topical Alginate-Based Wound Gel Fixated with Metal-based Nanoparticles and Tranexamic Acid as a Haemostatic Wound Healing System” – to “*BioNanoScience*”. (submitted)
2. X. Nqoro¹, S. A. Adeyemi², P. Ubanako², D.T. Ndinteh³, P. Kumar², Y.E. Choonara², B. A. Aderibigbe¹ “Wound Healing Potential of Sodium Alginate-Based Topical Gels Loaded with a Combination of Essential Oils, Iron Oxide Nanoparticles and Tranexamic Acid” – to “*Polymer Bulletin*”. (submitted)

Book chapters

1. B. Buyana, S. Alven, X. Nqoro, B. A. Aderibigbe. Antibiotics Encapsulated Scaffolds as Potential Wound Dressings. In: *Antibiotic Materials in Healthcare*, Chapter 7, Elsevier, 2020.
2. X. Nqoro, S. Alven, B. Buyana, Z. Feketshane, B.A. Aderibigbe. Alginate-based wound dressings for skin healing and regeneration. In: *Natural Polymers in Wound Healing and Repair*, Chapter 15, Elsevier, 2022.
3. V. Khwaza, B. Buyana, X. Nqoro, R. Ngonidzashe, O.O. Oyedeji, B.A. Aderibigbe. Polymeric beads for targeted drug delivery and healthcare applications. In: *Polymeric Biomaterials for Healthcare Applications*, Chapter 2, Elsevier, 2022.

4. V. Khwaza, B. Buyana, X. Nqoro, S. Peter, Z. Mbese, Z. Feketshane, S. Alven, B.A. Aderibigbe. Strategies for delivery of antiviral agents. In: Viral Infections and Antiviral Therapies, Chapter 19, Elsevier, 2023.

Conference proceedings

1. Nqoro. X and Aderibigbe. B.A. Synthesis and characterization of 4-aminoquinolinebased hybrid compounds as potential antimalarials. BIO-Africa Convention, Durban, 27-29 August 2018.
2. Nqoro X. and B.A. Aderibigbe. Synthesis, characterization, and *in vitro* evaluation of antifolates as potential antimalarials. University of Fort Hare Postgraduate Day, 8 November 2019.
3. Nqoro X. and B.A. Aderibigbe. 4-Aminosalicylic Acid-based Hybrid Compounds as Potentially Active Antimalarial Drugs. H3D Symposium “Celebrating a Decade of Infectious Diseases Drug Discovery in Africa” 2020.



University of Fort Hare
Together in Excellence

List of Abbreviations

SA: Sodium alginate

CMC: Carboxymethylcellulose.

EO: Essential oils

TA: Tranexamic acid

CS: Chitosan

CMCS: Carboxymethylchitosan

Lav: Lavender oil

Rose: Rosemary oil

Euc: Eucalyptus oil

NPs: nanoparticles

RBC: Red blood cells

HA: Hyaluronic acid

PVA: Polyvinyl acid

PEO: Polyethylene oxide

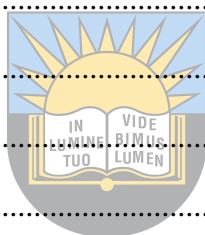
PEG: Polyethylene glycol



University of Fort Hare
Together in Excellence

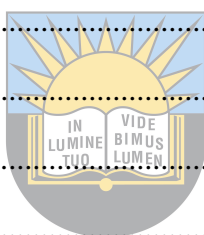
Table of Contents

Declaration	i
Dedication	ii
Abstract	iii
Acknowledgements	iv
Conference and Publications	v
Manuscripts submitted for publication	v
Book chapters	v
Conference proceedings	vi
List of Abbreviations	vii
Table of Contents	viii
List of Figures	xi
List of Tables	xii
List of schemes	xiii
Chapter 1	1
1. Introduction	1
1.1. Problem statement	4
1.2. Motivation and Rationale	5
1.3. Aim of Research	6
1.4. Objectives of Research	6
1.5. The Novelty of the Research	7
References	7
Chapter 2	13
2. Literature Review	13
2.1. Wound Healing	13
2.2. Types of Wound	15
2.3. Classification of Wound Dressings	16



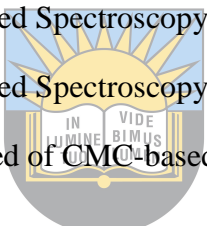
University of Fort Hare
Together in Excellence

2.4. Healing Effects.....	17
2.4.1. Chitosan	17
2.4.2. Gelatin.....	22
2.4.3. Cellulose.....	30
2.4.4. Hyaluronic Acid.....	34
2.4.5. Alginate.....	39
2.5. Application of Organic Drugs and Nanoparticles in Wound Healing	48
2.6. Essential Oils in the Management of Wounds	54
2.7. Commercially Available Haemostatic Wound Dressings.....	57
2.8. Four mathematical models of <i>in vitro</i> drug release.....	59
2.9. Impact of Microorganisms in wound healing	61
References	62
Chapter 3	79
3. MATERIALS	79
3.1. Solvents and Reagents	79
3.2. EXPERIMENTAL	79
3.2.1. Preparation of Ag nanoparticles.....	79
3.2.2. Preparation of ZnO nanoparticles	79
3.2.3. Preparation of MgO nanoparticles	80
3.2.4. Preparation of Fe ₃ O ₄ Nanoparticles	80
3.2.5. Preparation of topical gels.....	80
3.3. CHARACTERIZATION	82
3.3.1. Fourier Transform Infrared Spectroscopy (FTIR)	82
3.3.2. Spreadability	82
3.3.3. Viscosity.....	82
3.3.4. pH evaluation & stability studies	82
3.3.5. X-ray Diffraction (XRD)	82



University of Fort Hare
Together in Excellence

3.3.6. Scanning Electron Microscope (SEM)	83
3.3.7. <i>In vitro</i> drug release kinetics	83
3.3.8. <i>In vitro</i> antibacterial analysis	84
3.3.9. Whole blood clot assay	84
3.3.10. Cytotoxicity evaluation	85
3.3.11. Wound healing assay	85
3.3.12. Statistical analysis	85
References	86
Chapter 4	89
4. RESULTS AND DISCUSSION	89
4.1. Fourier-Transform Infrared Spectroscopy (FTIR)	89
4.1.1. Fourier-Transform Infrared Spectroscopy of SA-based gels	89
4.1.2. Fourier-Transform Infrared Spectroscopy of SA/EO-based gels	92
4.1.3 Fourier-Transform Infrared of CMC-based gels	95
4.2. SEM and XRD	96
4.3. Spreadability and viscosity of the topical gels	99
4.4. Drug release studies	102
4.5. <i>In vitro</i> antibacterial assay	108
4.5.1. <i>In vitro</i> antibacterial assay of SA-based topical gels	108
4.5.2 <i>In vitro</i> antibacterial assay of SA/EO-based topical gels	111
4.5.3. <i>In vitro</i> antibacterial assay of CMC-based topical gels	113
4.6. <i>In vitro</i> whole blood clot assay	114
4.6.1. <i>In vitro</i> whole blood clot assay of SA-based topical gels	114
4.6.2. <i>In vitro</i> whole blood clot assay of SA/EO-based topical gels	116
4.6.3. <i>In vitro</i> whole blood clot assay of CMC-based topical gels	117
4.7. <i>In vitro</i> cytotoxicity	118
4.7.1. <i>In vitro</i> cytotoxicity of SA-based topical gels	118



University of Fort Hare
Together in Excellence

4.7.2. <i>In vitro</i> cytotoxicity of SA/EO-based topical gels	119
4.7.3. <i>In vitro</i> cytotoxicity of CMC-based topical gels.....	120
4.8. <i>In vitro</i> wound scratch assay	121
References	126
Chapter 5	132
5. CONCLUSION	132
5.1. Limitation of these studies	133
Appendix	134

List of Figures

Figure 1: Phases of wound healing	13
Figure 2: Classes of wound dressings	17
Figure 3: Summary of the composition of amino acids in gelatin	23
Figure 4: Schematic presentation of bacterial pathogens.....	62
Figure 5: FTIR spectra of X1, X3 and X9	90
Figure 6: FTIR spectra of topical gels X2, X5, and X11	90
Figure 7: FTIR spectra of topical gels X4 and X10.....	91
Figure 8: FTIR spectra of topical gels X8 and X14	91
Figure 9: FTIR spectra of topical gels X7 and X13	92
Figure 10: FTIR spectra of topical gels X6 and X12	92
Figure 11: (a) FTIR spectra of Euc & SA/Euc, (b) FTIR spectra SA/Euc/Fe ₃ O ₄ & SA/Euc/Fe ₃ O ₄	93
Figure 12: (a) FTIR spectra of Rose & SA/Rose, (b) FTIR spectra SA/Rose/Fe ₃ O ₄ & SA/Rose/Fe ₃ O ₄	94
Figure 13: (a) FTIR spectra of Lav & SA/Lav, (b) FTIR spectra SA/Lav/Fe ₃ O ₄ & SA/Lav/Fe ₃ O ₄	95
Figure 14a-c: FTIR spectra of CMC-based topical gels	96
Figure 15: SEM images of a) Fe ₃ O ₄ , b) GO, c) MgO, d) rGO, and e) ZnO-NPs	98
Figure 16: Shows cumulative % DR of TA from CMC/TA and X2	103
Figure 17: Shows cumulative % DR of TA from X4 & CMC/TA/Ag	103
Figure 18: Shows cumulative % DR of TA from CMC/TA/MgO & CMC/TA/ZnO.....	104

Figure 19: Shows cumulative % DR of rGO from X8 & X14.....	104
Figure 20: Shows cumulative % DR of MgO from X4 and X10.....	105
Figure 21: Shows cumulative % DR of MgO from CMC/TA/MgO	105
Figure 22: Shows cumulative % DR of AgNPs from X6 & X12	106
Figure 23: Shows cumulative % DR of AgNPs plotted against time	106
Figure 24: Shows cumulative % DR of ZnO from X5 & X11	107
Figure 25: Shows cumulative % DR of ZnO plotted against time.....	107
Figure 26: Haemostatic evaluation of SA-based topical gels (error bars = \pm std) n= 3 *** p-value \leq 0.0002, ** p-value \leq 0.002 * p-value \leq 0.05	115
Figure 27: Haemostatic evaluation of SA/EO-based gels (error bars = \pm std) n= 3 *** p-value \leq 0.0002, ** p-value \leq 0.002 * p-value \leq 0.05	117
Figure 28: Haemostatic evaluation of CMC-based topical gels (error bars = \pm std) n= 3 *** p-value \leq 0.0002 ** p-value \leq 0.002 * p-value \leq 0.05	117
Figure 29: % Cell viability of HaCaT cells treated with SA-based gel formulations (error bars = \pm std) n = 3.....	118
Figure 30: Figure 4.7b: % Cell viability of HaCaT cells treated with X14 (error bars = \pm std) n = 3	119
Figure 31: % Cell viability of HaCaT cells treated with SA/EO-based gel formulations (error bars = \pm std) n = 3	120
Figure 32: % Cell viability of HaCaT cells treated with CMC-based gel formulations (error bars = \pm std) n = 3	121
Figure 33: Scratch assay images showing wound healing potential of untreated, X4, and X12 (T0-T96).....	123
Figure 34: Presents scratch assay images showing wound healing potential of untreated, SAT/Lav/Fe3O4, and CMC/TA/MgO (T0-T96)	124
Figure 35: Presents scratch assay images showing wound healing potential of untreated at 10% FBS (T0-T96).....	125

List of Tables

Table 1: Summary of Haemostatic Materials	5
Table 2: Summary of polymer-based dressings with haemostatic activity.....	43
Table 3: Summary of commercially available haemostatic dressings	58
Table 4: The coefficient constant of diffusion [193–196].	61
Table 5: Formulations used to prepare SA-based topical gels.....	80

Table 6: Formulations used to prepare SA/EO-based topical gels	81
Table 7: Formulations used to prepare CMC-based topical gels	81
Table 8: Different bacterial strains used in the in vitro antibacterial studies.....	84
Table 9: Spreadability, pH, and stability results of the prepared SA topical gels	99
Table 10: Spreadability, pH, and stability results of the prepared SA/EO-based topical gels	101
Table 11: Spreadability, pH, and stability results of the prepared CMC-based topical gels .	102
Table 12: A summary of in vitro drug release of the prepared formulations.....	108
Table 13: In vitro MIC of SA-based gels, TA, and nanoparticles	110
Table 14: In vitro MIC of SA/EO-based gels	112
Table 15: In vitro MIC of CMC-based topical gels	113
Table 16: Summary of wound closure for untreated, X4, X12, SAT/Lav/Fe ₃ O ₄ , and CMC/TA/MgO (mean ± STD, n=3)	125

List of schemes

Scheme 1: Shows deacetylation of chitin to chitosan.....	18
Scheme 2: Chemical structure of gelatin.....	24
Scheme 3: Carboxymethylation of cellulose to form carboxymethylcellulose.....	31
Scheme 4: Structure of Hyaluronic acid.....	35
Scheme 5: M and G-block structure of alginate	39



University of Fort Hare
Together in Excellence

Chapter 1

1. Introduction

Skin is the largest part of the body, and protects the body from foreign materials. It acts as the first line of defence by providing biological hindrance against infections and maintaining haemostasis [1–3]. A wound is a breakdown or injury in the skin that leads to the interruption of the skin's defensive role, disrupting its physical barrier properties against the external environment and thereby exposing it to the infectious pathogen [4–7]. Skin injuries may be caused by a wide variety of incidents, including burns, genetic disorders, car accidents, gunshots, stabs, *etc.* Wounds can be categorized as acute (friction, electricity, chemicals, freezing, and cuts) or chronic (leg ulcers, diabetic foot ulcers, pressure ulcers, and burns) depending on the time they take to heal [4,8,9]. Acute wounds heal in a timely manner, while chronic wounds fail to heal at the expected time, resulting in a prolonged healing process and trauma [7,8]. Wound healing is the body's innate response to injury [10], and it involves four phases: haemostasis, the first phase after injury where the body stops bleeding by forming clots [11], inflammation, the 2nd phase, proliferation, the 3rd phase, and remodelling, the 4th phase of wound healing where the wound fully closes and forms a scar [12–15].

Haemostasis is the first step that occurs directly after an injury, and managing this phase is very important to achieving progressive wound healing. This stage can be hampered by various factors like diseases, wound depth, biological materials, the use of anticoagulants and blood thinners, *etc.*, leading to excessive or uncontrolled bleeding. The body's inability to stop bleeding is termed haemorrhage and may lead to several complications [16]. In the present time, haemorrhage is one of the leading causes of death in emergency and pre-hospital cases [17–19]. In 2016, excessive bleeding was reported to account for over 10% of the annual death toll annually, which is more than 5.8 million deaths worldwide [20,21]. Liang *et al.* reported that haemorrhage is responsible for 40% of deaths during injury and is also the leading cause of traumatic deaths [22]. Despite threatening human lives, uncontrolled haemorrhage also hinders wound healing, leading to complications such as bacterial infection, acidosis, organ failure, coagulopathy, hypothermia, anaemia, *etc.* [23,24]. Controlling excessive bleeding is a crucial step for pre-hospital treatment and a life-saving protocol to prevent excessive bleeding [16,22,25]. The primary clinical treatment of bleeding wounds is the use of traditional gauze, applying pressure to the wound, and blood transfusion in severe cases of excessive blood loss

[26]. However, a blood transfusion after a haemorrhage may lead to multiple organ failure, infection, coagulation dysfunction, and many other complications [27].

Haemorrhage normally cannot be managed by the body's innate mechanisms. However, it can be avoided if suitable care and ideal haemostatic agents or dressings are immediately available to control excessive bleeding [17]. Haemostatic dressings offer a life-saving treatment in both intraoperative and pre-hospital conditions for victims of haemorrhage. The use of topical haemostatic dressings has been practised in many cases of haemorrhaging wounds. Topical haemostatic dressings can be categorized as synthetic sealants, active or adhesive materials, external dressings, mechanical agents, blood concentrators, *etc.* [28]. These types of haemostatic dressings are derived from or composed of organic or inorganic materials, natural or synthetic polymers, plant-based extracts, essential oils, proteins, tissue factors, *etc.*, and they promote haemostasis through the different haemostatic mechanisms. Based on the type and size of the wound, they are developed in different forms, such as gels, ointments, hydrogels, woven and non-woven sheets, films, powder, sponge, glue, nanofibers, lipids, nanocrystals, and microspheres [29]. Haemostatic dressings stop bleeding via one or more of the following mechanisms: they concentrate the blood by absorbing water, adhere to the tissue, platelets, and red blood cells, activate platelet aggregation, strengthen natural stypsis, induce vasoconstriction, accelerate the production of tissue factors, and form a viscous gel in contact with blood [30].

University of Fort Hare
Together in Excellence

A variety of haemostatic dressings such as Celox™, Quikclot combact gauze, Traumacel, Floseal, Tisseel, GelFoam®, Kaltostat™, WoundStat™, or Arista™ are commercially available [31–37]. However, the use of these dressings is accompanied by several limitations, such as being expensive, suffering from host rejection, requiring professional treatment, having the possibility of causing infection, and causing severe pain, including elevated temperatures at the wound site leading to superficial burns [19,38,39]. Therefore, developing more effective haemostatic agents that are more accessible and cost-effective with fewer limitations and high haemostatic ability is a pressing need.

An open wound is prone to infection, and it is important to develop wound dressings with the potential not just to promote haemostasis but also to hinder bacterial infection and rapid wound closure. The use of metal-based nanoparticles due to their outstanding features such as optical, catalytic, magnetic, bio-separation of DNA and proteins, and antibacterial properties has enabled their wide range of use in various fields. Shabanova *et al.* reported thrombin- Fe₃O₄-

NPs for the management of internal bleeding. These NPs displayed non-toxicity against HeLa cell lines and promoted rapid local haemostasis effects [40]. A recent report by Buyana *et al.* showed that loading an antifibrinolytic material (aminocaproic acid) and ZnO nanoparticles into SA-based gels resulted in a synergistic haemostatic effect *in vitro* [41]. Masood and co-workers reported CS/PEG hydrogels loaded with AgNPs to inhibit bacterial cell growth of both gram-negative and gram-positive strains of bacteria, and they further promoted wound healing, showing significant keratinocyte migration and scar formation with no scabs [42]. Liu *et al.* formulated PCL/Gel electrospun nanofibers fabricated with MgO NPs for the management of infected wounds and reported their antibacterial activity to be directly proportional to an increase in the concentration of MgO NPs [43].

Biopolymers such as CMC can promote coagulation by dissolving in the blood due to their high solubility, thereby increasing the viscosity of the blood and eventually stopping blood loss [44]. Aoshima *et al.* revealed that CMC acts as a bridge for fibrin polymerization when it is dissolved in the blood, thereby promoting the formation of thick fibrin fiber, leading to improved blood coagulation [45]. Wang *et al.* designed self-expanding porous composites from the combination of CMC and polyvinyl alcohol (PVA) that could be easily removed without causing re-bleeding after achieving haemostasis at the wound site [37]. Moreover, higher platelet adhesion was observed when the content of CMC was increased, suggesting that CMC can promote platelet aggregation. Mahmoodzadeh *et al.* developed cellulose-based aerogels with a high drug (tranexamic acid) release rate of 90% within 6h [46]. These scaffolds exhibited high adherence to the affected site, forming a milky gel in contact with the plasma that resulted in rapid blood clotting. Liu *et al.* designed formulations of alginate-based paste dressings loaded with lipidated tissue factors to induce haemostasis within 75 s [47]. The haemostatic capability of these dressings was dependent on the concentration of alginate. Increasing alginate concentration increased the clotting time of the scaffolds, suggesting that lower concentrations of alginate played a significant role in blood clotting.

Huang *et al.* designed haemostatic microspheres composed of silk fibroin with different formulations of alginate [27]. A shorter blood clotting time was observed in formulations with low alginate concentrations. Zhong *et al.* designed TA-loaded formulations of CMCS/SA composite films with drug release recorded in the range of 60–80% [48]. It was also notable that pure SA films exhibited a shorter clotting time than pure CMCS films [48]. Khezri *et al.* designed polymer-based nanostructured lipid carriers (NLC) impregnated with rosemary essential oil to induce collagen production, reepithelialization, fibroblast infiltration, increased

vascularization, and display antibacterial activity against *S. epidermidis*, *E. coli*, *L. monocytogenes*, *P. aeruginosa*, and *S. aureus* bacterial strains, and they promoted complete wound healing within 12 days [49]. It is important to select an ideal wound dressing for the management of haemostasis and in this study, topical gels composed of SA, carbopol, and CMC were prepared. The gels were impregnated with tranexamic acid (an antifibrinolytic agent), nanoparticles (Ag, MgO, ZnO, Fe₃O₄, graphene oxide, and reduced graphene oxide), and essential oils (lavender, rosemary, and eucalyptus). The prepared topical gels were analyzed using FTIR, pH, viscosity, spreadability, *in vitro* cytotoxicity, *in vitro* wound healing, haemolysis assay, and *in vitro* antibacterial evaluation.

1.1. Problem statement

Haemorrhage is a life-threatening and dreadful condition in injury, and it is fatal. Uncontrolled blood loss remains a leading cause of approximately 50% of traumatic deaths, with 8% resulting from the inability to apply pressure on the wound [32,50]. This can be attributed to limited options to prevent excessive blood loss by first responders [51]. Annually, more than 5.8 million deaths worldwide have been reported due to excessive uncontrolled bleeding [21], and haemorrhage may prevent progressive wound healing, causing several complications. A range of haemostatic dressings are commercially available, and these dressings play a crucial role in controlling excessive blood loss. However, some of them are associated with severe side effects. Applying pressure to a bleeding wound can cause the patient tremendous pain. Fibrin and thrombin-based haemostatic products (Tisseel and Evicel) have a high risk of host rejection, immune response, causing infection, high cost, and short shelf life [35]. Oxidized cellulose (Surgicel® and Traumastem®) delays wound healing by causing tissue inflammation as its hydroxyl groups are converted into acidic forms of carboxylic acid [29]. Collagen (Instat, Helistat, and Avitene) [52], causes allergic reactions and viral infections. Starch powder (Arista™) is expensive, collapses easily after water absorption, and its crosslinking agent is toxic to the human body [36,53]. Chitosan haemostats (CELOX™, HemCon® bandage) have been associated with high wound re-bleeding and have to be removed after application [54]. Zeolite-based haemostats (Quikclot) induce an exothermic reaction at the wound site, which may cause burns and necrosis [47,51,55]. Kaolin dressings (Quikclot) are toxic to the endothelial cells *in vitro* and may enter the bloodstream, resulting in complications [56–58]. Therefore, it is very important to design and develop more effective haemostatic agents that are more accessible and cost-effective with fewer limitations and high haemostatic ability. The bacterial infection and biofilm resistance also pose a major threat to progressive wound healing.

Metal-based nanoparticles have been reported to possess high antibacterial activity. Alavi *et al.* reported that the application of AgNPs in medical fields is hampered by their toxicity on animal cells [59]. A summary of the advantages and modes of action associated with haemostatic materials is presented in **Table 1** below.

Table 1: Summary of Haemostatic Materials

Agents	Mode of action	Advantages	Disadvantages	References
QuikClot gauze	Initiates the clotting process by activating factor XII of the clotting cascade	It stops bleeding when applied with pressure.	It may cause skin re-damage, and cause exothermic reactions. Expensive	[17]
HemCom bandage	Crosslink with erythrocytes to form a mucoadhesive barrier.	Stops bleeding and promotes clot formation.	It may cause skin re-damage and be painful.	[38,56]
Fibrin	Supply the clotting cofactors in a much higher concentration.	Promote growth factors and mimic the final stage of blood clotting.	Expensive, may cause infection, and is difficult to apply to certain wounds.	[33]
QuikClot zeolite	initiates the clotting process by activating factor XII of the clotting cascade.	Easy application, rapidly stops bleeding, and forms clots.	Raises a body's temperature to 40-42°C causing burns at the site of action. Expensive	[33,39,60]
Kaolin dressings	Initiates the previously termed 'intrinsic' clotting cascade.	Stops bleeding and forms blood clots.	Toxic to the endothelial cells <i>in vitro</i> , may enter the bloodstream, resulting in complications.	[56–58]

1.2. Motivation and Rationale

A wide range of haemostatic agents commercially available present different mechanisms of action against clot formation and are undoubtedly effective. However, these agents are hampered by several limitations, such as host rejection, being time-consuming, being expensive, allergenic, painful, causing skin burns, exposing the wound to infections, being mostly imported, and not being locally available [19,38,39]. Limitations associated with

the presently used dressings can be overcome by combining two biopolymers or biopolymers with synthetic polymers. Khezri *et al.* designed polymer-based nanostructured lipid carriers (NLC) impregnated with rosemary essential oil to induce collagen production, reepithelialization, fibroblast infiltration, increased vascularization, and display antibacterial activity against *S. epidermidis*, *E. coli*, *L. monocytogenes*, *P. aeruginosa*, and *S. aureus* bacterial strains, and they promoted complete wound healing within 12 days [49]. The combination of CMC and PVA reported by Wang *et al.* resulted in porous composites that could be easily removed from the wound site without causing re-bleeding [37]. Recently, the use of cellulose-based dressings for the management of traumatic bleeding has been one of the main improvements for controlled haemostasis [61].

A CMC-based dressing increases blood viscosity by dissolving when in contact with the blood and eventually promotes haemostasis [44]. Alginate-based dressings have drawn a lot of attention due to their low cost, biodegradability, biocompatibility, skin regenerative properties, anti-inflammation, haemostasis, *etc.* [62]. Zhong *et al.* reported high SA content-based films that promoted rapid drug release and haemostasis when combined with CMCS and chitosan (CS) [48]. Furthermore, topical gels with haemostasis effects have been reported, where activity results from their capability to penetrate the skin and also promote controlled drug release [41]. Based on the improved efficiency of the polymer-based dressings reported by many researchers, SA and CMC-based topical gels were prepared and incorporated with selected essential oils to promote safe and rapid haemostasis.

1.3. Aim of Research

To develop polymer-based topical gels loaded with bioactive materials for the management of bleeding wounds.

1.4. Objectives of Research

- Preparation of nanoparticles by known synthetic routes.
- Characterization of nanoparticles by SEM, FTIR, and XRD
- Preparation of polymer-based topical gels that are loaded with bioactive materials
- Characterization of the topical gels using pH, FTIR, spreadability, viscosity, and drug release
- *In vitro* biological studies (cell viability, haemolysis assay, antibacterial studies, and wound healing/scratch assay)

1.5. The Novelty of the Research

The commercially available wound dressings suffer from several limitations. The use of biopolymers is a promising approach to overcome some of the limitations associated with the presently used wound dressings. To the best of our knowledge, there are no reports on topical gels composed of the following formulations (1:1) alginate/carbopol and carboxymethylcellulose/carbopol for the management of bleeding wounds. Moreover, loading of TA in combination with essential oils and a range of nanoparticles has not been reported. In this reported work, TA was combined with selected essential oils and a range of nanoparticles in topical gels. The gels promoted cell proliferation, displayed good antibacterial activity, and had excellent haemostatic effects. They were biocompatible without causing toxic side effects, making them potential wound dressings for the treatment of infected and bleeding wounds, but further studies are required.

References

- [1] Dang Q, Zhang Q, Liu C, Yan J, Chang G, Xin Y, Cheng X, Cao Y, Gao H, Liu Y. Decanoic acid functionalized chitosan: Synthesis, characterization, and evaluation as potential wound dressing material. *Int J Biol Macromol* 2019;139:1046–53. <https://doi.org/10.1016/j.ijbiomac.2019.08.083>.
- [2] Pan H, Fan D, Cao W, Zhu C, Duan Z, Fu R, Li X, Ma X. Preparation and characterization of breathable hemostatic hydrogel dressings and determination of their effects on full-thickness defects. *Polymers (Basel)* 2017;9. <https://doi.org/10.3390/polym9120727>.
- [3] Hu F, Yun J. Hemostatic, anti-inflammatory and antibacterial effects of Sanqixiantao dressing in vivo and in vitro 2017;16:2239–44.
- [4] Naseri-nosar M, Maria Z. Wound dressings from naturally-occurring polymers: A review on homopolysaccharide-based composites. *Carbohydr Polym* 2018;189:379–98. <https://doi.org/10.1016/j.carbpol.2018.02.003>.
- [5] Pawar H V, Tetteh J, Debrah P, Boateng JS. Comparison of in vitro antibacterial activity of streptomycin-diclofenac loaded composite biomaterial dressings with commercial silver based antimicrobial wound dressings. *Int J Biol Macromol* 2019;121:191–9. <https://doi.org/10.1016/j.ijbiomac.2018.10.023>.
- [6] Gupta A, Kowalczyk M, Heaselgrave W, Britland ST. The production and application of hydrogels for wound management : A review. *Eur Polym J* 2019;111:134–51. <https://doi.org/10.1016/j.eurpolymj.2018.12.019>.
- [7] Fahimirad S, Ajallouei F. Naturally-derived electrospun wound dressings for target delivery of bio- active agents. *Int J Pharm.* 2019;566:307–28. <https://doi.org/10.1016/j.ijpharm.2019.05.053>.

- [8] Dhivya S, Vijaya V, Santhini E. Review article Wound dressings – a review 2015;5:24–8. <https://doi.org/10.7603/s40>.
- [9] Robson MC, Steed DL, Franz MG. Wound healing: biologic feature and approaches to maximize healing trajectories, *Curr Prob Surge* 2. 2001;38:72-139.
- [10] Hima BT, Vidyavathi M, Kavitha K, Sastry TP. Preparation and evaluation of ciprofloxacin loaded chitosan-gelatin composite films for wound healing activity 2010;2:173–82. <https://doi.org/10.5138/ijdd.2010.0975.0215.02027>.
- [11] Stricker-Krongrad A-H, Alikhassy Z, Matsangos N, Sebastian R, Marti G, Lay F, Harmon JW. Efficacy of Chitosan-Based Dressing for Control of Bleeding in Excisional Wounds. *Eplasty* 2018;18:122-130.
- [12] Negut I, Grumezescu V, Grumezescu AM. Treatment Strategies for Infected Wounds. *Molecules*. 2018;23:1–23. <https://doi.org/10.3390/molecules23092392>.
- [13] Zahedi P, Rezaeian I, Ranaei-siadat S. A review on wound dressings with an emphasis on electrospun nanofibrous polymeric bandages. *Polym Adv Technol*. 2010;21:77-95. <https://doi.org/10.1002/pat.1625>.
- [14] Ghadi R, Jain A, Khan W, Domb AJ. Microparticulate polymers and hydrogels for wound healing. vol. 2. Elsevier Ltd.; 2016. *Wound Healing Biomaterials*; Chapter 10; 203-225. <https://doi.org/10.1016/B978-1-78242-456-7.00010-6>.
- [15] Rivera AE, Spencer JM. Clinical aspects of full-thickness wound healing. *Clin. Dermatol* 2007;25:39–48. <https://doi.org/10.1016/j.clindermatol.2006.10.001>.
- [16] Liu J, Li Y, Hu Y, Cheng G, Ye E, Shen C, Xu F. Hemostatic porous sponges of crosslinked hyaluronic acid/cationized dextran by one self-foaming process. *Mater Sci Eng C* 2018;83:160–8. <https://doi.org/10.1016/j.msec.2017.10.007>.
- [17] Bennett BL. Bleeding Control Using Hemostatic Dressings: Lessons Learned. *Wilderness Environ Med* 2017;28:S39–49. <https://doi.org/10.1016/j.wem.2016.12.005>.
- [18] Hou Y, Xia Y, Pan Y, Tang S, Sun X, Xie Y, Guo H, Wei J. Influences of mesoporous zinc-calcium silicate on water absorption, degradability, antibacterial efficacy, hemostatic performances and cell viability to microporous starch based hemostat. *Mater Sci Eng C* 2017;76:340–9. <https://doi.org/10.1016/j.msec.2017.03.094>.
- [19] Barba BJD, Tranquilan-aranilla C, Abad L V. Hemostatic potential of natural/synthetic polymer based hydrogels crosslinked by gamma radiation. *Radiat Phys Chem* 2016;118:111–3. <https://doi.org/10.1016/j.radphyschem.2015.02.022>.
- [20] Wang Y, Fu Y, Li J, Mu Y, Zhang X, Zhang X, Zhang K, Liang M, Feng C, Chen X. Multifunctional chitosan/dopamine/diatom-biosilica composite beads for rapid blood coagulation. *Carbohydr Polym* 2018;200:6–14. <https://doi.org/10.1016/j.carbpol.2018.07.065>.
- [21] Tavakoli S, Kharaziha M, Nemati S, Kalateh A. Nanocomposite hydrogel based on carrageenan-coated starch/cellulose nanofibers as a hemorrhage control material. *Carbohydr Polym* 2021;251:117013. <https://doi.org/10.1016/j.carbpol.2020.117013>.

- [22] Liang Y, Xu C, Li G, Liu T, Liang JF, Wang X. Graphene-kaolin composite sponge for rapid and riskless hemostasis. *Colloids Surf. B* 2018;169:168–75. <https://doi.org/10.1016/j.colsurfb.2018.05.016>.
- [23] Wang Y, Yin M, Li Z, Liu Y, Ren X, Huang TS. Preparation of antimicrobial and hemostatic cotton with modified mesoporous particles for biomedical applications. *Colloids Surf. B* 2018;165:199–206. <https://doi.org/10.1016/j.colsurfb.2018.02.045>.
- [24] Chan LW, Kim CH, Wang X, Pun SH, White NJ, Kim TH. PolySTAT-modified chitosan gauzes for improved hemostasis in external hemorrhage. *Acta Biomater* 2016;31:178–85. <https://doi.org/10.1016/j.actbio.2015.11.017>.
- [25] Aydemir U, Kocer Z, Sahin İ, Aru B, Yan G. Oxidized regenerated cellulose crosslinked gelatin microparticles for rapid and biocompatible hemostasis: A versatile cross-linking agent 2018;200:624–32. <https://doi.org/10.1016/j.carbpol.2018.07.074>.
- [26] Gao Y, Sarode A, Kokoroskos N, Ukidve A, Zhao Z, Guo S, Flaumenhaft R, Gupta AS, Saillant N, Mitragotri S. A polymer-based systemic hemostatic agent. *Sci Adv* 2020;6:1–13. <https://doi.org/10.1126/sciadv.aba0588>.
- [27] Huang X, Fu Q, Deng Y, Wang F, Xia B, Chen Z, Chen G. Surface roughness of silk fibroin/alginate microspheres for rapid hemostasis in vitro and in vivo. *Carbohydr Polym* 2021;253:117256. <https://doi.org/10.1016/j.carbpol.2020.117256>.
- [28] Huang L, Liu GL, Kaye AD, Liu H. Advances in Topical Hemostatic Agent Therapies: A Comprehensive Update. *Adv Ther* 2020;37:4132–48. <https://doi.org/10.1007/s12325-020-01467-y>.
- [29] Biranje SS, Madiwale P V., Patankar KC, Chhabra R, Bangde P, Dandekar P, Adivarekar RV. Cytotoxicity and hemostatic activity of chitosan/carrageenan composite wound healing dressing for traumatic hemorrhage. *Carbohydr Polym* 2020;239:116106. <https://doi.org/10.1016/j.carbpol.2020.116106>.
- [30] Di Lena F. Hemostatic polymers: The concept, state of the art and perspectives. *J Mater Chem B* 2014;2:3567–77. <https://doi.org/10.1039/c3tb21739f>.
- [31] Barba BJD, Aranilla CT, Rellve LS, Cruz VRC, Vista JR, Abad L V. Hemostatic granules and dressing prepared from formulations of carboxymethyl cellulose, kappacarrageenan and polyethylene oxide crosslinked by gamma radiation. *Radiat Phys Chem* 2018;144:180–8. <https://doi.org/10.1016/j.radphyschem.2017.08.009>.
- [32] Chen J, Ai J, Chen S, Xu Z, Lin J, Liu H, Chen Q. Synergistic enhancement of hemostatic performance of mesoporous silica by hydrocaffeic acid and chitosan. *Int J Biol Macromol* 2019;139:1203–11. <https://doi.org/10.1016/j.ijbiomac.2019.08.091>.
- [33] Neuffer MC, McDivitt J, Rose D, King K, Cloonan CC, Vayer JS. Hemostatic dressings for the first responder: A review. *Mil Med* 2004;169:716–20. <https://doi.org/10.7205/MILMED.169.9.716>.
- [34] Aydemir Sezer U, Kocer Z, Aru B, Demirel GY, Gulmez M, Aktekin A, Ozkara S, Sezer S. Combination of gelatin and tranexamic acid offers improved haemostasis and safe use on internal hemorrhage control. *RSC Adv* 2016;6:95189–98. <https://doi.org/10.1039/c6ra16790j>.

- [35] Spotnitz WD, Burks S. Hemostats, sealants, and adhesives III: A new update as well as cost and regulatory considerations for components of the surgical toolbox. *Transfusion* 2012;52:2243–55. <https://doi.org/10.1111/j.1537-2995.2012.03707.x>.
- [36] Wang Y, Liu G, Wu L, Qu H, Song D, Huang H, Wu C, Xu M. Rational design of porous starch/hyaluronic acid composites for hemostasis. *Int J Biol Macromol* 2020;158:1319–29. <https://doi.org/10.1016/j.ijbiomac.2020.05.018>.
- [37] Wang Y, Zhao Y, Qiao L, Zou F, Xie Y, Zheng Y, Chao Y, Yang Y, He W, Yang S. Cellulose fibers-reinforced self-expanding porous composite with multiple hemostatic efficacy and shape adaptability for uncontrollable massive hemorrhage treatment. *Bioact Mater* 2021;6:2089–104. <https://doi.org/10.1016/j.bioactmat.2020.12.014>.
- [38] Liu X, Jia G. Modern Wound Dressing Using Polymers/Biopolymers. *J Material Sci. Eng.* 2018;7:7–10. <https://doi.org/10.4172/2169-0022.1000454>.
- [39] Liu X, Niu Y, Chen KC, Chen S. Rapid hemostatic and mild polyurethane-urea foam wound dressing for promoting wound healing. *Mater Sci Eng C* 2017;71:289–97. <https://doi.org/10.1016/j.msec.2016.10.019>.
- [40] Shabanova EM, Drozdov AS, Fakhardo AF, Dudanov IP, Kovalchuk MS, Vinogradov VV. Thrombin@Fe₃O₄ nanoparticles for use as a hemostatic agent in internal bleeding. *Sci Rep* 2018;8:1–10. <https://doi.org/10.1038/s41598-017-18665-4>
- [41] Buyana B, Aderibigbe BA, Ndinteh DT, Fonkui YT, Kumar P. Alginate-pluronic topical gels loaded with thymol, norfloxacin and ZnO nanoparticles as potential wound dressings. *J Drug Deliv Sci Technol* 2020;60:101960. <https://doi.org/10.1016/j.jddst.2020.101960>.
- [42] Masood N, Ahmed R, Tariq M, Ahmed Z, Masoud MS, Ali I, Asghar R, Andleeb A, Hasan A. Silver nanoparticle impregnated chitosan-PEG hydrogel enhances wound healing in diabetes induced rabbits. *Int J Pharm* 2019;559:23–36. <https://doi.org/10.1016/j.ijpharm.2019.01.019>.
- [43] Liu M, Wang X, Li H, Xia C, Liu Z, Liu J, Yin A, Lou X, Wang H, Mo X, Wu J. Magnesium oxide-incorporated electrospun membranes inhibit bacterial infections and promote the healing process of infected wounds. *J Mater Chem B* 2021;9:3727–44. <https://doi.org/10.1039/d1tb00217a>.
- [44] Gu H, He J, Huang Y, Guo Z. Fabrication of oxidized sodium carboxymethylcellulose from viscose fibers and their viscosity behaviors. *Fibers Polym* 2013;14:1266–70. <https://doi.org/10.1007/s12221-013-1266-1>.
- [45] Aoshima M, Tanabe K, Kohno I, Jo Y, Takahashi K, Sugo T, Matsuda M. Hemostatic mechanisms of a soluble fraction of plant-derived sodium carboxymethyl cellulose. *Japanese J Thromb Hemost* 2012;23:387–98. <https://doi.org/10.2491/jjsth.23.387>.
- [46] Mahmoodzadeh A, Moghaddas J, Jarolmasjed S, Ebrahimi Kalan A, Edalati M, Salehi R. Biodegradable cellulose-based superabsorbent as potent hemostatic agent. *Chem Eng J* 2021;418:129252. <https://doi.org/10.1016/j.cej.2021.129252>.
- [47] Liu C, Shi Z, Sun H, Mujuni CJ, Zhao L, Wang X, Huang F. Preparation and characterization of tissue-factor-loaded alginate: Toward a bioactive hemostatic material. *Carbohydr Polym* 2020;249:116860.

<https://doi.org/10.1016/j.carbpol.2020.116860>.

- [48] Zhong QK, Wu ZY, Qin YQ, Hu Z, Li SD, Yang ZM, Li P. Preparation and properties of carboxymethyl chitosan/alginate/tranexamic acid composite films. *Membranes (Basel)* 2019;9. <https://doi.org/10.3390/membranes9010011>.
- [49] Khezri K, Farahpour MR, Mounesi Rad S. Accelerated infected wound healing by topical application of encapsulated Rosemary essential oil into nanostructured lipid carriers. *Artif Cells, Nanomedicine Biotechnol* 2019;47:980–8. <https://doi.org/10.1080/21691401.2019.1582539>.
- [50] Hattori H, Amano Y, Nogami Y, Takase B, Ishihara M. Hemostasis for severe hemorrhage with photocrosslinkable chitosan hydrogel and calcium alginate. *Ann Biomed Eng* 2010;38:3724–32. <https://doi.org/10.1007/s10439-010-0121-4>.
- [51] Burnett LR, Richter JG, Rahmany MB, Soler R, Steen JA, Orlando G, Abouswareb T, Van Dyke ME. Novel keratin (KeraStat™) and polyurethane (Nanosan®-Sorb) biomaterials are hemostatic in a porcine lethal extremity hemorrhage model. *J Biomater Appl* 2014;28:869–79. <https://doi.org/10.1177/0885328213484975>.
- [52] Pourshahrestani S, Zeimaran E, Kadri NA, Mutlu N, Boccaccini AR. Polymeric Hydrogel Systems as Emerging Biomaterial Platforms to Enable Hemostasis and Wound Healing. *Adv Healthc Mater* 2020;9. <https://doi.org/10.1002/adhm.202000905>.
- [53] Chen Y, Qian JQ, Zhao CY, Yang LC, Ding J, Guo H. Preparation and evaluation of porous starch/chitosan composite cross-linking hemostatic. *Eur Polym J* 2019;118:17–26. <https://doi.org/10.1016/j.eurpolymj.2019.05.039>.
- [54] Wang Y, Wang C, Qiao L, Feng J, Zheng Y, Chao Y, He W, Xei Y, Shuai W, Li M. Shape-adaptive composite foams with high expansion and absorption used for massive hemorrhage control and irregular wound treatment. *Appl Mater Today* 2018;13:228–41. <https://doi.org/10.1016/j.apmt.2018.09.009>.
- [55] Fan X, Li Y, Li N, Wan G, Amir M, Tang K. Rapid hemostatic chitosan/cellulose composite sponge by alkali/urea method for massive haemorrhage 2020;164:2769–78. <https://doi.org/10.1016/j.ijbiomac.2020.07.312>.
- [56] Granville-Chapman J, Jacobs N, Midwinter MJ. Pre-hospital haemostatic dressings: A systematic review. *Injury* 2011;42:447–59. <https://doi.org/10.1016/j.injury.2010.09.037>.
- [57] Serena TE, Kushnir I, Kushnir A, Yaakov RA, Eckert KA. The safety of an autologous whole blood clot product applied to full thickness dermal wounds in a porcine model for up to 18 days. *Chronic Wound Care Manag Res* 2019;Volume 6:39–49. <https://doi.org/10.2147/cwcmr.s189836>.
- [58] Lundin JG, McGann CL, Daniels GC, Streifel BC, Wynne JH. Hemostatic kaolinpolyurethane foam composites for multifunctional wound dressing applications. *Mater Sci Eng C* 2017;79:702–9. <https://doi.org/10.1016/j.msec.2017.05.084>.
- [59] Alavi M, Varma RS. Antibacterial and wound healing activities of silver nanoparticles embedded in cellulose compared to other polysaccharides and protein polymers. *Cellulose* 2021;28:8295–311. <https://doi.org/10.1007/s10570-021-04067-3>
- [60] Lena F. and perspectives 2014:3567–77. <https://doi.org/10.1039/c3tb21739f>.

- [61] Khoshmohabat H, Paydar S, Makarem A, Karami MY, Dastgheib N, Zahraei SAH, Rezaei R, Sadat G, Nezhad M. A review of the application of cellulose hemostatic agent on trauma injuries. *Open Access Emerg Med* 2019;11:171–7. <https://doi.org/10.2147/OAEM.S205006>.
- [62] Lee, KY, Mooney DJ. Alginate: Properties and biomedical applications. *Prog Polym Sci* 2012;37:106–26.



University of Fort Hare
Together in Excellence

Chapter 2

2. Literature Review

2.1. Wound Healing

Wound healing is the body's intrinsic mechanism in response to skin breakdown, which involves a cascade of events to restore or regenerate tissue in the affected skin area. Wound healing is also responsible for stopping blood loss [1], the first and most important step for progressive healing. However, several factors may affect the body's natural reaction to wound healing, like old age, bacterial infection, mishandled wound dressings, health diseases (haemophilia, diabetes), *etc.* These factors may delay wound closure and transform the wound into an even worse condition, leading to chronic wounds [2]. The body on its own may suffer to heal certain wounds depending on the depth and size of the wound, which causes scar formation. To overcome this challenge, the application of wound dressings is exercised to rapidly stop blood loss, inhibit bacterial infection, cause less or no pain, accelerate wound healing, and exhibit less or no scar formation. Biopolymer-based or a combination of both natural and synthetic polymer-based wound dressings is reported to be advantageous compared to only using synthetic-based wound dressings [3]. Nevertheless, normal wound healing requires a complicated interaction of four overlapping stages: haemostasis, inflammation, proliferation, and maturation **Figure 1** [4–7].



Figure 1: Phases of wound healing

Haemostasis is the body's first line of defence in response to injury [8], and it involves a complex interaction of platelets, clotting factors, fibrinolytic proteins, cytokine mediators, *etc.* and takes place in three major stages: vascular spasms, vasoconstriction, and platelet plug formation, respectively. Upon wound formation, haemostatic mechanisms (activation of clotting factors, which leads to the conversion of prothrombin → thrombin → fibrinogen → fibrin) take place to stop bleeding by forming a blood clot and holding the platelet plug formation that covers the affected blood vessel together [9,10]. Growth factors are then released, and the

factors responsible for growth diffuse into the surrounding tissue and attract neutrophils (useful against infection) and monocytes (transform into macrophages, which bring about a series of activities that are essential for the wound healing process) [11–13] preparing for the second stage of wound healing. This stage of wound healing lasts for seconds up to minutes, depending on the depth and size of the wound, and also determines how soon a wound dressing has been applied to the wound.

Inflammation is the second phase right after haemostasis, where swelling, warmth, and redness in the affected area are observed due to white blood cells (exudate) leaked by blood vessels [14]. Wound exudate also provides a moist environment, which is important for wound healing. In this stage, neutrophils located in blood vessels migrate to the wound bed, enabling their concentration and that of monocytes in response to the degranulation of platelets and foreign materials. This interaction leads to the transformation of monocytes into macrophages, which protect the wound from infection by clearing microorganisms, pathogens, and debris through the release of reactive oxygen species (ROS) and proteases [11,18–20]. Macrophages not only clear debris, microorganisms, and pathogens, but they also liberate enzymes and cytokines, which produce growth factors that later help in the initiation of granulation tissue formation for the post-inflammation stage [8,17]. Moreover, the liberation of enzymes and cytokines produces fibroblasts and myofibroblasts, which contract and reconstruct the wound site and thereby narrow its size. This stage lasts for hours or days.

The third phase of wound healing is proliferation, which starts with the migration of fibroblasts and myofibroblasts, which are essential in the formation of granulation tissue. This phase is characterized by neovascularization, phase epithelialization, and the formation of granulation tissue at the wound site, constructing a newly developed extracellular matrix [18]. The extracellular matrix is responsible for angiogenesis, a process where the structural framework and restoration of the new vessel at the wound site are achieved by endothelial cells [8,17]. The migration of keratinocytes to the wound site matures, proliferates, and reconstructs thereby covering the wound bed [8]. This stage can last for days or weeks. Collagen, a structural protein essential in all phases of wound healing, plays a significant role in both the proliferation and remodelling phases. The fourth and final phase of wound healing is remodelling which can last for months or years. Finally, the wound is covered, and scar formation is observed. At this stage, most involved cells (macrophages, endothelial cells, myofibroblast, fibroblast, *etc.*) leave the wound site, and some undergo apoptosis [9,17]. Replacement of collagen (type III) with collagen (type

I) takes place, leading to increased scar strength. The formed scar tissue differs from that of unwounded tissue in that it has lower mechanical strength. The hair follicles and sweat glands might not be regenerated or healed after chronic wound damage.

2.2. Types of Wound

Wounds can be characterized based on their biological nature of repairing themselves as acute or chronic. Acute wounds are the type of wounds that typically heal within 1–3 months [19], progressing through the normal phases of wound healing at the expected rate without any complications. These types of wounds can regenerate without external care and form minimal scars. Primary causes of acute wounds include frictional contact of skin on a rough surface, paper cuts, animal bites, knife stabs, gunshots, burns (superficial, partial-thickness, and full thickness), corrosive chemicals, incisions, and electricity [20] that destroy the underlying skin tissue [21]. Typical types of acute wounds include non-penetrating (bruises, lacerations [22], concussions, and abrasions) and penetrating (animal bite, gunshot, cuts, surgical [23], stabs, and burns [24]). However, at any stage of wound healing, an acute wound can turn into a chronic wound if the progressive normal phases of wound healing are hampered by different factors like an imbalanced immune system, health diseases, and bacterial biofilm, leading to an extended healing time [25,26].

Chronic wounds unlike acute wounds fail to heal within 2–3 months and thus require additional medical attention. The literature revealed that the majority of chronic wounds approximately 70% or more, are a result of biofilm infection [27]. Impaired re-epithelialization and angiogenesis, increased protease activity, and dysregulated growth factors with persistent inflammation characterize chronic wounds as they lead to delayed progression of wound healing [4]. The most common and different types of chronic wounds include venous ulcers, diabetic foot ulcers, arterial ulcers, pressure ulcers, infectious wounds, radiation poisoning, and ischemic wounds. Bagher *et al.* reported that over 25 billion dollars are spent annually on the management of chronic wounds, with approximately 6.5 million people affected in the US [28]. Wounds can also be classified based on their depth as full-thickness (affecting the hypodermis and dermis), partial-thickness (affecting the dermis and epidermis), or superficial wound (affecting only the epidermis). Appropriate understanding of the type of wound and proper care of the wound is key to preventing chronic wounds. Treatment of chronic wounds varies depending on the wound type and wound site; therefore, a proper wound dressing has to be selected and applied accordingly. Polymer-based wound dressings play a major role in the treatment of different types of wounds.

2.3. Classification of Wound Dressings

Wounds that are deep, partial, minor, or major require suitable medical treatment to avoid further complications. The practice of treating wounds requires different approaches, which can be termed (wound dressings), leading to different classifications of these wound dressings as follows: (I) traditional or passive, (II) skin substitutes, (III) interactive materials, and (IV) bioactive dressings (**Figure 2**) [29,30]. Wound dressings should be easily accessible and easy to use by non-trained people in cases of emergency and in places far from where medical attention can be offered. Wound dressings play various roles in each phase of wound healing; some are suitable for a specific stage, while others are commonly used in every phase of wound healing. An ideal wound dressing should have a good water vapour transmission rate (WVTR), tensile strength, be biocompatible, biodegradable, non-toxic, absorb exudate, be patient-compliant, provide a wet environment at the wound site, prevent the formation of scars, *etc.*

Traditional or passive wound dressings are designed to protect the wound from the outside environment by covering the wound and thereby stopping excessive loss of blood; they also act as wound cushions, absorb wound exudates, and provide a dry wound environment [30,31]. Regardless of the aforementioned advantages, this type of wound dressing requires frequent changing and can lead to skin re-damage and severe pain [29,32]. Bandages, wool dressings, plaster, and gauze are examples of traditional or passive wound dressings [29–31].

Skin substitutes are wound dressings designed to substitute the injured skin and are made up of epidermal and dermal tissue layers made from keratinocytes and fibroblasts on a collagen matrix [29,33]. The application of skin substitutes is limited due to limited survival time on the wound site, host rejection, and possibilities of infection and transmission; examples include allografts, autografts, and acellular xenografts [30,33]. Interactive materials are wound dressings prepared from natural (alginate, chitosan, gelatin, *etc.*) or synthetic (PEG, PVA, *etc.*) polymers [30]. They provide a wet environment for the wound, acting as a cushion and barrier against infection from microorganisms, enhancing granulation, modifying the physiology of the wound site, displaying good tensile strength, and improving water vapour transmission rate [29–31,34]. This type of wound dressing can be divided into different forms like sprays, films, foams, hydrogels, sponges, *etc.*

Bioactive wound dressings are capable of promoting wound healing and can be incorporated with active materials, which they deliver to the target site of action to promote faster wound healing and improve their biological activity. Active materials like antimicrobials, vitamins,

metal nanoparticles, stem cells, *etc.* are usually fabricated in these types of dressings, and they are in different forms, such as gels, nanofibers, wafers, foams, sponges, hydrogels, membranes, and films [30,35]. These dressings are designed from a variety of naturally occurring biopolymers such as cellulose, hyaluronic acid, collagen, gelatin, alginate, pectin, chitosan, silk fibroin, *etc.*, or synthetic polymers (PEO, PVA, PEG, *etc.*) [3,5,7]. Bioactive dressings reported in current studies are biocompatible, biodegradable, promote wound healing, are antibacterial, promote WVTR, have good tensile strength, patient compliance, and have environmentally friendly characteristics [29,36]. Biopolymers can be used solely or in combination with other polymers and biologically active materials like vitamins, organic drugs, growth factors, metal nanoparticles, *etc.* for direct delivery to the affected area.

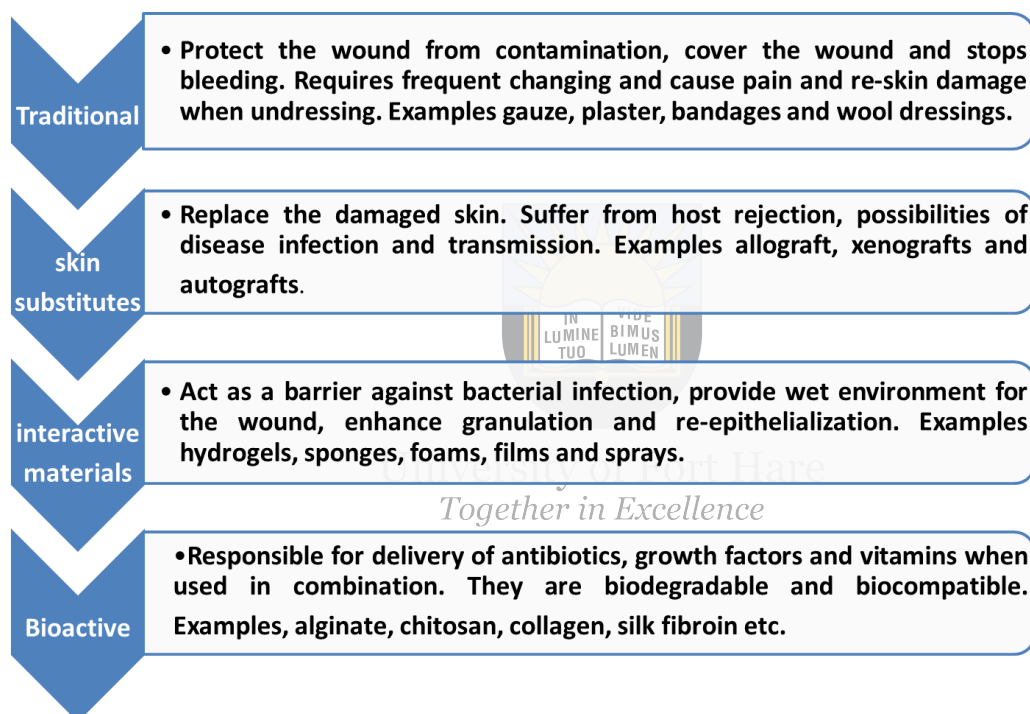


Figure 2: Classes of wound dressings

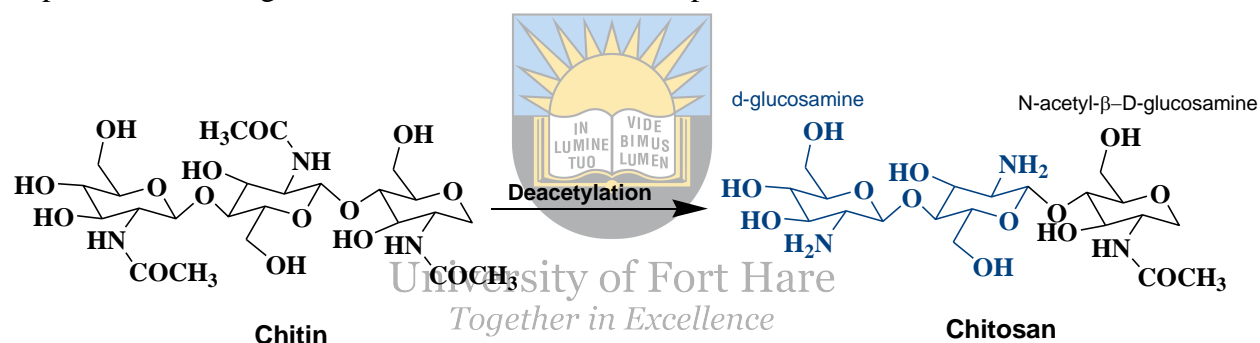
2.4. Biopolymers used in the Design of Wound Dressings with Haemostatic Wound

2.4. Healing Effects

2.4.1. Chitosan

Chitosan (a straight natural polymer resulting from the deacetylation of chitin) is composed of D-glucosamine and N-acetyl- β -D-glucosamine and is obtained from fungi and the exoskeleton of crustaceans [37–39]. Deacetylation of chitin results in the formation of amine groups, which give chitosan its cationic characteristic [39–41]. Generally, cationic biopolymers often possess an antimicrobial effect [39,42], which is no surprise given chitosan's ability to inhibit bacterial

growth against several bacterial strains, leading to the promotion of wound healing [43]. When applied to the body, it is easily recognized by the body cells, leading to its degradation by enzymes and promoting the activation of macrophages. Moreover, it stimulates the synthesis of hyaluronic acid, which is produced by the body to enhance blood clotting [44]. Wound dressings fabricated from chitosan have been reported to exhibit a great coagulation effect even in the presence of coagulopathy [45]. Chitosan has been repeatedly reported to possess excellent haemostatic properties both *in vitro* and *in vivo*. The haemostatic properties of chitosan seem to be charge-dependent [46]. The positively charged chitosan, due to the presence of amino groups, crosslinks with the negatively charged membranes of red blood cells, leading to a higher degree of platelet adhesion and wound surface constriction [1,39]. It is also reported that the degree of deacetylation may influence the haemostatic activity of chitosan. Bano and co-workers reported solid chitosan with a high degree of deacetylation to have a high haemostatic effect and higher platelet adhesion [1]. Moreover, chitosan can be easily attracted to platelets, resulting in thrombosis and activation of platelets.



Scheme 1: Shows deacetylation of chitin to chitosan

Bagher and co-workers prepared hesperidin-loaded alginate/chitosan hydrogels and analysed their wound-healing potential in a rat model. Two formulations of the hydrogels were prepared based on the concentration of hesperidin (1 and 10%) and tested for their wound healing potential. The *in vitro* drug release showed a sustained release in 14 days of $77.03 \pm 8.71\%$, and the hydrogels with or without hesperidin exhibited good haemocompatibility [28]. The presence of hesperidin in the hydrogels made no significant difference when tested for haemolysis. Hydrogels without hesperidin displayed a higher number of bacterial colonies, while hydrogels containing 10% hesperidin exhibited a lower number of bacterial colonies, followed by 1% hesperidin-loaded hydrogel. This implies that the addition of hesperidin to the hydrogels played a significant role in improving the antibacterial activity of the hydrogels, which is dependent on the concentration. A similar trend was also observed in the cytotoxicity

assay results, and the gels were not only cytocompatible but also promoted cell proliferation, which increased with an increase in the concentration of hesperidin. This proliferative effect was linked to hesperidin's remarkable positive cell growth effect. *In vivo* wound healing studies revealed incomplete wound healing with inflammation and infection in the plain hydrogel-treated wound, while hesperidin hydrogels exhibited full wound healing with no signs of infection or inflammation. The commercial wound dressing exhibited 32 and 59% wound closure on days 7 and 14, respectively, while hesperidin 10% hydrogel exhibited 82 and 98% wound closure post-injury, respectively.

Chen and co-workers reported porous starch/chitosan composites crosslinked with sodium trimetaphosphate (STMP) labelled (SPC) and tested their wound healing activity on a rat model [47]. These composites exhibited swelling ratios of 355.0% and a water absorption ratio of 150.8%. They were reported to be hemocompatible with a 0.12 ± 0.02 haemolytic absorbance, and they showed a high cell adhesion area against the rat tail. *In vitro* blood loss was recorded at 0.070 ± 0.031 g with 164.42 ± 8.67 s clotting time, compared to the medical gauze with 0.27 ± 0.091 g and 230.8 ± 10.30 s, respectively. Using the rat tail and the liver haemorrhaging models, the blood loss and clotting time were recorded at 0.29 ± 0.023 g and 147.25 ± 15.80 s and 145.2 ± 19.2 s, respectively, with a 20 mg SPC dosage. Sundaram *et al.* prepared injectable chitosan composite hydrogels for rapid haemostasis. The prepared hydrogels were adhesive, haemocompatible ($1 \pm 0.5\%$), and non-toxic with $96.6 \pm 5.9\%$ cell viability and 112 ± 12 s clotting time *in vitro*. *In vivo* investigation of the femoral artery and rat liver haemorrhage revealed shorter clotting times compared to the marketed haemostatic agents like Floseal and Fibrin sealant, with 20 ± 10 s, 105 ± 31 s, 76 ± 15 s, 218 ± 46 s, and 77 ± 26 s, 204 ± 58 s, respectively [48]. Wang *et al.* prepared a porous haemostatic sponge from chitosan/alginate and Bletilla striate polysaccharide (CS/Alg/Bsp) [49]. All the prepared sponges with varying ratios of Alg (5, 10, 15, 20% w/w) and Bsp (2.5, 5, 7.5, and 10% w/w) exhibited more than 90% porosity. A CS/Alg10/Bsp composite sponge was selected for further experimental studies because it exhibited significant pore size and water absorption results. The blood clotting kinetics of this sponge were greater than those of the plain CS, and they were found to be better as Bsp concentration increased. They exhibited a minimal BCI of 22.41%. These composite sponges showed an increase in cell growth of 3T3 cells, as they exhibited cell viability in the range of 109-117% after 48h of incubation. Using the rabbit ear artery haemorrhage model, the *in vivo* blood clotting time was recorded at 68.82s with 0.03 g of blood loss. The ternary

composite sponge exhibited shorter clotting time and blood loss compared to the marketed gelatin sponge.

Mohandas *et al.* prepared loaded VEGF fibrin nanoparticle composites from chitosan/hyaluronic acid (CS/HA) sponges to enhance angiogenesis in wounds. Porosity and swelling ratios for all the tested samples were in the range of 65–75% and 8–12%, respectively, with degradation percentages between 10–20% from the 1st week, which gradually increased to 30–35% from the 2nd week. The haemostatic behaviour of CS/HA-VFNPs sponges was compared to that of CS/HA sponges and Koltastat, a commercially available haemostatic dressing, and it was found that CS/HA-VFNPs exhibited the highest blood clotting ability, which was attributed to the presence of fibrin nanoparticles. Cell viability studies were performed against human umbilical vein endothelial cells (HUVECs) and human dermal fibroblast (HDF) cells using the Alamar blue assay. CS/HA-VFNPs sponges exhibited a maximum of approximately 85% against HDF cells and 98% against HUVECs. VEGF released from the fibrin nanoparticle composite sponges is significantly the most potent growth factor that promotes angiogenesis, which induces endothelial cell proliferation and migration [50]. Their results suggest that CS/HA-VFNPs sponges are promising scaffolds for the enhancement of angiogenesis. However, further studies still need to be done to evaluate the *in vivo* wound-healing properties of these sponges.

He *et al.* prepared alginate/carboxymethyl-chitosan/kangfuxin (ACK) sponges to enhance blood clotting and the management of full-thickness wounds. Different concentrations of kangfuxin (5, 10, and 15%) were used to evaluate its wound healing properties compared to plain AC and alginate. Blood coagulation tests showed that alginate sponges had poor blood clotting ability as compared to AC, ACK-5, ACK-10, and ACK-15, with blood completely clotting in contact with these sponges at a record time of less than 60 seconds. The antibacterial assay revealed that *S. aureus* was more resistant to all the treatment groups, with bacterial colonies decreasing by less than 65%, while in *E. coli*, all treatment groups exhibited similar antibacterial activity of more than 80%, with ACK-5 showing the highest number of bacterial colonies killed. hGFs cells were selected to check the cytocompatibility of these sponges, and ACK-10 and ACK-15 presented the highest number of attached hGFs as compared to the other treatment groups. *In vivo* wound healing was done for 14 days, and on day 4, the ACK-15 composite sponge exhibited a greater wound closure as compared to all other groups. From days 9 to 14, the ACK-10 composite sponge exhibited significant wound reduction, greater than all other treatment groups [5]. These results signify that a high concentration of kangfuxin

may lead to fast drug release, which influences the initial fast healing properties of ACK-15; however, a controlled release is more beneficial for the treatment of wounds, and after the 14th day, ACK10 sponge-treated wound was almost covered by regenerated skin.

Hao and co-workers fabricated alginate and chitosan-based composite sponges with fucoidan (ACF) to enhance hair follicle regeneration and angiogenesis for the treatment of full-thickness wounds [51]. Different compositions of fucoidan (AC, ACF-1, ACF-2, and ACF-3) were used to investigate its wound-healing properties. Evaluation of haemostatic assay for these composite sponges showed high blood clotting ability as follows: ACF-1 > ACF-2 > AC > ACF-3, signifying high fucoidan concentrations induced lower haemostatic ability and the blood clotting ability of AC was influenced by both chitosan and alginate. The antimicrobial evaluation revealed that the activity of AC is influenced by the antibacterial properties of CS and SA, and the fabrication of fucoidan decreased the antimicrobial ability of these polymers as it increased in concentration against *E. coli* (a gram-negative bacterial strain). These findings suggest that the antibacterial activity of these sponges is dependent on the concentration of fucoidan, and lower concentrations exhibit high antibacterial activity. Despite the influence of fucoidan on haemostatic and antimicrobial activity, ACF-1 and ACF-3 exhibited great cell viability against human gingival fibroblasts (hGFs). *In vivo* studies on rat full-thickness wounds were performed using AC, ACF-1, and ACF-3 composite sponges and sterile gauze as the control group for 21 days. All the samples appeared to have normal subcutaneous tissue with no evidence of infection. However, there was no visible wound contraction. The control group showed scabs and was haemorrhagic at the wound site on day 4. On day 9, ACF-1 exhibited the highest wound contraction, which was significantly closer to the one for ACF-3, with control and AC showing lesser wound contraction. On days 14–20, ACF-1 greatly accelerated wound healing, with wound contraction of over 98%, while there was no significant difference between AC and ACF-3, with both exhibiting less than 80% wound healing, whereas the control exhibited over 80% wound healing. The ACF-1 composite sponge enhanced wound healing by promoting cell proliferation, inflammatory cell infiltration, and angiogenesis.

Wang *et al.* prepared (CDDs) dopamine bio-glued beads from the combination of chitosan with diatom-biosilica to promote fast blood clotting. These beads showed large and fast absorption of water, which was linked to their porous internal structure, as confirmed by a scanning electron microscope (SEM). L929 cells were used to evaluate the cytotoxicity of the composite beads, and the cell viability of these composite beads was above 80% regardless of the concentration, reaching above 90% after 48 hrs [52]. According to GB/T 16886.5-2003 (ISO

10993-5: 1999), a material exhibiting 75% or more cell viability is considered noncytotoxic [53]. Cell viability that exceeded 100% was observed after 72 hrs, showing that the prepared composite beads also stimulate cell growth. The clotting time of CDDs composite beads was compared to other prepared formulations: CS (chitosan beads), CD (chitosan dopamine composite beads), and powder of chitosan (CP). The clotting time was recorded at 3.19 min, 3.08 min, 2.23 min, and 1.35 min for CP, CS, CDs, and CDDs, respectively. CDDs exhibited the shortest blood clotting time, and this is in relation to the fast and rapid water absorption of these composite beads. This shows that the CDDs blood clotting mechanism could involve water absorption within the blood cells, concentrating in them, and thereby forming a sticky blood clot that hinders blood flow or loss.

The addition of polydopamine significantly shortened the clotting time of the composite beads, as CDs and CDDs exhibited shorter times compared to other treatment groups. As observed by SEM, CDs exhibited a significant increase in blood cells on their surface, while CDDs revealed a large number of blood cells and a dense network of fibrin, indicating an excellent haemostatic effect. Polydopamine has a hydrophilic surface, which aids in the absorption of the composite beads, leading to the accelerated aggregation of coagulation cascades. Moreover, its phenolic hydroxyl groups may cause adhesion, leading to calmed blood clots and the closure of blood vessels. It is evident that chitosan, dopamine, and diatom-biosilica significantly exhibited a synergistic effect to promote rapid blood clots.



2.4.2. Gelatin

Gelatin is a high molecular weight protein extracted from the hydrolysis of collagen from plants or animals [54,55], and it is used in various pharmaceutical practices due to its biocompatibility, biodegradability, haemocompatibility, *etc.* [56,57]. Based on the hydrolysis procedure used (alkali or acid hydrolysis) during their manufacture, they can be classified as either type B or type A, respectively [58]. Its polypeptide chain is composed of a high number of amino acids [58], with proline, hydroxyproline, and glycine being the most dominant residues in its structure (**Figure 3**) [59,60]. The gelling effect of gelatin is influenced by a temperature of 35–40°C, including the dominance of proline and hydroxyproline [58,61]. In wound healing applications, it has been proven to promote a fast migration of healed cells [62]. Its wide application in the management of external haemorrhage and the clinical prevention of internal bleeding during surgery has made it a reliable agent in tissue regeneration.

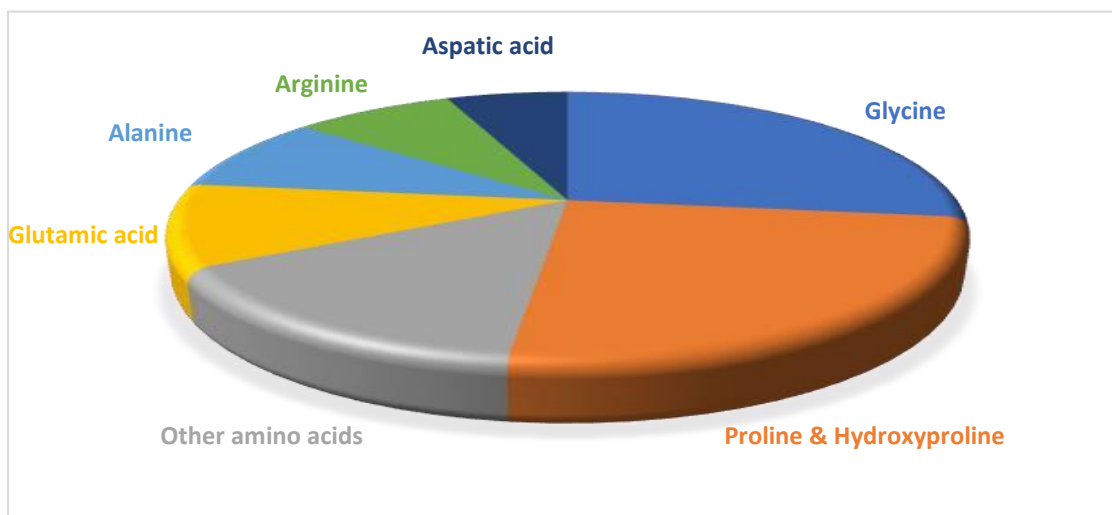
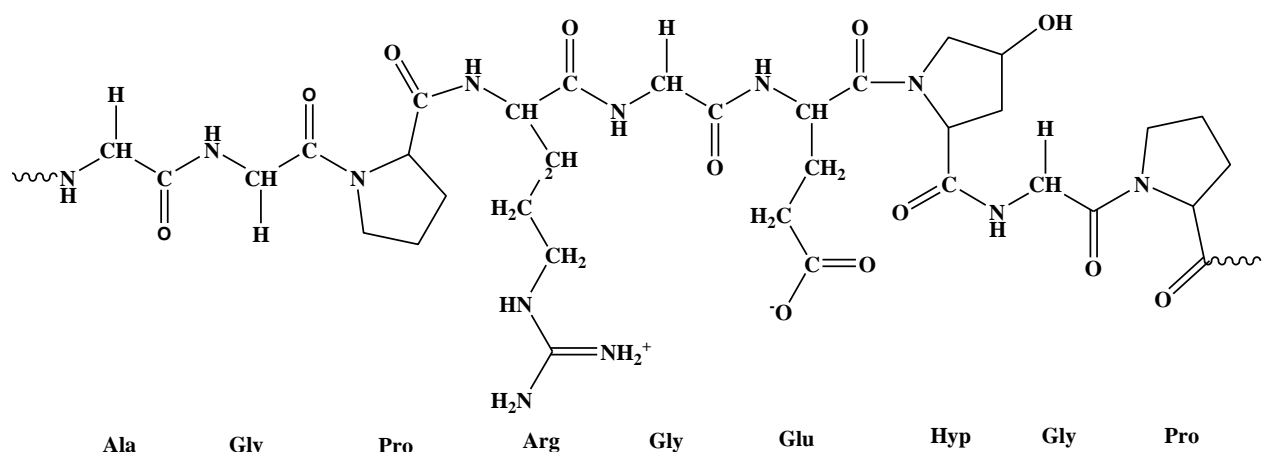


Figure 3: Summary of the composition of amino acids in gelatin [59,60]

Owing to its adhesive potential, recent studies have reported that gelatin-based scaffolds are advantageous in the rapid control of haemorrhage, as they accelerate the coagulation cascades [63] by adhering to RBCs and platelets *via* electrostatic interaction, which additionally promotes thrombus formation. Moreover, Alipal *et al.* reported that its swelling properties can limit blood flow by providing a site for fibrin clots and thereby forming a stable matrix around the broken blood vessel [64]. Gelatin's bio-adhesion properties can be linked to the high number of hydrogen bond-forming moieties available in its structure (-OH, -NH₂, and -OOC). Wang *et al.* reported its cellular adhesion and proliferation properties to be facilitated by its similar peptide chain to that of collagen [65]. Han *et al.* reported that its adhesion is influenced by the arginine-glycine-asparagine (RGD) sequence present in its molecular structure, which further promotes migration [66]. It can also activate the intrinsic blood clotting pathway as it is extracted from collagen. Nevertheless, its application in the critical control of haemorrhage conditions is limited as a result of its high water solubility, poor mechanical strength, and poor swelling capacity. Moreover, it also plays an important role in the 2nd phase of wound healing by facilitating the healing processes of the inflammation phase and the proliferation phase [67]. Drug release kinetics and incorporation capacity of gelatin-based scaffolds in the drug delivery system can be monitored by either varying their degree of crosslinking, molecular weight, or selection of type A or B [61].



Scheme 2: Chemical structure of gelatin

Huang *et al.* prepared gelatin/silver nanoparticle-based biodegradable composite cryogels and checked their potential to inhibit *Pseudomonas aeruginosa* (*P. aeruginosa*)-infected burn wound, biofilm, and haemostatic activity [68]. The prepared cryogels exhibited haemolysis ratios below 5% when their concentration was as high as 5 mg/mL, signifying good haemocompatibility of the cryogels. *In vitro* cytocompatibility showed that a concentration below 20 mg/mL exhibited no significant cell toxicity with both Gel/AgNPs-0.5 and Gel/AgNPs cryogels, with cell viability equivalent to that of Gel cryogel. Moreover, the cell viability of L929 cells in contact with Gel/AgNPs-0.5 and Gel/AgNPs revealed no significant difference as compared to that of Gel cryogel ($P > 0.05$) in 1, 3, and 5 days of incubation; this suggests that the addition of AgNPs did not affect the cell viability and haemocompatibility of the prepared cryogels. The live/dead staining revealed a green spindle-like morphology of the cells and almost no evidence of dead cells recorded in 1 day of cryogels in contact with the cells. The antibacterial activity of these cryogels was evaluated against *P. aeruginosa*, *E. coli*, and MRSA bacterial strains, where 80 mL of the sample was added to 10 mL of 10⁵ central forming units/mL of the microorganism's solution incubated at 37°C. The untreated bacterial solution showed OD₆₀₀ values that increased with increasing time for up to 24 h, and they then remained constant for all three bacterial strains. Gel cryogel exhibited similar results to those of the untreated bacterial solution, signifying that gelatin does not have any significant antimicrobial activity against the treated bacterial strains. Gel/AgNPs-0.5 exhibited good antimicrobial activity against *E. coli* and MRSA in the 1st 12 h, while against *Pseudomonas aeruginosa*, such activity was observed within 24 h. Gel/AgNPs cryogels exhibited the best antimicrobial activity against MRSA and *P. aeruginosa* strains, where all the bacteria were killed within 48 h. These results were outstanding and indicated that the bacterial activity was

dependent on the amount of AgNPs loaded within the cryogels. Similarly, the antibacterial results of the blank and gel cryogel treated with selected bacterial strains showed no significant difference in the biofilm biomass. The removal ratio of the biofilm biomass for Gel/AgNPs was recorded at 70%.

In vivo haemostatic capacity for the prepared cryogels was compared to that of the commercially available gelatin sponge, medical gauze, and untreated group using a mouse liver trauma model. The recorded blood loss was 350 mg for the untreated, 230 mg, 121 mg, 82 mg, and 81 mg for the medical gauze, gelatin sponge, Gel cryogel, and Gel/AgNPs cryogels, respectively. The slight difference between Gel cryogel and Gel/AgNPs shows that silver nanoparticles have no significant haemostatic activity and did not influence the swelling water absorption capacity of the Gel cryogels. The bleeding time was faster (2.5 min) for the gel sponge, gel cryogel, and Gel/AgNPs treated groups, while the gauze-treated bleeding time was 3.3 min and 5 min for the untreated. The fast healing potential was linked to gelatin's potential to bind or activate platelets, thereby leading to the formation of blood clots as well as swelling and porosity, which may concentrate the blood after absorption. *In vivo* haemostasis assay against the rat liver defect model revealed a short bleeding time for Gel/AgNPs of 3.3 min, greater than that of Gel cryogels (4.1 min) and untreated (6.7 min). *In vivo* wound healing of Gel/AgNPs cryogels exhibited wound contraction of 96%, higher than that of Gel cryogel and commercially available Tegaderm™ with 75% and 56%, respectively. Moreover, the collagen content increased with treatment time, with the Gel/AgNPs cryogel-treated group exhibiting higher collagen content as compared to Tegaderm™ after the 1st and 2nd weeks of treatment.

Cao and co-workers formulated porous gelatin microspheres fabricated with vancomycin (Van) and checked their haemostatic efficacy. The specific surface area and porosity were recorded at 22.9 m²/g and 40.1% for plain porous microspheres (P-MS), with no significant difference with those of vancomycin porous gelatin microspheres (Van/Gel-MS) with 23.3 m²/g and 39.6%, respectively. Water absorption of Van/Gel-MS was 1460%, P-MS (1450), and 1330 for crosslinked gelatin microspheres (CL-MS). This proves that porous Gel microspheres exhibit a higher absorption capacity than crosslinked Gel microspheres, and the fabrication of Van slightly aided the porosity and water uptake of the microspheres. The prepared samples exhibited *in vitro* coagulation more than three times better than those of the untreated and Yunnan Baiyao (a haemostatic material from China) treatment groups, with CL-MS exhibiting 136 s, Gel-MS 133 s, and P-MS 80 s. Moreover, across different concentrations of Van/Gel-MS, they all exhibited similar clotting times to those of P-MS, indicating that Van had no

significant effect on the blood clotting effect of the microspheres. Van/Gel-MS were proven to promote cell adhesion as the SEM images revealed an accumulation of fibrin and RBC on their surface [69]. Drug release kinetics of 8, 4, and 2% concentrations of Van from Van/Gel-MS were recorded in 5 days. Upon the 1st hour, Van/Gel-MS 8, 4, and 2% initial bursts of 12.22%, 14.47%, and 19.68% release were followed by 61.18%, 68.01%, and 76.71% in 24 h, and lastly 78.05%, 86.95%, and 91.67% in 120 h, respectively. The trend in these findings indicates that lower concentrations of Van lead to higher drug release from the microspheres, and vice versa. Gel microspheres without Van exhibited no antibacterial activity against *S. aureus*, while Van/Gel-MS 8% revealed the highest antibacterial inhibition (8.5 mm), 4% (7.5 mm), and 2% (7 mm). Comparing drug release kinetics and antibacterial activity, it can be said that slower and controlled drug release positively played a significant role in the inhibition of *S. aureus*. *In vivo* haemostatic results on the liver lacerated model revealed contrary results in comparison to the *in vitro* haemostatic results on all the tested samples.

The untreated liver model had the longest clotting time, while CL-MS had a better clotting time than Gel-MS. Yunnan Baiyao exhibited a shorter time than both of them. However, shorter haemostatic times were recorded for P-MS (1.25 min) and Van/Gel-MS (1.55 min), which can be linked to their high porosity and water absorption capacity. Similar blood clotting times were observed for Van/Gel-MS irrespective of the difference in their concentrations, indicating that blood coagulation was dependent on gelatin's haemostatic potential and porosity of the microspheres. *In vivo* infected wound repair showed a nearly sealed, bright, and moist surface in all Van/Gel-MS treated groups with muscle lesion reduction filled with fibrous connective tissue over 10 days of treatment. Although there were no bleeding spots across all groups, the PMS-treated group showed the presence of exudate and inflammation. Furthermore, histological analysis revealed a larger number of scattered macrophage permeation, fibroblasts, neovascularization, and myocyte necrosis for all the Van/Gel-MS concentrations. However, Van/Gel-MS 2% exhibited a higher number of new capillaries formed compared to all other groups, while P-MS showed severe exudate and inflammation.

Atashgahi *et al.* prepared gelatin nanofibers covering epinephrine-entrapped chitosan nanoparticles (E/CS/Gel) for fast haemostasis. The composition of this nanofiber material was as follows: chitosan (15 % w/v), epinephrine (300 µg/ml), and gelatin (1.5% w/v). Epinephrine exhibited concentration-dependent cytotoxicity, which increased with an increase in concentration. However, it exhibited reduced cytotoxicity when fabricated with chitosan NPs and even displayed good biocompatibility when treated as E/CS/Gel. This shows that chitosan

and gelatin significantly improved the biocompatibility of epinephrine. *In vitro* haemolytic assay displayed haemolysis ratios of 3.4% and 2.1% for E/CS/Gel and CS NPs, respectively. As stated, haemoglobin release is classified as haemolytic at >5%, slightly haemolytic at 2–5%, and non-haemolytic at 0–2% [70]. *In vitro* blood clotting of E/CS/Gel nanofiber was compared to that of the commercially available dressing (GelFoam®). The whole blood (WB) and normal saline (NS) absorptions were recorded at 300% and 270%, respectively, for E/CS/Gel, while GelFoam® absorbed 210% and 200%, respectively. Using citrated human blood, the clotting time for E/CS/Gel was recorded at 20 seconds, 52 seconds for the base pad containing E/CS NPs, 70 seconds for GelFoam®, and 110s for the base pad. The application of blood cells on the surface of E/CS/Gel revealed immediate blood clotting as the E/CS/Gel nanofibers showed activation of agglutination and coagulation procedures. SEM images showed a substantial adherence of RBCs to the surface of nano-biomaterials, forming thrombus and thereby activating platelets. Plasma prothrombin time (PT) and activated partial thromboplastin time (aPTT) revealed about a 20% notable decrease in PT compared to aPTT, with no significant change after applying E/CS/Gel. *In vivo* haemostatic assay on ruptured femoral arteries was performed for E/CS/Gel, GelFoam®, base pad containing E/CS NPs, and blank, and the haemostatic time was recorded at 99 s, 140 s, 163 s, and 203 s, respectively. The lower blood loss could be linked to gelatin's adhesive nature and the fact that in high dosage, it causes blood clotting through platelet adhesion [70]. Using a ruptured liver model, the bleeding time was recorded at 33s for E/CS/Gel, 54s GelFoam®, 75s base pad containing E/CS NPs, 97s blank, and 104s for untreated wounds, with 50% of the animals still haemorrhaging throughout the end of the experiment. *In vivo* haemostatic evaluation of these nanofibers concludes that they are potentially active materials for rapid blood clotting, and a combination of gelatin and chitosan yielded a synergistic effect.

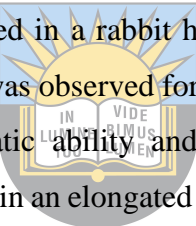
Aydemir and co-workers prepared sodium oxidized regenerated cellulose as a cross-linker of gelatin-based microparticles (Gel/NaORC) to stimulate fast haemostasis [71]. NaORC exhibited no notable swelling capability, while different formulations of NaORC (1, 5, 10, 25, and 50%) used to crosslink the gelatin microparticles exhibited 21.59%, 21.03%, 16.63%, 15.21%, and 14.63% swelling capabilities, respectively. The swelling ratios of the microparticles decreased with an increase in the concentration of NaORC. The *in vitro* coagulation time of the microparticles was compared to that of NaORC as a control and Celox®, a marketed product. The coagulation time for the Gel/NaORC formulation presented a shorter time for NaORC-1 which increased with concentration as Gel/NaORC-50 had the

longest blood clotting time. However, there was a notable difference between Gel/NaORC-1 and Gel/NaORC-5 despite their similar swelling capabilities, suggesting that the haemostatic activity of the microparticles did not solely depend on swelling ratios but also the concentration of NaORC. Celox® displayed the shortest time compared to all the tested groups, while NaORC revealed a short time against all other Gel/NaORC formulations except for Gel/NaORC-1. Gel and NaORC synergistically played a key role in reducing the blood clotting time of Gel/NaORC-1. Gel/NaORC-1 was selected for further studies, and the calcification profiles for Gel/NaORC-1 and Celox® were similar with shorter calcification periods than in the control and Gel groups, while NaORC presented the shortest calcification period ($p < 0.05$). *In vitro* cytotoxicity was performed against human umbilical vein endothelial cells (HUVEC) incubated for three days, and Celox®, Gel/NaORC-1, and Gel displayed more viable cells than the control and NaORC groups. MTT assay conducted for 6, 12, and 24 h showed that all treatment groups except the control exhibited an increase in cell viability that increased with time. However, there was a notable decrease in cell viability for Gel groups in the 24th h, while Celox® showed an exceptionally increased cell viability.

Wang *et al.* designed photo-crosslinkable hybrid haemostatic injectable and *in situ* hydrogels composed of gelatin methacryloyl (GelMA) and pectin methacrylate (PECMA). Their polymer combination therapy resulted in a highly porous structure, mechanical properties, tunable rheology, biodegradability, and controllable swelling of the hybrid injectable hydrogel. These properties were achieved by varying the polymer (1.5–7.0%) and calcium (0–15 mM) content used in the sequence of crosslinking the hybrid hydrogels *via* UV-photopolymerization and calcium gelation. These hybrid hydrogels showed a synergistic effect in their haemostatic activity and biocompatibility, and their highly porous structure aided in rapid blood clotting and quick blood absorption properties [72]. They were further proven to show rapid photo-crosslinking and can be easily injected into the affected area, halting blood loss and thereby reducing blood clotting time by 39%. These hybrid hydrogels could be easily removed from the site of treatment without causing skin re-damage.

Nagahama *et al.* also reported combined haemostatic dressings already on the market [Gel sponge (GelFoam®) and fibrin glue (Tisseel)] for improved haemostatic effect and in neurosurgical applications. Treating a 51-year-old female who suffered from brisk venous bleeding due to a tear at the sigmoid sinus junction, using the fibrin/Gelfoam immediately controlled the bleeding and remained uncomplicated for the remainder of the resection of the tumour operation [73].

Yan *et al.* formulated a collagen sponge reinforced with chitosan/calcium pyrophosphate nanoflowers (CPNFs-Col sponge) for fast haemostasis [74]. These sponges were formulated at different concentrations of collagen (0, 15, 30, and 40%). *In vitro* and *in vivo* biological studies were performed for these sponges, and there was no evident cytotoxicity on both HUVEC cells past 2 days and mice appeared normal with no sudden change in their behaviour. Using 2% rabbit haemocyte the sponges also showed excellent *in vitro* compatibility during the haemolysis test. CPNFs-Col-30% exhibited overall excellent results in all the *in vitro* biological tests. Platelet adhesion was more significant for the CPNFs-Col-30 sponge with $\pm 80\%$, followed by the collagen sponge with $\pm 53\%$ and the chitosan sponge with $\pm 53\%$. The haemoglobin adsorption test revealed that the CPNFs-Col-30 sponge exhibited the highest ratios of approximately 50% within the initial 2 minutes compared to other groups with less than 25%. However, from 3-5 min, the collagen sponge exhibited similar ratios with CPNFs-Col30 sponge, with a maximum of $\pm 90\%$ in 5 min. These results prove that the CPNFs-Col-30 sponge will enhance the rate of blood clotting at the very beginning of post-injury. *In vivo* haemostatic evaluations were performed in a rabbit hepatic trauma model and an ear artery model. The shortest haemostatic time was observed for the groups treated with CPNFs-Col-30 sponge, exhibiting the best haemostatic ability and showing minimal blood loss. Other treatment groups achieved haemostasis in an elongated time frame with more blood loss. These sponges are undoubtedly the best candidates for the management of haemorrhage in a shorter time to hinder excessive blood loss.



University of Port Harcourt
Together in Excellence

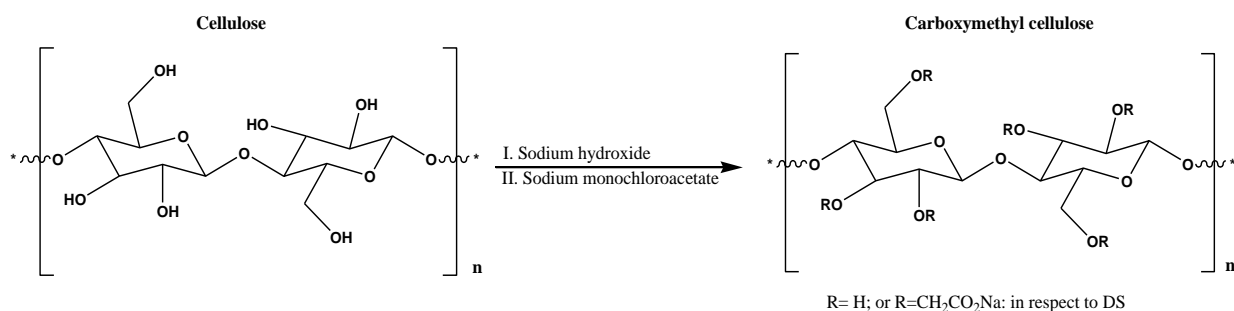
Arunagiri *et al.* formulated haemostatic microparticles composed of crosslinked polyelectrolyte Gelatin-Tannic acid- κ -Carrageenan (GTC) [75], and the prepared microparticles were found to be stable at 86 μm (GTC^k), 63 μm (GTC^l), and 46 μm (GTC^m). The swelling and water absorption properties of these formulations increased with a decrease in the particle size of the microparticle, with GTC^m showing the highest swelling (273%) and water absorption (2400%) properties. The prepared scaffolds exhibited haemolysis ratios below 0.5%, showing their good haemocompatibility. Using the FE-SEM analyser, the microparticles exhibited high cell adhesion of RBC and platelets, which increased with an increase in the particle size. Pseudopodia structure was deformed due to the high number of platelet adhesion, and deformed pseudopodia aided in forming platelet plugs, which help to strengthen fibrin and thereby stop blood loss [76]. A blood clotting index was performed for the prepared microparticles and compared to that of tannic acid, gelatin, and κ -Carrageenan. The microparticles revealed a significant BCI than the other groups, with GTC^m displaying the lowest percentage of 10.33%

and κ -Carrageenan with the highest of 68.44%. GTC^m was selected for further studies, and the cell toxicity was checked using a range of 10–1000 $\mu\text{g}/\text{mL}$. Cell viability was dependent on the concentration of GTC^m, as lower concentrations of 10–60 $\mu\text{g}/\text{mL}$ displayed over 100% cell viability, 80–500 $\mu\text{g}/\text{mL}$ displayed >90% viability, and lastly, 1000 $\mu\text{g}/\text{mL}$ showed >80% viability. Despite the decrease, all these concentrations are still considered safe. The blood clotting and blood loss properties for GTC^m were recorded at 50 s and 66.77 mg, respectively, showing a rapid coagulation time.

2.4.3. Cellulose

Cellulose is an environmentally friendly polymer composed of a linear series of D-glucose molecules linked by β -glycosidic bonds [77,78]. It is extracted from plant fibre cell walls, and it is also available in algae and bacteria in small proportions. It is a widely distributed natural polymer compound and offers several advantages, such as sustainability, renewability, biocompatibility, biodegradability, patient compliance, and affordability. A composite sponge prepared from cellulose absorbed blood rapidly and stimulated thrombosis to achieve haemostasis [79]. Cellulose can be modified to produce a variety of its derivatives, which can be used in different fields of biomedical research, depending on their structure, and some of them have been widely used in wound healing and as haemostatic materials (oxidized cellulose, carboxymethyl cellulose, *etc.*). CMC is derived from cellulose, where, depending on the degree of substitution (DS), the hydroxyl groups present in the cellulose structure are modified into carboxymethyl groups. The DS varies between 0.4 and 1.5 [80]. The substitution of the hydroxyl groups with carboxymethyl groups has increased the water solubility of CMC and it is widely used in sodium salt form. Owing to these features, CMC has been widely applied in a variety of different industries (such as lubricants in eye drops in healthcare and food thickeners in the food industry). It has been used in regenerative medicine, wound healing, and drug delivery [81]. CMC can promote coagulation by dissolving in the blood due to its high solubility, thereby increasing the viscosity of the blood and eventually stopping blood loss [82]. Aoshima and co-workers revealed in their work that CMC operated as a bridge for fibrin polymerization when it is dissolved in the blood, thereby promoting the formation of thick fibrin fibre and, as a result, improving blood coagulation [83]. As reported by Ribeiro *et al.*, a variety of commercially available CMC dressings have been widely used in different stages of wound healing, like IntraSiteTM Gel (which promotes fast wound healing by removing hard-boiled tissue on the affected area), SilvercelTM (used in chronic wounds to hinder microbial

infection), Aquacel Ag™ and GranuGel™ (which suppress microbial infection and treat full-thickness wounds, respectively) [84].



Scheme 3: Carboxymethylation of cellulose to form carboxymethylcellulose

Ohta and co-workers formulated non-woven sheets composed of carboxymethylcellulose (CMC) with varying degrees of substitution (DS) for the management of haemostasis [81]. The DS significantly played a notable role in the absorption properties and biodegradability of the sheets, as an increase in DS increased their biodegradability and decreased the absorption potential of the nonwoven sheets. Using clot signal, nonwoven sheets without CMC had less haemostatic ability compared to those with CMC which significantly improved the formation of hard blood clots, which could be linked to the incorporation of CMC into fibrin fibres. The clotting time was short for the CMC-treated group compared to the groups treated with normal saline. They discovered that the prepared CMC scaffold accelerates the development of clots thereafter, but it does not shorten the initiation of clotting. The high DS of CMC sheets increased the viscosity of the blood as they dissolved in contact with it. Using rat tail, the haemostatic evaluation of the CMC sheets was recorded to significantly shorten the bleeding time regardless of the DS, with the shortest bleeding time of 7.5 min being lower than that of the native cellulose nonwoven sheet by 3.3 min.

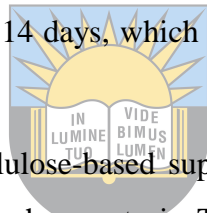
Fan *et al.* prepared CS/cellulose composite sponges loaded with sodium dodecyl sulphate (SDS) for the management of excessive bleeding using a variation of CS to cellulose (9:1, 7:3, 5:5, 3:7, and 1:9). The porosity of these formulations was in the range of 95.9-79.3% with Cel9/CS1 exhibiting the highest ratios. There was no significant difference in the water absorption ratios of the formulations though there was a slight difference between Cel5/CS5 and Cel9/CS1, showing better absorption, respectively. The haemoglobin absorbance of the reported sponges was significantly low compared to that of a commercial gelatin sponge, pure cellulose gel, and gauze, implying that the presence of CS improved the haemostasis of the

sponges [79]. *In vitro* blood clotting time was recorded at 3 min for gelatin sponge and gauze, while the sponges stopped bleeding within the range of 98–35s, with the shortest time recorded for Cel5/CS5. These sponges revealed good adhesion properties as the amount of CS was increased, showing a great number of RBCs on their surface, and their haemolytic ratios were below 5%, showing good haemocompatibility. Moreover, these sponges exhibited antibacterial activity against *P. aeruginosa*, *S. aureus*, and *E. coli*. With no surprise, the cell viability rate increased with an increase in the content of CS, and the sponges promoted cell growth as recorded from day 1-3 with viability rates in the range of 89.6–106.9% and 102.1-115.2%, respectively. *In vivo* haemostatic evaluation revealed the shortest bleeding time for Cel5/CS5 on rat liver (20 s), leg artery (34 s), and tail amputation (29 s), compared to gelatin sponge-treated groups with 131 s, 372 s, and 159 s, clotting times, respectively.

Liu and co-workers prepared carboxylated cellulose nanofibers (CNF/Gel/AgNPs) with gelatin loaded with aminated silver nanoparticles of (0.2 and 0.5) varying concentrations. Equilibrium fluid uptake of these nanofibers was compared to that of plain CNF, and CNF exhibited better fluid uptake of simulated blood fluid (SBF) compared to the blood. However, this was significantly lower than that of CNF/Gel/AgNPs formulations, which showed similar SBF and blood absorption that increased with an increase in AgNPs. Haemoglobin absorbance was significantly lower for CNF/Gel/AgNPs scaffolds compared to that of CNF, however, they were all non-haemolytic with absorbances lower than 0.18. Expectedly, CNF/Gel/AgNPs exhibited the highest number of platelets adhered to their surface, and a similar trend was observed for the thrombin-antithrombin complex. The *in vitro* cytotoxicity against normal neonatal human dermal fibroblast displayed cell viability greater than 100% for the tested dressings, and the CNF/Gel/AgNPs_{0.5} scaffold exhibited the best antibacterial inhibition compared to the other tested groups over *S. aureus* and *P. aeruginosa* bacterial strains [85]. Wound healing results revealed that approximately 90% of the wound was closed in 14 days, with a survival rate of 83% for the treated mice, while CNF-treated mice did not survive more than 7 days.

Barbar *et al.* formulated haemostatic granules from gamma radiation cross-linked CMC/kappacarrageenan (KC) and polyethylene oxide (PEO) [86]. Two formulations were achieved, CMC (20% w/w CMC, irradiated at 40 kGy) and KPP (2.5% KC, 2.5% PEG, 5% PEO, irradiated at 25 kGy), which were further designated –G (granules) or –D (pasted in medical gauze). Swelling ratios showed water absorption to be high and reaching equilibrium within the first 4h for CMC and 7h for KPP. The prepared CMC-G scaffold could absorb 10

times more of its amount, despite a significant decrease in saline solution absorption. KPP-D presented a restricted swelling capacity, which was linked to the gauze backing and high crosslinking by PEO. *In vitro* haemostatic evaluation displayed no significant difference over KPP-D and CMC-D scaffolds, with a BCI lower (1:2 sample-to-blood ratio) than that of commercially available agents Celox®, medical gauze, and QuickClot®. Blood clotting results presented a relatively faster blood coagulation time for the two formulations as compared to that of the commercially marketed haemostats. Platelet adhesion results showed less adhesion observed for QuickClot® and CMC formulations, whereas KPP formulations presented high adhesion of platelets on their surface. KPP-D was suggested to work as an adhesive material and to attract and aggregate platelets, while CMC-G was more of a tissue factor dehydrator, concentrating RBCs. *In vitro* cytotoxicity of the formulations revealed cell viability of 85% (CMC) and 87% (KPP). *In vivo* blood coagulation investigation using 20 rat femoral arteries showed treatment with CMC-G and KPP-D exhibited 100% survival in 7 and 14 days, regardless of the age of the rat, and induced blood clotting in less than 90 s. These formulations displayed complete wound closure in 14 days, which was comparable to a popular chitosan-based product.



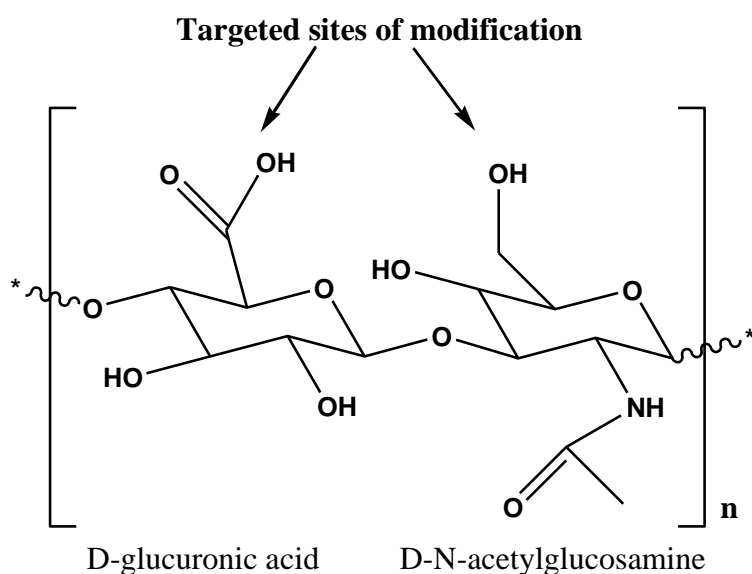
Mahmoodzadeh *et al.* formulated cellulose-based superabsorbents (aerogels and hydrogels) loaded with tranexamic acid to promote haemostasis. The prepared formulations revealed that the aerogels had a higher porosity (~70%) than the hydrogels, and they exhibited higher swelling and blood absorption ratios (60 times their size) by trapping the RBCs. The commercial dressings (Gelita-Cel® and Traumastem®) exhibited no significant swelling ratios [87]. Aerogels formulation exhibited adherence to the bleeding site of 1.5 cm² area with an average stress of 82 ± 6 kPa, even greater than that of commercial fibrin glue (15–20 kPa), Traumastem® (23 kPa), and Gelita-Cel® (18 kPa). The release of tranexamic acid was recorded at 41% in 4h and 90% in 6h. For aerogels, 90% release was achieved. Aerogel formulations were used for further studies, and they exhibited good cytocompatibility, including non-haemolytic behaviour (0.66 ± 0.05% haemolytic ratio), including a BCI of 0.8%. BCI and RBC attachment of Traumastem® and Gelita-Cel® were recorded at (60 and 30%) and (20 and 4%), while the aerogel scaffold exhibited an 80% RBC attachment. The clotting was more rapid for the aerogel scaffold forming a milky gel in contact with the plasma, while the Traumastem® and Gelita-Cel® clotting times were recorded at nearly 240 s. *In vivo* studies using a rat femoral artery showed the amount of blood loss and coagulation time of (0.8 g and

179s), (3.6.g and 380s), and (3.42 g and 402s for aerogel scaffold, Traumastem®, and Gelita-Cel®, respectively.

2.4.4. Hyaluronic Acid

Hyaluronic acid (HA) is a biopolymer that is naturally occurring in most body parts and is more abundant in synovial fluid (SF) and articular cartilage. It is a glycosaminoglycan forming the main component of the extracellular matrix (ECM) [88,89]. Its structure is composed of repeating linear disaccharides, made up of D-N-acetylglucosamine and D-glucuronic acid [90], linked together by β -1,3 and β -1,4 glycosidic bonds [91]. It is non-allergic, biocompatible, biodegradable, bioresorbable, and non-toxic [88,90]. Moreover, it acts as a shock-absorber, lubricant, flow resistance regulator, and joint structure stabilizer [92]. Its structural formula is composed of a large number of hydroxyl and carboxylic acid groups and a few acetamide groups, which aid in its high water absorption ability and hydrophilic behaviour as its molecules have the potential to swell up to 1000 times. It is involved in all stages of wound healing, and just after an injury, it is increased at the site of injury as it promotes angiogenesis, decreases the inflammatory process, and regulates tissue remodelling [93].

During the process of wound healing, high levels of HA are reported in granulation tissue, and its hydrophilic character makes it bind to fibrin, making the fibrin clot soft and more susceptible to being colonized by the cells. It can be composed of 25 000 repeating disaccharides and more, and this determines the role it plays in the body, concluding that its activity is dependent on its molecular weight [91]. Low molecular weight HA molecules stimulate angiogenesis, pro-inflammatory cytokines, migration, and vascular endothelial cell proliferation [91], allowing sufficient blood supply at the broken blood vessel [94]. Contrary, high molecular weight HA inhibits angiogenesis, migration, and vascular endothelial cell proliferation; however, it stimulates the anti-inflammatory response [95]. When applied to the body, HA is ineffective until it attaches to the cluster determinant 44 (CD44) receptor, and when that happens, it induces fibroblast migration [94]. Its binding to CD44 triggers its fragmentation from high molecular weight to low molecular weight oligomers thereby regulating cellular activity that recruits monocytes and leucocytes and thus sustains the inflammatory response [92,93]. However, its interaction with CD44 has been reported to slow down the movement of leukocytes, affecting neutrophils' adhesion to the broken blood vessel [95]. HA-based hydrogels have been reported to play a positive role in cartilage haemostasis, proliferation, wound healing, cellular signalling, and biomechanical integrity [96].



Scheme 4: Structure of Hyaluronic acid

Chen *et al.* reported an *in vitro* evaluation of a composite powder (RapidClot) composed of hyaluronic acid and alginate for the management of excessive bleeding wounds. The water absorption properties of these composites were compared to those of the commercially available dressings, *i.e.*, Celox and WoundSeal. The swelling ratios were recorded at 1124% RC, 372% CX, and 201% WS. Distilled water was used to simulate the blood clotting time and contact time with the PBS, WS exhibited the longest clotting time of 705 s, while RC and CX were 95 and 80 s, respectively. Using blood, the clotting time for WS remained at 705 s, while a significant difference was observed between CX and RC with increased or prolonged clotting times of 132.7 and 378.7 s, respectively. This shows that RC has better haemostatic ability than the two commercially available dressings. The haemolysis assay for these dressings was tested using different concentrations, and results revealed that the haemolysis of WS and RC was not dependent on their concentration, while CX revealed an increase in concentration to negatively affect its haemocompatibility. At the highest concentration used, (20 mg/mL), the haemolytic ratio for these dressings was recorded at $46.3 \pm 6.5\%$, $36.4 \pm 9.1\%$, and $4.2 \pm 1.5\%$ for WS, CX, and RC, respectively [97]. Enzymatic degradation studies using hyaluronidase and lysozyme revealed a decreased weight of CX and RC from day 1 (35%) and day 7 (55%), while WS revealed no notable difference. While in the lysosome, CX was more susceptible with 40% remaining after digestion on day 7, while RC showed 50% remaining. Using NIH/3 T3 fibroblasts, the cell viability was recorded at $98.4 \pm 4.1\%$ for CX, $90.7 \pm 3.1\%$ for RC, and $49.6 \pm 14.4\%$ for WS.

Liu and co-workers prepared hyaluronic acid/cationized dextran (HA/Dex) sponges, and these sponges were composed of poly((2-dimethyl amino)-ethyl methacrylate)-grafted dextran (DexPDM) and partially-quaternized Dex-PDM crosslinked using sodium trimetaphosphate (STMP). These sponges were labelled SHDP and SHDQ, respectively. Amongst formulations of SHDP depending on STMP, 50 mg STMP (SHDP-2) was selected for further wound healing studies accompanied by SHDQ due to its high water absorption and swelling capacity of 1035% and 1159%, respectively. Lower haemolysis ratios below 0.5% were observed for both SHDP-2 and SHDQ, moreover, they further exhibited cell viability of over 70%, revealing the cytocompatibility of the sponges against HEK 293 cells. SEM images confirmed the blood compatibility of SHDP-2 and SHDQ with red blood cells (RBCs), showing a biconcave disk morphology even after treatment. Compared to sterile gauze (65% haemoglobin content), the whole-blood clotting assay after the 60s revealed SHDP-2 and SHDQ sponges with significant haemoglobin content of about 30%. This rapid blood clotting could be linked to the highly porous and swelling ratios of these sponges. Complete blood clotting was observed in 2 min in treatment with SHDQ and 3 min for SHDP-2, while sterile gauze did not reveal blood clotting formation after 3 min. These results signify that excessive bleeding cannot be solely stopped by the body's natural mechanisms, thereby requiring an effective haemostatic wound to play a vital role in rapid haemostasis. Application of optical microscopy showed that the SHDQ sponge was more effective when compared to all other tested treatments, revealing more aggregated RBCs on its surface. The high haemostatic ability of SHDQ was linked to its high cationic charge, which might have interacted with the negatively charged blood cells to inhibit blood loss. *In vivo* haemostatic performance was done using blank (no treatment), sterile gauze, SHDP-2 and SHDQ on bleeding livers treated for 60 s, then later covered the affected area with filter paper for another 60s. [98]. SHDP-2 and SHDQ displayed promising haemostatic ability *in vitro* and *in vivo* and are promising materials for haemorrhaging wounds.

An *et al.* formulated a highly haemostatic tissue-adhesive hydrogel (HA-serotonin) through the oxidative crosslinking of serotonin molecules combined with the HA backbone. This scaffold, due to serotonin's nucleophilic activity of oxidative intermediates, exhibited outstanding biocompatibility against human adipose-derived stem cells and HepG2 cells cultured for 7 days. The blood clotting time of HA-serotonin was compared to that of an existing haemostatic agent (Fibrin glue) as a positive control, and the HA-serotonin hydrogel exhibited a significantly decreased bleeding time of 30 s in comparison with fibrin glue. The blood clotting kinetics of HA-serotonin was dose-dependent as compared to those of fibrin glue, signifying

that in diverse clinical applications, it may be more efficient and easier to control haemostatic performance [99]. Control of blood clotting kinetics can be achieved by changing the material doses, revealing the competitive advantage of HA-serotonin hydrogel over conventional haemostatic agents for realistic applications. The amount of blood loss was checked using filter paper on a mouse liver model, and the HA-serotonin hydrogel and the fibrin glue exhibited minimal blood loss compared to the untreated group. However, the mass of blood lost was significantly reduced by HA-serotonin hydrogel compared to all other treatment groups. These findings imply that HA-serotonin hydrogels could promote greater haemostatic activity than the fibrin-based agents already on the market. The HA-serotonin hydrogel not only promotes rapid blood clotting but also prevents massive blood loss. Histological analysis of the liver after treatment revealed no unusual immune response for the HA-serotonin hydrogel-treated groups, confirming their biocompatibility and safety for further clinical evaluations. These adhesive hydrogels exhibited anti-adhesion behaviour for tissues surrounding the injured tissue and the formation of a thin layer on the bleeding area. However, out of 9 treated animals, there was only one single case where 11% of abnormal tissue adhesion was observed, while all others exhibited 44% for the untreated groups and 66% for the fibrin glue-treated groups. Furthermore, the haemostatic potential of the scaffold was studied using a haemophilic (B6;129S-F8^{tm1Kaz}/J) mouse strain on the ruptured liver. A fatal haemorrhage was observed in the untreated groups, in contrast to the HA-serotonin hydrogel-treated groups, which had decreased bleeding mass. After 1 min of treatment, only a few blood spots were observed on the filter paper for HA-serotonin-treated mice, while excessive bleeding was still observed in the untreated mice. Regardless of almost impossible blood clotting in haemophilic mice, histological analysis showed almost complete haemostasis when treated with HA-serotonin, with a clot-like structure noted in the bleeding area of the liver retrieved from the mice. The factor VIII-mediated coagulation pathway is thought to be the target site for complete haemostasis by HA-serotonin hydrogel, as it is deficient in haemophilia. The scaffolds reported in this research have a promising haemostatic ability. However, more clinical studies need to be done to confirm their activity.

Wang *et al.* reported HA-catechol hydrogels by drafting dopamine hydrochloride into HA (CHI-HA) to manage haemostatic wounds. This material was crosslinked using a varying concentration of H₂O₂ and horseradish peroxidase (HRP) to form CHI-HA-R₁ and CHI-HA-R₂. After 24 h, CHI-HA exhibited the highest swelling ratios compared to CHI-HA-R₁ and CHI-HA-R₂. However, it was noticeable that an increase in HRP and H₂O₂ ratios significantly

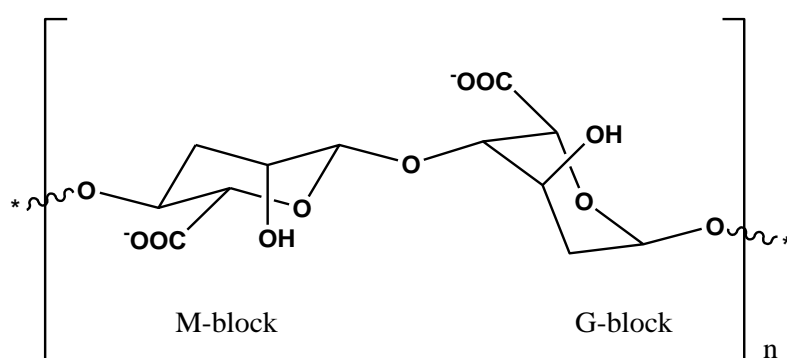
decreased the swelling capability of the hydrogels, as CHI-HA exhibited 3115.86%, CHI-HAR₁ (1112.76%), and CHI-HA-R₂ (889.70%). The cytocompatibility of the hydrogels was tested against L929 cells, and none of the hydrogels exhibited a negative cell growth rate effect, as CHI-HA exhibited 82%, CHI-HA-R₁ (93%), and CHI-HA-R₂ (98%). The haemostatic capability of these hydrogels was evaluated using a rat liver defect model, and the untreated group after 20 min of treatment exhibited 70 mg of blood loss, while CHI-HA showed 18 mg of blood loss in 12 min, and CHI-HA-R₂ revealed rapid control of bleeding and good haemostatic properties. Further studies were performed in a rat leg artery haemorrhage model, and the results were similar to those of the liver model, with CHI-HA-R₂ revealing almost no notable bleeding. This outstanding performance was linked to its elastic and adhesion properties [100]. The wound closure of these hydrogels was investigated in comparison with that of the surgically sutured wound for 9 days. On day 6, CHI-HA-R₂ exhibited better wound closure than the suture and CHI-HA. However, on day 9, there was no significant difference between CHI-HAR₂ and suture-treated wounds with 97% wound closure.

Wang and co-workers formulated wound dressings composed of starch and HA cross-linked with sodium trimetaphosphate (STMP) with varying concentrations of HA and STMP. The swelling ratios of these scaffolds increased with an increase in HA content; however, an increase in STMP had a different trend, where it increased from a concentration of 5–10% and decreased from 10–20%. BCI results showed that an increase in HA significantly decreased BCI sharply to (0.025), and a similar trend for STMP was observed. A correlation between the swelling behaviour and the blood coagulation behaviour of the dressings was also observed. The selected composite dressing containing 15% HA and 5% STMP exhibited improved haemostatic ability than the marked dressings (Yunnan Baiyao®, Arista™, and Quickclean® particles [101]. *In vitro* cytotoxicity evaluation using MTT assay against L929 cells revealed that for a concentration of 12.25–100%, the prepared composite exhibited 111.2–124.0% cell viability, revealing their safety for the cell and capability to promote proliferation. The haemolysis ratio was recorded at 0.97% ± 0.21%, showing a non-haemolytic effect, and the *in vivo* histocompatibility after 14 days showed no signs of oedema, exothermic burns, redness, or bleeding at all stages. Haemostatic evaluation of the S5/S/HA15 composite compared to that of Quickclean® particles was performed against rabbit ear artery, liver, back, and ear vein injuries. There was no significant difference observed between the haemostatic potential of the composite dressings in terms of blood loss and clotting time. S5/S/HA15 had better haemostatic

potential when applied to the ear vein, with reduced blood loss in a few seconds compared to Quickclean® particles.

2.4.5. Alginate

Alginate (alginic acid) is a readily available and naturally occurring anionic biopolymer extracted from the cell walls of brown seaweed [102-104]. It is used and investigated for many biomedical applications due to its low toxicity, biocompatibility, mild gelation, and relatively low cost [104]. The polysaccharide backbone is composed of (1-4) linked α -L-guluronate (G-blocks) and β -D-mannuronate (M-blocks) and followed by segments of repeatedly linked MG blocks [105]. Alginate-based wound dressings promote a moist environment with reduced bacterial invasion [104]. Alginate dressings also promote good inflammatory properties such as skin regeneration, biodegradability, moderate water transmission rate, good antimicrobial activity, promising mechanical strength, *etc.* Alginate hydrogels prepared from natural or biopolymers are used as wound dressings for different types of wounds, including burn wounds. These alginate-based hydrogels help in the maintenance of an optimally moist environment and an appropriate temperature for the wound [106–108]. A wound dressing material that is used must be selected depending on the condition of the wound [109,110] and must be easily removed from the wound without causing trauma to the healed tissue. Modified alginate-based wound dressings play a fundamental role in absorbing large amounts of wound exudates to prevent infection at the wound site; they are biocompatible, non-toxic, remove wound debris, stop bleeding, create a moist environment, and act against bacterial infections [111–115].



Scheme 5: M and G-block structure of alginate

Feng *et al.* prepared alginate-based TEMPO-mediated oxidized cellulose nanocrystal (TOCN) composites to target the first phase (haemostasis) of wound healing. The size of the produced nanocrystal composites was in the expected and acceptable range, which has been reported in the literature. The prepared SA/TOCN composites were divided into different concentrations

and cross-linked with calcium chloride. Outstanding water absorption properties were observed in SA/TOCN-30 composite sponge (1399.1%), and SA/TOCN-30 composite film (75.2%) in all the testing materials, contrary to alginate sponge (825.9%) and film (43.35%), which presented the lowest water uptake. Haemolysis *in vitro* assay was conducted using 2% rabbit erythrocyte suspension. Haemolysis was evident in the positive control (distilled water) compared to SA solution (4 and 6 mg/mL), TOCN solution (1 and 4 mg/mL), and SA/TOCN composite extracts, which did not cause any haemolysis. These results prove that SA, TOCN, and SA/TOCN composites have outstanding haemocompatibility and are suitable for wound dressing applications. The CCK-8 method was used to perform cytocompatibility for 48 h. The cell viability on the control was set to 100%. The cell viability for the composites was 99% after 48 h, showing that all the composites were non-toxic to Hela cells despite different concentrations (0.1, 0.5, 2.5, and 5 mg/mL). SEM revealed that the erythrocytes kept their characteristic morphology of a bio-concave disk with a large amount gathered on the SA/TOCN composites, and none exhibited deformation or aggregation. *In vivo* studies were performed on a rabbit liver injury model and an ear artery injury model [116]. The bleeding amount in the liver injury model was recorded as 0.539 ± 0.069 g, 0.826 ± 0.075 g, and 1.735 ± 0.055 g for SA/TOCN-30 composite sponge, SA/TOCN-30 composite film, and gauze as compared to all other materials, respectively. Similar results were observed for the ear artery injury model; however, they were comparably lower in this model. Moreover, the SA/TOCN-30 composite sponge's haemostatic time (76 ± 8.13 s) was significantly shorter than in all other groups. The SA/TOCN composite sponge groups presented a more rapid haemostatic time when compared to all other materials and SA/TOCN composite films, with the SA/TOCN-30 composite sponge (70 ± 5.93 s) haemostatic speed which was the shortest.

Jin *et al.* prepared sodium alginate, carboxymethyl chitosan, and collagen haemostatic microspheres (CMCSM) with an average particle size of 13.33 and 39.33 surface area and volume, respectively, and tested their activity *in vivo*. These microspheres were haemocompatible with haemolysis ratios of $0.051 \pm 0.008\%$. The haemostatic performance of the microspheres was compared to that of a marketed compound microporous polysaccharide haemostatic powder (CMPHP) and wet gauze on an amputated rat tail. The wet gauze groups after haemostasis showed a block of blood clots, while in the CMCSM and CMPHP groups, there was no apparent clot observed, with a small volume of powder stuck. The coagulation time was recorded at 249.2 ± 44.7 s, 370.0 ± 43.1 s, and 428.0 ± 83.3 s for the CMCSM, CMPHP and gauze groups, respectively. Blood loss was 665.2 ± 51.3 mg for the wet gauze

group, 54.5 ± 24.6 mg for CMPHP, and 37.6 ± 8.1 mg for CMCSM. The hybridization of SA, CMCS, and collagen produced a synergistic effect in promoting wound healing. The CMCS led to the aggregation of RBCs, thereby forming a barrier of a blood clot, while SA activated clotting factors with the eggshell skeleton consisting of Cs^{2+} , and collagen strengthened platelet aggregation by activating intrinsic pathways for rapid haemostasis [117]. The wound-healing assay showed rapid healing for CMCSM-treated groups in the first 2 days compared to the control; however, they exhibited similar wound healing with no significant difference at day 12 with >80% wound closure.

Liu *et al.* prepared alginate paste and hydrogels containing lipidated tissue factor (TF) to form a controllable haemostatic material. The formulated scaffolds had varying concentrations of alginate (1%, 2%, and 3% w/v). The drug release kinetics revealed a sequential decrease as the concentration of alginate increased in the scaffolds. TF-hydrogels exhibited drug release kinetics that was not dependent on alginate concentration. After 2h, all the hydrogels released 35% TF and 40% in 4h. These hydrogels followed a Fickian diffusion mechanism, while the release from a 1% scaffold followed a case-II diffusion mechanism [118]. The TF-paste scaffolds exhibited high drug release compared to the TF-hydrogel scaffolds. TF-paste scaffolds exhibited the shortest blood clotting time (1.5 min, 3.2 min, and 5.1 min) compared to the TF-hydrogels (4.3 min, 8.2 min, and 8.9 min), which increased with an increase of alginate concentration, respectively. The untreated group showed a coagulation time of 14.2 min. *In vitro* cytotoxicity was performed using the Calcein AM/PI dual-staining survival assay on NIH 3T3 cells. The TF-hydrogels and TF-paste scaffolds exhibited similar results, with the cells stained green showing no signs of toxicity on NIH 2T3 cells and almost no PI-positive cells noted.

Jin and co-workers formulated alginate microspheres coated with different amounts of berberine (B1, B5, and B10%) for the management of bleeding wounds and bacterial-infected wounds [119]. The microspheres were termed SCC as they contained SA, carboxymethylchitosan, and collagen. The particle size and surface area average size of the microspheres increased with an increase in berberine, respectively. The swelling ratios of these microspheres showed an increasing behaviour in relation to the increase in berberine amount, and SCC-B10 exhibited the highest of 4300% in the first 5 min and a maximum of 4800% in 10 min. Biodegradability studies revealed that all the tested microspheres exhibited more than 90% degradation after 90 min. Haemolysis evaluation using 2% rabbit RBC suspension proved that all the microspheres were haemocompatible with less than 2% haemolytic activity, and the

encapsulation of berberine significantly aided in the haemocompatibility of the microspheres. *In vivo* haemostatic activity on rat tails revealed that mixing plain S/C/C and berberine did not induce blood coagulation, with a clot forming after 12 min which could be attributed to the self-clotting mechanism. However, when these were used in the form of microspheres, SCC-B10 expectedly showed the shortest clotting time of 180.33 ± 6.11 s, followed by SCC-B1, SCCB5, and plain SCC microspheres with 209.7 ± 42.4 s, 217.0 ± 26.1 s, and 249.2 ± 44.7 s, respectively, greater than that of the commercially available compound microporous polysaccharide haemostatic powder 'CMPHP' (370.0 ± 43.1 s). Blood loss was evaluated for SCC-B10, SCC, and CMPHP and was found to be 26.3 mg, 37 mg, and 54.5 mg, respectively. Antibacterial activity evaluation revealed that the plain SCC microspheres did not exhibit antibacterial activity against *S. aureus*, while SCC-B1 exhibited the highest antibacterial inhibition, which is in line with its rapid drug release. These results suggest that berberine has a high antibacterial activity dependent on its concentration, and its influence on the swelling capacity of the microspheres makes it suitable for haemostasis and controlled drug release.


Sutar *et al.* prepared *Croton oblongifolius* extract-coated alginate/pectin dressings for the management of bleeding. The prepared dressing had the morphology of a highly porous sponge of 90% porosity, and the simulated wound fluid absorption was greater for A/P-CO and A/P (5.2 g) compared to the marketed gauze (4.1 g) [120]. The dressings were biodegradable; however, their slow rate of degradation was linked to their swelling capacity, and coating them with CO did not affect the rate of degradation. Drug release kinetics revealed a controlled release of CO, which was 72% in 72h of incubation. The BCI of the dressing was compared to the untreated group, and CO-coated dressing exhibited a lower BCI percentage of approximately 15% compared to plain A/P dressing 27%, and untreated 39%. The clotting ability of A/P-CO dressing was linked to tannins presently available in CO extract. The A/P-CO dressing exhibited a high thrombin-antithrombin complex (TAT) concentration of 41.36 mg/mL compared to other groups with minimal TAT levels. The *in vitro* cell biocompatibility of the dressings was performed using primary HDF cells, and they were non-toxic to the cells with 82% cell viability. Antibacterial activity of the dressing compared to that of plain CO extract was evaluated on *S. aureus* and *E. coli*, and the bacterial inhibition was observed to be more efficient for plain CO extract with 15 mm and 14 mm zones of inhibition, respectively, while A/P-CO exhibited none and 8 mm, respectively.

Huang and co-workers formulated silk fibroin/alginate microspheres (SF/SA) with varying concentrations of alginate 2 and 4% to promote fast blood clotting. The swelling ratios of the

microspheres were recorded at $3311 \pm 30.5\%$ for SF/SA2, $2868.3 \pm 50.6\%$ SF/SA4, $2810.6 \pm 52.2\%$ SA, and $712 \pm 40.1\%$ SF. Similarly, the *in vitro* water absorption ratios were highest for SF/SA2 ($4775 \pm 478 \%$) than all other groups. *In vitro* cytotoxicity of the microspheres was investigated using an MTT assay on L929 cells, and they were reported to not only be biocompatible but also promote cell growth of the L929 cells [121]. The cell viability was recorded at $139.0 \pm 8.39 \%$ for SF/SA4, $134.9 \pm 5.12\%$ for SF/SA2, $131.8 \pm 3.66\%$ for SA, and $128.4 \pm 7.91 \%$ for SF. *In vitro* simulated blood clotting tests revealed a 122 ± 2.05 s clotting time for SF/SA2, followed by SF/SA4 (173 ± 5.43 s), SA (188 ± 1.41 s), and lastly SF (287 ± 8.57 s). The *in vitro* blood clotting evaluation showed that SF/SA2 exhibited the shortest time of 2.33 ± 0.20 min, followed by SA (3.06 ± 0.23 min), SF/SA4 (3.36 ± 0.37 min), and SF microspheres (4.93 ± 0.76 min), while the control groups exhibited 6.86 ± 0.21 . The whole blood clotting kinetics also confirmed that SF/SA2 have better haemostatic potential than other groups, as it exhibited the lowest absorbance values in all treated times. Biodegradation studies revealed the greatest degradation for SA microspheres compared to other groups, and SF/SA4 had better degradation than SF/SA2, showing that SA is more degradable than SF. In relation to the *in vitro* blood clotting assay, the *in vivo* coagulation evaluation on the rat tail exhibited similar results, with SF/SA2 showing the shortest blood clotting time of 65.6 ± 6.7 s and SA the longest of 203 ± 11.1 s. The amount of blood loss was recorded at 7.1 ± 2.5 mg for SF/SA2, 13.4 ± 2.3 mg (SA), 16.8 ± 2.6 mg (SF), and 17.4 ± 3.9 mg (SF/SA4) microspheres. These findings were similar to those of the rat liver laceration model, however, the amount of blood loss and clotting time were a bit slower than in the rat model, as the liver produces a greater amount of blood compared to the tail.

Table 2: Summary of polymer-based dressings with haemostatic activity

<i>Polymer</i>	<i>Hybridized polymer</i>	<i>Type of wound dressing</i>	<i>Material loaded</i>	<i>Advantages</i>	<i>Reference</i>
Chitosan	alginate	Sponge	Kungfuxin	Fast blood clotting, active against <i>E. coli</i> ,	[5]
				Rapid wound healing ability.	

alginate	Hydrogel	Hesperidin	Fast wound closure, hinder microbial infection, exhibits anti-inflammatory, haemocompatible	[28]
starch	Sponge		Haemocompatible, high cell adhesion, promotes haemostasis	[47]
	Injectable hydrogels		Non-toxic, haemocompatible, reduces the bleeding time	[48]
Alginate, Bletilla striate polysaccharide	Sponge		promote cell growth, haemocompatible, promote fast blood clotting and less blood loss	[49]
 <p>University of Fort Hare Together in Excellence</p>				
Hyaluronic acid	Sponge	VEGF fibrin nanoparticle	Cytocompatible, high blood clotting ability, promotes angiogenesis	[50]
Alginate	Sponge	Fucoidan	Blood clotting, active against <i>E. coli</i> at lower concentrations, non-toxic.	[51]

Diatom-biosilica	Beads	Dopamine	Cytocompatible, stimulates cell growth, fast blood clotting time	[52]
Gelatin	Cryogel	AgNPs	Haemocompatible, non-toxic, hinders bacterial infection, removes biofilm biomass, haemostatic	[68]
	microspheres	vancomycin	Rapid blood clotting, cell adhesive, <i>S. aureus</i> inhibition, accelerated healing of an infected wound	[69]
Chitosan	Nanofibers	Epinephrine	Haemocompatible, cytotocompatible, cell adhesive, rapid blood clotting,	[70]
Na oxidized regenerated cellulose	Microparticles		Blood clotting, promoted cell viability and cell growth	[71]
Pectin methacrylate	Injectable & <i>in situ</i> hydrogel		Biodegradable, biocompatible, haemostatic, easily removed	[72]
Fibrin glue	Sponge		Immediate control of bleeding	[73]



University of Fort Hare
Together in Excellence

	κ -Carrageenan	Microparticles		Non-haemolytic, high cell adhesion, fast blood clotting, non-toxic	[75]
Carboxymethyl cellulose	Chitosan	Sponge	Na dodecyl sulphate	Haemocompatible, haemostatic, rapid blood clotting, cell adhesive, antibacterial inhibition, increased cell growth	[79]
		Nonwoven sheets		Biodegradable, accelerate blood clotting, haemostatic	[81]
	Gelatin	Nanofibers	AgNPs	Non-haemolytic, platelet adhesive, proliferative, antibacterial, promoted wound healing	[85]
	κ -Carrageenan, polyethylene oxide	granules		Fast blood clotting, high platelet adhesion, tissue factor dehydrator, nontoxic, accelerate wound healing	[86]
		Aerogel & hydrogel	Tranexamic acid	High blood absorption rates, adhesive, fast drug release kinetics,	[87]





University of Fort Hare
Together in Excellence

				cytocompatible, non-haemolytic, haemostatic	
Hyaluronic acid	Alginate	Powder		Haemostatic, haemocompatible	[97]
	poly((2dimethyl amino)-ethyl methacrylate)	Sponge	Dextran	Non-haemolytic, non-toxic, fast blood clotting, aggregate RBC	[98]
		Hydrogel	Serotonin	Biocompatible, decreased bleeding time, tissue adhesive,	[99]
		Hydrogel	Dopamine	Cytocompatible, reduce blood loss, fast blood clotting, and accelerated wound closure	[100]
	Starch			Haemocompatible, non-toxic, promote cell growth, haemostatic	[101]
Alginate	Oxidized cellulose	Sponge & film		Non-toxic, fast blood clotting, minimizes blood loss	[116]
	Carboxymethyl chitosan, collagen	Microspheres		Non-haemolytic, biocompatible, aggregate RBC, haemostatic	[117]



University of Fort Hare
Together in Excellence

	Paste & hydrogel	Lipidsted tissue factor	Reduce bleeding time, biocompatible	[118]
	Microspheres	Berberine	Non-haemolytic, blood clotting, antibacterial	[119]
Pectin	Sponge	<i>Croton oblongifolius</i>	Biodegradable, controlled drug release, haemocompatible, biocompatible, antibacterial, blood clotting	[120]
Silk fibroin	Microspheres		Non-toxic, promotes proliferation, nonhaemolytic, fast blood clotting <i>in vivo</i> and minimal blood loss	[121]


 University of Fort Hare
Together in Excellence

2.5. Application of Organic Drugs and Nanoparticles in Wound Healing

Nanomaterials should have a dimension of at least 1–100 nm [122]. Their size is even smaller than the body cells, allowing them to have high uptake to interact with biomaterials within the cells or on their surface [123]. Nanomaterials come in many forms, such as polymeric nanoparticles, solid lipid nanoparticles, nano-emulsions, lipids, inorganic (metal oxides or metals) nanoparticles, *etc.* The use of metal-based nanoparticles has evolved in the research industry since their discovery. Their unique and outstanding features, such as optical, electronic, catalytic, magnetic, bio-separation of DNA and proteins, and antibacterial properties, have enabled their wide range of use in various fields. They can be prepared from the synthesis of inorganic compounds or from natural plants. Farooq *et al.* reported that titanium oxide (TiO₂) and zinc oxide nanoparticles (ZnO-NPs) possess antibacterial activity by generating reactive oxygen species (ROS), leading to radical stress in the bacterial organism.

ZnO NPs oxidize bacterial proteins and destroy DNA synthesis, thus inhibiting bacterial growth [78]. They further reported that the antibacterial activity of ZnO is dependent on the electronic state, surface energy, roughness, surface charge, shape, surface area, and particle size [78].

Gel formulations containing ZnO were reported by Buyana *et al.* and the gels exhibited good antimicrobial activity [124]. Manuja *et al.* reported nanocomposites of sodium alginate, gum acacia, and ZnO. These nanocomposites increased the rate of wound healing in full-thickness excisional rabbit wounds and also promoted an anti-inflammatory response and cell adhesion and proliferation [125]. Norouzi *et al.* formulated PVA-ZnO nanofibers that possess antibacterial properties against *S. aureus* and *E. coli*; higher antibacterial inhibition was observed when tested *in vivo*, including fast wound healing and better cell attachment [126]. Soubhagya *et al.* formulated CS/pectin-ZnO NPs-based films for the management of wounds and reported their antimicrobial activity against both gram-positive and gram-negative bacterial strains. Moreover, they promoted an increased rate of cell growth and migration with a non-toxic effect against primary human dermal fibroblast cells [127]. Zhang *et al.* prepared hydrogels composed of alginate/chitosan oligosaccharides-ZnO and reported their antimicrobial activity against *C. albicans*, *E. coli*, *B. subtilis*, and *S. aureus*. They further reported their biocompatibility against 293T cells, RBCs, and 3T3 cells [128]. Yang *et al.* reported ZnONPs' negative effect on prothrombin and thrombin regeneration by absorbing these coagulation factors and thereby delaying blood clotting [129]. However, there's limited research on the interaction of ZnO with the haemostatic pathways.

Iron oxide nanoparticles (Fe_nO_n) can be found in different forms in nature as hematite (α - Fe_2O_3), maghemite (γ - Fe_2O_3), and magnetite (Fe_3O_4) [130]. Shabanova *et al.* reported thrombin@ Fe_3O_4 NPs for the management of internal bleeding; these NPs displayed nontoxicity against HeLa and HELF cells, and they rapidly promoted local haemostasis and stopped bleeding [131]. Li *et al.* developed iron oxide exosomes derived from mesenchymal stem cells. The exosomes increase collagen expression and enhance proliferation and the migration of endothelial cells, resulting in reduced scar formation [132]. Yadav *et al.* fractionated iron oxide NPs with *Trianthema portulacastrum L.* to inhibit glycogen synthase kinase-3- β associated with delayed wound healing. The prepared ointment was reported to accelerate wound contraction and epithelialization processes and promote high hydroxyproline content and tensile strength [133]. Sathiyaseelan *et al.* prepared CS/PVA nanocomposite sponges fabricated with iron oxide NPs for the management of anaemia-associated diabetic

wounds [134]. These composite sponges exhibited moderate antidiabetic, antioxidant, and considerable antibacterial activity, with lower concentrations of NPs exhibiting increased cell growth in HEK293 cells [134]. The antibacterial activity of magnesium oxide (MgO) NPs is influenced by their particle size. Yaroslavovytch *et al.* reported MgO NPs with particle size less than 10 nm to intensively promote cell death of *B. subtilis* and *S. aureus* bacterial strains, while those of 50 nm had partial activity against *B. subtilis* and *E. coli* [135].

Liu *et al.* formulated PCL/Gel electrospun nanofibers fabricated with MgO NPs for the management of infected wounds. The antibacterial activity of the nanofibers increased with an increase in the concentration of MgO NPs with 90%, 94%, and 98% inhibition against *S. aureus*, *S. epidermidis*, and *E. coli*, respectively [136]. These nanospun fibres promoted the healing of full-thickness wounds in a rat model and were non-toxic against NIH 3T3 fibroblasts and HUVECs. In another report, Liu *et al.* focused on MgO NPs-fabricated PCL/Gel electrospun membranes to improve the healing of diabetic wounds and promote angiogenesis. These scaffolds showed cytocompatibility with VEGF cells and a fast degradation profile in rat models [137]. Upon subcutaneous implantation, these membranes exhibited the formation of a robust blood vessel within the first week, including newly formed capillary networks. They further promoted angiogenesis, boosted the formation of granulation tissue, and accelerated the rate of diabetic wound healing by suppressing the inflammatory response [137]. Sukumaran *et al.* prepared composite films from CS/Gel polymers fabricated with MgO, and these scaffolds displayed high antibacterial activity against *E. coli* and *S. aureus*, including an antifungal effect against *C. albicans*, while lower concentrations of MgO NPs showed increased cell proliferation, migration, and biocompatibility on C3H10 T1/2 cells [138]. MgO NPs on reported reviews showed most of their antibacterial activity against *E. coli* and *S. aureus* compared to other bacterial strains, including an increased activity observed at lower concentrations and smaller particle sizes.

The application of silver nanoparticles (AgNPs) in the medical field is hampered by their toxicity against animal cells. This limitation is overcome by loading AgNPs into polymer-based dressings [139]. Polymer-based dressings containing AgNPs have been widely used for infected wounds to inhibit microorganisms on the wound site. Fabrication of AgNPs into fabric wound dressings and other textiles has significantly promoted their antibacterial activity against a wide range of gram-negative and gram-positive bacterial strains and the inhibition of biofilm [140]. The AgNPs bind to the bacterial cell wall and disturb enzymes essential for their metabolism. Masood *et al.* reported AgNP loaded in CS/PEG hydrogels to inhibit bacterial cell

growth of *P. aeruginosa*, *B. subtilis*, *E. coli*, and *S. aureus* compared to plain AgNPs and gels of this form, and they further promoted wound healing, showing significant keratinocyte migration and scar formation with no scabs [141]. On day 4, a 47% wound contraction occurred in the hydrogel loaded with the nanoparticles compared to the plane hydrogels, which had a 12% contraction. Huang *et al.* reported xerogels containing AgNPs and ZnO NPs. These hybrid scaffolds synergistically killed microorganisms (*S. aureus* and *E. coli*) by 99.85 and 99.9%, respectively [142]. These xerogels exhibited good biocompatibility, and complete wound healing was observed within 10 days of post-injury in the animal model. Their outstanding results make them suitable for the treatment of infected or chronic wounds.

Yang *et al.* prepared ϵ -poly(L-lysine)-modified PVACS/AgNPs hydrogels and reported their non-cytotoxicity on mouse fibroblasts and antibacterial activity against *E. coli* and *S. aureus*. These hydrogels were suitable for accelerated wound healing and increased the formation of collagen fibers, the integrity of the epidermal tissue, and thickness [143]. Choudhary *et al.* formulated AgNPs and calcium alginate nanoparticle-impregnated CS hydrogels for the management of full-thickness diabetic wounds [144]. These hydrogels showed good antibacterial activity against *B. subtilis*, *S. aureus*, *E. coli*, and *P. aeruginosa*, and almost complete wound closure of 83.5% on day 15 compared to the marketed Silverex Heal (60.3%) on diabetic rats. Graphene oxide (GO), a derivative of graphene, is a 2D nanomaterial composed of a large number of carbon and oxygen atoms in its structure. Many reports have shown its activity against a large variety of bacterial strains, haemocompatibility and haemostatic, hydrophilicity, and biocompatibility. Yang *et al.* reported GO nanosheet's antibacterial activity to be arbitrated by reactive oxygen species and destructive extraction of bacterial phospholipids, leading to damaged cell membrane integrity and bacterial death [89]. Zhang *et al.* formulated sponges composed of *N*-alkylated chitosan (AC) and GO for the management of haemostasis in emergencies [145]. These sponges were reported to be biocompatible and promote increased blood clotting efficiency with an increase in GO ratios when tested *in vitro*. *In vivo* performance on rabbit femoral artery revealed that the sponges containing 20% GO ratios exhibited shorter haemostatic times compared to those of Celox®, a marketed haemostatic material. Additionally, they were proven to promote RBC and platelet adhesion and haemostasis by activating platelets and intracellular Ca⁺. Li *et al.* reported polydopamine-reinforced GO sponges that stopped bleeding within 105 s with a BCI of approximately 22% and blood loss of less than 1g [146].

Liang *et al.* reported GO-kaolin composite sponges that promoted haemostasis in 73 s on rabbit arteries, also showing RBC adhesion on their interface [147]. Guajardo *et al.* prepared positively and negatively charged aerogels composed of GO and Gel with improved haemostatic activity [148]. Positively charged aerogels showed greater structural properties as they promoted H bonding compared to negatively charged aerogels. However, negatively charged aerogels exhibited a superior blood clotting potential of 95.6% and promoted coagulation without using common mechanisms. Moreover, negatively charged aerogels induced the growth of fibroblasts and were biocompatible. Borges-Vilchez *et al.* reported Gel-GO aerogels reinforced with grape skin extract high in proanthocyanidins and evaluated their haemostatic potential [149]. The addition of 5 and 10% proanthocyanidins significantly increased blood clotting by 36.6 and 24.5%, respectively, compared to Gel-GO aerogels. Moreover, these aerogels were non-toxic and promoted platelet adhesion, forming a stable fibrin network. Reduced graphene oxide (rGO) is a precursor of GO with fewer oxygen-containing groups. Singh *et al.* reported that reduced graphene oxide (rGO) is not endowed with any prothrombotic or platelet-stimulating characteristics because of the loss of oxygen-containing groups [146]. Zhao *et al.* formulated Gel-rGO/tannic acid cryogel, and the haemostatic ability was influenced by the concentration of tannic acid more than rGO [150]. However, rGO-Gel cryogels exhibited haemolysis ratios below 5% together with cryogels containing tannic acid, showing it is safe to be applied to bleeding wounds despite its low blood-clotting kinetics.

Haemostatic activity using organic compounds such as antifibrinolytic agents promotes haemostasis through a different mechanism compared to most inorganic or metal-based nanomaterials. There are several organic haemostatic materials such as antifibrinolytic agents (tranexamic acid, aprotinin [151], and aminocaproic acid) [152]. TA is a synthetic compound derived from the amino acid lysine and is responsible for the inhibition of fibrinolysis by hindering plasminogen activation and thus reducing plasmin formation, preventing fibrin network destruction that leads to stable blood clot formation [87,153–155]. It is commonly used systemically (orally or intravenously) [156] and can reduce the need for blood transfusions [157]. TA, though it has been mostly used systemically, has also been used in topical formulations to control bleeding [153]. Huang *et al.* reported that the use of TA in neurosurgical settings can cause neurotoxicity and hyperexcitability [158]. Xi *et al.* reported enhanced haemostatic efficiency of starch by encapsulation of TA in its porous form [159]. Sasmal and Datta formulated PVA/CS (1:1 and 3:2) nanofibers fabricated with 40 mg/mL of TA to control

haemorrhaging wounds [160]. All the prepared nanofibers exhibited haemolysis ratios below 5%; however, it was evident that loading of TA had the potential to increase the haemolysis of the scaffolds. Plain 3:2 PVA/CS exhibited high water absorption ratios compared to the plain 1:1 PVA/CS formulation, 3:2 PVA/CS-TA, and 1:1 PVA/CS-TA. However, 1:1 PVA/CS-TA exhibited the shortest blood clotting time (167 ± 6 s) compared to all other groups, followed by 1:1 PVA/CS, 3:2 PVA/CS-TA, and 3:2 PVA/CS. These results suggest that an appropriate ratio of CS to TA has a synergistic effect in promoting rapid coagulation time. These nanofibers also showed anti-biofilm characteristics.

Zhong and co-workers formulated CMCS/SA composite films impregnated with 0.01 g/mL TA, and the drug release was recorded in the range of 60–80%, with the 1:2 CMCS: SA formulation showing the highest release profiles, followed by the 1:1 formulation [161]. The drug release kinetics of the 1:2 CMCS: SA formulation exhibited the shortest blood clotting time (115 s), followed by 1:1. This shows that TA played a significant role in controlling bleeding. It was also notable that pure SA films exhibited a shorter clotting time than pure CMCS films. Bhattacharya *et al.* prepared TA-loaded gellan gum-based polymeric beads, and the drug release kinetics revealed a prolonged cumulative release of TA at pH 7.4 up to 90% compared to pH 1.2, which was less than 20% [162]. Saporito *et al.* reported TA-impregnated CS acetate dressings with glycosaminoglycan (HA or chondroitin sulphate), and the release profiles for all the prepared dressings were 50% in 30 min and reached the plateau value in 3 h [163]. The reported formulations were all biocompatible and promoted proliferation and blood coagulation. However, the CS-containing formulation promoted fast blood clotting, resulting in a synergistic effect of CS and TA. Buyana *et al.* reported SA/pluronic F127 topical gels impregnated with ZnO and aminocaproic acid. These gels exhibited absorbance values below 0.25 in whole blood clot analysis, revealing their potential application in bleeding wounds [124]. Koumentakou *et al.* reported CS dressings containing levofloxacin (LEV) and inorganic additives [iron (III) sulphate "FS", aluminium sulphate hydrate "AS", and aluminium chloride "ACl"] [164]. The drug release from the prepared dressings reached 80% within 30 min and 100% in 6 h, which was sustained for 12 h, except for CS-LEV, which had less than 70% drug release within 5 h. However, CS-LEV dressings exhibited the fastest blood clotting time below 50 s, followed by CS/ACl-LEV, with no significant difference between the two. This suggests that the antibiotic LEV has a haemostatic ability. Regardless of the shorter haemostatic time displayed by CSLEV, haemolysis ratios were slightly above 5% which was significantly decreased to 2% by addition of ACl.

Zhang *et al.* prepared hydroxybutyl CS-containing dopamine (HBCS-DA) hydrogels with a non-toxic effect against L929 cells with haemolysis ratios below 3% [165]. The haemolysis ratios decreased with an increase in DA content, and the inhibition zone increased with an increase in DA concentration against *E. coli* and *S. aureus*. However, it was more effective against *S. aureus* compared to *E. coli*. The haemolysis test on the scaffolds containing a higher content of DA displayed the shortest clotting time (95.6 s) compared to all other tested hydrogels. Lv *et al.* reported cotton-like mat dressings of poly (L-lactic acid) (PLLA)/SA grafted with dopamine and fabricated with Fe³⁺ to exhibit excellent antibacterial activity against both *E. coli* and *S. aureus* [166]. These scaffolds possessed great cytocompatibility, haemocompatibility, and histocompatibility. The *in vitro* blood clotting evaluation showed the shortest time of 47 s when treated with the scaffolds. The application of these scaffolds *in vivo* in the rat liver model displayed a decreased clotting time of 23 s and a bleeding volume of 0.097g. Wang *et al.* prepared DA-hydrochloride-grafted CS/HA hydrogels with H₂O₂ and horseradish as triggers [100]. These hydrogels significantly shortened haemostasis time and showed less than 20 mg of blood loss. Wang *et al.* reported CS/DA/diatom-biosilica composite beads with 83 s of coagulation time and less than 5% haemolytic ratios [52]. Additionally, these composite beads were biocompatible displaying more than 80% cell viability.

2.6. Essential Oils in the Management of Wounds

Essential oils (EOs) are mostly extracted from natural products like plants and are applied in a large number of different industries, including cosmetics, pharmaceuticals, and medication. They contain semi-volatile and volatile organic compounds responsible for the smell, aroma, and flavour of plants [167]. Due to their biocompatibility, they can be applied directly to the skin; however, some can irritate, mostly on broken skin, and are not stable at room temperature. In the preparation of wound dressings using EOs, it is evident that loading them into polymer-based dressings and loading bioactive materials significantly reduced their toxicity, volatility, increased stability, wound healing, and biological potential. The loading of essential oils into polymer-based gels leads to the formation of emulsified dressing. Emulsions can be categorized into different forms, for example, nano-emulsion, micro-emulsion, *etc.*, depending on their nanoparticle size, and these formulations serve different advantages in drug delivery systems. Nanoemulsions have great potential for the protection, encapsulation, and delivery of nanoparticles and organic drugs to the targeted site. Emulsions can be primarily prepared at room temperature using water, oil, and emulsifiers and are noted as oil-in-water (O/W) emulsions or water-in-oil emulsions (W/O). Furthermore, they can also be formulated as double

solvent emulsions as water in oil in water (W/O/W) or oil in water in oil (O/W/O) emulsions, which are often unstable and require lipophilic and hydrophilic emulsifiers in the presence of high-pressure and high-energy approaches [168]. Other types of dressings containing EOs have been developed and applied in wound healing, including films, hydrogels, patches, sponges, nanofibers, *etc.*

Djemaa *et al.* prepared *lavandula aspic L.* (lavender EO)-based ointment and reported its wound healing and antioxidant potential [169]. The ointment possessed low antioxidant activity compared to ascorbic acid. However, the wound healing contraction in the rat model was recorded at 98% for 14 days post-injury, proving that the lavender EO-based ointment can promote tissue repair within a short time. Mahmood *et al.* prepared gellan gum-based hydrogel films loaded with lavender or tea tree EO and ofloxacin, followed by *in vitro* and *in vivo* wound healing activity [170]. The antibacterial activity showed that the zone of inhibition against *E. coli* and *S. aureus* was independent of the concentration of ofloxacin, as there was no significant difference observed in films containing different ofloxacin ratios. The films containing EO 25% (*w/w*) displayed the highest zone of inhibition of 21 mm for the films containing lavender and 31 mm for the films containing tea tree EO. Using films loaded with 25% (*w/w*) of EO and 9 mg of ofloxacin, antibacterial activity was significantly improved, showing the synergistic effect of the drug and the essential oils in the bacterial strains. A great synergistic effect was observed when lavender EO was used in combination with ofloxacin. *In vivo* wound healing showed 98% wound contraction in 10 days when using both films containing the drug and lavender or tea tree EO films, compared to the control and films containing only EO. A completely healed epidermis was observed using histological images. These findings suggest that wound dressings containing antibiotics and EO are good candidates for accelerated wound healing.

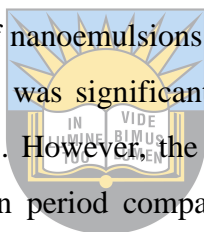
Liakos and co-workers formulated SA film loaded with a variety of EO (lavender, eucalyptus, elicriso italic, lemongrass, cinnamon, peppermint, tea tree, chamomile blue, and lemon) and reported their wound healing and antimicrobial potential against *C. albicans* fungi and *E. coli* bacteria [171]. The antimicrobial activity of the films increased with an increase in the concentration of EO. Films containing cinnamon, lemongrass, peppermint, and tea tree EO exhibited the highest inhibition zone, followed by lavender EO. Eucalyptus, lemon, and elicriso EO only showed activity against *C. albicans*, while chamomile blue had no antimicrobial activity. Araujo and co-workers topically applied rosemary EO to cutaneous mouse wounds, and enhanced wound healing occurred within 14 days and developed hair follicles by day 21.

Rosemary EO-treated groups also showed regeneration of granulation tissue, reepithelialization, reduced inflammation, angiogenesis, and collagen deposition [172]. Wound healing effects of topically applied rosemary EO were also reported by Umasanar *et al.*, and it accelerated wound contraction in diabetic and non-diabetic wounds compared to antibiotic (streptozotocin)-treated groups [173]. Khezri *et al.* loaded rosemary EO on polymer-based nanostructured lipid carriers (NLC), and they promoted complete wound healing within 12 days for rosemary-NLC and rosemary topical gels [174]. The prepared NLCs induced collagen production, re-epithelialization, fibroblast infiltration, increased vascularization, and displayed antibacterial activity against *S. epidermidis*, *E. coli*, *L. monocytogenes*, *P. aeruginosa*, and *S. aureus* bacterial strains.

Godoi *et al.* reported nanoemulsions containing eucalyptus EO to possess high cell viability and be non-haemolytic at lower concentrations [175]. These findings suggest that eucalyptus oil-based polymer dressings are suitable for application in wound management. Labib *et al.* reported CS-films loaded with tea tree oil and rosemary oil to synergistically promote fast wound healing compared to the sole encapsulation of these oil formulations [176]. Additionally, the histopathological analysis also presented complete re-epithelialization and suitable formulations of these EOs that promoted wound healing at different stages. Kazemi *et al.* prepared nanoemulsions composed of lavender EO, licorice (rhizome and root of *Glycyrrhiza glabra*) extract, tween (20 and 80), glycerine, and PEG and loaded them in Eucerine cream (Mahdarou, Iran) for healing of deep-skin wounds [177]. The prepared nanoemulsion accelerated wound contraction, with approximately 90% wound closure on day 10 and 98% on the 14th day. These nanoemulsions also up-regulated both collagen I and III expressions, including TGF- β -1. Histopathological analysis showed complete re-epithelialization in groups treated with the nanoemulsion, showing that the nanoemulsions are good candidates for the rapid healing of wounds. Bhalke *et al.* developed topical gels containing curcuminoids, tulsi/holy basil oil, and eucalyptus oil and checked their anti-inflammatory effects [178]. The reported formulation exhibited no apparent skin irritation, *i.e.*, oedema or erythema, in the albino Wistar rats. Formulations that induced a higher anti-inflammatory effect were those containing a higher content of curcuminoids, and their anti-inflammatory activity was significantly close to that of diclofenac sodium.

Sofi *et al.* reported that lavender oil and AgNPs loaded into polyurethane (PU) nanofibers had high antibacterial activity against *E. coli* and *S. aureus* [179]. Selective formulations of these nanofibers exhibited cell growth of up to 260% on day 6. These results show that these scaffolds

can promote the healing of infected wounds and thus promote proliferation and granulation. However, more studies based on the application of these scaffolds *in vivo* for wound healing are needed. Manikandan *et al.* reported murivenna oil-impregnated polyurethane nanofibers with low haemolytic activity and improved surface properties, which led to delayed blood clotting in both prothrombin and activated partial thromboplastin time [180]. Manzouerh *et al.* reported dill (*Anethum graveolens*) EO-loaded ointment decreased inflammation, triggered the proliferation stage and regulated collagen in MRSA-infected wounds when topically administered [181]. García-Salinas *et al.* reported polycaprolactone (PCL) electrospun patches loaded with EOs (thymol and tyrosol) and reported these dressings had high cell viability when containing lower concentrations of EOs [182]. The pro-inflammatory gene in thymol-treated groups was more down-regulated compared to other treatment groups. Additionally, it represented low cell attachment affinity, which may delay wound integration and adherence. Pivveta *et al.* reported thymol-loaded nanostructured lipid carriers that presented anti-inflammatory activity and improved the wound healing of infected wounds [183]. Alam *et al.* studied the wound-healing potential of nanoemulsions containing clove oil [184]. The wound healing time for these nanoemulsions was significantly close to that of pure clove oil and gentamycin-treated groups in 24 days. However, the nanoemulsions and gentamycin group exhibited the shortest epithelialization period compared to the pure clove oil group. The nanoemulsions were non-toxic, and there were no signs of inflammatory cells observed using histopathological analysis.



2.7. Commercially Available Haemostatic Wound Dressings

Excessive blood loss hugely contributes to the death toll globally, mostly during accidents, on battlefields, delayed treatment of stabs, gunshots, *etc.* The management of bleeding wounds is a vital step in people's lives even before they reach professional medical help. Haemostatic dressings have been developed to stop bleeding and are readily available on the market. Haemostatic dressings should be easy to use even by non-professional candidates because bleeding is usually due to unplanned circumstances (*e.g.*, accidents, fights, *etc.*). The commercially available haemostatic dressings are in the form of hydrogels, woven and non-woven sheets, films, powder, sponges, [185] ointments, glue, gels, nanofibers, lipids, nanocrystals, and microspheres. A variety of these haemostatic materials are prepared from polymers, organic and inorganic compounds, biologically derived from proteins and tissue factors that biologically promote haemostasis and synthetic materials. An ideal haemostatic dressing for pre-hospital bleeding control should possess the following characteristics: easily

prepared and used by non-trained candidates, stop blood loss rapidly even at a site with a blood pool, sustain haemostasis until professional help arrives, easily removed without complication, biodegradable, prolonged shelf-life, cost-effective, and biocompatible [155].

Powder haemostatic materials are mostly applicable in cases of emergency injuries and prehospital medication before the wounded person reaches the healthcare centre. Haemostatic powder materials can be easily used even by untrained personnel; however, they have poor biodegradability properties and have to be removed at the wound site before the medical intervention, a process that may cause re-bleeding [86]. Commercially available powder haemostatic materials include CeloxTM, QuikClot, Surgicel®, TraumaDEX *etc.* [86,186,187]. CeloxTM is biocompatible and stops bleeding rapidly, however, it has to be removed after use from the body, and *in vivo*, it may cause long-term inflammatory response [188,189]. Quikclot® zeolite also rapidly stops bleeding, but it induces an exothermic reaction at the wound site, which may cause burns and necrosis [79,87,190]. AristaTM is a hemisphere used in surgical procedures, and the crosslinkers used to prepare it cause side effects in humans and are toxic [101]. XSTAT®, a polymer-based sponge, induces haemostasis and acts by absorbing blood within a short space of time, however, it's not suitable for uncontrolled bleeding [191]. Other commercially available haemostatic dressings are Oxicel®, Evarrest, ActCel, Traumacel, Gelita-Cel®, Floseal, Tisseel, GelFoam®, KaltostatTM, WoundStatTM, ARTISS, Stypro®, HEMOBLASTTM *etc.* **Table 3** below shows the summarized properties of commercially available haemostatic dressings.

Table 3: Summary of commercially available haemostatic dressings

Product name	Product type	Mechanism of action	disadvantage
QuickClot	Powder	Concentrates blood	Cause burns and necrosis
Celox	Granules	Quickly forms blood clots	Inflammation
XSTAT	Sponge	Absorbs blood and stops bleeding	Only suitable for minor wounds
Tisseel	Sealant	Forms fibrin clot and triggers coagulation cascade	Expensive, short shelf-life and expensive

WoundSeal	Powder	Absorbs water in the blood and thus forming clots	The risk of viral transmission must be removed before wound closure
Tranexamic acid	Powder, tablets	Prevents fibrin clot degradation	No apparent effects
GelFoam	Sponge, foam, powder	Covers wound area and absorbs surrounding fluid while forming blood clots	Vascular structure compression
Oxycel	Woven, sponge, gauze	Forms local artificial brown clot in contact with blood	Inflammation, necrosis, and rebleeding during removal
Floseal	Sealant	Forms fibrin clot and triggers coagulation cascade	Requires removal and might cause rebleeding
Instat	Paste, nonwoven sheets, pads	Forms clot by binding clotting factors	Might cause pain or numbness
Hemostat	Sheets, liquid	Adhesive vasoconstriction and forms clots	Requires removal, and might be allergic to some patients
Thrombostat	Spray, liquid	Initiates blood clotting cascades	Risk of disseminated coagulopathy if thrombin enters the circulatory system
Drysol	Liquid	Vasoconstriction	May cause irritation

2.8. Four mathematical models of *in vitro* drug release

Zero-order release equation

$$Q = K.t + Q_0$$

Where Q is the amount of drug dissolved in time t, Q_0 is the initial amount of drug in the gels, and K is the zero-order release constant expressed. This equation refers to a release profile where the release rate of the drug is independent of the pharmaceutical dosage concentration and time [192]. This release model applies to slow drug release. The data obtained from *in vitro* drug release studies was plotted as the cumulative amount of drug released versus time.

Higuchi release equation

$$Q = K \sqrt{t}$$

Where K is the Higuchi dissolution constant, t is the time, and Q is the amount of drug released in time t. This equation refers to a system where the release of drugs is by diffusion. This model is suitable for porous matrix. This model is based on the hypotheses that (i) the initial concentration of drug in the drug delivery system is higher when compared to the drug solubility; (ii) drug diffusion occurs *via* one dimension only whereby the edge effect is negligible; (iii) drug particles are smaller than the thickness of the system; (iv) the system swelling and dissolution are negligible; (v) drug diffusivity is constant, and (vi) perfect sink conditions are attainable in the release environment [193]. The data obtained were plotted as cumulative percentage of drug release versus the square root of time.

Korsmeyer-Peppas:

$$Q = M_t / M_\infty$$

$$M_t / M_\infty = K.t^n$$

Where M_t / M_∞ is the amount of drug released at time t, K is the release rate constant, and n is the release exponent. The n value is used to characterize the release profile. This release model illustrates drug release from a polymeric system equation [194]. To find out the mechanism of drug release, only the first 60% of drug release data are fitted in the Korsmeyer-Peppas model. To study the release kinetics, data obtained from *in vitro* drug release studies were plotted as log cumulative percentage drug release versus log time. The diffusion coefficient (n) is used to calculate the mechanism of release.

Table 4: The coefficient constant of diffusion [193–196].

Coefficient of diffusion value	Mechanism of release
$n < 0.5$	Quasi-Fickian diffusion
$n = 0.5$	Fickian diffusion
$0.5 < n < 1.0$	Anomalous (non-Fickian)
$n = 1$	Non-Fickian case II. It means a zero-order release profile.
$n > 1.0$	Non-Fickian super case II.

2.9. Impact of Microorganisms on wound healing

Microorganisms are one of the major challenges associated with delayed wound healing, resulting from their resistance to multiple drug scaffolds used in wound management. Various types of bacterial microorganisms are classified as gram-negative and gram-positive. *P. aeruginosa* is a gram-negative strain of bacteria most commonly found in chronic and burn wounds [197,198]. This bacterial pathogen delays wound healing by weakening mechanisms associated with the repair of epithelial tissue and damaging epithelial cells [199]. *P. aeruginosa* is resistant to a vast number of drugs used in wound healing, including antibiotics [200]. The resistance of *P. aeruginosa* is linked to its ability to form biofilm and genetic mutations allowing it to adapt to different environments [199-201]. *S. aureus* is a common strain of gram-positive bacteria responsible for various wound infections. It is commonly found in the wound's top layer [202]. *B. subtilis* is a gram-positive pathogen that forms endospores that enable it to survive harsh conditions such as alkaline, acidic, osmotic, and nutrition-lacking environments [203].

S. aureus contributes to delayed wound healing by producing virulent factors such as coagulase, α -toxin, metalloprotease, and enterotoxins that destruct cell membranes, resulting in cell death [204]. Moreover, molecules covering its cell membrane, such as lipoprotein and peptidoglycan, induce an enhanced pro-inflammatory response by activating immune cells through pathogen recognition receptors [204]. The mechanism of resistance for *S. aureus* to various antibiotics includes its β -lactamase enzymes, which are responsible for breaking β -lactam antibiotic's ring [205]. *E. faecalis* is commonly found in diabetic and burn wounds, delays re-epithelialization, and has developed resistance due to its acquired and intrinsic resistance to a range of antibiotics [203].

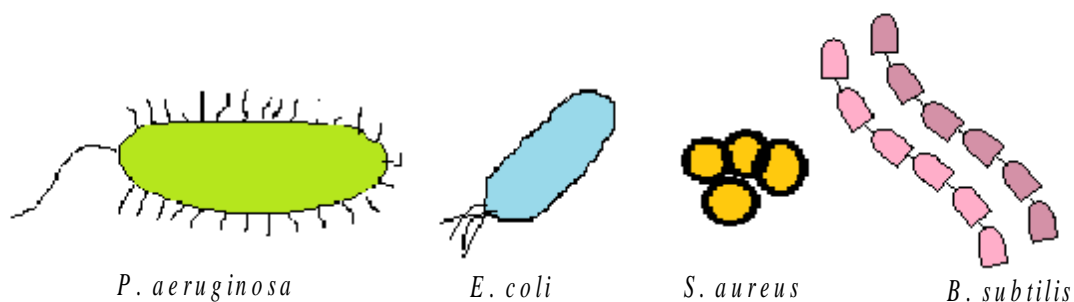


Figure 4: Schematic presentation of bacterial pathogens

References

- [1] Bano I, Arshad M, Yasin T, Ghauri MA, Younus M. Chitosan: A potential biopolymer for wound management. *Int J Biol Macromol* 2017;102:380–3. <https://doi.org/10.1016/j.ijbiomac.2017.04.047>.
- [2] Riaz A, Sohail M, Usman M, Khaliq T, Kousar M, Khan S, Hussain Z, Munir A. Bioinspired sodium alginate based thermosensitive hydrogel membranes for accelerated wound healing. *Int J Biol Macromol* 2020;155:751–65. <https://doi.org/10.1016/j.ijbiomac.2020.03.248>.
- [3] Ali Khan Z, Jamil S, Akhtar A, Mustehsan Bashir M, Yar M. Chitosan based hybrid materials used for wound healing applications- A short review. *Int J Polym Mater Polym Biomater* 2020;69:419–36. <https://doi.org/10.1080/00914037.2019.1575828>.
- [4] Cordenonsi ML, Faccendini A, Rossi S, Bonferoni CM, Malavasi L, Raffin R, Schapoval EES, Del Fante C, Vigani B, Miele D, Sandri G, Ferrari F. Platelet lysate loaded electrospun scaffolds: Effect of nanofiber types on wound healing. *Eur. J. Pharm. Biopharm.* 2019;142:247–57. <https://doi.org/10.1016/j.ejpb.2019.06.030>.
- [5] He Y, Zhao W, Dong Z, Ji Y, Li M, Hao Y, Zhang D, Yuan C, Deng J, Zhao P, Zhou Q. A biodegradable antibacterial alginate/carboxymethyl chitosan/Kangfuxin sponges for promoting blood coagulation and full-thickness wound healing. *Int J Biol Macromol* 2021;167:182–92. <https://doi.org/10.1016/j.ijbiomac.2020.11.168>.
- [6] Ahmed S, Ikram S. Chitosan Based Scaffolds and Their Applications in Wound Healing. *ALS* 2016;10:27–37. <https://doi.org/10.1016/j.als.2016.04.001>.
- [7] Hamedi H, Moradi S, Hudson SM, Tonelli AE. Chitosan based hydrogels and their applications for drug delivery in wound dressings: A review. *Carbohydr Polym* 2018;199:445–60. <https://doi.org/10.1016/j.carbpol.2018.06.114>.
- [8] Ambekar RS, Kandasubramanian B. Advancements in nanofibers for wound dressing: A review. *Eur. Polym. J.* 2019;117:304–36. <https://doi.org/10.1016/j.eurpolymj.2019.05.020>.
- [9] Mendes BB, Gómez-Florit M, Babo PS, Domingues RM, Reis RL, Gomes ME. Blood derivatives awaken in regenerative medicine strategies to modulate wound healing. *Adv Drug Deliv Rev* 2018;129:376–93. <https://doi.org/10.1016/j.addr.2017.12.018>.
- [10] Panawes S, Ekabutr P, Niamlang P, Pavasant P. Journal of Drug Delivery Science and Technology Antimicrobial mangosteen extract infused alginate-coated gauze wound

- dressing. *J Drug Deliv Sci Technol* 2017;41:182–90.
<https://doi.org/10.1016/j.jddst.2017.06.021>.
- [11] Diegelmann, R.F.; Cohen, I.K.; Kaplan AM. The role of macrophages in wound repair: A review. *Plast Reconstr Surg* 1981;68, 107–113.
- [12] Folkman, J.; Klagsbrun M. Angiogenic factors. *Science* 1987;235, 442–447.
- [13] Kiritsy, C.P.; Lynch, A.B.; Lynch SE. Role of growth factors in cutaneous wound healing: A review. *Crit Rev Oral Biol Med* 1993;4, 729–760.
- [14] Buyana B, Alven S, Nqoro X, Aderibigbe BA. Antibiotics Encapsulated Scaffolds as Potential Wound Dressings. Elsevier Inc.; 2020. Antibiotic Materials in Healcare; Chapter 7; 111-128. <https://doi.org/10.1016/b978-0-12-820054-4.00007-0>.
- [15] Frykberg, R.G.; Banks J. Challenges in the treatment of chronic wounds. *Adv Wound Care (New Rochelle)* 2015;4, 560–82.
- [16] Homaeigohar S, Boccaccini AR. Acta Biomaterialia Antibacterial biohybrid nanofibers for wound dressings. *Acta Biomater* 2021;107:25–49. <https://doi.org/10.1016/j.actbio.2020.02.022>.
- [17] Kiya K, Kubo T. Neurochemistry International Neurovascular interactions in skin wound healing. *Neurochem Int* 2019;125:144–50. <https://doi.org/10.1016/j.neuint.2019.02.014>.
- [18] Moeini A, Pedram P, Makvandi P, Malinconico M, Gomez d’Ayala G. Wound healing and antimicrobial effect of active secondary metabolites in chitosan-based wound dressings: A review. *Carbohydr Polym* 2020;233:115839. <https://doi.org/10.1016/j.carbpol.2020.115839>.
- [19] Varaprasad K, Jayaramudu T, Kanikireddy V, Toro C, Sadiku ER. Alginate-based composite materials for wound dressing application: A mini review. *Carbohydr Polym* 2020;236:116025. <https://doi.org/10.1016/j.carbpol.2020.116025>.
- [20] Boateng J, Catanzano O. Advanced Therapeutic Dressings For Effective Wound Healing n.d.:1–80.
- [21] Saghazadeh S, Rinoldi C, Schot M, Kashaf SS, Derakhshandeh H, Yue K, Swieszkowski W, Memic A, Tamayol A, Khademhosseini A. Drug Delivery Systems and Materials for Wound Healing Applications. *Adv. Drug Deliv. Rev.* 2019;127:138–166. <https://doi:10.1016/j.addr.2018.04.008>.
- [22] Frykberg RG, Banks J. Challenges in the Treatment of Chronic Wounds. *Adv. Wound Car.* 2015;4: 560–582. <https://doi: 10.1089/wound.2015.0635..>
- [23] McLaren AC, Estes CS. Orthopaedic applications of injectable biomaterials. *Biomaterials.* 2011:202–226. <https://doi: 10.1533/9780857091376.2.202>.
- [24] Kona GS, Wadajkar AS, Nguyen KT. Tissue engineering applications of injectable biomaterials. *Biomaterials* 2011 142–182. <https://doi: 10.1533/9780857091376.2.142>.
- [25] Shamloo A, Sarmadi M, Aghababaie Z, Vossoughi M. Accelerated full-thickness wound healing via sustained bFGF delivery based on a PVA/chitosan/gelatin hydrogel

- incorporating PCL microspheres. *Int J Pharm* 2018;537:278–89. <https://doi.org/10.1016/j.ijpharm.2017.12.045>.
- [26] Ahmed A, Getti G, Boateng J. Ciprofloxacin-loaded calcium alginate wafers prepared by freeze-drying technique for potential healing of chronic diabetic foot ulcers. *Drug Deliv Transl Res* 2018;8:1751–68. <https://doi.org/10.1007/s13346-017-0445-9>.
- [27] Matica MA, Aachmann FL, Tøndervik A, Sletta H, Ostafe V. Chitosan as a wound dressing starting material: Antimicrobial properties and mode of action. *Int J Mol Sci* 2019;20:1–33. <https://doi.org/10.3390/ijms20235889>.
- [28] Bagher Z, Ehterami A, Hossein M, Khastar H. Journal of Drug Delivery Science and Technology Wound healing with alginate / chitosan hydrogel containing hesperidin in rat model. *J Drug Deliv Sci Technol* 2020;55:101379. <https://doi.org/10.1016/j.jddst.2019.101379>.
- [29] Dhivya S, Vijaya V, Santhini E. Review article Wound dressings – a review *Biomedicine*. 2015;5:24–28. <https://doi.org/10.7603/s40681-015-0022-9>.
- [30] Aderibigbe BA, Buyana B. Alginate in Wound Dressings. *Pharmaceutics*. 2018;10:119. <https://doi.org/10.3390/pharmaceutics10020042>.
- [31] Sharma S, Dua A, Malik A. Third generation materials for wound dressing. *Int. J. Pharm. Sci. Res.* 2014;5:2113–2124.
- [32] Koehler J, Brandl FP, Goepferich AM. Hydrogel wound dressings for bioactive treatment of acute and chronic wounds. *Eur Polym J* 2018;100:1–11. <https://doi.org/10.1016/j.eurpolymj.2017.12.046>.
- [33] Mir M, Najabat M, Afifa A, Ayesha B, Munam G, Shizza A. Synthetic polymeric biomaterials for wound healing: a review. *Prog Biomater* 2018;7:1–21. <https://doi.org/10.1007/s40204-018-0083-4>.
- [34] Andreu V, Mendoza G, Arruebo M, Irusta S. Smart Dressings Based on Nanostructured Fibers Containing Natural Origin Antimicrobial, Anti-Inflammatory, and Regenerative Compounds 2015:5154–93. <https://doi.org/10.3390/ma8085154>.
- [35] Fahimirad S, Ajallouei F. Naturally-derived electrospun wound dressings for target delivery of bio-active agents. *Int J Pharm* 2019;566:307–28. <https://doi.org/10.1016/j.ijpharm.2019.05.053>.
- [36] Naseri-nosar M, Maria Z. Wound dressings from naturally-occurring polymers: A review on homopolysaccharide-based composites. *Carbohydr Polym* 2018;189:379–98. <https://doi.org/10.1016/j.carbpol.2018.02.003>.
- [37] Jayakumar R, Prabakaran M, Sudheesh Kumar PT, Nair S V., Tamura H. Biomaterials based on chitin and chitosan in wound dressing applications. *Biotechnol Adv* 2011;29:322–37. <https://doi.org/10.1016/j.biotechadv.2011.01.005>.
- [38] 31130-Article Text-125205-2-10-20200726.pdf n.d.
- [39] Wang K, Pan S, Qi Z, Xia P, Xu H, Kong W, Li H, Xue P, Yang X, Fu C. Recent Advances in Chitosan-Based Metal Nanocomposites for Wound Healing Applications. *Adv Mater Sci Eng* 2020:1-13. <https://doi.org/10.1155/2020/3827912>.

- [40] Conzatti G, Chamary S, Geyter N De, Cavalie S, Morent R, Tourrette A. Surface functionalization of plasticized chitosan films through PNIPAM grafting via UV and plasma graft polymerization. *Eur Polym J* 2018;105:434–41. <https://doi.org/10.1016/j.eurpolymj.2018.06.020>.
- [41] Singh R, Shitiz K, Singh A. Chitin and chitosan: biopolymers for wound management. *Int Wound J* 2017;14:1276–89. <https://doi.org/10.1111/iwj.12797>.
- [42] Gutha Y, Pathak JL, Zhang W, Zhang Y, Jiao X. Antibacterial and wound healing properties of chitosan/poly(vinyl alcohol)/zinc oxide beads (CS/PVA/ZnO). *Int J Biol Macromol* 2017;103:234–41. <https://doi.org/10.1016/j.ijbiomac.2017.05.020>.
- [43] Batista MP, Gonçalves VSS, Gaspar FB, Nogueira ID, Matias AA, Gurikov P. Novel alginate-chitosan aerogel fibres for potential wound healing applications. *Int J Biol Macromol* 2020;156:773–82. <https://doi.org/10.1016/j.ijbiomac.2020.04.089>.
- [44] Intini C, Elviri L, Cabral J, Mros S, Bergonzi C, Bianchera A, Flammini L, Govoni P, Barocelli E, Bettini R, McConnell M. 3D-printed chitosan-based scaffolds: An in vitro study of human skin cell growth and an in-vivo wound healing evaluation in experimental diabetes in rats. *Carbohydr Polym* 2018;199:593–602. <https://doi.org/10.1016/j.carbpol.2018.07.057>.
- [45] Stricker-Krongrad A-H, Alikhassy Z, Matsangos N, Sebastian R, Marti G, Lay F, Harmon JW. Efficacy of Chitosan-Based Dressing for Control of Bleeding in Excisional Wounds. *Eplasty* 2018;18:122-130.
- [46] Croisier F, Jérôme C. Chitosan-based biomaterials for tissue engineering. *Eur Polym J* 2013;49:780–92. <https://doi.org/10.1016/j.eurpolymj.2012.12.009>.
- [47] Chen Y, Qian JQ, Zhao CY, Yang LC, Ding J, Guo H. Preparation and evaluation of porous starch/chitosan composite cross-linking hemostatic. *Eur Polym J* 2019;118:17–26. <https://doi.org/10.1016/j.eurpolymj.2019.05.039>.
- [48] Sundaram MN, Mony U, Varma PK, Jayakumar R. Vasoconstrictor and coagulation activator entrapped chitosan based composite hydrogel for rapid bleeding control. *Carbohydr Polym* 2021;258:117634. <https://doi.org/10.1016/j.carbpol.2021.117634>.
- [49] Wang C, Luo W, Li P, Li S, Yang Z, Hu Z, Liu Y, Ao N. Preparation and evaluation of chitosan/alginate porous microspheres/Bletilla striata polysaccharide composite hemostatic sponges. *Carbohydr Polym* 2017;174:432–42. <https://doi.org/10.1016/j.carbpol.2017.06.112>.
- [50] Mohandas A, Anisha BS, Chennazhi KP, Jayakumar R. Chitosan-hyaluronic acid/VEGF loaded fibrin nanoparticles composite sponges for enhancing angiogenesis in wounds. *Colloids Surfaces B Biointerfaces* 2015;127:105–13. <https://doi.org/10.1016/j.colsurfb.2015.01.024>.
- [51] Hao Y, Zhao W, Zhang L, Zeng X, Sun Z, Zhang D, Shen P, Li Z, Han Y, Li P, Zhou Q. Bio-multifunctional alginate/chitosan/fucoidan sponges with enhanced angiogenesis and hair follicle regeneration for promoting full-thickness wound healing. *Mater Des* 2020;193:108863. <https://doi.org/10.1016/j.matdes.2020.108863>.

- [52] Wang Y, Fu Y, Li J, Mu Y, Zhang X, Zhang K, Liang M, Feng C, Chen X. Multifunctional chitosan/dopamine/diatom-biosilica composite beads for rapid blood coagulation. *Carbohydr Polym* 2018;200:6–14. <https://doi.org/10.1016/j.carbpol.2018.07.065>.
- [53] Pawar V, Dhanka M, Srivastava R. Cefuroxime conjugated chitosan hydrogel for treatment of wound infections. *Colloids Surfaces B Biointerfaces* 2019;173:776–87. <https://doi.org/10.1016/j.colsurfb.2018.10.034>.
- [54] Ahmadi S, Hivechi A, Bahrami SH, Milan PB, Sara S. Cinnamon extract loaded electrospun chitosan/gelatin membrane with antibacterial activity. *Int J Biol Macromol* 2021;173:580–90. <https://doi.org/10.1016/j.ijbiomac.2021.01.156>.
- [55] Khoirunnisa D, Rukmana TI. Isolation and Characteristics of Bovine Skin Gelatin and Analysis of Glycine, Proline, and Hydroxyproline by High-Performance Liquid Chromatography- Fluorescence. *Int. J. Appl. Pharm.* 2018;10:269-75. <https://doi.org/10.22159/ijap.2018.v10s1.60>.
- [56] Devi N, Sarmah M, Khatun B, Maji TK. Encapsulation of active ingredients in polysaccharide-protein complex coacervates. *Adv. Colloid Interface Sci.* 2016. <https://doi.org/10.1016/j.cis.2016.05.009>.
- [57] Ramos M, Valdés A, Beltrán A, Garrigós M. Gelatin-based films and coatings for food packaging applications. *Coatings* 2016;6:1–20. <https://doi.org/10.3390/coatings6040041>.
- [58] Kommareddy S, Vaccines T, Shenoy D, Amiji M. Gelatin Nanoparticles and Their Biofunctionalization. *Gelatin and Gelatin Derivatives*. Chapter 11. 2007:330-352 <https://doi.org/10.1002/9783527610419.ch11>.
- [59] Wilson HT, Amirkhani M, Taylor AG. Evaluation of Gelatin as a Biostimulant Seed Treatment to Improve Plant Performance. *Frontiers in Plant Science* 2018;9:1–11. <https://doi.org/10.3389/fpls.2018.01006>.
- [60] Zhu S, Huang M, Feng G, Miao Y, Wu H, Zeng M, Lo YM. Gelatin versus its two major degradation products, prolyl-hydroxyproline and glycine, as supportive therapy in experimental colitis in mice. *Food Sci Nutr.* 2018;6:1023–31. <https://doi.org/10.1002/fsn3.639>.
- [61] Ahmady A, Hayati N, Samah A. A review: Gelatine as a bioadhesive material for medical and pharmaceutical applications. *Int J Pharm* 2021;608:121037. <https://doi.org/10.1016/j.ijpharm.2021.121037>.
- [62] Zahiri M, Khanmohammadi M, Goodarzi A, Ababzadeh S. Encapsulation of curcumin loaded chitosan nanoparticle within poly (ε-caprolactone) and gelatin fiber mat for wound healing and layered dermal reconstitution. *Int J Biol Macromol* 2020;153:1241–50. <https://doi.org/10.1016/j.ijbiomac.2019.10.255>.
- [63] Di Lena F. Hemostatic polymers: The concept, state of the art and perspectives. *J Mater Chem B* 2014;2:3567–77. <https://doi.org/10.1039/c3tb21739f>.
- [64] Alipal J, Pu NASM, Lee TC, Nayan NHM, Sahari N, Basri H, Idris MI, Abdullah HZ. A review of gelatin: Properties, sources, process, applications, and commercialisation. *Mater Today Proc* 2021;42:240–50. <https://doi.org/10.1016/j.matpr.2020.12.922>.

- [65] Wang M, Li Y, Wu J, Xu F, Zuo Y, Jansen JA. In vitro and in vivo study to the biocompatibility and biodegradation of hydroxyapatite/poly(vinyl alcohol)/gelatin composite. *J Biomed Mater Res - Part A* 2008;85:418–26. <https://doi.org/10.1002/jbm.a.31585>.
- [66] Han K, Bai Q, Wu W, Sun N, Cui N, Lu T. Gelatin-based adhesive hydrogel with selfhealing , hemostasis , and electrical conductivity. *Int J Biol Macromol* 2021;183:2142– 51. <https://doi.org/10.1016/j.ijbiomac.2021.05.147>.
- [67] Sharma A, Puri V, Kumar P. Rifampicin-Loaded Alginate-Gelatin Fibers Incorporated within Transdermal Films as a Fiber-in-Film System for Wound Healing Applications 2021.
- [68] Huang Y, Bai L, Yang Y, Yin Z, Guo B. Journal of Colloid and Interface Science Biodegradable gelatin/silver nanoparticle composite cryogel with excellent antibacterial and antibiofilm activity and hemostasis for *Pseudomonas aeruginosa* infected burn wound healing. *J Colloid Interface Sci* 2022;608:2278–89. <https://doi.org/10.1016/j.jcis.2021.10.131>.
- [69] Cao S, Li L, Du Y, Gan J, Wang J, Wang T, Liu Y, Liu W, Zhou Y, Gao X, Li H, Liu T. Porous gelatin microspheres for controlled drug delivery with high hemostatic efficacy. *Colloids Surfaces B Biointerfaces* 2021;207:112013. <https://doi.org/10.1016/j.colsurfb.2021.112013>.
- [70] Atashgahi M, Ghaemi B, Valizadeh A, Moshiri A. Epinephrine-entrapped chitosan nanoparticles covered by gelatin nanofibers: A bi-layer nano-biomaterial for rapid hemostasis. *Int J Pharm* 2021;608:121074. <https://doi.org/10.1016/j.ijpharm.2021.121074>.
- [71] Aydemir U, Kocer Z, Sahin İ, Aru B, Yan G. Oxidized regenerated cellulose crosslinked gelatin microparticles for rapid and biocompatible hemostasis: A versatile cross-linking agent 2018;200:624–32. <https://doi.org/10.1016/j.carbpol.2018.07.074>.
- [72] Wang J, Tsai C, Tsai N, Chiang C, Lin R, Pereira RF, Li YE. An injectable , dual crosslinkable hybrid pectin methacrylate (PECMA)/ gelatin methacryloyl (GelMA) hydrogel for skin hemostasis applications. *Int J Biol Macromol* 2021;185:441–50. <https://doi.org/10.1016/j.ijbiomac.2021.06.162>.
- [73] Nagahama Y, Li L, Takeda M, Mitsuhashi T, Kurisu K, Howard MA, Hitchon PW, Yamaguchi S. Localized controlled fibrin glue application with gelatin sponge for hemostasis and dural defect repair : Technical note. *Interdiscip Neurosurg* 2019;18:100476. <https://doi.org/10.1016/j.inat.2019.100476>.
- [74] Yan T, Cheng F, Wei X, Huang Y, He J. Biodegradable collagen sponge reinforced with chitosan/calcium pyrophosphate nanoflowers for rapid hemostasis. *Carbohydr Polym* 2017;170:271–80. <https://doi.org/10.1016/j.carbpol.2017.04.080>.
- [75] Arunagiri V, Tsai H, Fentahun H, Wei H. Preparation of physically crosslinked polyelectrolyte Gelatin-Tannic acid- κ -Carrageenan (GTC) microparticles as hemostatic agents. *Int J Biol Macromol* 2021;191:324–34. <https://doi.org/10.1016/j.ijbiomac.2021.09.008>.
- [76] Li N, Yang X, Liu W, Xi G, Wang M, Liang B, Ma Z, Feng Y, Chen H, Shi C. Tannic Acid Cross-linked Polysaccharide-Based Multifunctional Hemostatic Microparticles

- for the Regulation of Rapid Wound Healing. *Macromol. Biosci.* 2018;1-16.
<https://doi.org/10.1002/mabi.201800209>.
- [77] Suchý P, Paprskářová A, Chalupová M, Marholdova L, Nešporová K, Klusáková J, Kuzmínová G, Hendrych M, Velebný V. Composite Hemostatic Nonwoven Textiles Based on Hyaluronic Acid, Cellulose, and Etamsylate. *Materials.* 2020;13:1–14.
[doi:10.3390/ma13071627](https://doi.org/10.3390/ma13071627).
- [78] Farooq A, Patoary MK, Zhang M, Mussana H, Li M, Naeem MA, Mushtaq M, Farooq A, Liu L. Cellulose from sources to nanocellulose and an overview of synthesis and properties of nanocellulose/zinc oxide nanocomposite materials. *Int J Biol Macromol* 2020;154:1050–73. <https://doi.org/10.1016/j.ijbiomac.2020.03.163>.
- [79] Fan X, Li Y, Li N, Wan G, Amir M, Tang K. Rapid hemostatic chitosan/cellulose composite sponge by alkali/urea method for massive haemorrhage 2020;164:2769–78. <https://doi.org/10.1016/j.ijbiomac.2020.07.312>.
- [80] Kanikireddy V, Varaprasad K, Jayaramudu T, Karthikeyan C, Sadiku R. Carboxymethyl cellulose-based materials for infection control and wound healing: A review. *Int J Biol Macromol* 2020;164:963–75. <https://doi.org/10.1016/j.ijbiomac.2020.07.160>.
- [81] Ohta S, Nishiyama T, Sakoda M, Machioka K, Fuke M, Ichimura S, Inagaki F, Shimizu A, Hasegawa K, Kokudo N, Kaneko M, Yatomi Y, Ito T. Development of carboxymethyl cellulose nonwoven sheet as a novel hemostatic agent. *J Biosci Bioeng* 2015;119:718–23. <https://doi.org/10.1016/j.jbiosc.2014.10.026>.
- [82] Gu H, He J, Huang Y, Guo Z. Fabrication of oxidized sodium carboxymethylcellulose from viscose fibers and their viscosity behaviors. *Fibers Polym* 2013;14:1266–70. <https://doi.org/10.1007/s12221-013-1266-1>.
- [83] Aoshima M, Tanabe K, Kohno I, Jo Y, Takahashi K, Sugo T, Matsuda M. Hemostatic mechanisms of a soluble fraction of plant-derived sodium carboxymethyl cellulose. *Japanese J Thromb Hemost* 2012;23:387–98. <https://doi.org/10.2491/jjsth.23.387>.
- [84] Ribeiro AM, Magalhães M, Veiga F, Figueiras A. Cellulose-Based Hydrogels in Topical Drug Delivery: A Challenge in Medical Devices 2019:1205–33. https://doi.org/10.1007/978-3-319-77830-3_41.
- [85] Liu R, Dai L, Si C, Zeng Z. Antibacterial and hemostatic hydrogel via nanocomposite from cellulose nanofibers. *Carbohydr Polym* 2018;195:63–70. <https://doi.org/10.1016/j.carbpol.2018.04.085>.
- [86] Barba BJD, Aranilla CT, Relleve LS, Cruz VRC, Vista JR, Abad L V. Hemostatic granules and dressing prepared from formulations of carboxymethyl cellulose, kappa-carrageenan and polyethylene oxide crosslinked by gamma radiation. *Radiat Phys Chem* 2018;144:180–8. <https://doi.org/10.1016/j.radphyschem.2017.08.009>.
- [87] Mahmoodzadeh A, Moghaddas J, Jarolmasjed S, Ebrahimi Kalan A, Edalati M, Salehi R. Biodegradable cellulose-based superabsorbent as potent hemostatic agent. *Chem Eng J* 2021;418:129252. <https://doi.org/10.1016/j.cej.2021.129252>.

- [88] Collins MN, Birkinshaw C. Hyaluronic acid based scaffolds for tissue engineering — A review. *Carbohydr Polym* 2013;92:1262–79. <https://doi.org/10.1016/j.carbpol.2012.10.028>.
- [89] Yang Y, Dong Z, Li M, Liu L, Luo H, Wang P, Zhang D, Yang X, Zhou K, Lei S. Graphene Oxide/Copper Nanoderivatives-Modified Chitosan/Hyaluronic Acid Dressings for Facilitating Wound Healing in Infected Full-Thickness Skin Defects *Int. J. Nanomed.* 2020;8231–47.
- [90] Alven S, Aderibigbe BA. Hyaluronic acid-based scaffolds as potential bioactive wound dressings. *Polymers (Basel)* 2021;13. <https://doi.org/10.3390/polym13132102>.
- [91] Longinotti C. The use of hyaluronic acid based dressings to treat burns: A review. *Burn Trauma* 2014;2:162–8. <https://doi.org/10.4103/2321-3868.142398>.
- [92] Gupta RC, Lall R, Srivastava A, Sinha A. Hyaluronic acid: Molecular mechanisms and therapeutic trajectory. *Front Vet Sci* 2019;6:1–24. <https://doi.org/10.3389/fvets.2019.00192>.
- [93] Graça MFP, Miguel SP, Cabral CSD, Correia IJ. Hyaluronic acid — Based wound dressings : A review. *Carbohydr Polym* 2020;241:116364. <https://doi.org/10.1016/j.carbpol.2020.116364>.
- [94] Cortes H, Caballero-Florán IH, Mendoza-Muñoz N, Córdova-Villanueva EN, EscutiaGuadarrama L, Figueroa-González G, Reyes-Hernández OD, Carmen MG, VarelaCardoso M, Magaña JJ, Florán B, Prado-Audelo MLD, Leyva-Gómez G. Hyaluronic acid in wound dressings. *Cell Mol Biol* 2020;66:191–8. <https://doi.org/10.14715/cmb/2020.66.4.23>.
- [95] Dovedytis M, Liu ZJ, Bartlett S. Hyaluronic acid and its biomedical applications: A review. *Eng Regen* 2020;1:102–13. <https://doi.org/10.1016/j.engreg.2020.10.001>.
- [96] Prasathkumar M, Sadhasivam S. Chitosan/Hyaluronic acid/Alginate and an assorted polymers loaded with honey, plant, and marine compounds for progressive wound healing — Know-how. *Int J Biol Macromol* 2021;186:656–85. <https://doi.org/10.1016/j.ijbiomac.2021.07.067>.
- [97] Chen Y, Lu C, Shen M, Lin S, Chen C. In vitro evaluation of the hyaluronic acid/alginate composite powder for topical haemostasis and wound healing 2020:394–404. <https://doi.org/10.1111/iwj.13285>.
- [98] Liu J, Li Y, Hu Y, Cheng G, Ye E, Shen C, Xu F. Hemostatic porous sponges of crosslinked hyaluronic acid/cationized dextran by one self-foaming process. *Mater Sci Eng C* 2018;83:160–8. <https://doi.org/10.1016/j.msec.2017.10.007>.
- [99] Cho SS. As featured in: *Materials Horizons* multifunctional hemostatic adhesives inspired by a 2019. <https://doi.org/10.1039/c9mh00157c>.
- [100] Wang D, Xu P, Wang S, Li W, Liu W. Rapidly curable hyaluronic acid-catechol hydrogels inspired by scallops as tissue adhesives for hemostasis and wound healing. *Eur Polym J* 2020;134:109763. <https://doi.org/10.1016/j.eurpolymj.2020.109763>.
- [101] Wang Y, Liu G, Wu L, Qu H, Song D, Huang H, Wu C, Xu M. Rational design of porous starch/hyaluronic acid composites for hemostasis. *Int J Biol Macromol* 2020;158:1319–29. <https://doi.org/10.1016/j.ijbiomac.2020.05.018>.

- [102] He X, Ding Y, Xie W, Sun RY, Hunt NC, Song J, Sun X, Peng C, Zeng Q, Tan Y, Liu Y. Rubidium-Containing Calcium Alginate Hydrogel for Antibacterial and Diabetic Skin Wound Healing Applications. *ACS Biomater Sci Eng* 2019;5:4726–38. <https://doi.org/10.1021/acsbiomaterials.9b00547>.
- [103] Hu C, Gong RH, Zhou FL. Electrospun sodium alginate/polyethylene oxide fibers and nanocoated yarns. *Int J Polym Sci* 2015;2015. <https://doi.org/10.1155/2015/126041>.
- [104] Lee, K.Y.; Mooney DJ. Alginate: Properties and biomedical applications. *Prog Polym Sci* 2012;37:106–26.
- [105] V. C. Polysaccharide-based biomaterials with antimicrobial and antioxidant properties. *Polimeros* 2013;23:287-297.
- [106] Brachkova, M.I.; Marques, P.; Rocha, J.; Sepodes, B.; Duarte, M.A.; Pinto JF. Alginate films containing *Lactobacillus plantarum* as wound dressing for prevention of burn infection. *J Hosp Infect* 2011;79, 375–377.
- [107] Dantas MDM, Cavalcante DRR, Araujo FEN, Barretto SR, Acirole GTS, Pinheiro ALB, Ribeiro MAG, Lima-Verde IB, Melo CM, Cardoso JC, Junior RLCA. Improvement of dermal burn healing by combining sodium alginate/chitosan-based films and low level laser therapy. *J Photochem* 2011;105, 51–59.
- [108] Peng CW, Lin HY, Wang HW, Wu WW. The influence of operating parameters on the drug release and anti-bacterial performances of alginate wound dressings prepared by three-dimensional plotting. *Sci Eng C* 2012;32, 2491–2500.
- [109] Mogoşanu GD, Grumezescu AM. Natural and synthetic polymers for wounds and burns dressing. *Int J Pharm* 2014;463(2):127–136.
- [110] Kanokpanont S, Damrongsakkul S, Ratanavaraporn JAP. An innovative bi-layered wound dressing made of silk and gelatin for accelerated wound healing. *Int J Pharm* 2012;436(1–2):141–153.
- [111] Ji F, Lin W, Wang Z, Wang L, Zhang J, Ma G, Chen S. Development of nonstick and drug-loaded wound dressing based on the hydrolytic hydrophobic poly(carboxybetaine) ester analogue. *ACS Appl Mater Interfaces* 2013;5(21):10489–10494.
- [112] Broussard KC, Powers JG. Wound dressings: selecting the most appropriate type. *Am J Clin Dermatol* 2013;14:449–459. <https://doi.org/10.1007/s40257-013-0046-4>.
- [113] Abdelrahman T, Newton H. Wound dressings: principles and practice. *Surgery* 2011;29(10):491–495. <https://doi.org/10.1016/j.mpsur.2011.06.007>.
- [114] Costache MC, Qu H, Ducheyne P D DI. Polymer-xerogel composites for controlled release wound dressings. *Biomaterials* 2010;31(24):6336–6343.
- [115] Rossi S, Faccendini A, Bonferoni MC, Ferrari F, Sandri G, Fante CD, Perotti C, Caramella CM. Sponge-like dressings based on biopolymers for the delivery of platelet lysate to skin chronic wounds. *Int J Pharm* 2013;440(2):207–215. <https://doi.org/10.1016/j.ijpharm.2012.07.056>.
- [116] Cheng F, Liu C, Wei X, Yan T, Li H, He J, Huang Y. repairation and Characterization of 2,2,6,6-Tetramethylpiperidine-1-oxyl (TEMPO)-Oxidized Cellulose

- Nanocrystal/Alginate Biodegradable Composite Dressing for Hemostasis Applications. 2017:2–11. <https://doi.org/10.1021/acssuschemeng.6b02849>.
- [117] Jin J, Ji Z, Xu M, Liu C, Ye X, Zhang W, Li S, Wang D, Zhang W, Chen J, Ye F, Lv Z. Microspheres of Carboxymethyl Chitosan, Sodium Alginate, and Collagen as a Hemostatic Agent in Vivo. *ACS Biomater Sci Eng* 2018;4:2541–51. <https://doi.org/10.1021/acsbioamater.8b00453>.
- [118] Liu C, Shi Z, Sun H, Mujuni CJ, Zhao L, Wang X, Huang F. Preparation and characterization of tissue-factor-loaded alginate: Toward a bioactive hemostatic material. *Carbohydr Polym* 2020;249:116860. <https://doi.org/10.1016/j.carbpol.2020.116860>.
- [119] Jin J, Xu M, Liu Y, Ji Z, Dai K, Zhang L, Wang L, Ye F, Chen G, Lv Z. Alginatebased composite microspheres coated by berberine simultaneously improve hemostatic and antibacterial efficacy. *Colloids Surfaces B Biointerfaces* 2020;194:111168. <https://doi.org/10.1016/j.colsurfb.2020.111168>.
- [120] Sutar T, Bangde P, Dandekar P, Adivarekar R. Herbal hemostatic biopolymeric dressings of alginate/pectin coated with Croton oblongifolius extract. *Carbohydr Polym Technol Appl* 2021;2:100025. <https://doi.org/10.1016/j.carpta.2020.100025>.
- [121] Huang X, Fu Q, Deng Y, Wang F, Xia B, Chen Z, Chen G. Surface roughness of silk fibroin/alginate microspheres for rapid hemostasis in vitro and in vivo. *Carbohydr Polym* 2021;253:117256. <https://doi.org/10.1016/j.carbpol.2020.117256>.
- [122] Huang YW, Wu CH, Aronstam RS. Toxicity of transition metal oxide nanoparticles: Recent insights from in vitro studies. *Materials (Basel)* 2010;3:4842–59. <https://doi.org/10.3390/ma3104842>.
- [123] Sharma H, Kumar K, Choudhary C, Mishra PK, Vaidya B. Development and characterization of metal oxide nanoparticles for the delivery of anticancer drug. *Artif Cells, Nanomedicine Biotechnol* 2016;44:672–9. <https://doi.org/10.3109/21691401.2014.978980>.
- [124] Buyana B, Aderibigbe BA, Ndinteh DT, Fonkui YT, Kumar P. Alginate-pluronic topical gels loaded with thymol, norfloxacin and ZnO nanoparticles as potential wound dressings. *J Drug Deliv Sci Technol* 2020;60:101960. <https://doi.org/10.1016/j.jddst.2020.101960>.
- [125] Manuja A, Raguvaran R, Kumar B, Kalia A, Tripathi BN. International Journal of Biological Macromolecules Accelerated healing of full thickness excised skin wound in rabbits using single application of alginate / acacia based nanocomposites of ZnO nanoparticles. *Int J Biol Macromol* 2020;155:823–33. <https://doi.org/10.1016/j.ijbiomac.2020.03.221>.
- [126] Norouzi MA, Montazer M, Harifi T, Karimi P. Flower buds like PVA/ZnO composite nanofibers assembly: Antibacterial, in vivo wound healing, cytotoxicity and histological studies. *Polym Test* 2021;93:106914. <https://doi.org/10.1016/j.polymertesting.2020.106914>.
- [127] Soubhagya AS, Moorthi A, Prabakaran M. Preparation and characterization of chitosan/pectin/ZnO porous films for wound healing. *Int J Biol Macromol* 2020;157:135–45. <https://doi.org/10.1016/j.ijbiomac.2020.04.156>.

- [128] Zhang M, Qiao X, Han W, Jiang T, Liu F, Zhao X. Alginate-chitosan oligosaccharide/ZnO composite hydrogel for accelerating wound healing. *Carbohydr Polym* 2021;266:118100. <https://doi.org/10.1016/j.carbpol.2021.118100>.
- [129] Yang JY, Bae J, Jung A, Park S, Chung S, Seok J, Roh H, Han Y, Oh J, Sohn S, Jeong J, Cho W. Surface functionalization-specific binding of coagulation factors by zinc oxide nanoparticles delays coagulation time and reduces thrombin generation potential in vitro. *PLoS One* 2017;12:1–15. <https://doi.org/10.1371/journal.pone.0181634>.
- [130] Ali A, Zafar H, Zia M, ul Haq I, Phull AR, Ali JS, Hussain A. Synthesis, characterization, applications, and challenges of iron oxide nanoparticles. *Nanotechnol Sci Appl* 2016;9:49–67. <https://doi.org/10.2147/NSA.S99986>.
- [131] Shabanova EM, Drozdov AS, Fakhardo AF, Dudanov IP, Kovalchuk MS, Vinogradov V V. Thrombin@Fe₃O₄ nanoparticles for use as a hemostatic agent in internal bleeding. *Sci Rep* 2018;8:1–10. <https://doi.org/10.1038/s41598-017-18665-4>.
- [132] Li X, Wang Y, Shi L, Li B, Li J, Wei Z, Lv H, Wu L, Zhang H, Yang B, Xu X, Jiang J. Magnetic targeting enhances the cutaneous wound healing effects of human mesenchymal stem cell-derived iron oxide exosomes. *J Nanobiotechnology* 2020;18:1–14. <https://doi.org/10.1186/s12951-020-00670-x>.
- [133] Yadav E, Yadav P, Verma A. In silico Study of *Trianthema portulacastrum* Embedded Iron Oxide Nanoparticles on Glycogen Synthase Kinase-3 β : A Possible Contributor to its Enhanced in vivo Wound Healing Potential. *Front Pharmacol* 2021;12:1–14. <https://doi.org/10.3389/fphar.2021.664075>.
- [134] Sathiyaseelan A, Saravanakumar K, Mariadoss AVA, Wang MH. Antimicrobial and wound healing properties of FeO fabricated chitosan/pva nanocomposite sponge. *Antibiotics* 2021;10. <https://doi.org/10.3390/antibiotics10050524>.
- [135] Yaroslavovych PO. Antimicrobial effect of wound healing nano-containing polymer materials. *The Moldovan Medical Journal*. 2017;60:35-38. <https://doi.org/10.5281/zenodo.1050962>.
- [136] Liu M, Wang X, Li H, Xia C, Liu Z, Liu J, Yin A, Lou X, Wang H, Mo X, Wu J. Magnesium oxide-incorporated electrospun membranes inhibit bacterial infections and promote the healing process of infected wounds. *J Mater Chem B* 2021;9:3727–44. <https://doi.org/10.1039/d1tb00217a>.
- [137] Liu M, Wang R, Liu J, Zhang W, Liu Z, Lou X, Nie H, Wang H, Mo X, Abd-Elhamid AI, Zheng R, Wu J. Incorporation of magnesium oxide nanoparticles into electrospun membranes improves pro-angiogenic activity and promotes diabetic wound healing. *Mater Sci Eng C* 2021:112609. <https://doi.org/10.1016/j.msec.2021.112609>.
- [138] Attayil Sukumaran S, Kalimuthu B, Selvamurugan N, Mani P. Wound dressings based on chitosan/gelatin/MgO composite films. *Int J Polym Mater Polym Biomater* 2021;0:1–10. <https://doi.org/10.1080/00914037.2021.1960342>.
- [139] Alavi M, Varma RS. Antibacterial and wound healing activities of silver nanoparticles embedded in cellulose compared to other polysaccharides and protein polymers. *Cellulose* 2021;28:8295–311. <https://doi.org/10.1007/s10570-021-04067-3>.

- [140] Krishnan PD, Banas D, Durai RD, Kabanov D, Hosnedlova B, Kepinska M, Fernandez C, Ruttkay-Nedecky B, Nguyen HV, Farid A, Sochor J, Narayanan VHB, Kizek R. Silver nanomaterials for wound dressing applications. *Pharmaceutics* 2020;12:1–27. <https://doi.org/10.3390/pharmaceutics12090821>.
- [141] Masood N, Ahmed R, Tariq M, Ahmed Z, Masoud MS, Ali I, Asghar R, Andleeb A, Hasan A. Silver nanoparticle impregnated chitosan-PEG hydrogel enhances wound healing in diabetes induced rabbits. *Int J Pharm* 2019;559:23–36. <https://doi.org/10.1016/j.ijpharm.2019.01.019>.
- [142] Huang B, Liu X, Li Z, Zheng Y, Wai Kwok Yeung K, Cui Z, Liang Y, Zhu S, Wu S. Rapid bacteria capturing and killing by AgNPs/N-CD@ZnO hybrids strengthened photo-responsive xerogel for rapid healing of bacteria-infected wounds. *Chem Eng J* 2021;414. <https://doi.org/10.1016/j.cej.2021.128805>.
- [143] Yang X, Wang B, Sha D, Liu Y, Xu J, Shi K, Yu C, Ji X. Injectable and antibacterial ϵ -poly(L-lysine)-modified poly(vinyl alcohol)/chitosan/AgNPs hydrogels as wound healing dressings. *Polymer (Guildf)* 2020. <https://doi.org/10.1016/j.polymer.2020.123155>.
- [144] Choudhary M, Chhabra P, Tyagi A, Singh H. Scar free healing of full thickness diabetic wounds: A unique combination of silver nanoparticles as antimicrobial agent, calcium alginate nanoparticles as hemostatic agent, fresh blood as nutrient/growth factor supplier and chitosan as base matrix. *Int J Biol Macromol* 2021;178:41–52. <https://doi.org/10.1016/j.ijbiomac.2021.02.133>.
- [145] Zhang Y, Guan J, Wu J, Ding S, Yang J, Zhang J, Dong A, Deng L. N-alkylated chitosan/graphene oxide porous sponge for rapid and effective hemostasis in emergency situations. *Carbohydr Polym* 2019;219:405–13. <https://doi.org/10.1016/j.carbpol.2019.05.028>.
- [146] Li G, Liang Y, Xu C, Sun H, Tao L, Wei Y, Wang X. Polydopamine reinforced hemostasis of a graphene oxide sponge via enhanced platelet stimulation. *Colloids Surfaces B Biointerfaces* 2019;174:35–41. <https://doi.org/10.1016/j.colsurfb.2018.10.074>.
- [147] Liang Y, Xu C, Li G, Liu T, Liang JF, Wang X. Graphene-kaolin composite sponge for rapid and riskless hemostasis. *Colloids Surfaces B Biointerfaces* 2018;169:168–75. <https://doi.org/10.1016/j.colsurfb.2018.05.016>.
- [148] Guajardo S, Figueroa T, Borges J, Aguayo C, Fernández K. Graphene oxide-gelatin aerogels as wound dressings with improved hemostatic properties. *Mater Today Chem* 2021;20. <https://doi.org/10.1016/j.mtchem.2020.100418>.
- [149] Aguayo C, Borges-vilches J, Figueroa T, Fern K. Improved hemocompatibility for gelatin-graphene oxide composite aerogels reinforced with proanthocyanidins for wound dressing applications 2021;206. <https://doi.org/10.1016/j.colsurfb.2021.111941>.
- [150] Zhao X, Zhang Z, Luo J, Wu Z, Yang Z, Zhou S, Tu Y, Huang Y, Han Y, Guo B. Biomimetic, highly elastic conductive and hemostatic gelatin / rGO-based nanocomposite cryogel to improve 3D myogenic differentiation and guide in vivo skeletal muscle regeneration. *Appl Mater Today* 2022;26:101365. <https://doi.org/10.1016/j.apmt.2022.101365>.

- [151] Dudnick R, Martin P, Friedman LS. Management of bleeding ulcers. *Med Clin North Am* 1991;75:947–65. [https://doi.org/10.1016/S0025-7125\(16\)30423-0](https://doi.org/10.1016/S0025-7125(16)30423-0).
- [152] Kaur R, Siegel D, Glick J. Achieving hemostasis in dermatology-Part II: Topical hemostatic agents. *Indian Dermatol Online J* 2013;4:172. <https://doi.org/10.4103/22295178.115509>.
- [153] Howe N, Cherpelis B. Obtaining rapid and effective hemostasis: Part I. Update and review of topical hemostatic agents. *J Am Acad Dermatol* 2013;69:659.e1-659.e17. <https://doi.org/10.1016/j.jaad.2013.07.014>.
- [154] Austin SK. Haemostasis Key points 2021:199–204. <https://doi.org/10.1016/j.mpmed.2021.01.004>.
- [155] Peng HT. Hemostatic agents for prehospital hemorrhage control: A narrative review. *Mil Med Res* 2020;7:1–18. <https://doi.org/10.1186/s40779-020-00241-z>.
- [156] Wong Y, Low JA, Chio MTW. Role of topical tranexamic acid in hemostasis of locally advanced basal cell carcinoma. *JAAD Case Reports* 2016;2:162–3. <https://doi.org/10.1016/j.jdc.2016.03.001>.
- [157] Bartley J. Should chitosan and tranexamic acid be combined for improved hemostasis after sinus surgery? *Med Hypotheses* 2013;81:1036–8. <https://doi.org/10.1016/j.mehy.2013.09.027>.
- [158] Huang L, Liu GL, Kaye AD, Liu H. Advances in Topical Hemostatic Agent Therapies: A Comprehensive Update. *Adv Ther* 2020;37:4132–48. <https://doi.org/10.1007/s12325-020-01467-y>.
- [159] Xi C, Zhu L, Zhuang Y, Wang S, Sun G, Liu Y, Wang D. Experimental Evaluation of Tranexamic Acid-Loaded Porous Starch as a Hemostatic Powder. *Clin Appl Thromb* 2018;24:279–86. <https://doi.org/10.1177/1076029617716770>.
- [160] Sasmal P, Datta P. Tranexamic acid-loaded chitosan electrospun nanofibers as drug delivery system for hemorrhage control applications. *J Drug Deliv Sci Technol* 2019;52:559–67. <https://doi.org/10.1016/j.jddst.2019.05.018>.
- [161] Zhong QK, Wu ZY, Qin YQ, Hu Z, Li SD, Yang ZM, Li P. Preparation and properties of carboxymethyl chitosan/alginate/tranexamic acid composite films. *Membranes (Basel)* 2019;9. <https://doi.org/10.3390/membranes9010011>.
- [162] Bhattacharya SS, Banerjee S, Chowdhury P, Ghosh A, Hegde RR, Mondal R. Tranexamic acid loaded gellan gum-based polymeric microbeads for controlled release: In vitro and in vivo assessment. *Colloids Surfaces B Biointerfaces* 2013;112:483–91. <https://doi.org/10.1016/j.colsurfb.2013.07.054>.
- [163] Saporito F, Sandri G, Rossi S, Bonferoni MC, Riva F, Malavasi L, Caramella C, Ferrari F. Freeze dried chitosan acetate dressings with glycosaminoglycans and tranexamic acid. *Carbohydr Polym* 2018;184:408–17. <https://doi.org/10.1016/j.carbpol.2017.12.066>.
- [164] Koumentakou I, Terzopoulou Z, Michopoulou A, Kalafatakis I. Chitosan dressings containing inorganic additives and levo fl oxacin as potential wound care products with enhanced hemostatic properties. *Int J Biol Macromol* 2020;162:693–703. <https://doi.org/10.1016/j.ijbiomac.2020.06.187>.

- [165] Zhang X, Sun G, Tian M, Wang Y, Qu C, Cheng X, Feng C, Chen X. Mussel-inspired antibacterial polydopamine/chitosan/temperature-responsive hydrogels for rapid hemostasis. *Int J Biol Macromol* 2019;138:321–33. <https://doi.org/10.1016/j.ijbiomac.2019.07.052>.
- [166] Lv C, Li L, Jiao Z, Yan H, Wang Z, Wu Z, Guo M, Wang Y, Zhang P. Improved hemostatic effects by Fe³⁺ modified biomimetic PLLA cotton-like mat via sodium alginate grafted with dopamine. *Bioact Mater* 2021;6:2346–59. <https://doi.org/10.1016/j.bioactmat.2021.01.002>.
- [167] Lammari N, Louaer O, Meniai AH, Fessi H, Elaissari A. Plant oils: From chemical composition to encapsulated form use. *Int J Pharm* 2021;601:120538. <https://doi.org/10.1016/j.ijpharm.2021.120538>.
- [168] Saffarionpour S. One-step preparation of double emulsions stabilized with amphiphilic and stimuli-responsive block copolymers and nanoparticles for nutraceuticals and drug delivery. *JCIS Open* 2021;3:100020. <https://doi.org/10.1016/j.jciso.2021.100020>.
- [169] Ben Djemaa FG, Bellassoued K, Zouari S, El Feki A, Ammar E. Antioxidant and wound healing activity of *Lavandula aspic L.* ointment. *J Tissue Viability* 2016;25:193–200. <https://doi.org/10.1016/j.jtv.2016.10.002>.
- [170] Mahmood H, Khan IU, Asif M, Khan RU, Asghar S, Khalid I, Khalid SH, Irfan M, Rehman F, Shahzad Y, Yousaf AM, Younus A, Niazi ZR, Asim M. In vitro and in vivo evaluation of gellan gum hydrogel films: Assessing the co impact of therapeutic oils and ofloxacin on wound healing. *Int J Biol Macromol* 2021;166:483–95. <https://doi.org/10.1016/j.ijbiomac.2020.10.206>.
- [171] Liakos I, Rizzello L, Scurr DJ, Pompa PP, Bayer IS, Athanassiou A. All-natural composite wound dressing films of essential oils encapsulated in sodium alginate with antimicrobial properties. *Int J Pharm* 2014;463:137–45. <https://doi.org/10.1016/j.ijpharm.2013.10.046>.
- [172] Thayanne J, Araujo C De, Pantoja FDO, Stefany P, Sá F. Effect of Essential Oil of *Rosmarinus officinalis L.* (Rosemary) on the Healing of Cutaneous Lesions in Mice. *J. Chem. Pharm. Res.* 2017;9:381–6.
- [173] Umasankar K, Nambikkairaj B, Backyavathy DM. Effect of Topical Treatment of *Rosmarinus Officinalis* Essential Oil on Wound Healing in Streptozotocin Induced Diabetic Rats 2012;11:1–5.
- [174] Khezri K, Farahpour MR, Mounesi Rad S. Accelerated infected wound healing by topical application of encapsulated Rosemary essential oil into nanostructured lipid carriers. *Artif Cells, Nanomedicine Biotechnol* 2019;47:980–8. <https://doi.org/10.1080/21691401.2019.1582539>.
- [175] Godoi SN De, Quatrin PM, SAGRILLO MR, Nascimento K, Wagner R, Klein B, Santos RCV, Ourique AF. Evaluation of Stability and In Vitro Security of Nanoemulsions Containing *Eucalyptus globulus* Oil 2017;2017.
- [176] Labib RM, Ayoub IM, Michel HE, Mehanny M, Kamil V, Hany M, Magdy M, Moataz A, Maged B, Mohamed A. Appraisal on the wound healing potential of *Melaleuca alternifolia* and *Rosmarinus officinalis L.* Essential oil-loaded chitosan topical preparations. *PLoS One* 2019;14:1–17. <https://doi.org/10.1371/journal.pone.0219561>.

- [177] Kazemi M, Mohammadifar M, Aghadavoud E, Vakili Z, Aarabi MH, Talaei SA. Deep skin wound healing potential of lavender essential oil and licorice extract in a nanoemulsion form: Biochemical, histopathological and gene expression evidences. *J Tissue Viability* 2020;29:116–24. <https://doi.org/10.1016/j.jtv.2020.03.004>.
- [178] Bhalke RD, Kirloskar GV, Bhutada RR, Jagtap NK, Giri MA. Design, Development And Evaluation Of Topical Antiinflammatory Herbal Gel *Int. J. Pharm. Sci. Res.* 2020;11:1467–72. [https://doi.org/10.13040/IJPSR.0975-8232.11\(3\).1467-72](https://doi.org/10.13040/IJPSR.0975-8232.11(3).1467-72).
- [179] Sofi HS, Akram T, Tamboli AH, Majeed A, Shabir N, Sheikh FA. Novel lavender oil and silver nanoparticles simultaneously loaded onto polyurethane nanofibers for wound-healing applications. *Int J Pharm* 2019;569. <https://doi.org/10.1016/j.ijpharm.2019.118590>.
- [180] Manikandan A, Mani MP, Jaganathan SK, Rajasekar R, Jagannath M. Formation of functional nanofibrous electrospun polyurethane and murivenna oil with improved haemocompatibility for wound healing. *Polym Test* 2017;61:106–13. <https://doi.org/10.1016/j.polymertesting.2017.05.008>.
- [181] Manzuoerh R, Farahpour MR, Oryan A, Sonboli A. Effectiveness of topical administration of Anethum graveolens essential oil on MRSA-infected wounds. *Biomed Pharmacother* 2019;109:1650–8. <https://doi.org/10.1016/j.biopha.2018.10.117>.
- [182] García-Salinas S, Evangelopoulos M, Gámez-Herrera E, Arruebo M, Irusta S, Taraballi F, et al. Electrospun anti-inflammatory patch loaded with essential oils for wound healing. *Int J Pharm* 2020;577:119067. <https://doi.org/10.1016/j.ijpharm.2020.119067>.
- [183] Pivetta TP, Simões S, Araújo MM, Carvalho T, Arruda C, Marcato PD. Development of nanoparticles from natural lipids for topical delivery of thymol: Investigation of its anti-inflammatory properties. *Colloids Surfaces B Biointerfaces* 2018;164:281–90. <https://doi.org/10.1016/j.colsurfb.2018.01.053>.
- [184] Alam P, Ansari MJ, Anwer MK, Raish M, Kamal YKT, Shakeel F. Wound healing effects of nanoemulsion containing clove essential oil. *Artif Cells, Nanomedicine Biotechnol* 2017;45:591–7. <https://doi.org/10.3109/21691401.2016.1163716>.
- [185] Biranje SS, Madiwale P V., Patankar KC, Chhabra R, Bangde P, Dandekar P, Adivarekar RV. Cytotoxicity and hemostatic activity of chitosan/carrageenan composite wound healing dressing for traumatic hemorrhage. *Carbohydr Polym* 2020;239:116106. <https://doi.org/10.1016/j.carbpol.2020.116106>.
- [186] Chen J, Ai J, Chen S, Xu Z, Lin J, Liu H, Chen Q. Synergistic enhancement of hemostatic performance of mesoporous silica by hydrocaffeic acid and chitosan. *Int J Biol Macromol* 2019;139:1203–11. <https://doi.org/10.1016/j.ijbiomac.2019.08.091>.
- [187] Neuffer MC, McDivitt J, Rose D, King K, Cloonan CC, Vayer JS. Hemostatic dressings for the first responder: A review. *Mil Med* 2004;169:716–20. <https://doi.org/10.7205/MILMED.169.9.716>.
- [188] Aydemir Sezer U, Kocer Z, Aru B, Demirel GY, Gulmez M, Aktekin A, Ozkara S, Sezer S. Combination of gelatin and tranexamic acid offers improved haemostasis and safe use on internal hemorrhage control. *RSC Adv* 2016;6:95189–98. <https://doi.org/10.1039/c6ra16790j>.

- [189] Spotnitz WD, Burks S. Hemostats, sealants, and adhesives III: A new update as well as cost and regulatory considerations for components of the surgical toolbox. *Transfusion* 2012;52:2243–55. <https://doi.org/10.1111/j.1537-2995.2012.03707.x>.
- [190] Burnett LR, Richter JG, Rahmany MB, Soler R, Steen JA, Orlando G, Abouswareb T, Van Dyke ME. Novel keratin (KeraStat™) and polyurethane (Nanosan®-Sorb) biomaterials are hemostatic in a porcine lethal extremity hemorrhage model. *J Biomater Appl* 2014;28:869–79. <https://doi.org/10.1177/0885328213484975>.
- [191] Wang Y, Zhao Y, Qiao L, Zou F, Xie Y, Zheng Y, Chao Y, Yang Y, He W, Yang S. Cellulose fibers-reinforced self-expanding porous composite with multiple hemostatic efficacy and shape adaptability for uncontrollable massive hemorrhage treatment. *Bioact Mater* 2021;6:2089–104. <https://doi.org/10.1016/j.bioactmat.2020.12.014>.
- [192] Escobar-Chávez JJ, López-Cervantes M, Naik A, Kalia YN, Quintanar-Guerrero D, GanemQuintanar A. Applications of thermo-reversible pluronic F-127 gels in pharmaceutical formulations. *J Pharm Pharm Sci* 2006;9:339–58.
- [193] Nkazi BD, Neuse EW, Sadiku ER, Aderibigbe BA. Synthesis, Characterization and Kinetic Release Profile of Iron Containing Polymeric Co-conjugates with Antiproliferative Activity. *J Inorg Organomet Polym Mater* 2014;24:302–14. <https://doi.org/10.1007/s10904-013-9968-9>.
- [194] Haidar ZS. Mathematical modeling for pharmacokinetic predictions from controlled drug release nano systems: A comparative parametric study. *Biomed Pharmacol J* 2018;11:1801–6. <https://doi.org/10.13005/bpj/1552>.
- [195] Naseri S, Lepry WC, Nazhat SN. Bioactive glasses in wound healing: Hope or hype? *J Mater Chem B* 2017;5:6167–74. <https://doi.org/10.1039/c7tb01221g>.
- [196] Yadav HK, Halabi A, Alsalloum NA. Nanogels as Novel Drug Delivery Systems-A Review. *J Pharm Pharm Res* 2017;1:5.
- [197] de Cassia K, de Almeida Silva F, Calomino MA, Deutsch G, de Castilho SR, de Paula GR, Esper LMR, Teixeira LA. Molecular characterization of multidrug-resistant (MDR) *Pseudomonas aeruginosa* isolated in a burn center. *Burns* 2017;43:137-143.
- [198] Nagoba BS, Selkar SP, Wadher BJ, Gandhi RC. Acetic acid treatment of pseudomonal wound infections — A review. *J Infect Public Health* 2013;6:410-415.
- [199] Ruffin M, Brochiero E. Repair Process Impairment by *Pseudomonas aeruginosa* in Epithelial Tissues: Major Features and Potential Therapeutic Avenues. *Front Cell Infect Microbiol* 2019;9:1-18.
- [200] Raizman R, Little W, Smith AC. Rapid Diagnosis of *Pseudomonas aeruginosa* in Wounds with Point-of-Care Fluorescence Imaging. *Diagnostics* 2021;11:1-13.
- [201] Wang G, Li Z, Li T, Wang S, Zhang L, Zhang L, Tang P. Negative-Pressure Wound Therapy in a *Pseudomonas aeruginosa* Infection Model. *Biomed Res Int* 2018:1-11.
- [202] Serrs R, Grande R, Butrico L, Rossi A, Settimio UF, Caroleo B, Amato B, Gallelli L, de Francis S. Chronic wound infections: the role of *Pseudomonas aeruginosa* and *Staphylococcus aureus*. *Expert Rev Anti Infect Ther* 2015:1-9.

- [203] Buyana B, Aderibigbe BA, Ray SS, Ndinteh DT, Theirry FY. Development, Characterization and *In Vitro* Evaluation of Water soluble Poloxamer/Pluronic-Mastic gum-Gum Acacia-based Wound Dressins. *J Appl Polym Sci* 2019;137:48728.
- [204] Yakota M, Haffner N, Kassier M, Brunner M, Shambat SM, Brennecke F, Schniering J, Maggio EM, Distler O, Zinkernagel AS, Maurer B. Staphylococcus aureus impairs dermal fibroblast functions with deleterious effects on wound healing. *FASEB J* 2021:1-16.
- [205] Ekawati ER, Darmanto W, Wahyuningsih SPA. Detection of Staphylococcus aureus in wound infection on the skin surface. *IOP Conf Ser: Eerth Environ Sci* 2020;456:1-5.



University of Fort Hare
Together in Excellence

Chapter 3

3. MATERIALS

3.1. Solvents and Reagents

Distilled water was used to prepare the topical gels. The materials used (alginate, carbopol 940, methylparaben, propylene glycol, sodium hydroxide, potassium hydroxide, triethylamine, graphene oxide (GO) (carbon content 42.0-52.0 %), reduced graphene oxide (rGO) (carbon content >75%), and tranexamic acid (TA) (grade: pharmaceutical secondary standards) were all purchased from Sigma Aldrich, South Africa. They were all used without further purification. Sodium dihydrogen phosphate (NaH_2PO_4), trisodium citrate, silver nitrate (AgNO_3), magnesium chloride (MgCl_2), ferrous sulfate heptahydrate ($\text{FeSO}_4 \cdot 7\text{H}_2\text{O}$), and Zinc chloride (ZnCl_2), with $\geq 95\%$ purity, were purchased from Associated Chemical Enterprises (ACE).

3.2. EXPERIMENTAL

3.2.1. Preparation of Ag nanoparticles

The nanoparticles were prepared according to the Turkevich method [1]. Sixty millilitres of 1 mM AgNO_3 solution was boiled and covered with a watch glass on a hot plate. The solution was stirred using a magnetic stirrer bar, and then 6 mL of 10 mM trisodium citrate was added dropwise per second to the boiling solution. When the solution was light yellow, it was removed from the hot plate, allowed to cool, and then stored in the fridge at 4 °C.



3.2.2. Preparation of ZnO nanoparticles

The zinc oxide nanoparticles were prepared according to the procedure reported by Jyoti *et al.* [2]. Distilled water (50 mL) was used to dissolve zinc chloride (2.75g) in a beaker. The resultant solution was stirred at 90 °C until the zinc chloride was completely dissolved in the distilled water. A solution of sodium hydroxide (8 mL of 5 M) was added to the solution of zinc chloride dropwise with constant stirring. A milky white colloid was formed without the formation of precipitation. The reaction was allowed to stir for 2 hours after the complete addition of sodium hydroxide. After 2 hours of stirring, the reaction was then allowed to cool the supernatant solution was removed with 5 mL of distilled water 5 times. After complete washing, the zinc nanoparticles were dried at 100 °C in an oven for 30 minutes resulting in white powder.

3.2.3. Preparation of MgO nanoparticles

Magnesium oxide nanoparticles were prepared according to a procedure reported by Chandrappa *et al.* [3]. Magnesium chloride (203.3 mg) was dissolved in 50 mL of ethanol and that was labelled as reaction (A). Sodium hydroxide pellets (80 mg) were also dissolved in a separate beaker containing 50 mL of ethanol (reaction B). Both solutions (A & B) were stirred at 60 °C for about 30 min and then B was added dropwise to the solution, A under vigorous stirring. The mixture was stirred at 60 °C for another 10 min, 20 mL of ethanol was then added to dilute the mixture with constant stirring. The resultant solution was centrifuged at 2000 rpm for 10 min. The pellet obtained was dried at 60 °C and then at 300 °C (calcined) for 1h, to obtain MgO NPs.

3.2.4. Preparation of Fe₃O₄ Nanoparticles

Iron oxide nanoparticles were prepared based on the method presented by Fatima and co-workers [4]. A solution of FeSO₄•7H₂O (0.2780 g) was prepared in 5 mL ethylene glycol to form a homogenous solution. Then KOH (0.5 M) was dissolved in 8 mL of ethanol in a separate beaker, and then this solution was added dropwise to the first solution with constant stirring to get a homogenous solution. The resultant solution was then put at 200 °C for 24 h and a black solid product obtained was separated using a magnet. The magnet-separated particles were washed with ethanol or water and were dried at 40 °C for 6 h.

University of Fort Hare
Together in Excellence

3.2.5. Preparation of topical gels

The topical gel formulations were prepared according to **Tables 5-7**. A ratio of 1:1 was used to prepare the topical gels in 10 mL distilled water, with continuous stirring at 200-600 rpm for 2 h or until a clear gel was formed at room temperature. Methylparaben was also added and used as a preservative for the gels. The required quantities of TA, nanoparticles and EOs were added to the prepared gels and continued stirring for 20 minutes. Triethylamine was used to adjust the pH of the gels to neutral and propylene glycol was used as a penetration enhancer. The prepared gel formulations were stored at 4°C prior to further characterization.

Table 5: Formulations used to prepare SA-based topical gels

Code	Polymers		Drug		NPs					Distilled water (mL)
	SA	Carbopol	TA	Ag	GO	MgO	rGO	ZnO	Fe ₃ O ₄	

X1	100 mg	100 mg	-	-	-	-	-	-	-	10
X2	100 mg	100 mg	70 mg	-	-	-	-	-	-	10
X3	100 mg	100 mg	70 mg	-	-	-	-	-	50 mg	10
X4	100 mg	100 mg	70 mg	-	-	50 mg	-	-	-	10
X5	100 mg	100 mg	70 mg	-	-	-	-	50 mg	-	10
X6	100 mg	100 mg	70 mg	1 mL	-	-	-	-	-	10
X7	100 mg	100 mg	70 mg	-	50 mg	-	-	-	-	10
X8	100 mg	100 mg	70 mg	-	-	-	20 mg	-	-	10
X9	100 mg	100 mg	-	-	-	-	-	-	50 mg	10
X10	100 mg	100 mg	-	-	-	50 mg	-	-	-	10
X11	100 mg	100 mg	-	-	-	-	-	50 mg	-	10
X12	100 mg	100 mg	-	1 mL	-	-	-	-	-	10
X13	100 mg	100 mg	-	-	50 mg	-	-	-	-	10
X14	100 mg	100 mg	-	-	-	-	20 mg	-	-	10



Table 6: Formulations used to prepare SA/EO-based topical gels

Code	Polymers		Drug		Essential oils			NPs	Distilled water (mL)
	SA	Carbopol	TA	Lav	Rose	Euc	Fe ₃ O ₄		
SA/Rose	100 mg	100 mg	-	-	2 mL	-	-	10	
SA/Euc	100 mg	100 mg	-	-	-	2 mL	-	10	
SA/Lav	100 mg	100 mg	-	2 mL	-	-	-	10	
SA/Rose/Fe₃O₄	100 mg	100 mg	-	-	2 mL	-	30 mg	10	
SA/Euc/Fe₃O₄	100 mg	100 mg	-	-	-	2 mL	30 mg	10	
SA/Lav/Fe₃O₄	100 mg	100 mg	-	2 mL	-	-	30 mg	10	
SAT/Euc/Fe₃O₄	100 mg	100 mg	70 mg	-	-	2 mL	30 mg	10	
SAT/Rose/Fe₃O₄	100 mg	100 mg	70 mg	-	2 mL	-	30 mg	10	
SAT/Lav/Fe₃O₄	100 mg	100 mg	70 mg	2 mL	-	-	30 mg	10	

Table 7: Formulations used to prepare CMC-based topical gels

Code	Polymers (mg)	Drug	NPs (mg)
------	---------------	------	----------

	CMC	Carbopol	TA (mg)	Ag	GO	MgO	rGO	ZnO	Fe ₃ O ₄	Distilled water (mL)
CMC	100	100	-	-	-	-	-	-	-	10
CMC/TA	100	100	70	-	-	-	-	-	-	10
CMC/TA/Fe₃O₄	100	100	70	-	-	-	-	-	50	10
CMC/TA/MgO	100	100	70	-	-	50	-	-	-	10
CMC/TA/ZnO	100	100	70	-	-	-	-	50	-	10
CMC/TA/Ag	100	100	70	1 mL	-	-	-	-	-	10
CMC/TA/GO	100	100	70	-	50	-	-	-	-	10
CMC/TA/rGO	100	100	70	-	-	-	20	-	-	10

3.3. CHARACTERIZATION

3.3.1. Fourier Transform Infrared Spectroscopy (FTIR)

FTIR was performed on an FTIR spectrometer (Spectrum Two) PerkinElmer on the topical gels. The spectra were recorded in the range of 4000-500 cm⁻¹ and analysed using OMNIC software.

3.3.2. Spreadability

Spreadability was used to determine the rate at which the gels can be spread throughout the wound. 0.1 g or an initial gel diameter of 1-1.3 cm gel was placed in round glass slides on a flat surface and a second glass slide was carefully placed on top of the slide containing the gel. A known mass was placed on top of the two glass slides for about 10 min and the spreadability was determined in cm [5–9].

3.3.3. Viscosity

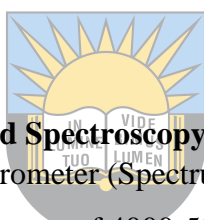
Brookfield viscometer (DV-1) was used to determine the viscosity (cP) of the prepared topical gel formulations. Spindle 63 (LV3) was rotated at a speed of 50 rpm. The reading was recorded at 1 and 2-minute time intervals, and the samples were measured at 25 °C.

3.3.4. pH evaluation & stability studies

The pH of the topical gel formulations was evaluated using pH strips and a digital pH meter.

3.3.5. X-ray Diffraction (XRD)

XRD thermographs were reported on a Bruker D8 Discover equipped with a proportional counter using Cu-K α radiation. Data were collected within the range of 2 θ =5-80°, scanning



University of Fort Hare
Together in Excellence

at $1.5^\circ \text{ min}^{-1}$ with a time constant filter of 0.38s per step and 6.0 mm slit width. Samples were mounted on a slide with a silicone wafer [10]. The X-ray diffraction data were handled using the Profex program (evaluation curve fitting). It was used to study the crystalline nature of synthesized nanoparticles, and the Debye–Scherrer equation was used to calculate the particle size using the high-intensity peaks [11].

$$D = \frac{0.9\lambda}{\beta \cos\theta} \quad \text{(Equation 1)}$$

3.3.6. Scanning Electron Microscope (SEM)

The SEM was used to evaluate the surface morphology and elemental composition of the nanoparticles. The samples were solidified and coated with gold. It was performed on a JEOL (JSM- 6390 LV) Scanning Electron Microscope, Japan, at an accelerating voltage of 15 kV.

3.3.7. *In vitro* drug release kinetics

The drug release profile of the topical gels was evaluated at pH 7.4 and 37 °C. Fifty milligrams of the topical gel loaded with Ag, Fe₃O₄, MgO, ZnO nanoparticles, rGO, GO and TA were placed in 10 mL of buffer solution of pH 7.4. The dissolved solution was transferred to a dialysis membrane, and the membrane was placed in a vial containing 40 mL of pH 7.4 buffer solution. The vial was then placed in a shaking incubator at 37 °C. At 5, 10, 15, 20, 25 30, 45, and 60 min intervals the release media was collected and replaced with a fresh buffer then was collected per hr. The release of Ag, Fe₃O₄, MgO, ZnO nanoparticles, rGO, GO and TA from the topical gels was evaluated using UV-vis spectroscopy at a UV wavelength of 424 nm, 303 nm, 282 nm, 271 nm, 263 nm, 267 nm and 266 nm, respectively, see **Appendix**. All the obtained data were expressed as % cumulative drug release. The concentration of Ag, Fe₃O₄, MgO, ZnO nanoparticles, rGO, GO and TA released from the topical gels was evaluated by the application of a calibration curve and plotted as % drug release against time. All the measurements were carried out in triplicate for each topical gel. The percentage of drug release was calculated using the following equation [12].

$$\% \text{ drug release} = \frac{\text{amount drug released}}{\text{amount drug loaded}} \times 100 \quad \text{(Equation 2)}$$

Selected release models were used to determine the release mechanisms of Ag, Fe₃O₄, MgO, ZnO nanoparticles, rGO, GO and TA from the topical gels. The release of drugs from the gels was evaluated by Higuchi, Zero order, First order, and Korsmeyer-Peppas equations.

3.3.8. *In vitro* antibacterial analysis

The antibacterial evaluation was conducted to determine the effectiveness of the wound dressings against selected bacterial strains. Three controls were used, streptomycin (STM), ampicillin (AMP), and nalidixic acid (NLD) with their MIC against different bacteria strains (Table 8). MIC of the studied compounds was carried out following Fonkui *et al.* [13]. Stock solutions were prepared by dissolving 4 mg of each gel in 5 mL of a mixture of DMSO and dH₂O (4:1, v/v). These solutions were then serially diluted (6 times) in 100 μ L of Muller-Hinton nutrient broth in 96 well plates to the desired concentrations (400, 200, 100, 50, 25 and 12.5 μ g/mL). Then after, 100 μ L of each of these solutions was placed in duplicate and seeded with 100 μ L of an overnight bacterial culture brought to 0.5 Mc Farland in nutrient broth. Streptomycin, ampicillin and nalidixic acid were used as positive control and negative control was prepared to contain 50% nutrient broth in DMSO.

Table 8: Different bacterial strains used in the *in vitro* antibacterial studies

	code
<i>Bacillus subtilis</i> (ATCC19659)	BS
<i>Enterococcus faecalis</i> (ATCC13047)	EF
<i>Mycobacterium smegmatis</i> (MC2155)	MS
<i>Staphylococcus epidermidis</i> (ATCC14990)	SE
<i>Escherischia coli</i> (ATCC25922)	EC
<i>Enterobacter cloacae</i> (ATCC13047)	ECL
<i>Klebsiella oxytoca</i> (ATCC8724)	KO
<i>Proteus vulgaris</i> (ATCC6380)	PV
<i>Pseudomonas aeruginosa</i> (ATCC27853)	PA
<i>Proteus mirabilis</i> (ATCC7002)	PM
<i>Staphylococcus aureus</i> (ATCC25923)	SA
<i>Klebsiella pneumonia</i> (ATCC13882)	KP

3.3.9. Whole blood clot assay

The *in vitro* haemostasis analysis was performed according to the procedure described by Catanzano *et al.* [14]. A two-tailed *t*-test using GraphPad by Dotmatics was used to evaluate the significant difference between the formulations and the control. The wound dressing (10mg) was immersed with 200 μ L of the whole blood and the gel was placed in 15 mL tubes.

Blood coagulation on the formulations after covering was activated by adding 20 μL of CaCl_2 . The wound dressings were then further incubated in a thermostatic incubator for 10 minutes at 37°C with gentle shaking. Deionized water (6 mL) was used to haemolyse the Red Blood Cells (RBCs) that were not trapped in the clot. The deionized water was added inside the wall of the tubes by dripping. A spectrophotometer was used to measure the relative absorbance (A) of the blood samples that were diluted to 25 mL at a wavelength of 540 nm [14].

3.3.10. Cytotoxicity evaluation

The *in vitro* cytotoxicity of the wound dressings was performed to evaluate the biocompatibility of the developed topical gels employing the MTT assay. The gels were screened against HaCaT cells (immortalized human keratinocytes) which were seeded at a density of 5×10^4 cells/mL in 96-well plates at a volume of 90 μL per well. Twenty-four hours later, the cells were treated in triplicates with 10 μL of gel solution per sample, making final concentrations of 200, 100, 50, 25, and 12.5 $\mu\text{g}/\text{mL}$. Cells treated with $1 \times \text{PBS}$ and 10% DMSO served as the negative and positive controls, respectively. The 96-well plates were incubated for 48 h after which MTT reagent was added, the plates were incubated for 4 h, solubilized overnight using DMSO, and the absorbance values were measured at 570 nm [8]. The experiments were run in triplicate three times. The cytotoxicity results of the wound dressings were analysed by calculating the percentage cell viability of each gel against untreated cells using:

$$\% \text{ Cell viability} = \frac{(\text{OD}_s - \text{OD}_c)}{(\text{OD}_u - \text{OD}_c)} \times 100 \quad \text{(Equation 3)}$$

Where OD_s is the absorbance of the test compound and OD_c is the absorbance of the control. OD_u is the absorbance of the untreated cells.

3.3.11. Wound healing assay

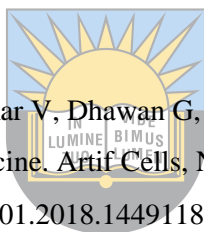
In vitro wound healing assay was evaluated based on a procedure adapted from Felice *et al.*, Suarez-Arnedo *et al.*, Cheng *et al.*, and Ranzato *et al.* [15–18]. Immortalized human keratinocyte (HaCaT) cells were cultured in a humidified incubator at 37°C and 5% CO_2 to 90% confluency in DMEM containing 10% (v/v) fetal bovine serum (FBS) and 1% (v/v) penicillin-streptomycin (Penstrep) antibiotics. The cells were then trypsinized and viable cells were quantified using the trypan blue dye elimination method. The cell density was adjusted to 2.5×10^5 cells/mL and the cells were seeded in 6-well plates until cell monolayers were formed (48 hours later). Single scratch wounds per well were generated using a 200 μL micropipette tip. The cells were then washed once per well with 2 mL of $1 \times$ phosphate-buffered saline ($1 \times \text{PBS}$) to remove dislodged cells. Serum-poor DMEM medium (containing 1% FBS) was added to the wells

(1800 μL per well) and cells were treated with 200 μL of the reported topical gels of various concentrations that showed the highest viability on the MTT assay screen. Untreated cells cultured in Dulbecco's Modified Eagle's Medium (DMEM) containing 10% FBS were used as positive control while those cultured in 1% FBS in DMEM were used as the negative control. The Images were captured in duplicates at 0, 24, 48, 72, and 96 hours using the 4 \times objective and phase-contrast feature of an inverted light microscope (Olympus CKX53, Olympus, Tokyo, Japan). Cell migration was quantified using ImageJ image processing software [18]. Wound closure was calculated using the following equation [19]:

$$\% \text{wound closure} = \frac{\text{wound area day 0} - \text{wound closure day 96}}{\text{wound closure day 0}} \times 100 \quad \text{(Equation 4)}$$

3.3.12. Statistical analysis

The data obtained from the in vitro studies were evaluated via Student's unpaired t-test on GraphPad Prism version 9 (GraphPad Software, Inc., San Diego, CA, USA). The data obtained are expressed as mean \pm standard deviation, in triplicate (n=3) and a *p*-value \leq 0.05 is considered significant.



References

- [1] Chugh H, Sood D, Chandra I, Tomar V, Dhawan G, Chandra R. Role of gold and silver nanoparticles in cancer nano-medicine. *Artif Cells, Nanomedicine Biotechnol* 2018;46:1210–20. <https://doi.org/10.1080/21691401.2018.1449118>.
- [2] Jyoti M, Vijay D, Radha S. To Study the Role of Temperature and Sodium Hydroxide Concentration in the Synthesis of Zinc Oxide Nanoparticles. *Int J Sci Res Publ* 2013;3:2250–3153.
- [3] G CK, M PB. Generation of Nanostructured MgO Particles by Solution Phase Method Polymer blends View project electrodeposition of alloys View project 2015.
- [4] Fatima H, Lee DW, Yun HJ, Kim KS. Shape-controlled synthesis of magnetic Fe₃O₄ nanoparticles with different iron precursors and capping agents. *RSC Adv* 2018;8:22917–23. <https://doi.org/10.1039/c8ra02909a>.
- [5] Buyana B, Aderibigbe BA, Ndinteh DT, Fonkui YT, Kumar P. Alginate-pluronic topical gels loaded with thymol, norfloxacin and ZnO nanoparticles as potential wound dressings. *J Drug Deliv Sci Technol* 2020;60:101960. <https://doi.org/10.1016/j.jddst.2020.101960>.
- [6] Metwally F. Evaluation of Topical Gel Bases Formulated with Various Essential Oils for Antibacterial Activity against Methicillin- Resistant Staphylococcus Aureus 2013;12:877–84.

- [7] Choudhary M, Chhabra P, Tyagi A, Singh H. Scar-free healing of full-thickness diabetic wounds: A unique combination of silver nanoparticles as antimicrobial agent, calcium alginate nanoparticles as hemostatic agent, fresh blood as nutrient/growth factor supplier and chitosan as base matrix. *Int J Biol Macromol* 2021;178:41–52. <https://doi.org/10.1016/j.ijbiomac.2021.02.133>.
- [8] Khan AW, Kotta S, Ansari SH, Sharma RK, Kumar A, Ali J. Formulation development, optimization and evaluation of aloe vera gel for wound healing. *Pharmacogn Mag* 2013;9:S6–10. <https://doi.org/10.4103/0973-1296.117849>.
- [9] Siang R, Teo SY, Lee SY, Basavaraj AK, Koh RY, Rathbone MJ. Formulation and evaluation of topical pentoxifylline-hydroxypropyl methylcellulose gels for wound healing application. *Int J Pharm Pharm Sci* 2014;6:535–9.
- [10] Ngece K, Aderibigbe BA, Ndinteh DT, Fonkui YT, Kumar P. Alginate-gum acacia based sponges as potential wound dressings for exuding and bleeding wounds. *Int J Biol Macromol* 2021;172:350–9. <https://doi.org/10.1016/j.ijbiomac.2021.01.055>.
- [11] Choudhary M, Chhabra P, Tyagi A, Singh H. Scar free healing of full thickness diabetic wounds: A unique combination of silver nanoparticles as antimicrobial agent, calcium alginate nanoparticles as hemostatic agent, fresh blood as nutrient/growth factor supplier and chitosan as base matrix. *Int. J. Biol. Macromol* 2021;17:41–52.
- [12] Fu R, Li C, Yu C, Xie H, Shi S, Li Z, et al. A novel electrospun membrane based on moxifloxacin hydrochloride/poly(vinyl alcohol)/sodium alginate for antibacterial wound dressings in practical application. *Drug Deliv* 2016;23:828–39. <https://doi.org/10.3109/10717544.2014.918676>.
- [13] Fonkui TY, Ikhile MI, Muganza M, Fotsing MCD, Arderne C, Siwe-Noundou X, et al. Synthesis, Characterization and Biological Applications of Novel Schiff Bases of 2(Trifluoromethoxy)aniline. *J Chin Pharm Sci* 2018;27:307–323.
- [14] Catanzano O, D'Esposito V, Formisano P, Boateng JS, Quaglia F. Composite AlginateHyaluronan Sponges for the Delivery of Tranexamic Acid in Postextractive Alveolar Wounds. *J Pharm Sci* 2018;107:654–61. <https://doi.org/10.1016/j.xphs.2017.09.026>.
- [15] Felice F, Zambito Y, Belardinelli E, Fabiano A, Santoni T, Stefano R Di. International Journal of Biological Macromolecules Effect of different chitosan derivatives on in vitro scratch wound assay : A comparative study. *Int J Biol Macromol* 2015;76:236–41. <https://doi.org/10.1016/j.ijbiomac.2015.02.041>.
- [16] Suarez-arnedo A, Figueroa FT, Clavijo C, Arbela P, Cruz JC, Munoz-Camargo C. An image J plugin for the high throughput image analysis of in vitro scratch wound healing assays. *PLoS One* 2020;15:e0232565. <https://doi.org/10.1371/journal.pone.0232565>.

- [17] Cheng Y, Hu Z, Zhao Y, Zou Z, Lu S, Zhang B, et al. Sponges of Carboxymethyl Chitosan Grafted with Collagen Peptides for Wound Healing. *Int J Mol Sci* 2019;20:3890.
- [18] Ranzato E, Patrone M, Mazzucco L, Burlando B. Platelet lysate stimulates wound repair of HaCaT keratinocytes. *Br J Dermatol* 2008;159:537–45.
- [19] Ramya Devi D, Sowmiya Lakshna S, Veena Parvathi S, Vedha Hari BN. Investigation of wound healing effect of topical gel of Albizia amara leaves extract. *South African J Bot* 2018;119:400–9. <https://doi.org/10.1016/j.sajb.2018.10.005>.



University of Fort Hare
Together in Excellence

Chapter 4

4. RESULTS AND DISCUSSION

4.1. Fourier-Transform Infrared Spectroscopy (FTIR)

4.1.1. Fourier-Transform Infrared Spectroscopy of SA-based gels

The FTIR spectra of the prepared SA-based topical gels are shown in **Figures 5–10** below. The topical gels containing TA and nanoparticles were compared with the ones containing only nanoparticles. Similar characteristic peaks were observed for all the prepared topical gels, which can be attributed to the similar polymer composition used in their preparation. The spectra also showed that the nanoparticles, or TA, did not interact with the polymer network. The FTIR of all the prepared topical gels revealed absorption bands at 3310 cm^{-1} for O-H stretch, 1637 cm^{-1} for C=O stretch, and 1042 cm^{-1} for C-O stretch. Similar peaks were reported for alginate-based topical gels, which further confirmed the successful preparation of the gel formulations [1,2]. Pure SA powder revealed C=O stretch at 1604 cm^{-1} , O-H carboxylic group peaks at 3302 cm^{-1} , C-O stretch at 1026 cm^{-1} , and C-H stretch at 2936 cm^{-1} . The O-H stretch in the prepared topical gel confirmed the successful interaction of the polymers, SA and carbopol. The C-O stretch further confirmed an interaction between SA and carbopol. The FTIR spectrum of TA revealed absorption signals at 2936 cm^{-1} , 2830 cm^{-1} , 2959 cm^{-1} , 2205 cm^{-1} , 1651 cm^{-1} , 1549 cm^{-1} , 1379 cm^{-1} , and 1041 cm^{-1} , which are attributed to the O-H stretch carboxylic group, C-H stretch, C=O stretch, and C-O stretch, respectively. The FTIR spectra of the nanoparticles and rGO are shown as supplementary figures. The FTIR spectra of iron oxide nanoparticles revealed a characteristic peak of Fe-O stretch at 661 cm^{-1} . The peak at 661 cm^{-1} is attributed to the Fe-O stretching of iron oxide, and similar peaks have been reported between $620\text{--}660\text{ cm}^{-1}$ for maghemite nanoparticles [3,4]. The FTIR spectra of magnesium oxide nanoparticles displayed a characteristic peak of Mg-O vibration at 873 cm^{-1} , revealing the formation of hexagonal nanoparticles [5]. Zinc oxide nanoparticles also showed a characteristic peak of Zn-O stretching at 699 cm^{-1} [6]. FTIR spectra for the nanoparticles are presented in **Appendix**.

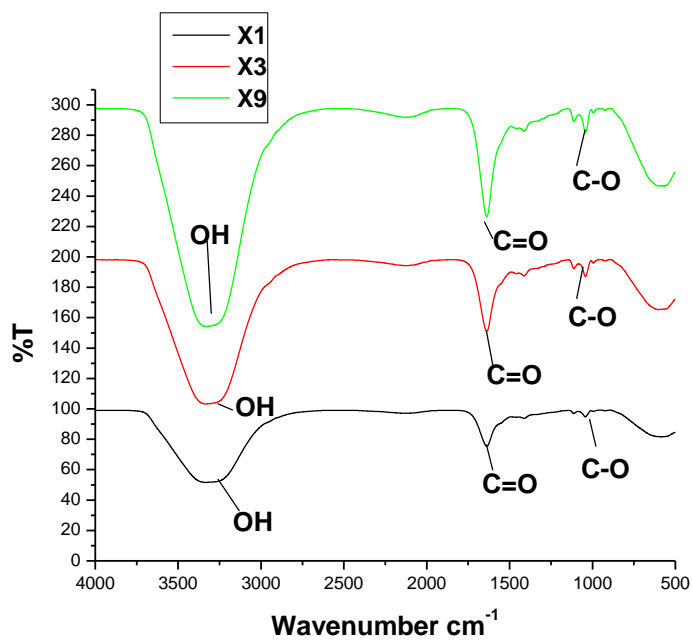


Figure 5: FTIR spectra of X1, X3 and X9

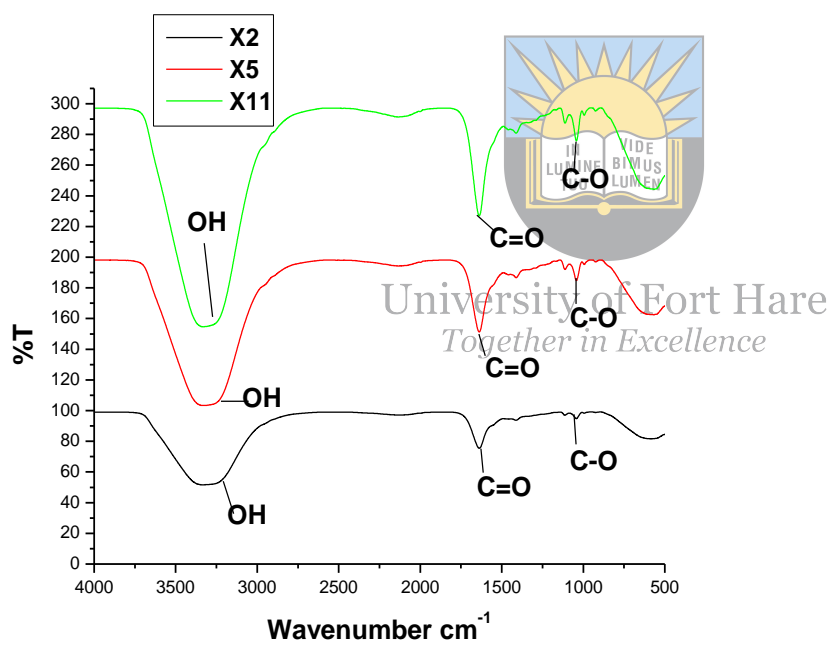


Figure 6: FTIR spectra of topical gels X2, X5, and X11

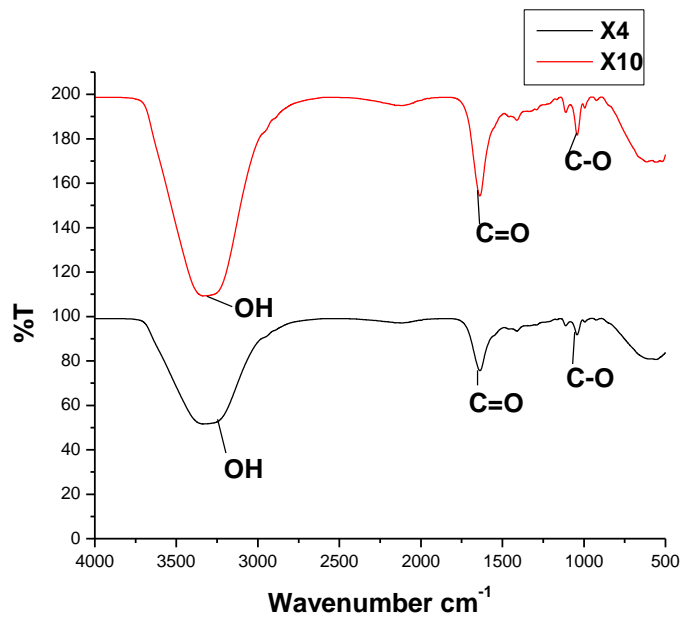


Figure 7: FTIR spectra of topical gels X4 and X10

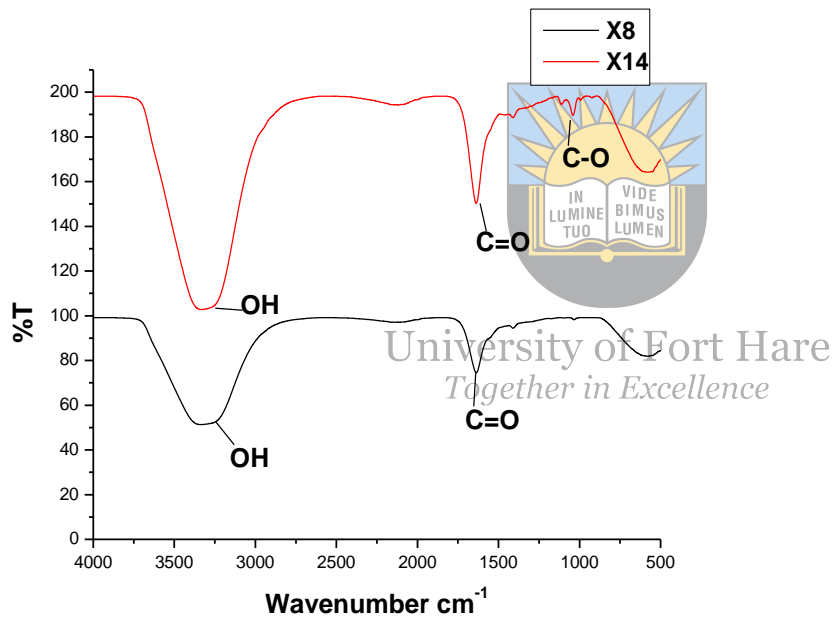


Figure 8: FTIR spectra of topical gels X8 and X14

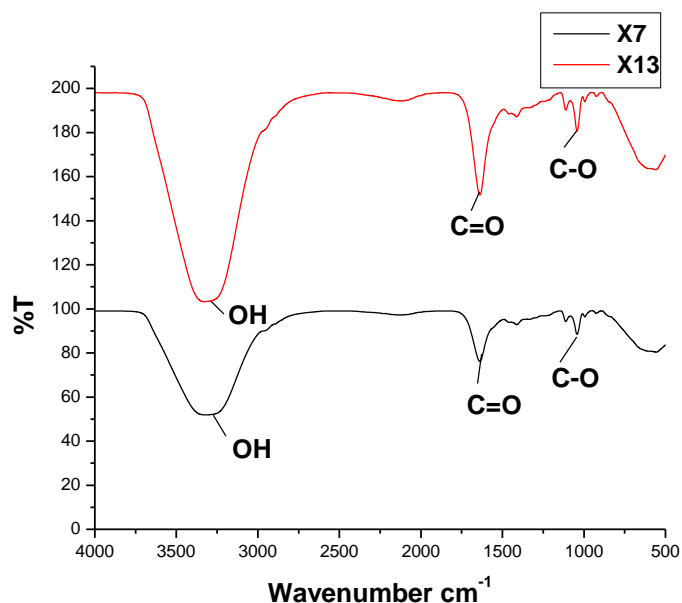


Figure 9: FTIR spectra of topical gels X7 and X13

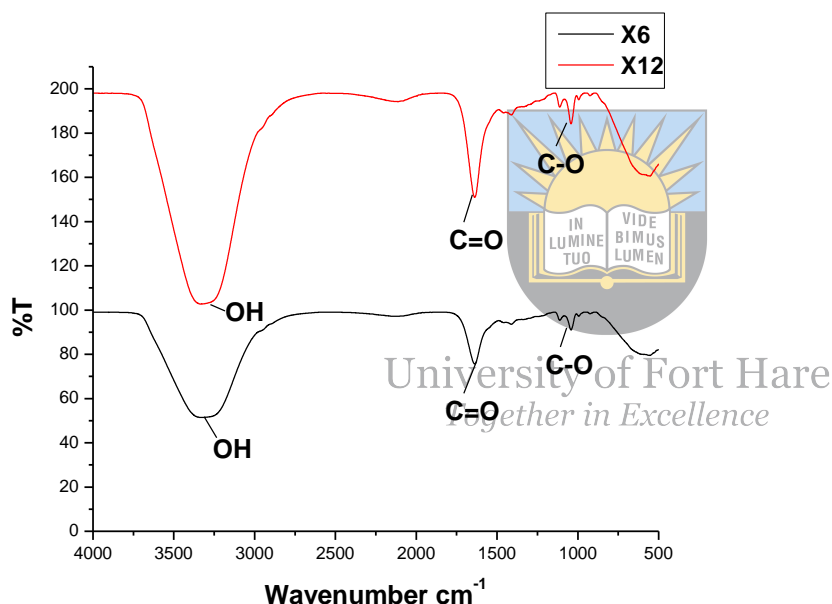


Figure 10: FTIR spectra of topical gels X6 and X12

4.1.2. Fourier-Transform Infrared Spectroscopy of SA/EO-based gels

Gel formulations of SA/Euc exhibited prominent characteristic peaks, as shown in **Figures 11a and b** below. **Euc-EO** showed a sharp vibration bend at 2948 cm^{-1} attributed to asymmetrical and symmetrical bending of C–H stretching [7]. The vibration bends at 968 cm^{-1} , $1079\text{--}1203\text{ cm}^{-1}$, and 1354 cm^{-1} correspond to the symmetrical bending of the CH_2 plane, C–O–C stretching, and C–O–H deformation, indicating the presence of 1,8-cineol and citronella the active compounds of eucalyptus oil. As in lavender oil-containing formulations, there was also no major difference between **SA/Euc**, **SA/Euc/Fe₃O₄**, and **SAT/Euc/Fe₃O₄** gel formulations. The presence of eucalyptus oil components was retained in all the formulations, with major

characteristic peaks visible at 968 cm^{-1} , $1079\text{--}1203\text{ cm}^{-1}$, 1354 cm^{-1} , and 2948 cm^{-1} related to the CH_2 plane, asymmetric C-O-C stretching, C-O-H deformation, and C-H symmetric bending, respectively. Additionally, a broad vibrational bend was observed at 3457 cm^{-1} constituting the O-H bending present in alginate. Hydrophobic interaction and hydrogen bonding were the main non-covalent bonds between eucalyptus oil and alginate gel [8].

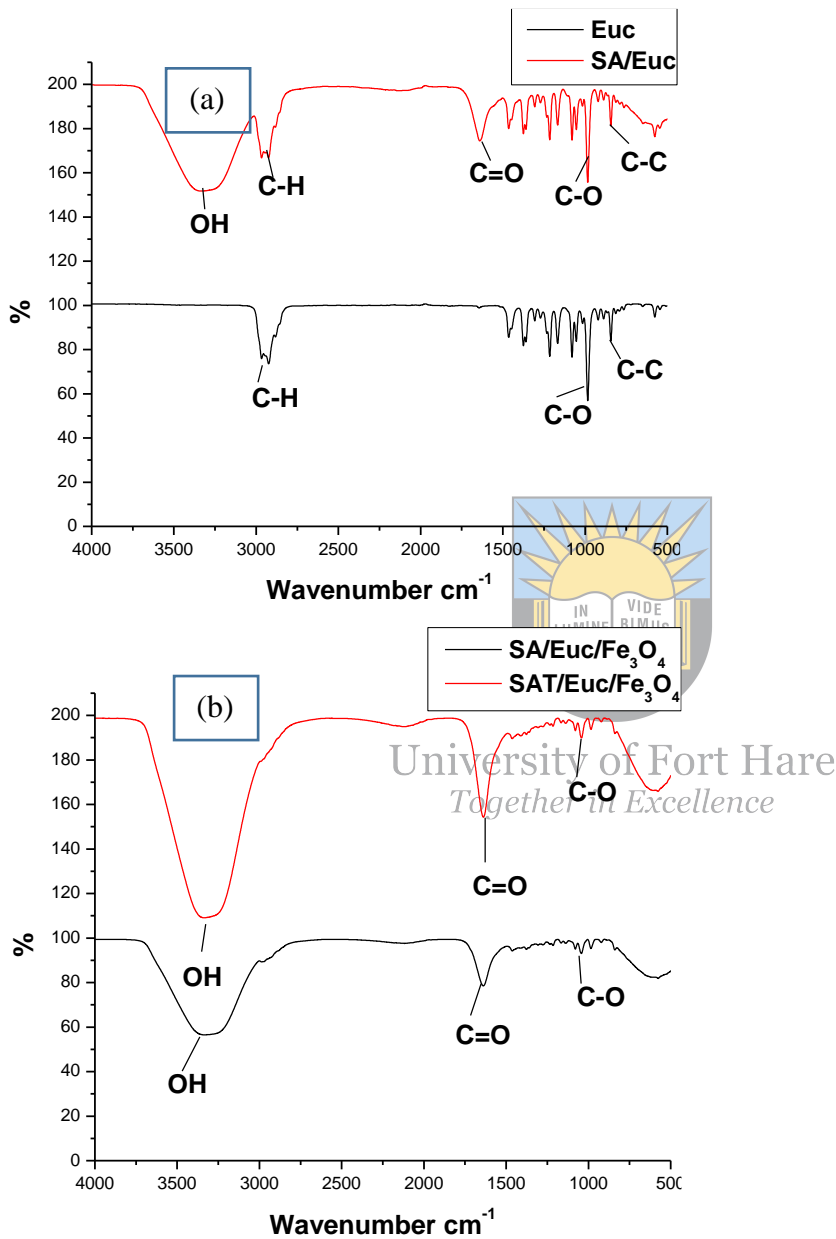


Figure 11: (a) FTIR spectra of Euc & SA/Euc, (b) FTIR spectra SA/Euc/Fe₃O₄ & SAT/Euc/Fe₃O₄

FTIR spectra of gels containing **Rose-EO** are displayed in **Figures 12a & 12b**. **Rose-EO** revealed vibration bending for C-H methylene group vibration and O-H alcohol at 2932 cm^{-1} and 3486 cm^{-1} , respectively [9,10]. The characteristic at 1723 cm^{-1} is attributed to the carbonyl

group C=O linked to camphor [10]. The vibration bands protruding at 833 cm^{-1} , 984 cm^{-1} , 1085 cm^{-1} , 1236 cm^{-1} , and 1330 cm^{-1} indicate the monoterpenes such as 1,8-cineole present in rosemary oil [11,12]. The FTIR SA/Rose, SA/Rose/Fe₃O₄, and SAT/Rose/Fe₃O₄ revealed similar absorption bands, and a broad O–H peak alcohol was observed at 3443 cm^{-1} . These formulations showed the presence of rosemary oil was stable in the polymeric matrix and did not interact significantly with the polymers functional groups, as the major vibration bands for monoterpenes were retained [13].

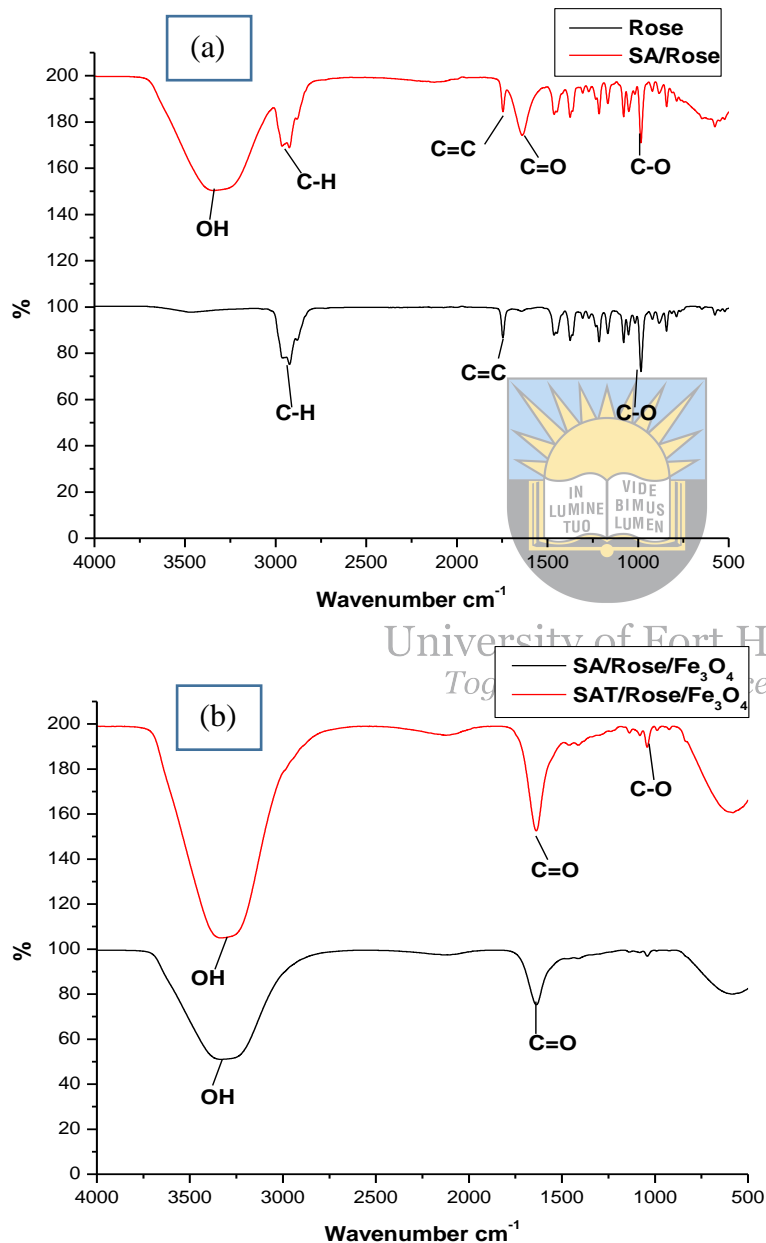


Figure 12: (a) FTIR spectra of Rose & SA/Rose, (b) FTIR spectra SA/Rose/Fe₃O₄ & SAT/Rose/Fe₃O₄

Figures 13a & 13b present absorption peaks of the formulation containing **Lav-EO**. Pure lavender oil exhibited an absorption peak at 3468 cm^{-1} linked to the O–H stretch alcohol, showing the presence of terpene-4-ol and linalool [14]. The intense C–H stretch at 2946 cm^{-1} is attributed to the aliphatic and aromatic groups. The strong peak at 1740 cm^{-1} is linked to the C=O carbonyl group indicating the presence of the major components of lavender oil such as Lavandula acetate, linalool, camphor, and linalyl acetate [15,16]. The C-O stretch bend visible at 1253 cm^{-1} further confirms the presence of the mentioned ester components of lavender oil [14,15]. The peaks at 917 cm^{-1} , 1018 cm^{-1} , and 1253 cm^{-1} correspond to the C–H deformations as that in camphor [15,16]. **SA/Lav/Fe₃O₄** and **SAT/Lav/Fe₃O₄** exhibited a broad characteristic peak at 3460 cm^{-1} corresponding to the O–H stretching alcohol present in the alginate polymer network [17]. The vibration bend at 2923 cm^{-1} is attributed to C–H stretch present in both polymer and lavender oil components. The twin peaks at 1641 cm^{-1} and 1732 cm^{-1} are linked to C=O stretching carbonyl group [14]. There was no major difference between spectra of **SA/Lav**, **SA/Lav/Fe₃O₄**, and **SAT/Lav/Fe₃O₄**, and it can be noted that components of lavender oil were retained in all formulations.

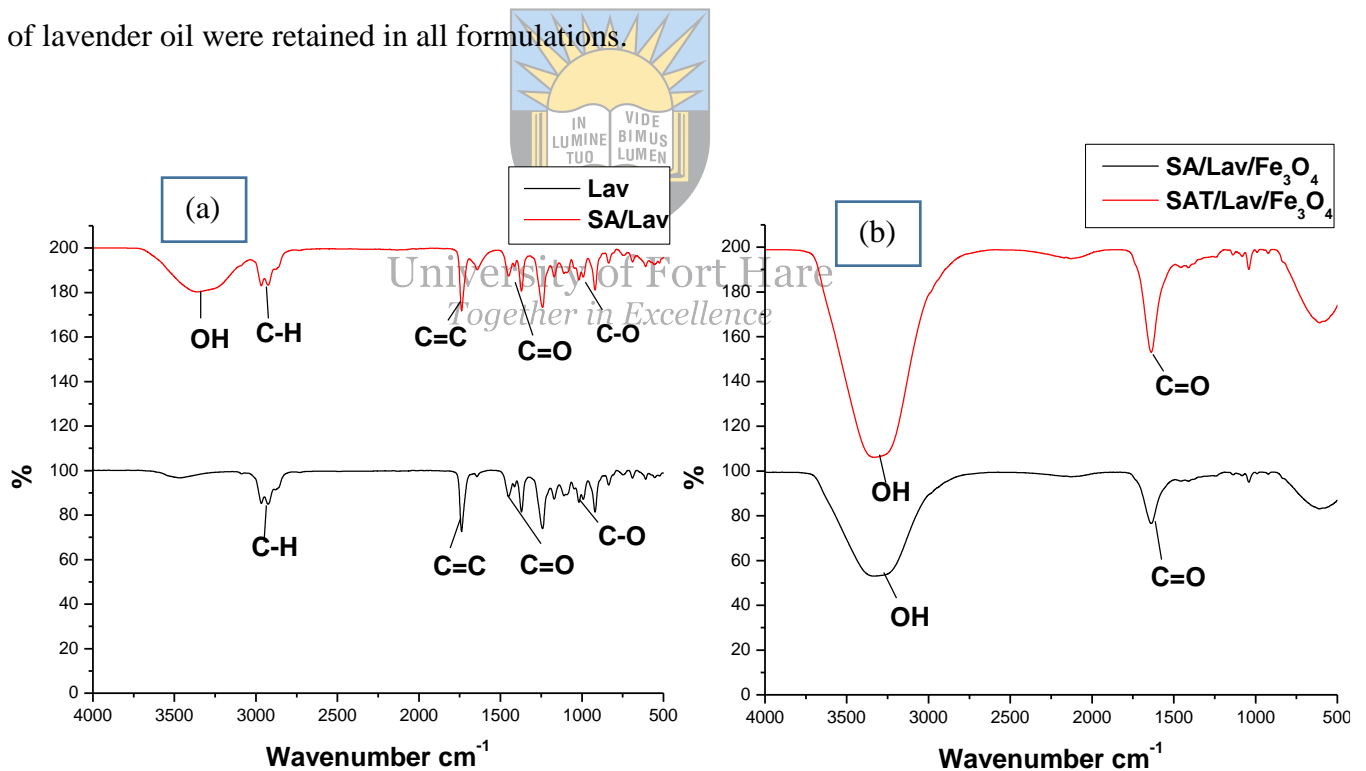


Figure 13: (a) FTIR spectra of Lav & SA/Lav, (b) FTIR spectra SA/Lav/Fe₃O₄ & SAT/Lav/Fe₃O₄

4.1.3 Fourier-Transform Infrared of CMC-based Gels

Figures 14a–c present FTIR spectra of CMC-based topical gels fabricated with TA and nanoparticles. This can be likened to the similar chemical structures of SA and CMC. Similar characteristic peaks were observed for all the prepared topical gels, which can be linked to a

similar polymer composition. The FTIR spectra of the topical gels also revealed the absence of an interaction between the nanoparticles, or TA, with the polymer network. Characteristic bands of these gel formulations were visible at 3548–3132 cm^{-1} O-H stretch, which can be linked to the CMC–carbopol intermolecular hydrogen bonding and 1667–1602 cm^{-1} C=O stretch, and 1040–1018 cm^{-1} C-O stretch can be linked to both CMC and carbopol.

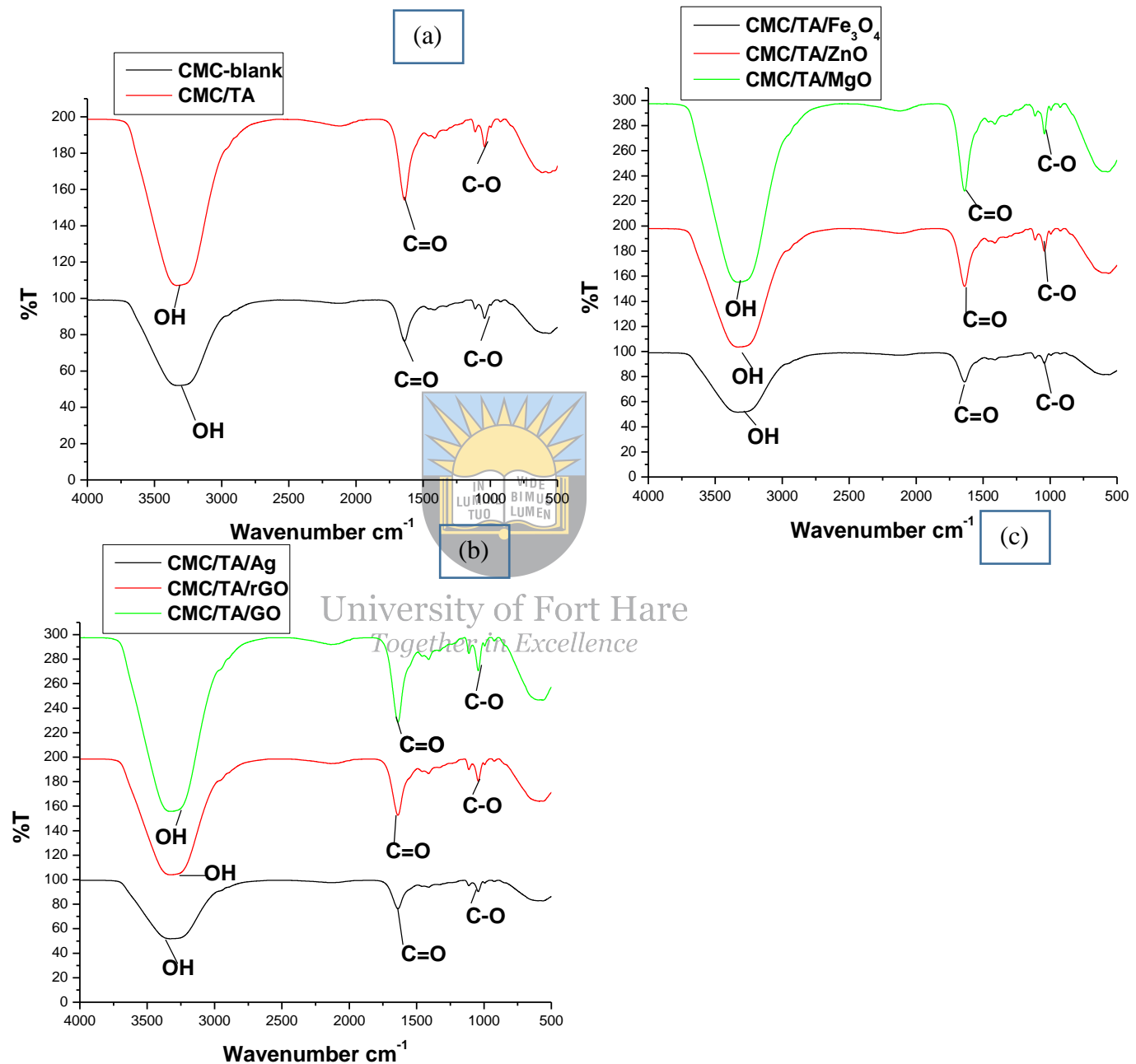


Figure 14a-c: FTIR spectra of CMC-based topical gels

4.2. SEM and XRD

Photomicrographs of various nanoparticles are presented in Figures 15a-e. The SEM image of Fe_3O_4 nanoparticles revealed aggregated and almost spherical morphology and similar morphology was reported by Gul *et al.* for Fe_3O_4 nanoparticles [18]. Pirsá *et al.* reported that

the particle aggregation of Fe₃O₄ nanoparticles is influenced by an increase in the particle's surface energy and decreased particle size [19]. The SEM image of ZnO NPs also showed a spherical, block-shaped with a solid dense structure morphology. Similar SEM morphology was reported by Mohammadi *et al.* for ZnO NPs [20]. The SEM image of MgO NPs showed spherical particles with larger particle clusters, and similar morphology was reported by Sushma *et al.* [21]. Photomicrographs of GO showed a block-shaped morphology with a smooth surface. rGO exhibited coarse and irregular morphology.



University of Fort Hare
Together in Excellence

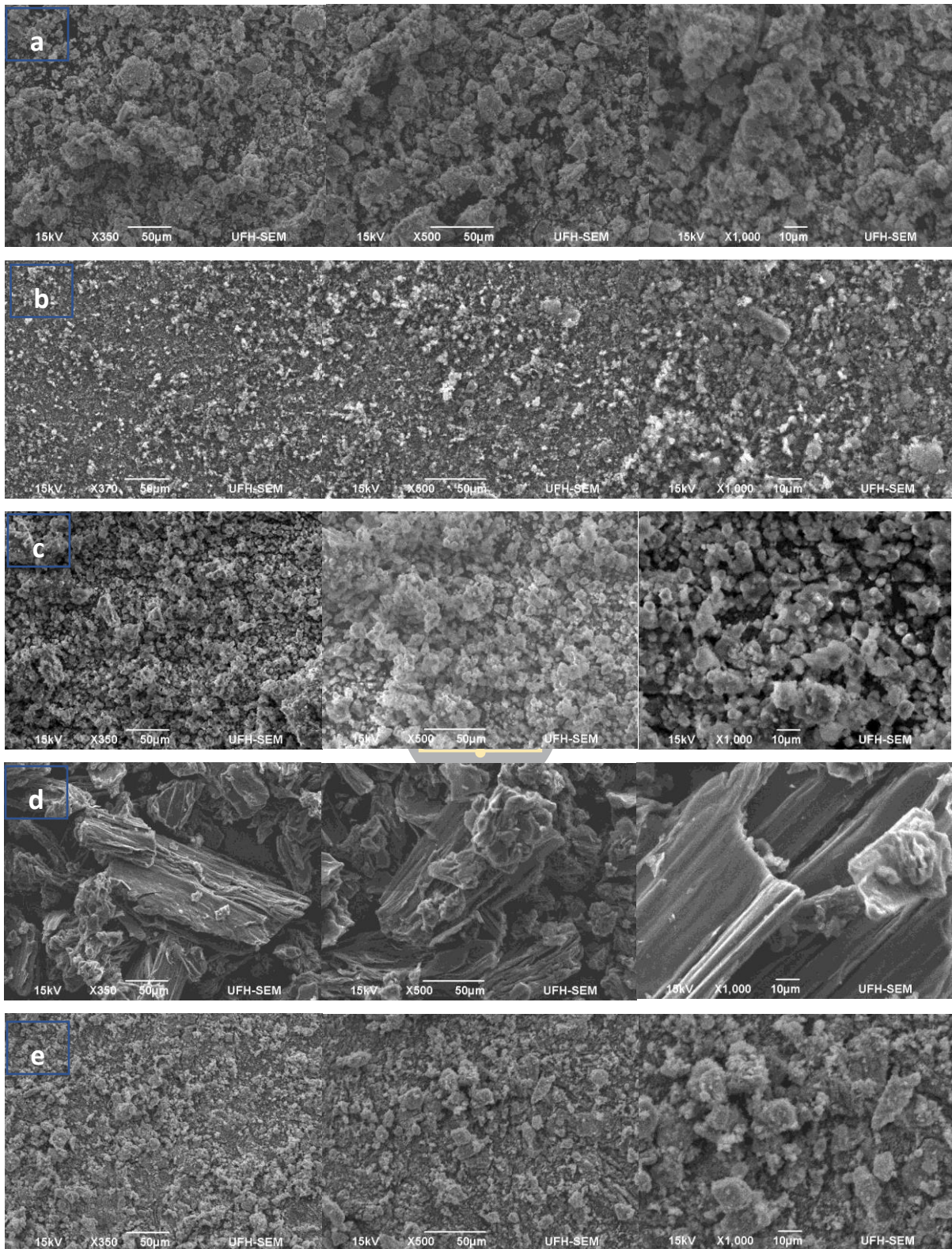


Figure 15: SEM images of a) Fe_3O_4 , b) GO, c) MgO, d) rGO, and e) ZnO-NPs

The X-ray diffraction graphs of all the reported molecules are presented in the Appendix. XRD graphs of the prepared nanoparticles displayed prominent crystalline characteristic 2θ peaks at 21.7° , 30.01° ,

31.01°, 36°, 43.6°, and 52.4° that were assigned to the crystal planes of (111), (220), (311), (222), (400), and (422) inverse cubic spinel magnetite, respectively, for Fe₃O₄ nanoparticles. Qureshi *et al.* investigated the systematic properties of hematite and magnetite nanoparticles, and they reported similar findings with a 44nm particle size for Fe₃O₄ nanoparticles calculated using the Debye-Scherrer equation [22]. The prepared ZnO revealed crystal 2 θ peaks at 11.8°, 30°, 32°, 34.9°, 36.5°, 48°, and 57°. Shalumon *et al.* also reported similar ZnO 2 θ peaks at 33.2° and 36.3° [23]. GO showed one major crystalline 2 θ peak at 26.4°. The MgO diffraction 2 θ peaks were visible at 11°, 18°, 25.5°, 27.9°, 33.5°, 36.5°, 43°, 45.5°, 53.1°, 56.3°, and a sharp peak at 31.9°. Similar diffraction peaks were reported by Sukumaran *et al.* and were attributed to (111), (200), (220), (311), and (222) [24]. Also using the sharp peak at 43.1° corresponding to the (200) lattice plane Sukumaran *et al.* calculated the size distribution of the prepared MgO nanoparticles to be 27nm by the Debye-Scherrer method [24]. Using the Debye-Scherrer equation, the average nanoparticle size of the most intense peak was 27.5nm for MgO, 15nm for ZnO, and 19nm for Fe₃O₄ nanoparticles. Also, the intensified peaks confirmed the crystalline properties of the nanoparticles [19].

4.3. Spreadability and viscosity of the topical gels

The gel formulations reported above were evaluated for their spreadability, pH, homogeneity, stability, and appearance, as shown in Table 9. The pH was recorded between 6.7- 7.2, which is in the range of normal skin pH. The good spreadability of the gels signifies that they can be easily administered to the skin. The prepared topical gels exhibited spreadability within the range of 6.1–10.1 cm. The good spreading feature of the gels is useful in uniform application and is also an ideal quality in topical formulations and an important feature in patient compliance treatment. Drug encapsulation had no obvious effect on the spreadability of the gel formulations. The healing efficiency of topical gels is influenced by their spreadability, which promotes uniform application [25]. The good spreadability range of the gels reveals that they can be easily applied to the wounds without overflowing from the wound bed, thereby indicating the capability to provide a wet contact time that provides moisture to the wound environment [26]. The prepared formulations were all clear and homogenous, with no phase separation. After the storage of the topical gels for 10 months in a refrigerator at 4 °C, all the gels maintained their physical and chemical states, showing their stability and long-term storage capabilities.

Table 9: Spreadability, pH, and stability results of the prepared SA topical gels

Sample ID	Spreadability – 10 months later	pH	Viscosity 50 rpm		10 months later	
			30 s	120 s	30 s	120 s

X1	10.1 cm – 9.8 cm	6.8	5424 cp	5381 cp	5420 cp	5380 cp
X2	8.5 cm – 8.6 cm	6.7	2376 cp	2316 cp	2371 cp	2312 cp
X3	8.5 cm – 8.7 cm	7.1	5796 cp	5820 cp	5793 cp	5815 cp
X4	6.9 cm – 7 cm	7.0	1765 cp	1692 cp	1763 cp	1688 cp
X5	6.7 cm – 6.6 cm	6.7	2068 cp	2052 cp	2067 cp	2050 cp
X6	10.6 cm – 10.4 cm	6.8	1152 cp	1116 cp	1150 cp	1111 cp
X7	10.1 cm – 10 cm	6.9	4272 cp	4260 cp	4271 cp	4258 cp
X8	7.6 cm – 7.5 cm	6.9	1584 cp	1584cp	1582 cp	1582cp
X9	6.1 cm – 6.2 cm	6.8	1548 cp	1512 cp	1544 cp	1506 cp
X10	10 cm – 10 cm	6.9	2700 cp	2724 cp	2698 cp	2720 cp
X11	9.3 cm – 9.4 cm	7.1	2364 cp	2436 cp	2366 cp	2439 cp
X12	7.2 cm – 7.4 cm	6.7	2064 cp	2100 cp	2066 cp	2102 cp
X13	10.5 cm – 10.1 cm	6.8	3912 cp	3972 cp	3911 cp	3971 cp
X14	9.1 cm – 10 cm	7.0	3360 cp	3360 cp	3362 cp	3362 cp

The viscosity of topical gels at 50 rpm (revolution per minute) was 5820–1116 cP, as shown in **Table 9** above. The viscosity of all the prepared topical gels was not dependent/affected by the type of drug-loaded. The permeation enhancer/gelling agent (carbopol) effect was not significant on the viscosity of the gels. The viscosity of gel formulations revealed consistency. The viscosity of formulations decreased with increasing shear rate, indicating a non-Newtonian flow (shear thinning). A non-Newtonian flow is acceptable because, when applied at high shear conditions, there is low flow resistance [27,28]. The reduced viscosity also suggests pseudoplastic behaviour which confirms a feature of high spreadability and the capability of the gel formulations to remain at the wound site after application without flowing off the site of application [29]. The viscosity of the gel formulations also revealed their good stability.

The prepared topical SA/EO gels were analysed for their spreadability, pH, stability, and viscosity, as **shown in Table 10**. The pH was recorded between 6.8-7.2. The prepared topical gels exhibited spreadability within the range of 5.4–10.1 cm. **SA/Rose** exhibited lower spreadability values compared to formulations loaded with iron oxide and both iron oxide and tranexamic acid, while **SA/Lav** formulations revealed a decreasing or good spreadability behaviour upon the addition of biomaterials. **SA/Euc** topical gels showed no notable spreadability trend after loading the bioactive materials. However, all the prepared **SA/Euc**

formulations exhibited good spreadability. The prepared formulations were all clear and in **the** form of emulsions with no phase separation. **SA/Rose/Fe₃O₄** and **SAT/Rose/Fe₃O₄** decreased with increasing shear rate, indicating a non-Newtonian flow (shear thinning), while all other formulations showed increasing consistency from 30 to 120 s. After 12 months of storage in a refrigerator, all the prepared formulations maintained their physical and chemical states, showing their stability and long-term storage capabilities.

Table 10: Spreadability, pH, and stability results of the prepared SA/EO-based topical gels

Sample ID	Spreadability – 10 months later	pH	Viscosity 50 rpm		10 months later	
			30 s	120 s	30 s	120 s
SA/Lav	9.1 cm – 9 cm	6.9	3396 cp	3444 cp	3393 cp	3443cp
SA/Rose	7.3 cm – 7.2 cm	6.8	2232 cp	2244 cp	2230 cp	2241 cp
SA/Euc	6.8 cm – 6.7 cm	7.1	2829 cp	2841 cp	2830 cp	2843 cp
SA/Lav/Fe ₃ O ₄	5.4 cm – 5.5 cm	6.8	3288 cp	3300 cp	3293 cp	3306 cp
SA/Rose/Fe ₃ O ₄	8.3 cm – 8.2 cm	7.2	1284 cp	1260 cp	1282 cp	1257 cp
SA/Euc/Fe ₃ O ₄	6.5 cm – 6.4 cm	7.0	2892 cp	2928 cp	2886 cp	2922 cp
SAT/Euc/Fe ₃ O ₄	7.5 cm – 7.6 cm	7.1	3060 cp	3108 cp	3058 cp	3105 cp
SAT/Rose/Fe ₃ O ₄	10 cm – 10.1 cm	6.9	1743 cP	1716 cP	1740 cP	1714 cP
SAT/Lav/Fe ₃ O ₄	6.2 cm – 6.1 cm	7.0	2232 cP	2280 cP	2233 cP	2281 cP

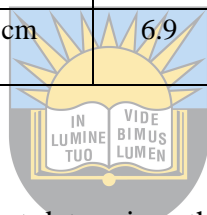
The physical properties of CMC-based gel formulations are presented in **Table 11** below. The spreadability and pH of these formulations were recorded between 5-11.2 cm and 6.7-7.3, respectively. Loading of TA and nanoparticles had no significant effect on the spreadability of the formulations, and they all maintained good spreadability for topical application. Upon storage for 10 months, these gel formulations displayed no signs of phase separation, chemical or physical change, or colour change, revealing good stability and long-term storage capabilities. Gel formulations **CMC/TA/Ag** and **CMC/TA/rGO** revealed their viscosity at a lower shear rate (20 rpm) compared to all other CMC-based formulations. The prepared CMC-based gels revealed consistency and showed a non-Newtonian flow. The viscosity of the gel formulations also showed the stability of these formulations.

Table 11: Spreadability, pH, and stability results of the prepared CMC-based topical gels

Sample ID	Spreadability – 10 months later	pH	Viscosity 50 rpm		10 months later	
			30 s	120 s	30 s	120 s
CMC-Blank	7.7 cm – 7.9 cm	6.7	11980 cP	11930 cP	11978 cP	11927 cP
CMC/TA	11.2 cm – 11 cm	7.2	4128 cP	4056 cP	4126 cP	4054 cP
CMC/TA/Fe ₃ O ₄	10.1 cm – 10 cm	6.9	7248 cP	7020 cP	7245 cP	7015 cP
CMC/TA/MgO	10.1 cm – 9.9 cm	7.2	5556 cP	5328 cP	5555 cP	5325 cP
CMC/TA/ZnO	8.5 cm – 8.6 cm	7	11870 cP	12000 cP	11874 cP	12000 cP
CMC/TA/GO	8.5 cm – 8.5 cm	7.3	5712 cP	5796 cP	5710 cP	5796 cP
			Viscosity 20 rpm		10 months later	
CMC/TA/Ag	8.5 cm – 8.5	7.1	27030 cP	26580 cP	27027 cP	26576 cP
CMC/TA/rGO	5 cm – 5.2 cm	6.9	23220 cP	21900 cP	23218 cP	21898 cP

4.4. Drug release studies

Drug release is an important feature that determines the rate at which the loaded drug will be released. Varied formulations containing TA (CMC/TA, X2, CMC/TA/ZnO, X4, CMC/TA/Ag, and CMC/TA/MgO), as presented in Figures 16-18, revealed a cumulative percentage of drug release $\geq 16\%$ in 20 minutes, a time used to evaluate haemostatic ability of the prepared dressings. The cumulative drug release was recorded at $\pm 53\%$ (CMC/TA/Ag), $\pm 58\%$ (CMC/TA), $\pm 62\%$ (CMC/TA/ZnO), $\pm 70\%$ (X4), $\pm 74\%$ (X2), and $\pm 74\%$ (CMC/TA/MgO) in 24 h. All the prepared formulations revealed cumulative drug release in the range of 71–88% recorded on day 3. Notably, the release of TA from gels loaded with both TA and nanoparticles was sustained.



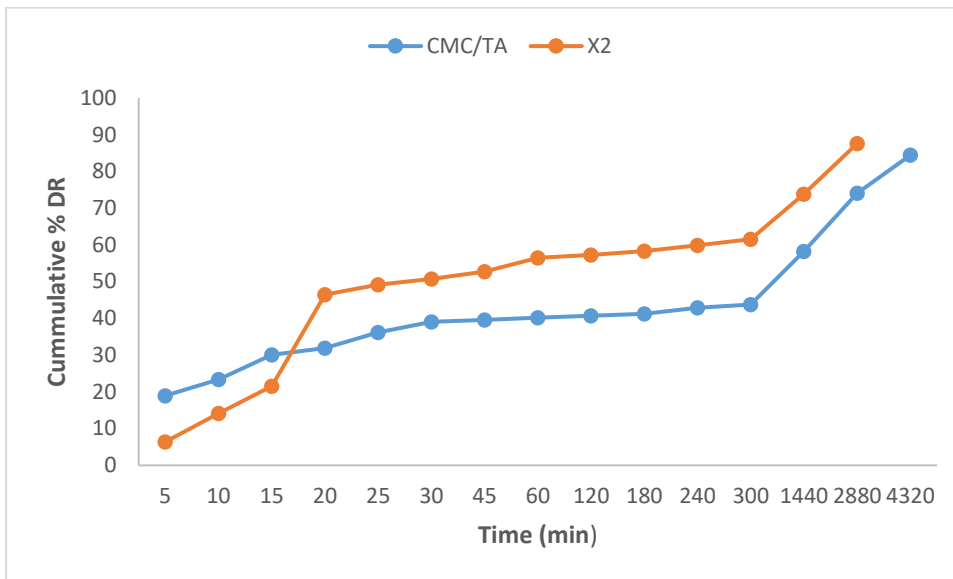


Figure 16: Shows cumulative % DR of TA from CMC/TA and X2

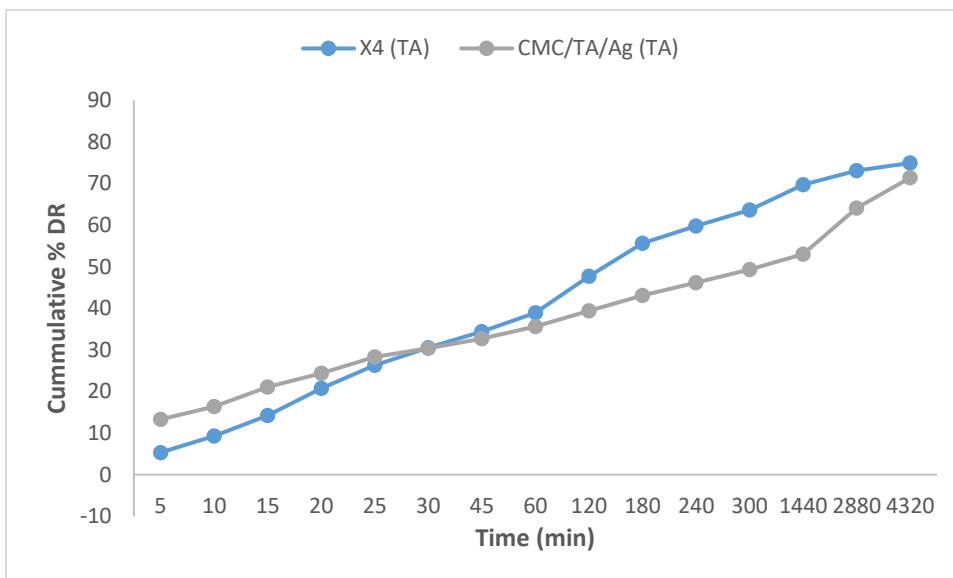


Figure 17: Shows cumulative % DR of TA from X4 & CMC/TA/Ag

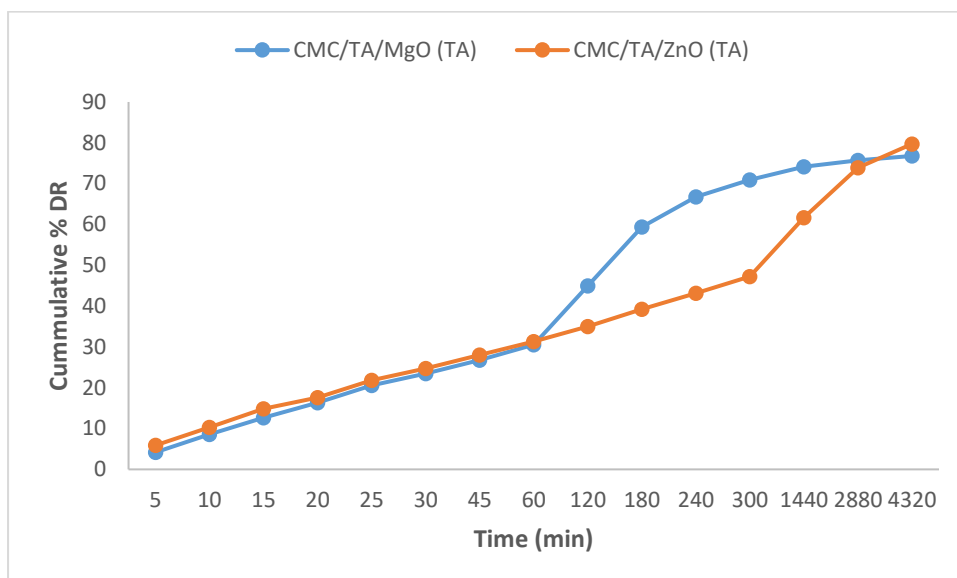


Figure 18: Shows cumulative % DR of TA from CMC/TA/MgO & CMC/TA/ZnO

The drug release kinetics of rGO is reported in **Figure 19**. **X8** loaded with rGO and TA exhibited a slow rate of drug release (39% within the first 5 h). However, the controlled drug release of rGO was observed in **X14** loaded with only graphene oxide, displaying $\pm 25\%$ in 20 min and a maximum of $\pm 73\%$ for 3 days. The controlled drug release exhibited by **X14** signifies that it will be suitable for microbial-infected and chronic wounds. However, drug release studies at pH 5.5 are required to compare its drug release kinetics.

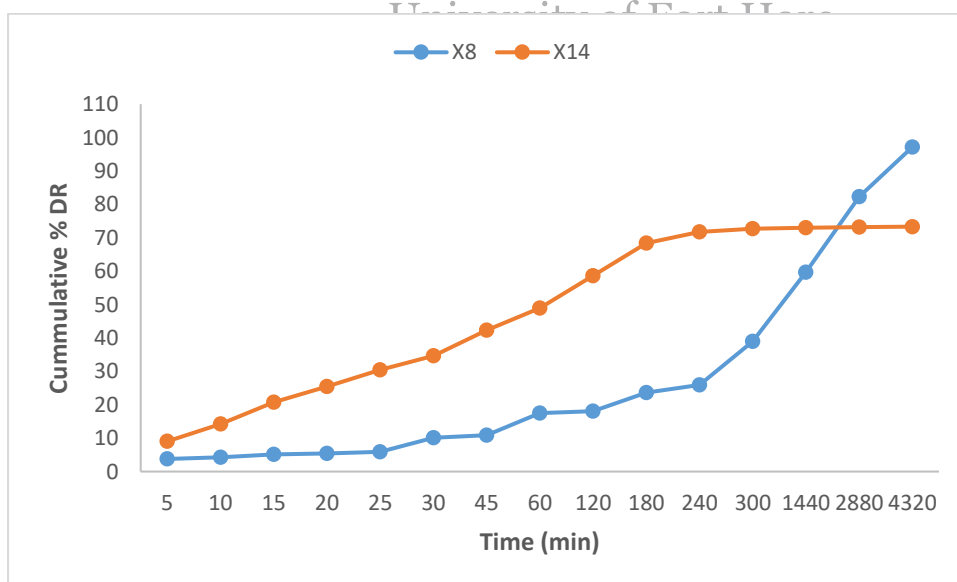


Figure 19: Shows cumulative % DR of rGO from X8 & X14

Figures 20 & 21 present the release profiles of MgO NPs from the gels. Topical gels fabricated with MgO showed the highest rate of drug release percentage, ranging between 91-97% within 3 days, as compared to other bioactive-loaded gels. The cumulative drug release exhibited by

these gels was observed at $\pm 27\%$ (**CMC/TA/MgO**), $\pm 31\%$ (**X4**), and $\pm 38\%$ (**X10**) after 20 min. Scaffolds loaded with both TA and MgO presented a linear cumulative percentage of drug release sustained until the final day of evaluation. **X10** fabricated with only MgO showed linear drug release kinetics for the first hour; however, after 60 min, a constant and slow drug release was observed.

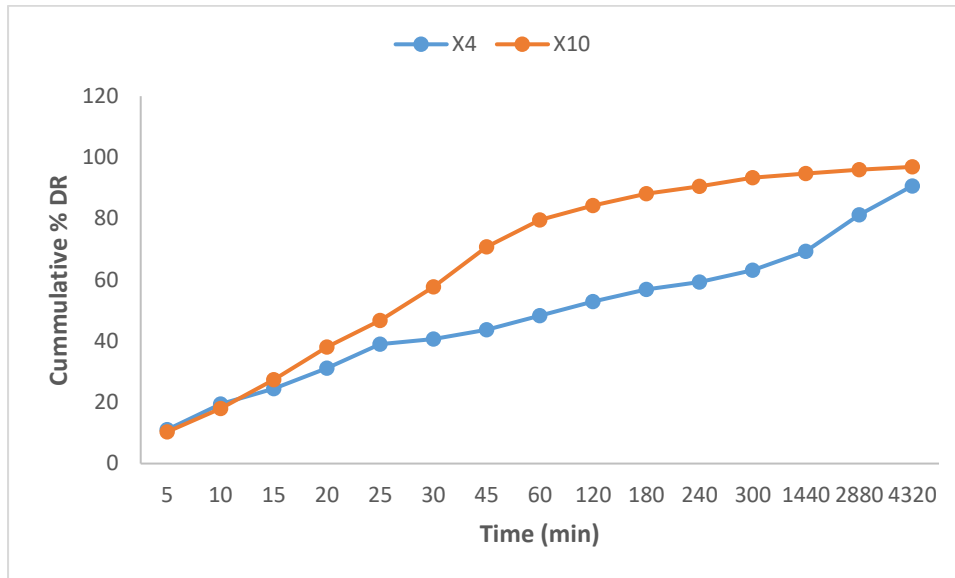


Figure 20: Shows cumulative % DR of MgO from X4 and X10

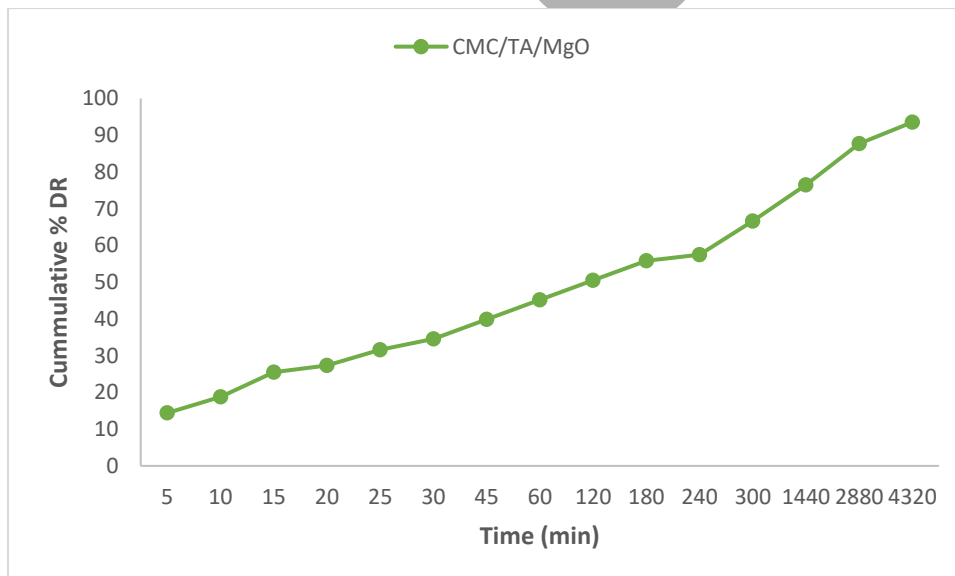


Figure 21: Shows cumulative % DR of MgO from CMC/TA/MgO

The lowest drug release kinetics recorded on the day of investigation are exhibited by **X6** showing $\pm 51\%$ release of AgNPs. **Figures 22 & 23** show gel formulations loaded with AgNPs (**X6**, **CMC/TA/Ag**, and **X12**) showed $\pm 13\%$, $\pm 17\%$, and $\pm 27\%$ cumulative % of drug release in 20 min, followed by $\pm 51\%$, $\pm 75\%$, and $\pm 73\%$ on day 3, respectively. Gel formulations loaded

with TA and AgNPs displayed low drug release in the early stages, however, it increased with time and was sustained.

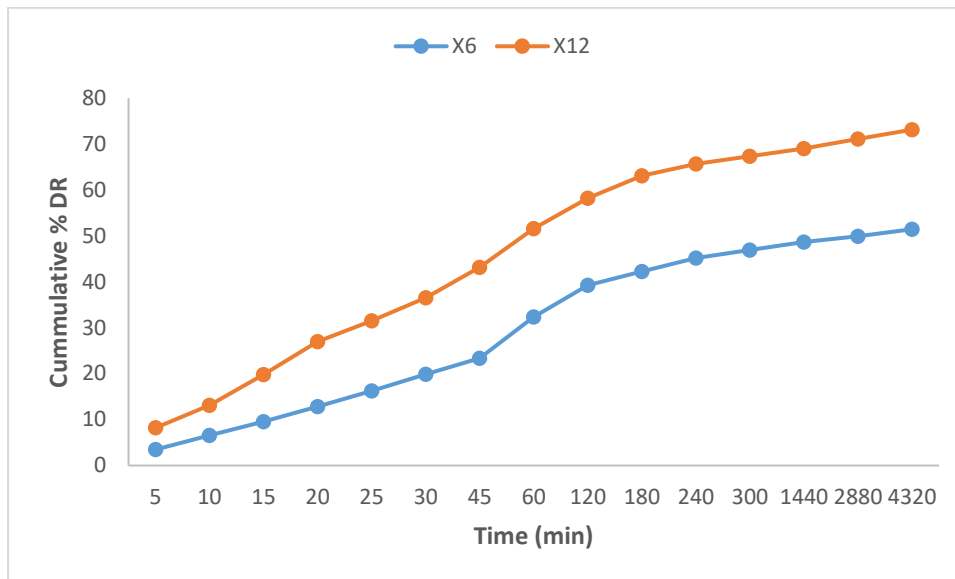


Figure 22: Shows cumulative % DR of AgNPs from X6 & X12

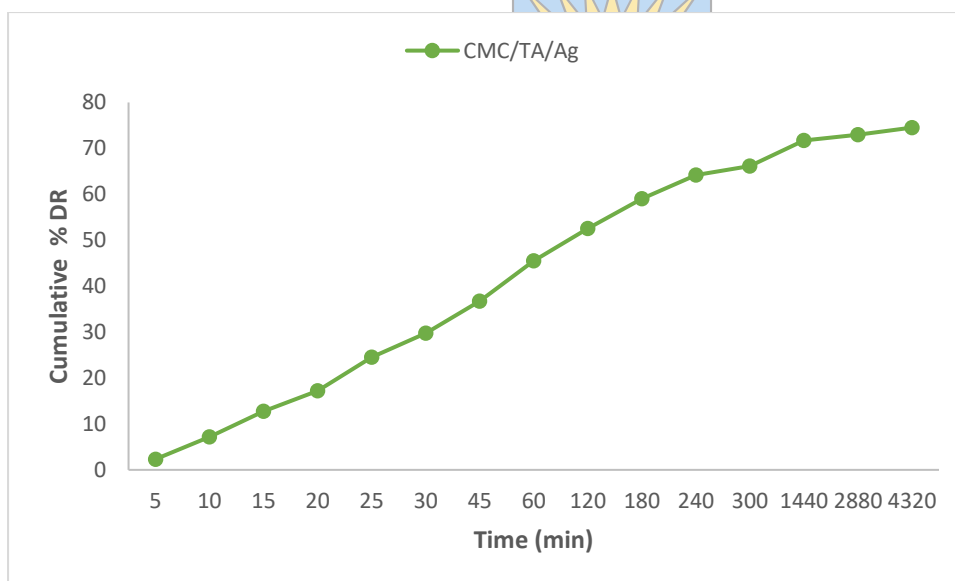


Figure 23: Shows cumulative % DR of AgNPs plotted against time

The cumulative % drug release of ZnO from varied topical gels (**X11**, **X5**, and **CMC/TA/ZnO**) is reported in **Figures 24 & 25**. **CMC/TA/ZnO** exhibited an initial burst release of 30% within the first 5 min, followed by a sustained release profile for day 3 showing 85% cumulative % of ZnO release. **X11** loaded with only ZnO showed a slower drug release of $\pm 3\%$ within the first 10 min, however, 93% of the drug on day 3 was released. **X5** fabricated with both TA and ZnO revealed a cumulative release of ZnO showing $\pm 40\%$ in 20 min and $\pm 76\%$ on day three.

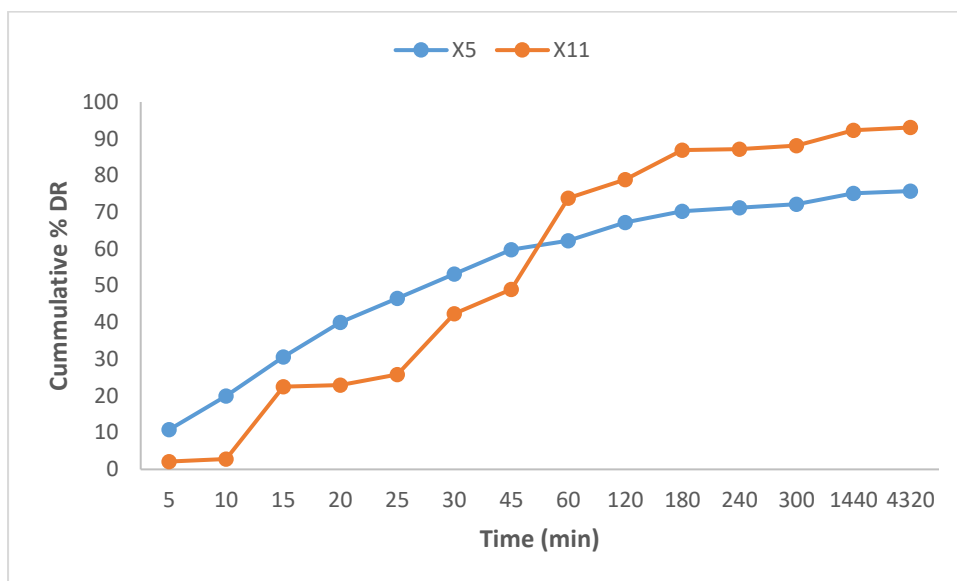


Figure 24: Shows cumulative % DR of ZnO from X5 & X11

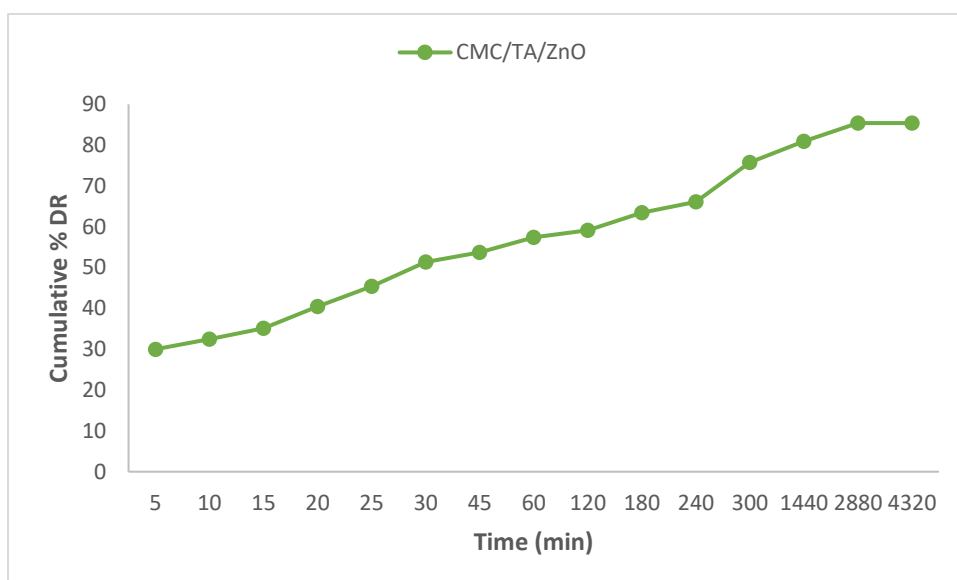


Figure 25: Shows cumulative % DR of ZnO plotted against time

Four mathematical models, Zero-order, First order, Higuchi and Korsmeyer Peppas were used to evaluate the drug release mechanisms of the gels. The values of n and R^2 were summarized, refer to the appendix for linear regression plots, and the drug release mechanism of each topical gel is presented in (Table 12). The drug release of CMC/TA and X7 was best fitted to the Higuchi model compared to other mathematical models, showing 0.926 and 0.9845 R^2 values, respectively. The drug release of CMC/TA/MgO displayed a 0.9695 R^2 value and was best fitted to the Zero-order model. X2, CMC/TA/ZnO (ZnO), CMC/TA/ZnO (TA), CM/TA/Ag (TA), X4 (MgO), and X6 (Ag NPs) all obeyed Korsmeyer Peppas with R^2 values equal to 0.6701, 0.9173, 0.9093, 0.8885, 0.8591, and 0.7495, respectively. The drug release of these

formulations displayed n-values below 0.5, representing a Quasi-Fickian release mechanism. Additionally, the drug release kinetics of **CMC/TA/Ag** (AgNPs), **CMC/TA/MgO** (TA), **X4** (TA), **X5** (ZnO), **X10** (MgO), **X11** (ZnO), **X12** (AgNPs), and **X14** (rGO) also obeyed the Korsmeyer Peppas model with R² values ranging between 0.8556-0.9757 and n-values greater than 0.5, representing a non-Fickian release mechanism. Notably, single fabrication of nanoparticles to the gels led to a non-Fickian release mechanism as seen in **X10**, **X11**, **X12**, and **X14** that all exhibited n-values above 0.5.

Table 12: A summary of in vitro drug release of the prepared formulations

Gels	Bioactive agent	Zero-order	First order	Higuchi	Korsmeyer Peppas	
		R ₂	R ²	R ²	n	R ²
CMC/TA	TA	0.8532	0.646	0.926	0.1653	0.8189
X2	TA	0.3776	0.1555	0.5419	0.4976	0.6701
CMC/TA/ZnO	ZnO	0.5176	0.4071	0.7097	0.2544	0.9173
CMC/TA/ZnO	TA	0.7301	0.4242	0.8856	0.455	0.9093
CMC/TA/Ag	Ag	0.3807	0.1973	0.5744	0.8655	0.8807
CMC/TA/Ag	TA	0.6656	0.4502	0.8187	0.2543	0.8885
CMC/TA/MgO	MgO	0.9695	0.4405	0.8274	0.36	0.9525
CMC/TA/MgO	TA	0.4295	0.278	0.6325	0.7007	0.963
X4	MgO	0.6023	0.3489	0.7559	0.3944	0.8591
X4	TA	0.4528	0.2607	0.6497	0.6018	0.9094
X5	ZnO	0.1835	0.1139	0.3571	0.8216	0.9757
X6	Ag	0.3623	0.2283	0.5535	0.3532	0.7495
X7	rGO	0.8987	0.5794	0.9845	0.5525	0.9567
X10	MgO	0.2556	0.1667	0.4212	0.5488	0.8556
X11	ZnO	0.2157	0.1081	0.4126	1.6226	0.8746
X12	Ag	0.3288	0.2112	0.5109	0.6582	0.9488
X14	rGO	0.3008	0.2152	0.4889	0.6181	0.9648

4.5. In vitro antibacterial assay

4.5.1. In vitro antibacterial assay of SA-based topical gels

Antibacterial activity for **X1-X14** is reported as displayed in **Table 13** below (experiments were repeated twice), and the activity of the formulations was compared to that of the controls (AMP, STM, and NLD). **X1**, **X3**, **X8**, **X10**, and **X11** displayed similar antibacterial activity against *E.*

faecalis, *S. aureus*, *M. smegmatis*, *E. cloacae*, *P. vulgaris*, *P. aeruginosa*, *E. coli*, and *K. pneumonia* bacterial strains, and this antimicrobial effect can be linked to the presence of SA. Similar antibacterial activity is displayed by pure TA, however, its encapsulation in the gel decreased its activity against *S. aureus*, as presented by **X2**. Moreover, **X9** also revealed a similar microbial effect to that of **X1**, **but** it did not show activity against *P. aeruginosa*. These findings are in line with those reported by many researchers, where dressings loaded with magnetite iron oxide NPs displayed limited or moderate antimicrobial effects. However, the pure **Fe₃O₄** NPs exhibited antibacterial activity against *B. subtilis*, a strain that showed resistance to almost all the formulations, *E. faecalis*, *M. smegmatis*, *E. cloacae*, *P. vulgaris*, *P. aeruginosa*, *P. mirabili*, *E. coli*, and *K. pneumonia*, suggesting that encapsulation of these NPs into the gels decreased their microbial activity.

X4 displayed antibacterial activity against all the tested strains except for *S. epidermidis* and *P. aeruginosa*. Liu *et al.* reported electrospun nanofibers with antibacterial activity dependent on the concentration of MgO NPs against *S. aureus*, *S. epidermidis*, and *E. coli* [30]. Similar results were reported by Sukumaran *et al.*, where chitosan/gelatin films incorporated with MgO NPs exhibited antibacterial activity (*S. aureus* and *E. coli*) that increased with an increase in the concentration of MgO NPs [24]. Moreover, Yaroslavovych *et al.* reported MgO NPs with particle sizes less than 10 nm to intensively promote cell death of *B. subtilis* and *S. aureus* bacterial strains, while those of 50 nm had partial activity against *B. subtilis* and *E. coli* [31]. These findings suggest that MgO NPs have a wide variety of antibacterial activity, however, it is dependent on their particle size, concentration, *etc.*

X5 displayed significant antibacterial activity against all strains of gram-negative bacteria, including *E. faecalis*, *S. aureus*, and *M. smegmatis*. The high antibacterial activity is due to the presence of ZnO NPs. However, several reports have proven ZnO-NPs to be effective against both gram-negative and gram-positive strains [32–34]. The antibacterial activity of ZnO-NPs is influenced by the electronic state, surface energy, roughness, surface charge, shape, surface area, and particle size [35]. Farooq *et al.* stated that ZnO-NPs antibacterial activity is through the oxidation of bacterial proteins, radical stress and destruction of DNA synthesis, thus inhibiting bacterial growth [35]. **X6** loaded with both TA and Ag NPs exhibited poor microbial inhibition compared to **X12** loaded with only Ag NPs, which showed maximum activity against all tested strains except for *B. subtilis* and *S. epidermidis*. These results are in agreement with those reported by Masood *et al.*, where AgNPs loaded in CS/PEG hydrogels inhibited bacterial cell growth of *P. aeruginosa*, *B. subtilis*, *E. coli*, and *S. aureus* compared to plain AgNPs and

gels of this form [36]. Choudhary *et al.* formulated AgNPs and calcium alginate nanoparticles loaded into CS hydrogels that displayed good antibacterial activity against *B. subtilis*, *S. aureus*, *E. coli*, and *P. aeruginosa* [25]. AgNPs bind to the bacterial cell wall and disturb enzymes essential for their metabolism.

The highest microbial inhibition against the broad bacterial spectrum is exhibited by **X7**, except for *B. subtilis*. Similar results were reported by Li *et al.*, where hydrogels composed of rose bengal, poly-vinyl alcohol, and GO exhibited antibacterial activity against both gram-negative and gram-positive bacterial strains [37]. Moreover, Prema *et al.* reported GO/ZnO (Cu)O nanocomposites with antibacterial activity against a variety of both gram-positive and negative strains, and their high antibacterial activity was linked to GO's large surface area [38]. Yang *et al.* reported that GO nanosheet's antibacterial activity results from reactive oxygen species and destructive extraction of bacterial phospholipids, leading to damaged cell membrane integrity and bacterial death [39]. **X14** was more efficient against *B. subtilis*, *E. faecalis*, *S. aureus*, *M. smegmatis*, *E. cloacae*, *K. oxytoca*, *P. aeruginosa*, *P. mirabili*, *E. coli*, and *K. pneumonia* microbial organisms. The formulations did not display any effect against *B. subtilis* except for **X4** and **X14**. As a spore-forming bacteria, *B. subtilis* is known to possess a much thicker proteinous cell wall, which hinders the permeability of nanoparticles [40]. However, all these formulations were active against *S. aureus* and *E. coli*, the most common and resistant strains of bacteria in wound therapy and responsible for several infections [41]. The high antibacterial efficacy displayed by these formulations against a broad bacterial spectrum suggests that they are potential wound dressings for the management of both acute and chronic wounds.

Table 13: *In vitro* MIC of SA-based gels, TA, and nanoparticles

Minimum inhibitory concentration (MIC, µg/mL)												
Sample ID	<i>Gram-positive</i>					<i>Gram-negative</i>						
	<i>BS</i>	<i>EF</i>	<i>SE</i>	<i>SA</i>	<i>MS</i>	<i>ECL</i>	<i>PV</i>	<i>KO</i>	<i>PA</i>	<i>PM</i>	<i>EC</i>	<i>KA</i>
X1	-	200	-	200	200	200	50	-	12.5	-	200	200
X2	-	200	-	-	400	400	12.5	-	12.5	-	200	200
X3	-	200	-	200	200	200	12.5	-	12.5	-	200	200
X4	15.625	125	-	62.5	500	15.625	15.625	15.625	-	15.625	500	500
X5	-	200	-	200	200	200	12.5	12.5	12.5	12.5	12.5	12.5
X6	-	500	-	-	500	500	-	15.625	-	-	500	500

X7	-	15.625	15.625	62.5	500	15.625	15.625	15.625	15.625	15.625	500	500
X8	-	200	-	200	200	200	12.5	-	12.5	-	200	200
X9	-	200	-	200	200	200	400	-	-	-	400	400
X10	-	200	-	200	200	200	12.5	-	12.5	-	200	200
X11	-	200	-	200	200	200	12.5	-	12.5	-	200	200
X12	-	15.625	-	62.5	500	15.625	15.625	15.625	15.625	15.625	500	500
X13	-	200	-	200	200	200	12.5	-	12.5	100	100	200
X14	15.625	15.625	-	31.5	500	15.625	-	15.625	15.625	15.625	500	500
TA	-	200	-	200	200	200	12.5	-	12.5	-	400	200
ZnO	-	50	50	50	100	200	12.5	-	12.5	100	50	100
MgO	-	15.625	-	15.625	500	15.625	-	15.625	15.625	15.625	500	500
Ag	12.5	12.5	-	200	200	200	12.5	-	12.5	100	100	100
Fe₃O₄	25	25	-	-	400	200	12.5	-	12.5	100	100	100
AMP	26	26	26	26	26	26	416	26	64	26	26	26
STM	16	128	8	256	4	512	128	16	128	128	64	512
NLD	16	>512	64	64	512	16	128	8	128	32	512	256

4.5.2 *In vitro* antibacterial assay of SA/EO-based topical gels

The antibacterial activity of SA/EO-based formulations is shown in **Table 14**. **Euc-EO** exhibited a minimum inhibitory concentration against *B. subtilis*, *E. faecalis*, *S. aureus*, *M. smegmatis*, *E. cloacae*, *K. oxytoca*, *P. aeruginosa*, *P. mirabilis*, *E. coli*, and *K. pneumonia*. However, gel formulations (**SA/Euc** and **SA/Euc/Fe₃O₄**) containing **Euc-EO** exhibited selective antibacterial activity against limited strains of microorganisms (*E. faecalis*, *S. aureus*, *M. smegmatis*, *E. cloacae*, *P. vulgaris*, *P. aeruginosa*, *E. coli*, and *K. pneumonia*). Additionally, **SAT/Euc/Fe₃O₄** showed similar microbial inhibition against *P. mirabilis*, a species in the same genus as *P. vulgaris*. The microbial inhibition displayed by these gel formulations against *S. aureus*, *E. coli*, and *P. aeruginosa*, the commonly resistant strains of bacteria that cause sepsis and other diseases [37,42,43]. Moreover, these bacterial strains are mostly found in infected and chronic wounds [37,42,43]. *P. vulgaris* causes biofilm and antibiotic resistance [44]. Notably, improved bacterial inhibition values (12.5 and 100 ug/mL) are observed in the SA/Euc formulation compared to pure Euc-EO (500 and 500 ug/mL) against *E. coli* and *K. pneumonia*, respectively, showing that the loading of Euc-EO, TA, and Fe₃O₄ NPs had a synergistic effect.

Lav-EO exhibited microbial inhibition identical to that displayed by **Euc-EO**. Even though **Lav-EO** displayed antibacterial activity similar to that of **Euc-EO**, its gel formulations presented microbial activity against a larger number of microorganisms compared to **Euc-EO** gel formulations. **SA/Lav** exhibited antibacterial effects against *E. faecalis*, *S. aureus*, *M. smegmatis*, *E. cloacae*, *P. vulgaris*, *P. aeruginosa*, *E. coli*, and *K. pneumonia*. Loading of iron oxide in this gel formulation led to a broad spectrum of microbial activity, and all bacterial forms were significantly inhibited, as displayed by **SA/Lav/Fe₃O₄**. Similar results were reported by Mahmood *et al.*, where hydrogel films containing Lav-EO were more efficient against *S. aureus* compared to *E. coli* [45]. **SAT/Lav/Fe₃O₄** exhibited antimicrobial activity similar to that of **SA/Lav/Fe₃O₄**, except that it did not impede *B. subtilis*. Lav-EO-containing gel formulations exhibited the best antibacterial efficacy against all the tested formulations that are reported. These findings imply that loading Lav-EO into gel formulations is a good approach for bacterial inhibition and the management of infected wounds

The antibacterial activity of **Rose-EO** was significant against all gram-positive strains of bacteria and all gram-negative strains, excluding *P. vulgaris*. Gel formulations, **SA/Rose** and **SA/Rose/Fe₃O₄**, inhibited the same bacterial strains (*B. subtilis*, *E. faecalis*, *S. aureus*, *M. smegmatis*, *E. cloacae*, *K. oxytoca*, *P. aeruginosa*, *P. mirabilis*, *E. coli*, and *K. pneumonia*). The identical antibacterial activity displayed by **SA/Rose** and **SA/Rose/Fe₃O₄** suggests that the loading of iron oxide played no significant impact. **SAT/Rose/Fe₃O₄** displayed significant antibacterial activity against a smaller antimicrobial spectrum (*E. faecalis*, *S. aureus*, *M. smegmatis*, *E. cloacae*, *P. vulgaris*, *P. aeruginosa*, *E. coli*, and *K. pneumonia*) compared to other formulations of this manner, suggesting that loading of two or more bioactive agents in the gels composed of **SA/Rose** decreased their activity, suggesting an antagonistic effect. Khezri *et al.* reported polymer-based nanostructured lipid carriers loaded with rose essential oil that inhibited the growth of *P. aeruginosa* and *S. aureus* [46]. The antimicrobial activity presented by the formulations implies that they will be suitable for the management of infected wounds.

Table 14: *In vitro* MIC of SA/EO-based gels

Minimum inhibitory concentration (MIC, µg/mL)												
Sample ID	<i>Gram-positive</i>					<i>Gram-negative</i>						
	<i>BS</i>	<i>EF</i>	<i>SE</i>	<i>SA</i>	<i>MS</i>	<i>ECL</i>	<i>PV</i>	<i>KO</i>	<i>PA</i>	<i>PM</i>	<i>EC</i>	<i>KP</i>

SA/Lav	-	200	-	200	200	200	12.5	-	12.5	-	100	200
SA/Rose	15.625	15.625	-	31.5	500	15.625	-	15.625	15.625	15.625	500	500
SA/Euc	-	200	-	200	400	200	12.5	-	12.5	-	12.5	200
SA/Lav/Fe₃O₄	15.625	15.625	15.625	62.5	500	15.625	15.625	15.625	15.625	15.625	500	500
SA/Rose/Fe₃O₄	15.625	15.625	-	31.5	500	15.625	-	15.625	15.625	15.625	500	500
SA/Euc/Fe₃O₄	-	200	-	200	200	200	12.5	-	12.5	-	100	200
SAT/Euc/Fe₃O₄	-	200	-	200	200	200	12.5	-	12.5	100	100	100
SAT/Rose/Fe₃O₄	-	200	-	200	200	200	25	-	12.5	-	100	200
SAT/Lav/Fe₃O₄	-	15.625	15.625	62.5	500	15.625	15.625	15.625	15.625	15.625	500	500
Rose-EO	15.625	15.625	15.625	62.5	500	15.625	-	15.625	15.625	15.625	500	500
Euc-EO	15.625	15.625	-	62.5	500	15.625	-	15.625	15.625	15.625	500	500
Lav-EO	15.625	15.625	-	62.5	500	15.625	-	15.625	15.625	15.625	500	500
AMP	26	26	26	26	26	26	416	26	64	26	26	26
STM	16	128	8	256	4	512	128	16	128	128	64	512
NLD	16	>512	64	64	512	16	128	8	128	32	512	256

4.5.3. *In vitro* antibacterial assay of CMC-based topical gels

CMC-based topical gels induced microbial inhibition, as reported in **Table 15**. All the reported CMC-based gels exhibited a 200 µg/mL minimum inhibitory concentration against *E. faecalis*, *S. aureus*, *M. smegmatis*, and *E. cloacae*, as well as against *K. pneumonia*, except for **CMC-Blank** (400 µg/mL). Loading of TA in the CMC gels significantly increased their antibacterial activity against *P. vulgaris* and *P. aeruginosa*, displaying 12.5 µg/mL MIC values in both strains. **CMC/TA/ZnO** and **CMC/TA/GO** exhibited similar microbial inhibition values to those presented by **CMC/TA**, suggesting that the antibacterial activity of these formulations was dependent on TA. The MIC values for **CMC/TA/Ag** against *P. vulgaris* were recorded at 100 µg/mL. Liu *et al.* reported CMC-based nanofibers showing antibacterial inhibition influenced by the concentration of Ag NPs over *S. aureus* and *P. aeruginosa* bacterial strains [47]. **CMC/TA/Fe₃O₄** revealed the best antibacterial efficacy against *E. coli* (12.5 µg/mL), compared to all other CMC gel formulations.

Table 15: *In vitro* MIC of CMC-based topical gels

Minimum inhibitory concentration (MIC, µg/mL)		
Sample ID	<i>Gram-positive</i>	<i>Gram-negative</i>

	<i>BS</i>	<i>EF</i>	<i>SE</i>	<i>SA</i>	<i>MS</i>	<i>ECL</i>	<i>PV</i>	<i>KO</i>	<i>PA</i>	<i>PM</i>	<i>EC</i>	<i>KP</i>
CMC-Blank	-	200	-	200	200	200	200	-	-	-	200	400
CMC/TA	-	200	-	200	200	200	12.5	-	12.5	-	200	200
CMC/TA/Fe₃O₄	-	200	-	200	200	200	12.5	-	12.5	-	12.5	200
CMC/TA/MgO	-	200	-	200	200	200	12.5	-	12.5	-	100	200
CMC/TA/ZnO	-	200	-	200	200	200	12.5	-	12.5	-	200	200
CMC/TA/Ag	-	200	-	200	200	200	100	-	-	-	200	200
CMC/TA/GO	-	200	-	200	200	200	12.5	-	12.5	-	200	200
CMC/TA/rGO	-	200	-	200	200	200	12.5	-	25	-	200	200
AMP	26	26	26	26	26	26	416	26	64	26	26	26
STM	16	128	8	256	4	512	128	16	128	128	64	512
NLD	16	>512	64	64	512	16	128	8	128	32	512	256

CMC/TA/rGO displayed a 25 µg/mL MIC value against *P. aeruginosa*. Ali *et al.* reported CMC hydrogels incorporated with rGO that inhibited the bacterial growth of *S. aureus* and *P. aeruginosa* [48]. Gel formulations reported in this study were mostly efficient against gram-negative strains, which are considered the most resistant and harmful bacterial microorganisms [49]. However, CMC-based formulations exhibited limited antibacterial activity compared to SA, SAT, and SA/EO-based formulations. The highest microbial efficiency is presented by SA/EO-based gel formulations against a broad bacterial spectrum including *B. subtilis*. These findings suggest that EOs have a broad bacterial efficacy against both gram-positive and gram-negative strains compared to the nanoparticles used in this study. Also, SA significantly improved microbial inhibition of the nanoparticles, suggesting a synergistic effect when compared to CMC.

4.6. *In vitro* whole blood clot assay

4.6.1. *In vitro* whole blood clot assay of SA-based topical gels

The *in vitro* haemostatic potential of the scaffolds was repeated three times, and the average absorbance value was used to plot the graphs. Haemostatic material should be able to form clots and thus stop bleeding within a limited amount of time to hinder excessive bleeding. Huang *et al.* stated that lower absorbance values yield a larger volume of blood clots [50]. Absorbance values of all the prepared topical gels were lower compared to that of the control (**Figure 26**), with *p*-value = (0.0021 "**X2**", 0.0014 "**X3**", 0.0043 "**X4**", 0.0017 "**X9**", 0.0121

"**X10**", 0.0054 "**X12**", and 0.0002 "**X14**") revealing that the formulations can promote blood clotting within a short time frame. Singh *et al.* reported that reduced graphene oxide (rGO) is not endowed with any prothrombotic or platelet-stimulating characteristics because of the loss of oxygen-containing groups [51]. Zhao *et al.* reported formulations containing rGO with a higher haemostatic ability influenced by tannic acid than rGO [52]. Contrary to these findings, **X14** containing rGO exhibited the lowest absorbance values compared to all other formulations (p -value < 0.05) however, it was not significantly different from that of **X3** (p -value > 0.05). This shows that the loading of reduced graphene oxide into SA-based gels promoted platelet aggregation.

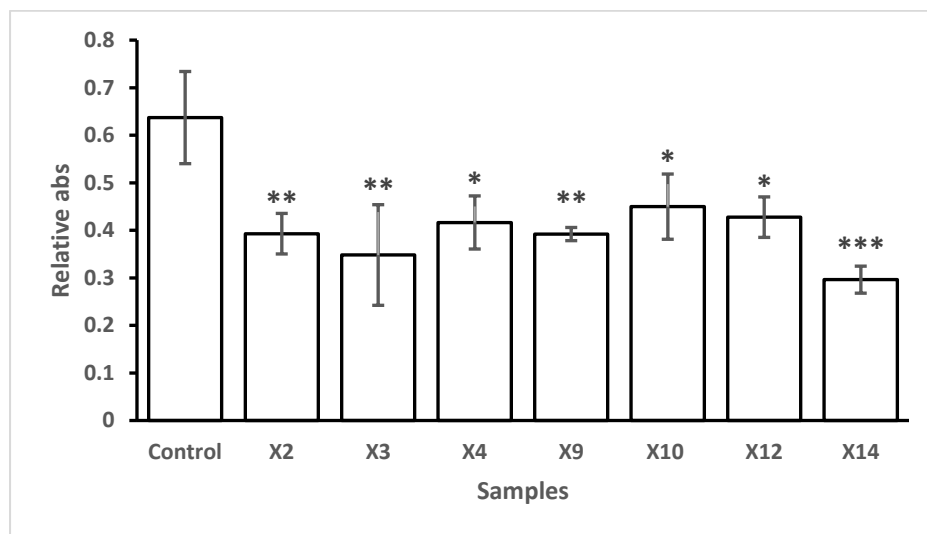


Figure 26: Haemostatic evaluation of SA-based topical gels (error bars = \pm std) $n=3$ *** p -value ≤ 0.0002 , ** p -value ≤ 0.002 * p -value ≤ 0.05

X3 containing both iron oxide and TA exhibited slightly lower absorbance values than formulations containing only TA (**X2**) and iron oxide (**X9**). Similarly, **X4** loaded with TA and MgO-NPs exhibited lower absorbance values than **X10** loaded with only MgO-NPs. This shows that the loading of the two bioactive agents resulted in a synergistic effect that is not statistically different from that of a single drug-loaded scaffold. Similar findings were reported in our group by Buyana *et al.* in which blood clotting of a single drug-loaded scaffold was not significant from that loaded with two bioactive agents [17].

X2 and **X9** exhibited similar blood clotting effects, suggesting that TA and the iron oxide nanoparticles promoted haemostasis through a similar pathway. Sasmal and Datta in their findings reported that an appropriate amount of polymer to that of TA plays a synergistic effect in promoting rapid coagulation time [53]. **X12** loaded with Ag-NPs also promoted blood clotting, suggesting that the loading of AgNPs aided in the haemostatic potential of the gel.

Nanoparticles reported in this study promoted haemostasis of the gels, and their encapsulation with TA resulted in a synergistic effect. The findings reported in this study suggest that the loading of an antifibrinolytic agent and metal nanoparticles in alginate-based wound dressings play a significant role in the haemostatic effect *in vitro*. Moreover, loading rGO to alginate-based dressings is a good approach to developing scaffolds that inhibit blood loss rapidly.

4.6.2. *In vitro* whole blood clot assay of SA/EO-based topical gels

The blood clotting potential of SA/EO-based gel formulations is presented in (Figure 27). Absorbance values of all the prepared topical gels were lower compared to that of the control with (p -values= 0.0051, 0.0255, 0.0177, 0.0188, 0.0196, and 0.0371) for **SA/Rose**, **SA/Lav**, **SA/Lav/Fe₃O₄**, **SAT/Euc/Fe₃O₄**, **SAT/Rose/Fe₃O₄**, and **SAT/Lav/Fe₃O₄**, respectively. These results suggest that the prepared gels can form a bigger clot volume within a limited time after application, as stated by Huang *et al.* that lower absorbance values are equivalent to larger blood clot size [50]. **SA/Rose** exhibited the lowest absorbance values compared to all other formulations, however, the difference was inconclusive (p -value > 0.05) except for **SA/Lav** (p -value = 0.0156). Amongst all other formulations, there was no significant difference (p -value > 0.05). Iron oxide and tranexamic acid played no significant role when loaded in the prepared SA/EO gels, and similar blood clotting behaviour was observed across all the essential oils used in this study. However, rose essential oil formulations revealed promising blood clotting potential as compared to lavender essential oil formulations (p -value < 0.05). The findings obtained in this study, suggest that SA/EO gels promote faster clot formation than when loaded with other bio-active materials and that rose essential oil is more potent for the management of bleeding wounds.

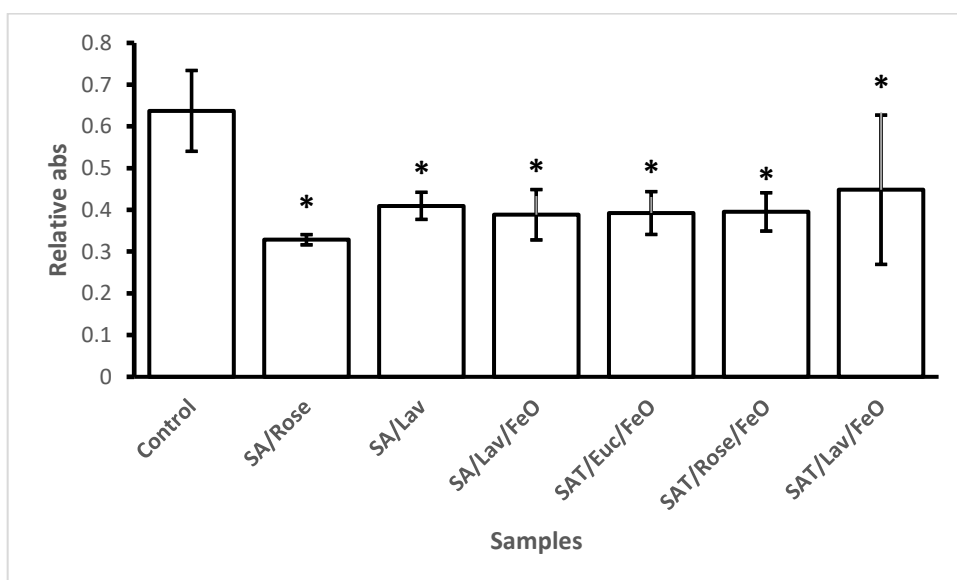


Figure 27: Haemostatic evaluation of SA/EO-based gels (error bars = \pm std) n= 3 *** p -value \leq 0.0002, ** p -value \leq 0.002 * p -value \leq 0.05

4.6.3. *In vitro* whole blood clot assay of CMC-based topical gels

In vitro blood clotting potential of CMC-based topical gels revealed absorbance values lower than that of the control with p -values (< 0.05) (**Figure 28**). The statistical difference presented by **CMC/TA** is (p -value = 0.0002), and all other formulations exhibited (p -value = 0.0001). Mahmoodzadeh *et al.* reported cellulose-based superabsorbent (aerogels and hydrogel) loaded with TA to promote fast blood clotting by forming a milky gel in contact with plasma [54]. The high blood coagulation potential induced by these gel formulations can be supported by the findings reported by Aoshima *et al.* in which CMC promoted blood coagulation by acting as a bridge for fibrin polymerization when dissolved in the blood, thereby stimulating thick fibrin fibre formation [55]. Gu *et al.* also reported that CMC-based dressing increases blood viscosity by dissolving when in contact with the blood and eventually promotes haemostasis [56]. There was no statistical significance between all other formulations except for **CMC/TA/ZnO** and **CMC/TA/GO** (p -value = 0.0439). **CMC/TA/ZnO** exhibited a significant haemostatic effect when compared to all other formulations. These data show that CMC-based topical gels containing TA and nanoparticles have high blood clotting ability compared to SA/EO-based and SA-based nanoparticle fabricated formulations. The blood clotting potential of these scaffolds compliments their antibacterial efficiency results, suggesting that they are good scaffolds for the management of wounds, hence their cell safety were considered.

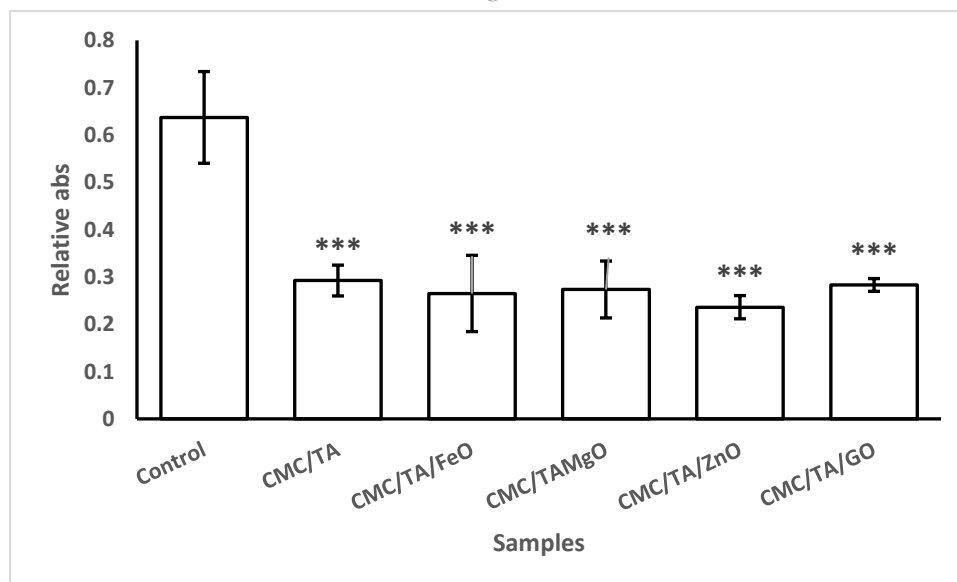


Figure 28: Haemostatic evaluation of CMC-based topical gels (error bars = \pm std) n= 3 *** p -value \leq 0.0002 ** p -value \leq 0.002 * p -value \leq 0.05

4.7. *In vitro* cytotoxicity

4.7.1. *In vitro* cytotoxicity of SA-based topical gels

A haemostatic material will be in direct contact with the open wound, and hence its safety profile is critical. The *in vitro* cytotoxicity assay on selected topical gel formulations (**X1**, **X2**, **X3**, **X4**, **X9**, **X10**, **X12**, and **X14**) was evaluated using HaCaT cells tested at different concentrations, as presented in **Figure 29**. The concentrations used for **X14** were as follows: 9.8, 4.9, 2.45, 1.225, and 0.6125 μM **Figure 30**. According to GB/ T 16886.5-2003 (ISO 10993-5: 1999), a material exhibiting $\geq 75\%$ cell viability is considered non-cytotoxic [57]. The cytotoxic effect of the prepared gels was concentration-dependent, as the highest concentration (200 μM) displayed the lowest cell viability in all the gel formulations. **X1** (blank) displayed moderate cytotoxic impact against the HaCaT cells regardless of a change in its concentration compared to all other gels, with 65% maximum cell viability at 50 μM . **X9** showed moderate cell viability to the HaCaT cells, displaying 76% HaCaT cell viability only at 100 μM . However, this difference was statistically insignificant. All other gel formulations (**X2**, **X3**, **X4**, **X10**, **X12**, and **X14**) were cytocompatible and promoted cell growth and migration. The loading of TA and metal-nanoparticles within the gels significantly improved their cell viability, migration, and growth. These results suggest that the prepared topical gels are promising systems for the enhancement of angiogenesis and rapid wound closure. In particular, **X12** and **X4** exhibited higher cell viability compared to other SA-based formulations and were selected for *in vitro* wound scratch assay.

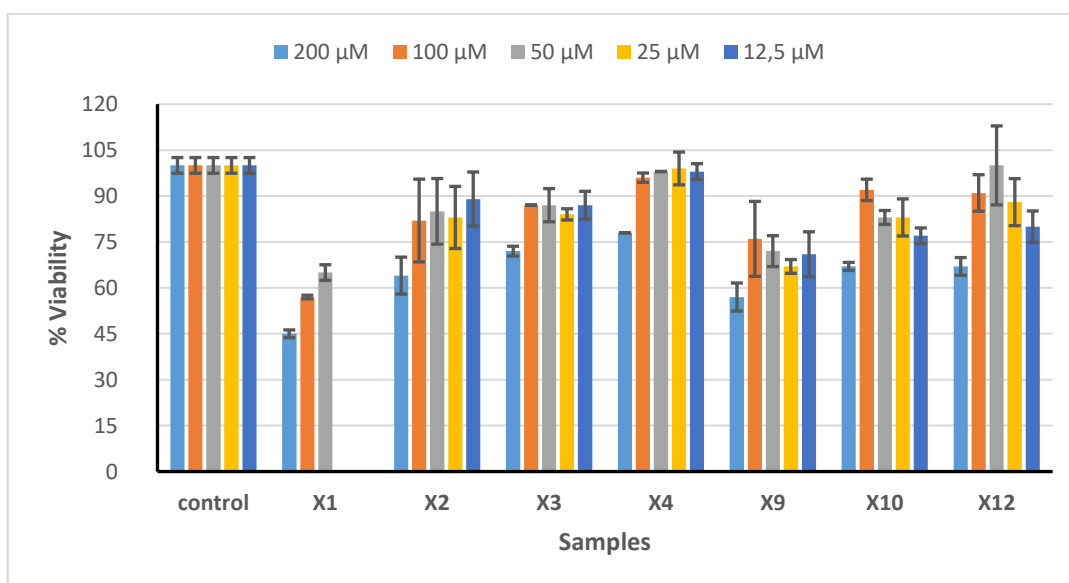


Figure 29: % Cell viability of HaCaT cells treated with SA-based gel formulations (error bars = \pm std) n = 3

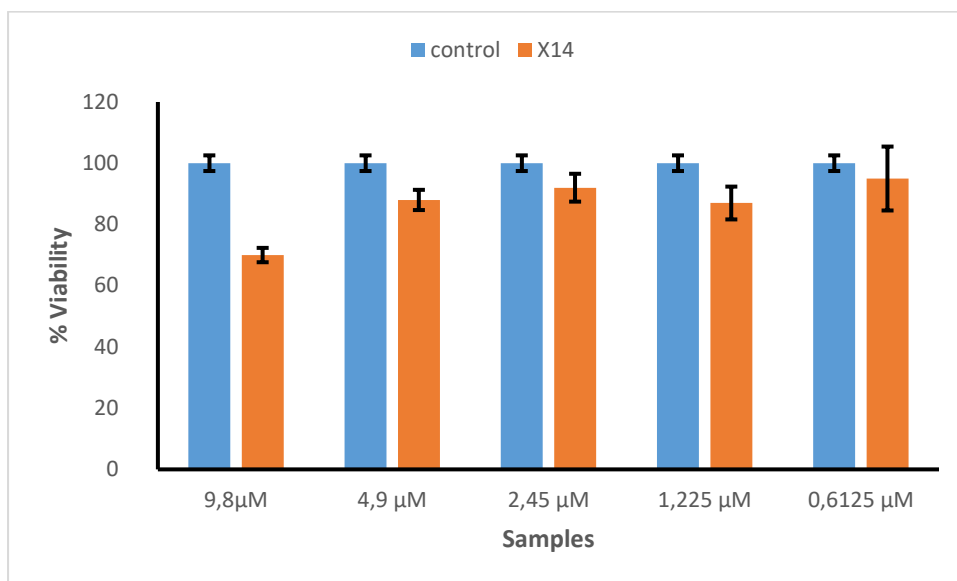


Figure 30: Figure 4.7b: % Cell viability of HaCaT cells treated with X14 (error bars = \pm std) n = 3

4.7.2. *In vitro* cytotoxicity of SA/EO-based topical gels

In relation to the above results for antibacterial activity and blood clotting kinetics, the essential oil-loaded gels revealed promising wound healing activity and showed no signs of toxicity even at a higher concentration of 200 μ M. Loading of essential oils and bioactive agents significantly improved the viability of these scaffolds (p -value < 0.05) at both 200 and 100 μ M compared to **SA-Blank**, as shown in **Figure 31**. However, there was no significant difference between the blank and **SAT/Rose/Fe₃O₄** at 50 μ M (p -value = 0.0984). The prepared SA/EO-based gels displayed the highest cell viability at 100 μ M and showed no significant difference compared to the control except for **SAT/Rose/Fe₃O₄** (p -value = 0.0037) and **SAT/Lav/Fe₃O₄** (p -value = 0.0024). Generally, **SAT/Lav/Fe₃O₄** exhibited >75% cell viability across all the concentrations tested and was selected for further analysis. All SA/EO-based topical gels reported in this study showed a non-cytotoxic effect against HaCaT cells, suggesting their safety for use in topical wound management.

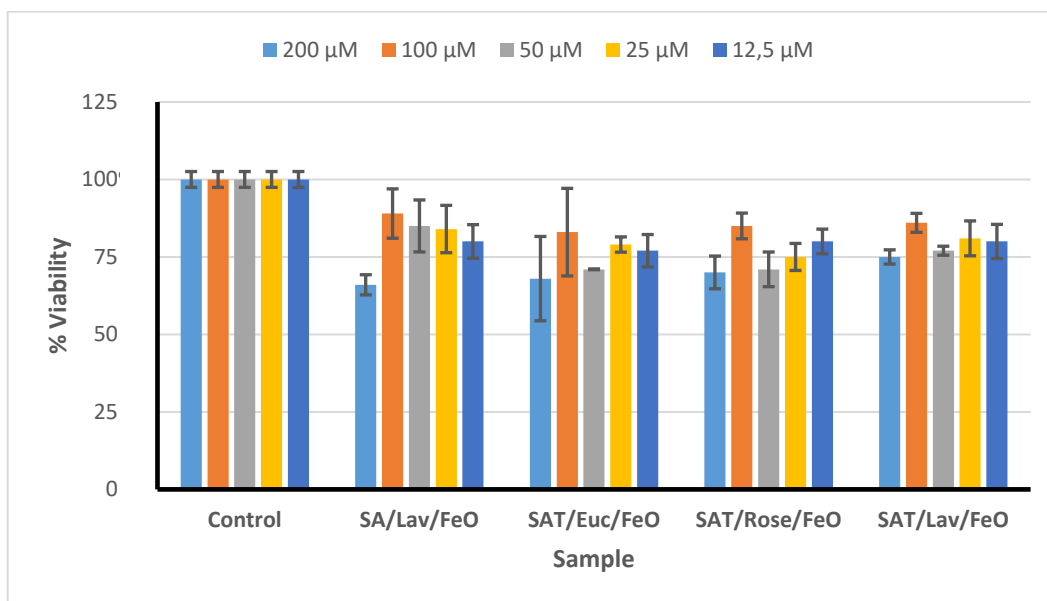


Figure 31: % Cell viability of HaCaT cells treated with SA/EO-based gel formulations (error bars = \pm std) n = 3

4.7.3. *In vitro* cytotoxicity of CMC-based topical gels

The *in vitro* cytotoxicity assay on selected CMC-based topical gel formulations is reported in **Figure 32**. The concentrations used for **CMC/TA/GO** were as follows: 9.8, 4.9, 2.45, 1.225, and 0.6125 μ M, respectively. Similarly, to the previously discussed SA-based formulations, CMC-based gels showed the lowest percentage of cell viability of HaCaT cells at 200 μ M. **CMC** (blank) displayed moderate cytotoxicity against the HaCaT cells regardless of the concentration used when compared to all other gel formulations, with 69% maximum cell viability at 50 μ M. **CMC/TA/Fe₃O₄** and **CMC/TA/GO** also revealed moderate cytotoxicity of 69% at 12.5 μ M and 74% at 4.9 μ M, respectively, on HaCaT cells. It can be noted that with **CMC/TA/Fe₃O₄**, when the concentration decreased from 200-12.5 μ M, the cytotoxicity also decreased, suggesting that lower concentrations of this formulation would be biocompatible to HaCaT cells. All other prepared topical gels were cytocompatible. The loading of TA and nanoparticles in the gels had a synergistic effect and significantly improved their cell viability on HaCaT cells. These results suggest that the prepared topical gels are promising scaffolds for application in tissue regeneration. **CMC/TA/MgO** was selected for complimentary studies as it showed the highest cell viability among the CMC-based formulations prepared in this study.

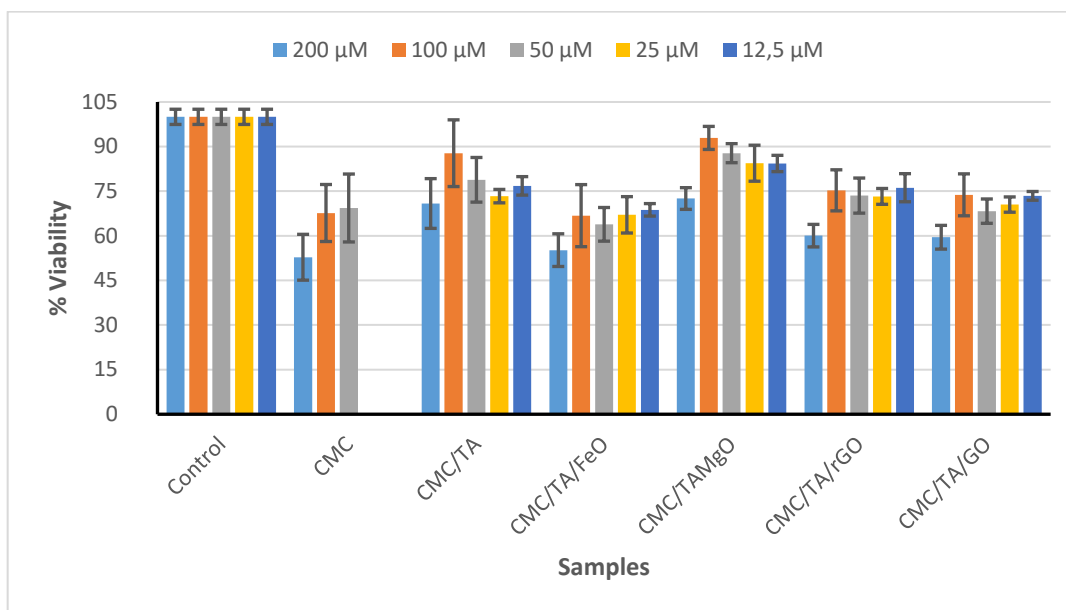
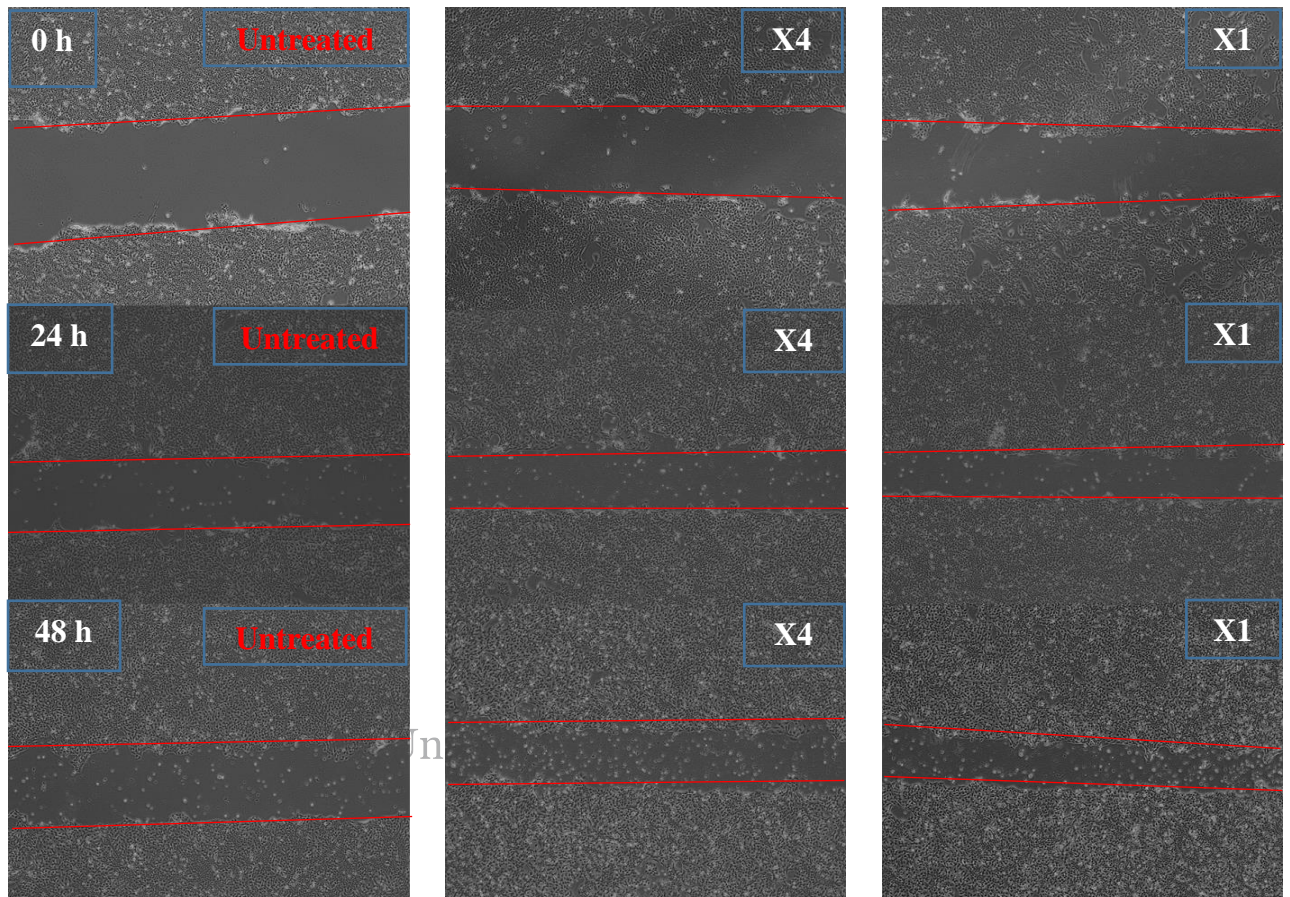


Figure 32: % Cell viability of HaCaT cells treated with CMC-based gel formulations (error bars = \pm std) n = 3

4.8. *In vitro* wound scratch assay

Formulations SAT/Lav/Fe₃O₄, and CMC/TA/MgO exhibited outstanding antibacterial activity, high cell viability, and rapid blood clotting potential, and their wound healing potential was investigated and compared to that of the untreated cells for 0-72 hours. Cell growth and migration are positive features of tissue regeneration and cellular interaction for progressive and complete wound healing. *In vitro* wound healing of **X4** and **X12** was compared to that of the untreated cells recorded daily from days 1-4. The wound healing of scratched cells at 1% FBS was evaluated through a **microscope**, and the HaCaT cell proliferation was imaged as shown in **Figures 33** and **34** for the treated and untreated groups. Topical gel-treated groups stimulated fibroblast proliferation higher than that of the untreated group 96 h post-scratching, except for **CMC/TA/ MgO**, as shown in **Table 4.8**. The untreated group displayed a slower rate of wound reduction (38% in 96 h), contrary to **X12** and **SAT/Lav/Fe₃O₄**, which showed a higher rate of HaCaT cell migration and proliferation with 62% and 86% wound closure, respectively. Elmowafy *et al.* stated that the viscosity of the material prolongs its time at the site of application, in turn prolonging its drug delivery [58]. However, the high cell migration exhibited by SAT/Lav/Fe₃O₄ also displayed dead cells within the surface of the micrograph. Similarly, to these findings, Kozics *et al.* reported that several essential oils, including lavender EO, possess high antibacterial activity and that a higher concentration [0.0469% (w/v)] of lavender EO exhibited 30% HaCaT cell viability [59]. Prashar *et al.* reported that cell safety of lavender essential oil is dose-dependent, as a concentration of 0.125% (v/v) showed 80–100%

viability, while an increase to 0.25% (v/v) showed a toxic effect on human skin cells *in vitro* [60]. Moreover, Miastkowska *et al.* revealed that the cytotoxic effect of commercial lavender EO on the HaCaT cells *in vitro* is influenced by its concentration as 0.025% (v/v) exhibited more than 100% cell viability and 0.390% (v/v) displayed ± 10 HaCaT cell viability [61]. Figure 35 shows an *in vitro* wound scratch assay at 10% FBS.



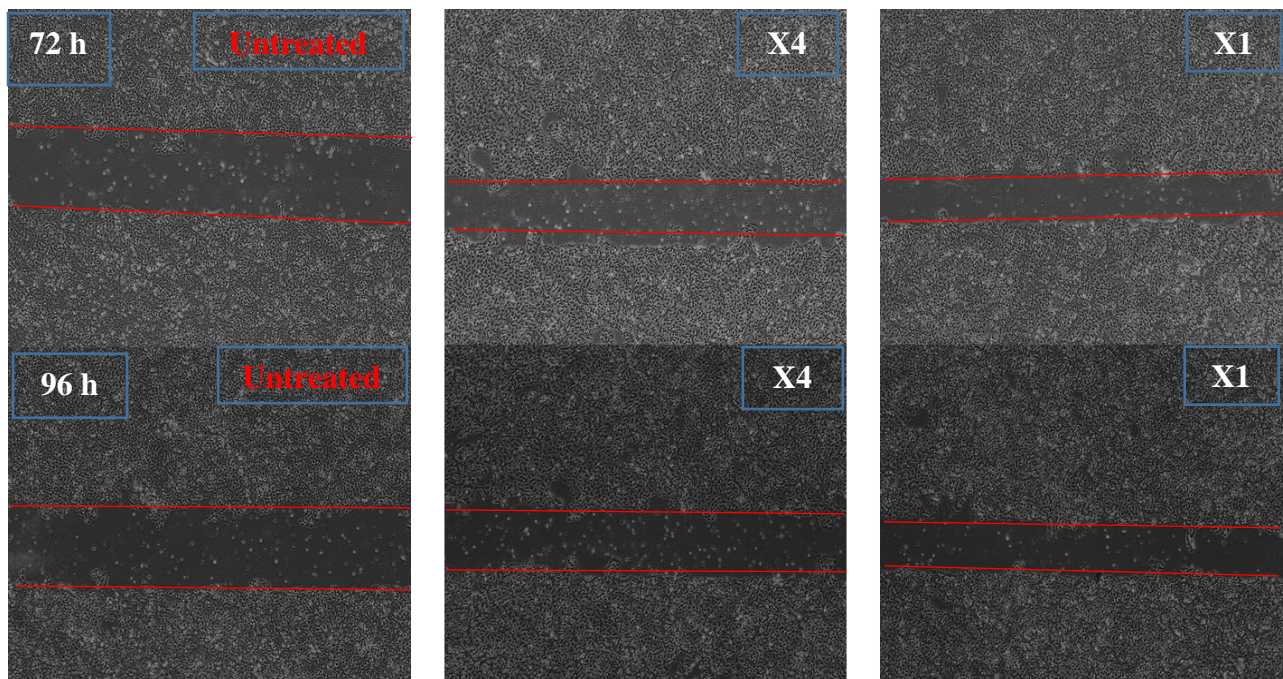


Figure 33: Scratch assay images showing wound healing potential of untreated, X4, and X12 (T0-T96)



University of Fort Hare
Together in Excellence

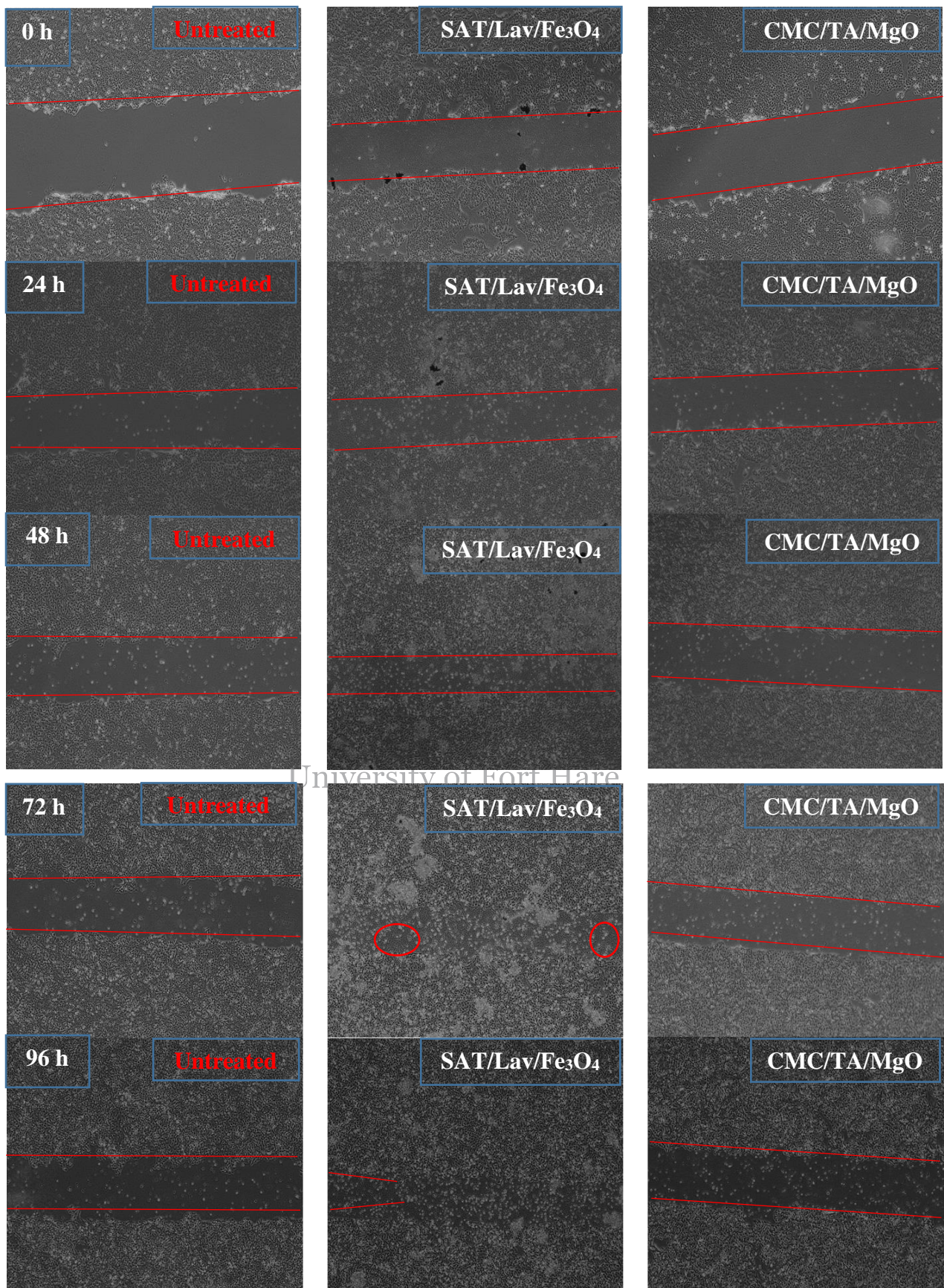


Figure 34: Presents scratch assay images showing wound healing potential of untreated, SAT/Lav/Fe₃O₄, and CMC/TA/MgO (T0-T96)

Table 16: Summary of wound closure for untreated, X4, X12, SAT/Lav/Fe₃O₄, and CMC/TA/MgO (mean ± STD, n=3)

Time (h)	Area (mm)				
	Untreated	X4	X12	SAT/Lav/Fe ₃ O ₄	CMC/TA/MgO
0	1094.54	860.25	692.20	534.859	915.05
24	707.84 ± 12.96	506.07 ± 51.63	384.25 ± 12.18	285.60 ± 31.92	663.32 ± 18.69
48	669.77 ± 25.01	389.55 ± 63.52	278.01 ± 40.78	117.82 ± 12.93	619.18 ± 7.07
72	636.11 ± 68.78	103.3 ± 79.55	131.18 ± 42.10	4.307 ± 1.49	620.95 ± 4.22
96	682.15 ± 9.24	446.83 ± 3.52	260.54 ± 69.69	75.83 ± 103.06	650.55 ± 8.954
Total reduction	412.39 = 38%	413.42 = 48%	431.66 = 62%	459.03 = 86%	264.50 = 29%

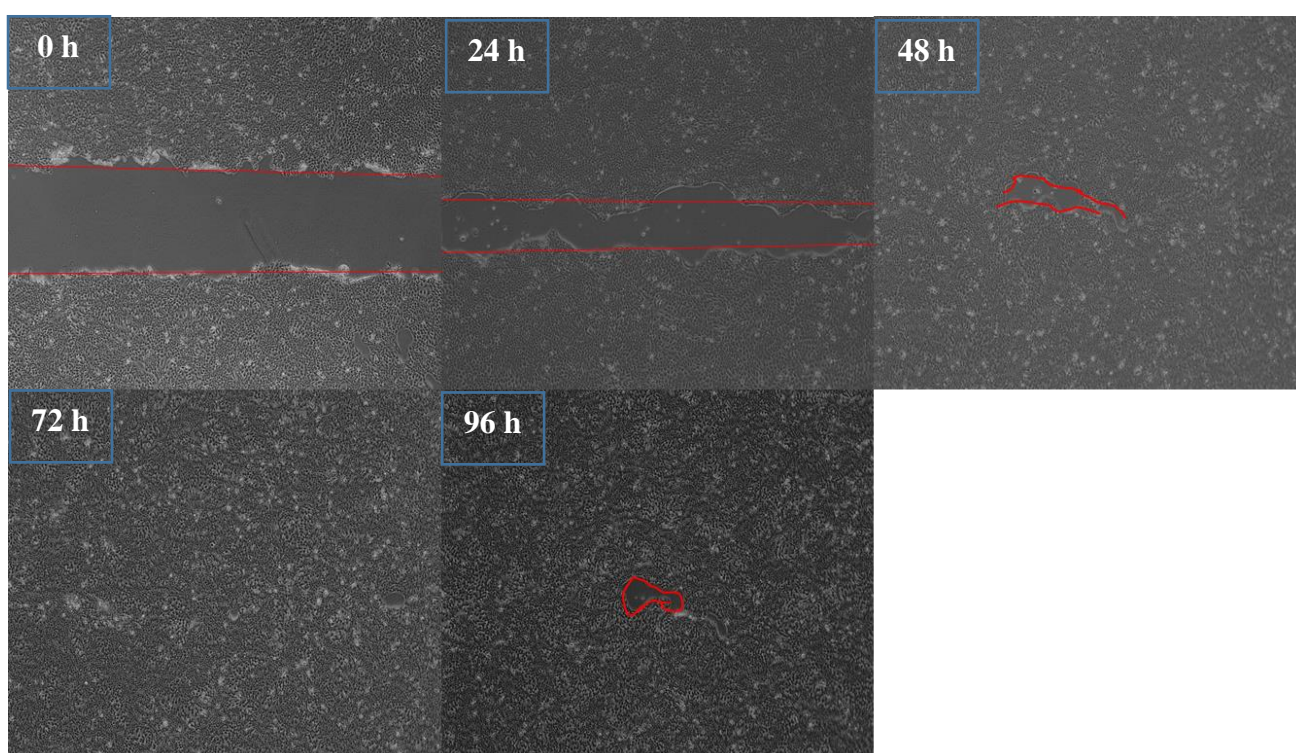


Figure 35: Presents scratch assay images showing wound healing potential of untreated at 10% FBS (T0-T96)

Findings reported in this study suggest that when using lavender EO-based material for direct application to the skin, proper precautions concerning its concentration must be considered. Nevertheless, Lav EO-fixated wound dressings do promote wound healing effects with the right concentration of Lav EO. Kazemi *et al.* reported nanoemulsions composed of lavender EO and licorice (rhizome and root of *Glycyrrhiza glabra*) extract to accelerate wound contraction, showing 98% on the 14th day, by increasing collagen type I and III expressions, including TGF- β -1 [62]. Djemaa *et al.* developed Lav EO-based ointment with a concentration of 4% that revealed 98% wound contraction in 14 days post-injury [63]. **CMC/TA/MgO** did not induce a

wound healing effect, presenting 29% HaCaT cell migration after 96 h of treatment. As reported by Ribeiro *et al.*, a variety of commercially available CMC dressings have been widely used in different stages of wound healing [64]. CMC-based dressings developed in this study are more suitable for the first phase of wound healing as a first-aid pre-hospital treatment to prevent haemorrhage.

X4 exhibited moderate wound closure (48%) on the final day of treatment. Findings presented in this study by the *in vitro* wound healing assay correlate with those of *in vitro* cell viability. A significant difference was observed between untreated and **X12** on day 4 with a *p*-value (0.0065). Chen *et al.* investigated the wound healing potential of PVA/alginate hydrogel formulations using scratch assay and reported that they enhanced mobility and migration of HaCaT cells, showing more than 90% wound reduction after 12 h with a *p*-value (<0.05) compared to the control [65]. Kong and co-workers reported similar PVA/alginate hydrogels loaded with different concentrations of 5-hydroxymethylfurfural [66]. The wound healing scratch assay of these formulations revealed that higher concentrations of 5-hydroxymethylfurfural induced faster wound reduction, showing $\pm 80\%$, and $\pm 38\%$ at the lowest concentration for 48 h against human skin fibroblast cells. Zheng *et al.* reported injectable thermos-sensitive hydrogels that stimulated the migration of HUVEC cells and showed 100% wound reduction in 12 h of treatment, imaged using fluorescent [67]. The *in vitro* wound healing efficacy displayed by these formulations is in agreement with *in vitro* cell viability and antimicrobial activity, revealing their capability to promote fast wound healing and hinder bacterial invasion, a key factor in delayed wound healing. Overall, this data demonstrated that the prepared SA-based gel formulations can stimulate cell migration and mitogenesis in wound healing compared to the CMC-based formulations. However, additional complementary tests *in vivo* are still needed.

References

- [1] Md S, Abdullah S, Alhakamy NA, Shaik RA, Eldakhakhny BM, Omar UM, Eid BG, et al. Development and evaluation of ginkgo biloba/sodium alginate nanocomplex gel as a long-acting formulation for wound healing. *Gels* 2022;19:1-19.
- [2] Siddique W, Zaman M, Waheed S, Sarfraz RM, Bhashir S, Minhas MU, Farooq U, et al. Development and optimization of ganciclovir-loaded carbopol topical gel by response surface methodology for enhanced skin permeation. *Polym. Bull* 2022;1-29.

- [3] Niraimathee VA, Subha V, Ravindran RE, Renganathan S. Green synthesis of iron oxide nanoparticles from *Mimosa pudica* root extract. *Int J Environ Sustain Dev* 2016;15:227-40.
- [4] Demirezen DA, Yıldız YŞ, Yılmaz Ş, Yılmaz DD. Green synthesis and characterization of iron oxide nanoparticles using *Ficus carica* (common fig) dried fruit extract. *J biosci bioeng* 2019;127:241-5.
- [5] Essien ER, Atasie VN, Okefor AO, Nwude DO. Biogenic synthesis of magnesium oxide nanoparticles using *Manihot esculenta* (Crantz) leaf extract. *Int Nano Lett* 2020;10:43-8.
- [6] Maheo AR, Vithiya BS, Prasad TA. Biosynthesis of chitosan and *Eupatorium adenophorum* mediated zinc oxide nanoparticles and their biological and photocatalytic activities. *MaterToday Proc* 2022;65:298-312
- [7] García C, Montero G, Coronado MA, Valdez B, Stoytcheva M, Rosas N, Torres R, Sagaste CA. Valorization of Eucalyptus Leaves by Essential Oil Extraction as an Added Value Product in Mexico. *Waste and Biomass Valor.* 2017;8:1187–97.
- [8] Wang H, Liu Y, Cai K, Zhang B, Tang S, Zhang W, Liu W. Antibacterial polysaccharide-based hydrogel dressing containing plant essential oil for burn wound healing. *Burn Trauma.* 2021;9:1–14.
- [9] Boughendjioua H. Fourier Transformed Infrared Spectroscopy Analysis of Constituents of Lemon Essential Oils from Algeria. *Am J Opt Photonics* 2017;5:30.
- [10] Rezanejad R, Ojagh SM, Heidarieh M, Raëisi M, Rafiee G, Alishahi A. Characterization of gamma-irradiated *rosmarinus officinalis* l. (rosemary). *Turkish J Pharm Sci* 2019;16:43–7.
- [11] Agatonovic-Kustrin S, Ristivojevic P, Gegechkori V, Litvinova TM, Morton DW. Essential oil quality and purity evaluation via ft-ir spectroscopy and pattern recognition techniques. *Appl Sci* 2020;10:1–12.
- [12] Agnieszka N, Danuta K, Malgorzata P, Agata C. Effects of thyme (*Thymus vulgaris* L.) and rosemary (*Rosmarinus officinalis* L.) essential oils on growth of *Brochothrix thermosphacta*. *African J Microbiol Res* 2013;7:3396–404.
- [13] Fernandes RV de B, Borges SV, Botrel DA, Oliveira CR de. Physical and chemical properties of encapsulated rosemary essential oil by spray drying using whey protein-inulin blends as carriers. *Int J Food Sci Technol* 2014;49:1522–9.
- [14] Balasubramanian K, Kodam KM. Encapsulation of therapeutic lavender oil in an electrolyte assisted polyacrylonitrile nanofibres for antibacterial applications. *RSC Adv* 2014;4:54892–901.
- [15] Sofi HS, Akram T, Tamboli AH, Majeed A, Shabir N, Sheikh FA. Novel lavender oil and silver nanoparticles simultaneously loaded onto polyurethane nanofibers for wound-healing applications. *Int J Pharm* 2019;569.
- [16] Mahmood H, Khan IU, Asif M, Khan RU, Asghar S, Khalid I, Khalid SH, et al. In vitro and in vivo evaluation of gellan gum hydrogel films: Assessing the co impact of therapeutic oils and ofloxacin on wound healing. *Int J Biol Macromol* 2021;166:483–95.

- [17] Buyana B, Aderibigbe BA, Ndinteh DT, Fonkui YT, Kumar P. Alginate-pluronic topical gels loaded with thymol, norfloxacin and ZnO nanoparticles as potential wound dressings. *J Drug Deliv Sci Technol* 2020;60:101960.
- [18] Gul W, Alrobei H, Riaz S, Shah A, Khan A. Effect of Iron Oxide Nanoparticles on the Physical Properties of Medium Density Fiberboard 2020.
- [19] Pirsa S, Asadzadeh F, Karimi Sani I. Synthesis of Magnetic Gluten/Pectin/Fe₃O₄ Nano-hydrogel and Its Use to Reduce Environmental Pollutants from Lake Urmia Sediments. *J Inorg Organomet Polym Mater* 2020;30:3188–98
- [20] Mohammadi FM, Ghasemi N. Influence of temperature and concentration on biosynthesis and characterization of zinc oxide nanoparticles using cherry extract. *J Nanostructure Chem* 2018; 8:93–102. <https://doi.org/10.1007/s40097-018-0257-6>.
- [21] John Sushma N, Prathyusha D, Swathi G, Madhavi T, Deva Prasad Raju B, Mallikarjuna K, et al. Facile approach to synthesize magnesium oxide nanoparticles by using *Clitoria ternatea*—characterization and in vitro antioxidant studies. *Appl Nanosci* 2016;6:437–44. <https://doi.org/10.1007/s13204-015-0455-1>.
- [22] Qureshi AA, Javed S, Javed HMA, Jamshaid M, Ali U, Akram MA. Systematic Investigation of Structural, Morphological, Thermal, Optoelectronic, and Magnetic Properties of High-Purity Hematite/Magnetite Nanoparticles for Optoelectronics. *Nanomaterials* 2022;12. <https://doi.org/10.3390/nano12101635>.
- [23] Shalumon KT, Anulekha KH, Nair S V, Nair S V, Chennazhi KP, Jayakumar R. International Journal of Biological Macromolecules Sodium alginate / poly (vinyl alcohol)/ nano ZnO composite nanofibers for antibacterial wound dressings. *Int J Biol Macromol* 2011;49:247–54. <https://doi.org/10.1016/j.ijbiomac.2011.04.005>.
- [24] Attayil Sukumaran S, Kalimuthu B, Selvamurugan N, Mani P. Wound dressings based on chitosan/gelatin/MgO composite films. *Int J Polym Mater Polym Biomater* 2021;0:1–10. <https://doi.org/10.1080/00914037.2021.1960342>.
- [25] Choudhary M, Chhabra P, Tyagi A, Singh H. Scar free healing of full thickness diabetic wounds: A unique combination of silver nanoparticles as antimicrobial agent, calcium alginate nanoparticles as hemostatic agent, fresh blood as nutrient/growth factor supplier and chitosan as base matrix. *Int J Biol Macromol* 2021;178:41–52. <https://doi.org/10.1016/j.ijbiomac.2021.02.133>.
- [26] Barkat A, Pottoo FH, Singh SP, Ahmad FJ. Therapeutic Intervention of Aloe Gel Containing Nano-Sized and Micron-Sized Silver Sulfadiazine Gel on Second-Degree Burn : A Comparative Study 2018. <https://doi.org/10.1177/1534734618791860>.
- [27] Mohammadi M, Mohammadi M. Non-Newtonian Shear-Thinning Fluid Passing Through a Duct with an Obstacle , Using a Power Law Model 2015;61:594–600. <https://doi.org/10.5545/sv-jme.2015.2650>.
- [28] Ontong JC, Singh S, Nwabor OF, Chusri S, Cytotoxicity ÁÁÁ. Potential of antimicrobial topical gel with synthesized biogenic silver nanoparticle using *Rhodomyrtus tomentosa* leaf extract and silk sericin. *Biotechnol Lett* 2020;42:2653–64. <https://doi.org/10.1007/s10529-020-02971-5>.

- [29] Carvalho C, Barbi MS, Hugo V, Sarmiento V, Chiavacci LA, Netto M, et al. Surfactant systems for nasal zidovudine delivery : structural , rheological and mucoadhesive properties 2010;430–9. <https://doi.org/10.1211/jpp/62.04.0004>.
- [30] Liu M, Wang X, Li H, Xia C, Liu Z, Liu J, et al. Magnesium oxide-incorporated electrospun membranes inhibit bacterial infections and promote the healing process of infected wounds. *J Mater Chem B* 2021;9:3727–44. <https://doi.org/10.1039/d1tb00217a>.
- [31] Yaroslavovytch PO. *Mmj-60-1-35-38* 2017;60. <https://doi.org/10.5281/zenodo.1050962>.
- [32] Norouzi MA, Montazer M, Harifi T, Karimi P. Flower buds like PVA/ZnO composite nanofibers assembly: Antibacterial, in vivo wound healing, cytotoxicity and histological studies. *Polym Test* 2021;93:106914. <https://doi.org/10.1016/j.polymertesting.2020.106914>.
- [33] Soubhagya AS, Moorthi A, Prabakaran M. Preparation and characterization of chitosan/pectin/ZnO porous films for wound healing. *Int J Biol Macromol* 2020;157:135–45. <https://doi.org/10.1016/j.ijbiomac.2020.04.156>.
- [34] Zhang M, Qiao X, Han W, Jiang T, Liu F, Zhao X. Alginate-chitosan oligosaccharide/ZnO composite hydrogel for accelerating wound healing. *Carbohydr Polym* 2021;266:118100. <https://doi.org/10.1016/j.carbpol.2021.118100>.
- [35] Farooq A, Patoary MK, Zhang M, Mussana H, Li M, Naeem MA, et al. Cellulose from sources to nanocellulose and an overview of synthesis and properties of nanocellulose/zinc oxide nanocomposite materials. *Int J Biol Macromol* 2020;154:1050–73. <https://doi.org/10.1016/j.ijbiomac.2020.03.163>.
- [36] Masood N, Ahmed R, Tariq M, Ahmed Z, Masoud MS, Ali I, et al. Silver nanoparticle impregnated chitosan-PEG hydrogel enhances wound healing in diabetes-induced rabbits. *Int J Pharm* 2019;559:23–36. <https://doi.org/10.1016/j.ijpharm.2019.01.019>.
- [37] Li Y, Wang J, Yang Y, Shi J, Zhang H, Yao X, et al. A rose bengal/graphene oxide/PVA hybrid hydrogel with enhanced mechanical properties and light-triggered antibacterial activity for wound treatment. *Mater Sci Eng C* 2021;118:111447. <https://doi.org/10.1016/j.msec.2020.111447>.
- [38] Prema D, Binu NM, Prakash J, Venkatasubbu GD. Photoinduced mechanistic activity of GO/Zn(Cu)O nanocomposite against infectious pathogens: Potential application in wound healing. *Photodiagnosis Photodyn Ther* 2021;34:102291. <https://doi.org/10.1016/j.pdpdt.2021.102291>.
- [39] Dong Z. Graphene Oxide / Copper Nanoderivatives-Modified Chitosan / Hyaluronic Acid Dressings for Facilitating Wound Healing in Infected Full-Thickness Skin Defects 2020:8231–47.
- [40] Ahmad NS, Abdullah N, Yasin FM. Toxicity assessment of reduced graphene oxide and titanium dioxide nanomaterials on gram-positive and gram-negative bacteria under normal laboratory lighting conditions. *Toxicol Reports* 2020;7:693–9. <https://doi.org/10.1016/j.toxrep.2020.04.015>.

- [41] Malathi S, Balashanmugam P, Devasena T, Kalkura SN. Enhanced antibacterial activity and wound healing by a novel collagen blended ZnO nanoparticles embedded niosome nanocomposites. *J Drug Deliv Sci Technol* 2021;63:102498. <https://doi.org/10.1016/j.jddst.2021.102498>.
- [42] Lin YH, Lin JH, Hong YS. Development of chitosan/poly- γ -glutamic acid/pluronic/curcumin nanoparticles in chitosan dressings for wound regeneration. *J Biomed Mater Res - Part B Appl Biomater* 2017;105:81–90. <https://doi.org/10.1002/jbm.b.33394>.
- [43] Augustine R, Rehman SRU, Ahmed R, Zahid AA, Sharifi M, Falahati M, et al. Electrospun chitosan membranes containing bioactive and therapeutic agents for enhanced wound healing. *Int J Biol Macromol* 2020;156:153–70. <https://doi.org/10.1016/j.ijbiomac.2020.03.207>.
- [44] Ngece K, Aderibigbe BA, Ndinteh DT, Fonkui YT, Kumar P. International Journal of Biological Macromolecules Alginate-gum acacia based sponges as potential wound dressings for exuding and bleeding wounds. *Int J Biol Macromol* 2021;172:350–9. <https://doi.org/10.1016/j.ijbiomac.2021.01.055>.
- [45] Mahmood H, Khan IU, Asif M, Khan RU, Asghar S, Khalid I, et al. In vitro and in vivo evaluation of gellan gum hydrogel films: Assessing the co impact of therapeutic oils and ofloxacin on wound healing. *Int J Biol Macromol* 2021;166:483–95. <https://doi.org/10.1016/j.ijbiomac.2020.10.206>.
- [46] Khezri K, Farahpour MR, Mounesi Rad S. Accelerated infected wound healing by topical application of encapsulated Rosemary essential oil into nanostructured lipid carriers. *Artif Cells, Nanomedicine Biotechnol* 2019;47:980–8. <https://doi.org/10.1080/21691401.2019.1582539>.
- [47] Liu R, Dai L, Si C, Zeng Z. Antibacterial and hemostatic hydrogel via nanocomposite from cellulose nanofibers. *Carbohydr Polym* 2018;195:63–70. <https://doi.org/10.1016/j.carbpol.2018.04.085>.
- [48] Ali NH, Amin MCIM, Ng SF. Sodium carboxymethyl cellulose hydrogels containing reduced graphene oxide (rGO) as a functional antibiofilm wound dressing. *J Biomater Sci Polym Ed* 2019;30:629–45. <https://doi.org/10.1080/09205063.2019.1595892>.
- [49] Ambekar RS, Kandasubramanian B. Advancements in nano fibers for wound dressing : A review 2019;117:304–36. <https://doi.org/10.1016/j.eurpolymj.2019.05.020>.
- [50] Huang X, Fu Q, Deng Y, Wang F, Xia B, Chen Z, et al. Surface roughness of silk fibroin/alginate microspheres for rapid hemostasis in vitro and in vivo. *Carbohydr Polym* 2021;253:117256. <https://doi.org/10.1016/j.carbpol.2020.117256>.
- [51] Li G, Liang Y, Xu C, Sun H, Tao L, Wei Y, et al. Polydopamine reinforced hemostasis of a graphene oxide sponge via enhanced platelet stimulation. *Colloids Surfaces B Biointerfaces* 2019;174:35–41. <https://doi.org/10.1016/j.colsurfb.2018.10.074>.
- [52] Zhao X, Zhang Z, Luo J, Wu Z, Yang Z, Zhou S, et al. Biomimetic , highly elastic conductive and hemostatic gelatin / rGO-based nanocomposite cryogel to improve 3D

- myogenic differentiation and guide in vivo skeletal muscle regeneration. *Appl Mater Today* 2022;26:101365. <https://doi.org/10.1016/j.apmt.2022.101365>.
- [53] Sasmal P, Datta P. Tranexamic acid-loaded chitosan electrospun nanofibers as drug delivery system for hemorrhage control applications. *J Drug Deliv Sci Technol* 2019;52:559–67. <https://doi.org/10.1016/j.jddst.2019.05.018>.
- [54] Mahmoodzadeh A, Moghaddas J, Jarolmasjed S, Ebrahimi Kalan A, Edalati M, Salehi R. Biodegradable cellulose-based superabsorbent as potent hemostatic agent. *Chem Eng J* 2021;418:129252. <https://doi.org/10.1016/j.cej.2021.129252>.
- [55] AOSHIMA M, TANABE K, KOHNO I, JO Y, TAKAHASHI K, SUGO T, et al. Hemostatic mechanisms of a soluble fraction of plant-derived sodium carboxymethyl cellulose. *Japanese J Thromb Hemost* 2012;23:387–98. <https://doi.org/10.2491/jjsth.23.387>.
- [56] Gu H, He J, Huang Y, Guo Z. Fabrication of oxidized sodium carboxymethylcellulose from viscose fibers and their viscosity behaviors. *Fibers Polym* 2013;14:1266–70. <https://doi.org/10.1007/s12221-013-1266-1>.
- [57] Pawar V, Dhanka M, Srivastava R. Colloids and Surfaces B : Biointerfaces Cefuroxime conjugated chitosan hydrogel for treatment of wound infections. *Colloids Surfaces B Biointerfaces* 2019;173:776–87. <https://doi.org/10.1016/j.colsurfb.2018.10.034>.
- [58] Elmowafy M, Al-Sanea MM. Nanostructured lipid carriers (NLCs) as drug delivery platform: Advances in formulation and delivery strategies. *Saudi Pharm J* 2021.
- [59] Kozics K, Bucková M, Puškárová A, Kalászová V, Cabicarová T, Pangallo D. molecules The Effect of Ten Essential Oils on Several Cutaneous Drug-Resistant Microorganisms and Their Cyto/Genotoxic and Antioxidant Properties. *Molecules* 2019;24:15.
- [60] Prashar A, Locke IC, Evans CS. Cytotoxicity of lavender oil and its major components to human skin cells. *Cell Prolif* 2004;37:221–9. <https://doi.org/10.1111/j.13652184.2004.00307.x>.
- [61] Miastkowska M, Kantyka T, Bielecka E, Kałucka U, Kamińska M, Kucharska M, et al. Enhanced biological activity of a novel preparation of *lavandula angustifolia* essential oil. *Molecules* 2021;26. <https://doi.org/10.3390/molecules26092458>.
- [62] Kazemi M, Mohammadifar M, Aghadavoud E, Vakili Z, Aarabi MH, Talaei SA. Deep skin wound healing potential of lavender essential oil and licorice extract in a nanoemulsion form: Biochemical, histopathological and gene expression evidences. *J Tissue Viability* 2020;29:116–24. <https://doi.org/10.1016/j.jtv.2020.03.004>.
- [63] Ben Djemaa FG, Bellassoued K, Zouari S, El Feki A, Ammar E. Antioxidant and wound healing activity of *Lavandula aspic L.* ointment. *J Tissue Viability* 2016;25:193–200. <https://doi.org/10.1016/j.jtv.2016.10.002>.
- [64] Ribeiro AM, Magalhães M, Veiga F, Figueiras A. Cellulose-Based Hydrogels in Topical Drug Delivery: A Challenge in Medical Devices 2019:1205–33. https://doi.org/10.1007/978-3-319-77830-3_41.

- [65] Chen G, He L, Zhang P, Zhang J, Mei X, Wang D, et al. Encapsulation of green tea polyphenol nanospheres in PVA/alginate hydrogel for promoting wound healing of diabetic rats by regulating PI3K/AKT pathway. *Mater Sci Eng C* 2020;110:110686. <https://doi.org/10.1016/j.msec.2020.110686>.
- [66] Kong F, Fan C, Yang Y, Hoon B, Wei K. International Journal of Biological Macromolecules 5-hydroxymethylfurfural-embedded poly (vinyl alcohol)/ sodium alginate hybrid hydrogels accelerate wound healing. *Int J Biol Macromol* 2019;138:933–49. <https://doi.org/10.1016/j.ijbiomac.2019.07.152>.
- [67] Zheng Z, Bian S, Li Z, Zhang Z, Liu Y, Zhai X, et al. Catechol modified quaternized chitosan enhanced wet adhesive and antibacterial properties of injectable thermosensitive hydrogel for wound healing. *Carbohydr Polym* 2020;249:116826. <https://doi.org/10.1016/j.carbpol.2020.116826>.

Chapter 5

5. CONCLUSION

The prepared topical gels presented promising wound healing characteristics, and the FTIR spectra confirmed that the loading of TA or nanoparticles did not affect the polymer composition of the gels. The high viscosity displayed by the gels suggests that they can be easily applied to the skin without flowing off during and after application. The decrease in viscosity of the gels with increased time showed that the gels have a shear-thinning behaviour. SEM and XRD confirmed the successful formation of the nanoparticles, revealing a crystalline peak in the range of 11–57° linked to their indices, showing a resemblance to that reported in the literature. *In vitro* drug release kinetics displayed by the prepared gel formulations revealed that they are mostly fitted to the Korsmeyer Peppas model compared to other mathematical models. The formulations followed Quasi-Fickian and non-Fickian release mechanisms. Loading of TA and nanoparticles significantly increased cell viability and antibacterial activity of the prepared topical gels, as pure topical gels **X1** and **CMC-blank** exhibited the lowest percentage of cell safety and the least microbial efficacy.

All the prepared gel formulations revealed significant antibacterial effects against the tested strains of bacteria. However, outstanding results were presented by **SA/Lav/Fe₃O₄**, which inhibited all strains of bacteria compared to all other formulations, followed by **X7**, **SAT/Lav/Fe₃O₄**, **SA/Rose**, **SA/Rose/Fe₃O₄**, **X4**, **X5**, **X12**, and **X14**. Overall, CMC-based formulations exhibited poor antibacterial activity against the tested bacterial strains. Importantly, the MIC values exhibited by these gels showed they have antibacterial activity against the common resistant strains of bacteria, *S. aureus* and *E. coli*. Nevertheless, CMC-

based gel formulations displayed optimum haemostasis compared to SA-based gels loaded with nanoparticles and SA-based gels loaded with different essential oils, TA, and iron oxide. **CMC/TA/ZnO** displayed the lowest absorbance values compared to **SA/Rose** (p -value = 0.0043) and **X14** (p -value = 0.0499) which displayed significant haemostasis in their respective groups. Evaluation of cell viability on HaCaT cells showed that SA-based formulations exhibited high cell viability, while CMC-based formulations displayed moderate cell viability.

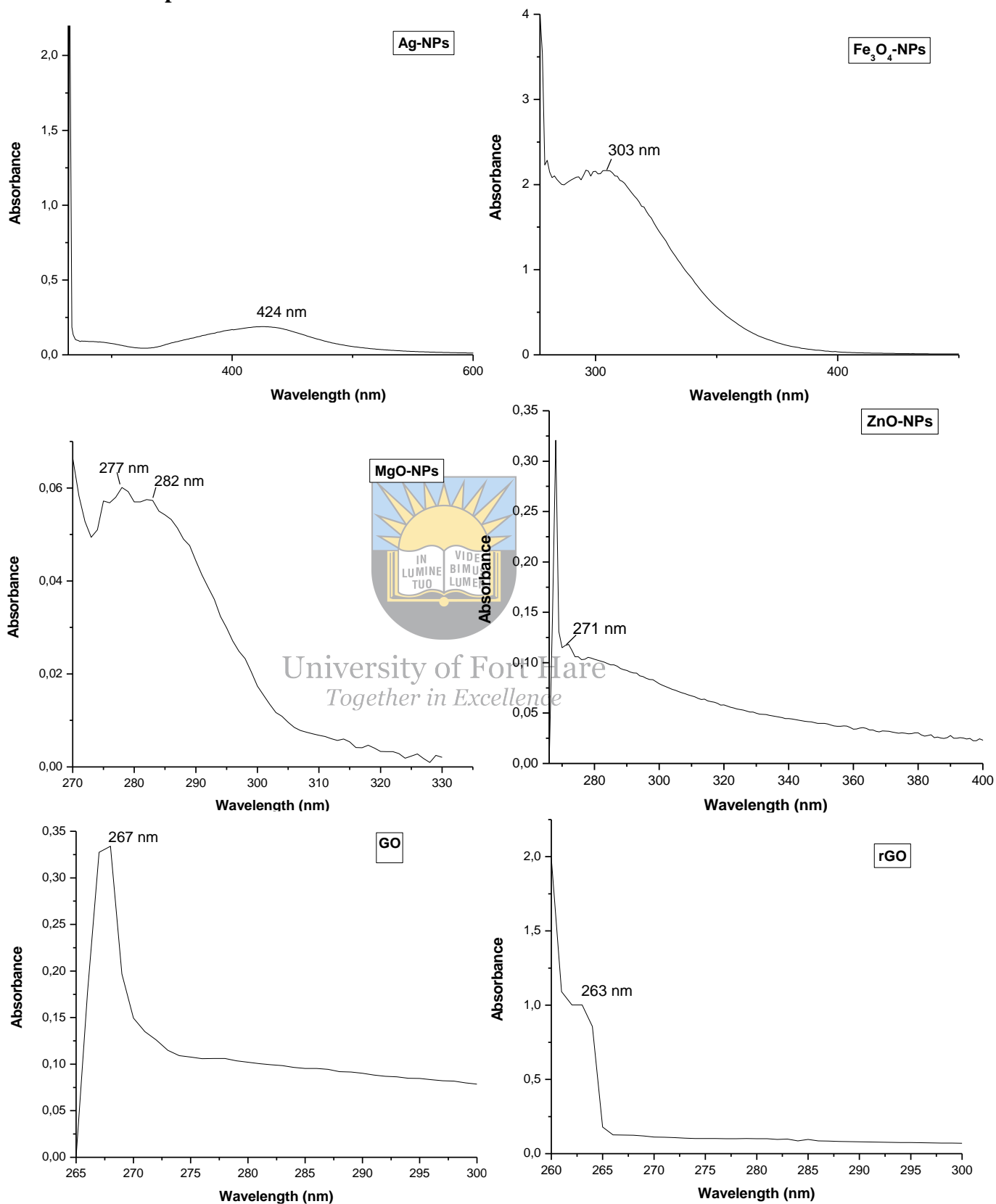
In vitro wound scratch assay results are co-related with the *in vitro* cell viability results, with SA-based gels fabricated with TA and nanoparticles showing a high rate of wound closure compared to CMC-based formulations loaded with the same bioactive agents. Gel formulations **X4** and **X12** displayed higher cell proliferation features compared to other gel formulations, and they increased HaCaT cell migration in the affected region. Interestingly, **SAT/Lav/Fe₃O₄** displayed high cell migration in the affected area, though there were also dead cells. The concentration of essential oils should be considered and controlled when preparing open wound dressings to enhance their safety. **CMC/TA/MgO** displayed no wound healing effect as investigated using the wound scratch assay throughout the tested period. Findings in this study show that SA-based topical gels loaded with TA, nanoparticles, and EO are promising scaffolds for the management of bleeding and microbial-infected wounds. CMC-based scaffolds were best suited for the first phase of wound healing, as all formulations in this category exhibited low absorbance values. CMC-based topical gels reported in this study are good materials for rapid blood clotting during accidents and pre-hospital cases. The high antibacterial efficacy displayed by SA-based topical gels makes them suitable for application to infected and chronic wounds. However, *in vitro* drug release studies at pH 5.5 that resemble those of chronic wounds are required. Additionally, *in vivo* studies are still needed to further confirm the wound-healing properties of these formulations and their pharmacokinetic compliance.

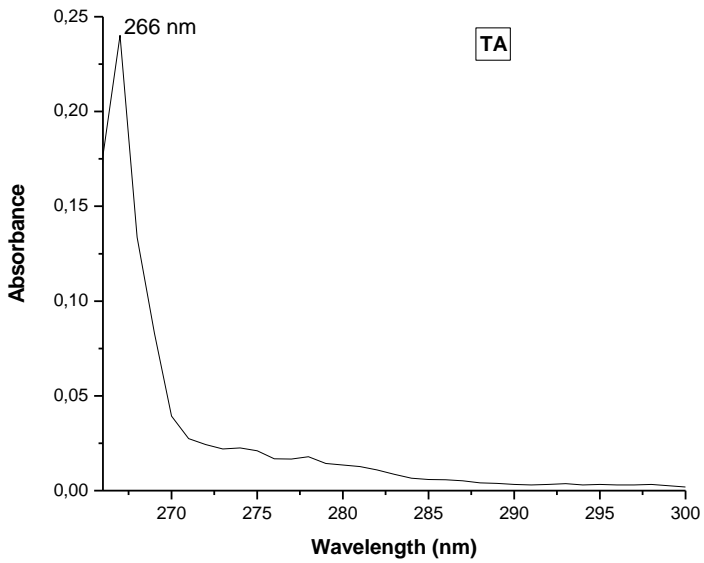
5.1. Limitation of these studies

The findings obtained from this study revealed the promising potential of topical gels loaded with essential oils for the management of infected and bleeding wounds. However, dilution of lavender EO is considered to promote cell safety when incorporated into topical gels. Haemolysis assay still needs to be performed mostly on CMC-based formulations, as they display promising haemostatic features and need to be checked for their safety on red blood cells. *In vivo* studies of the reported scaffolds are still needed to confirm the wound-healing effect of these formulations.

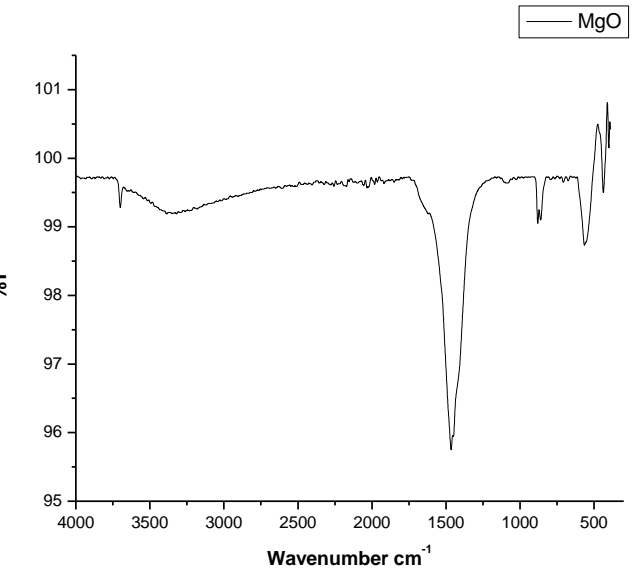
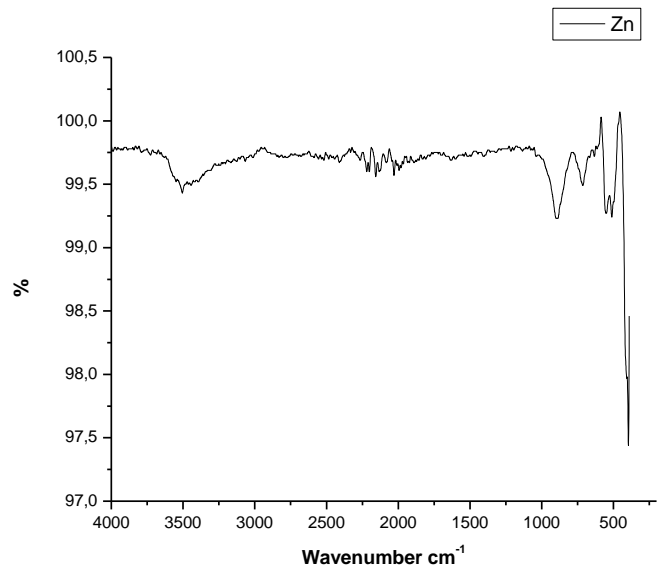
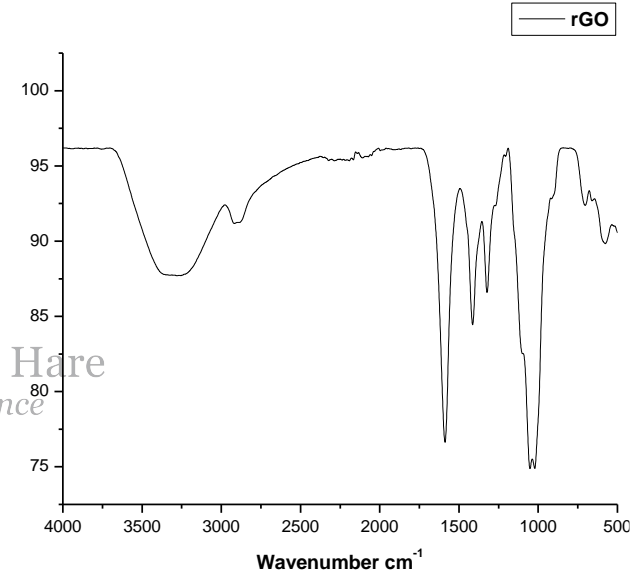
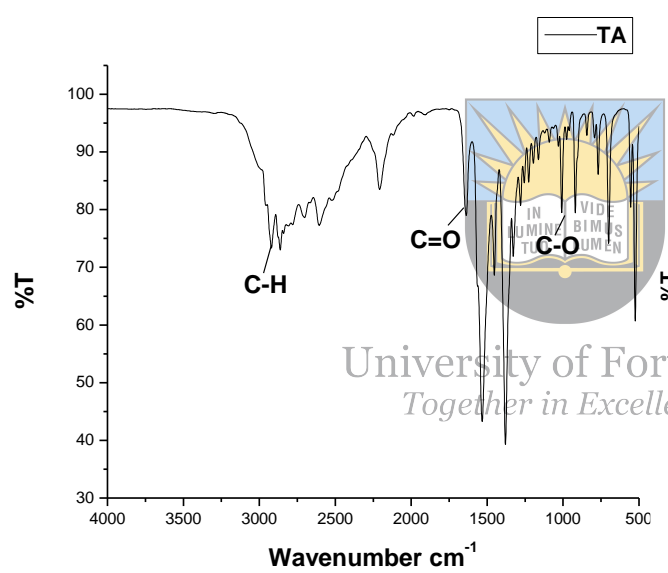
Appendix

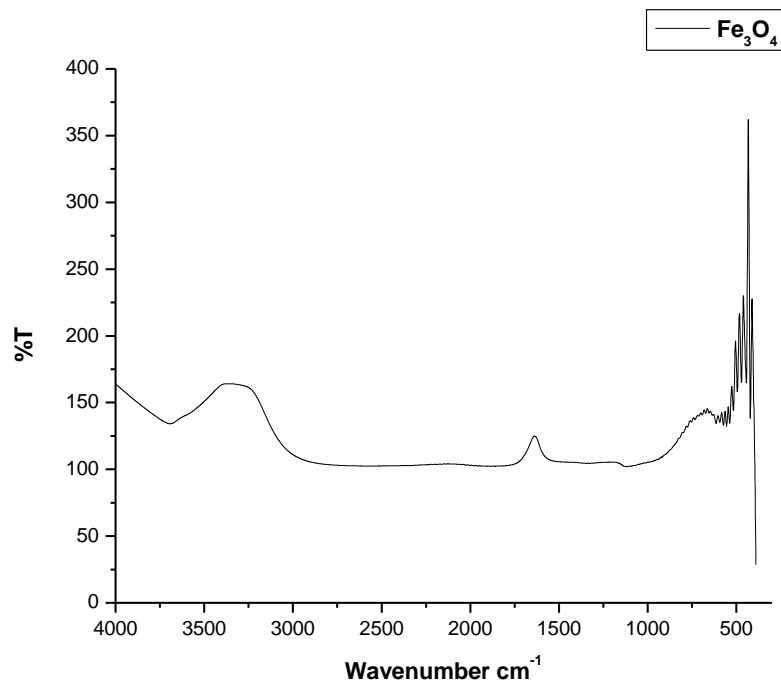
UV-Vis of Nanoparticles and TA



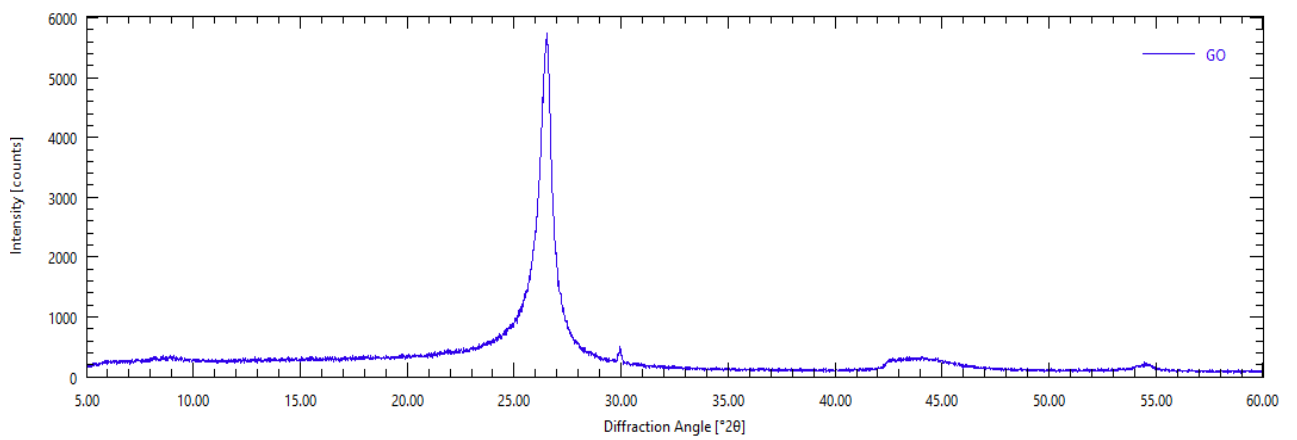
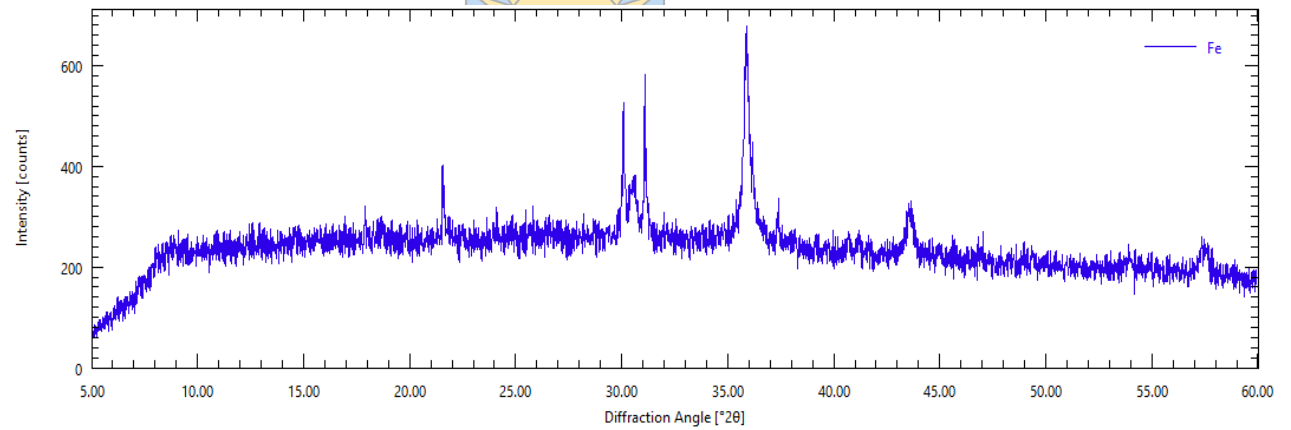


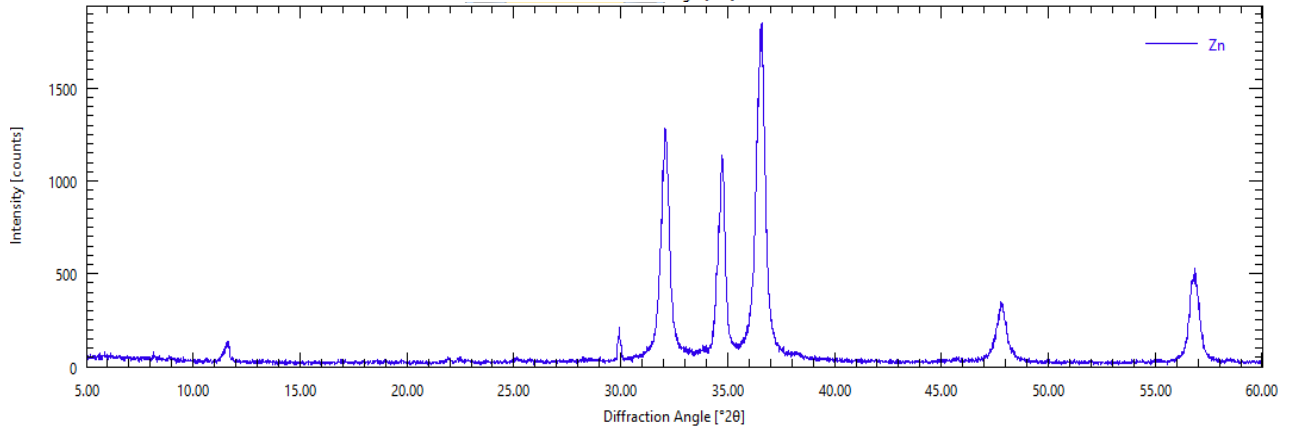
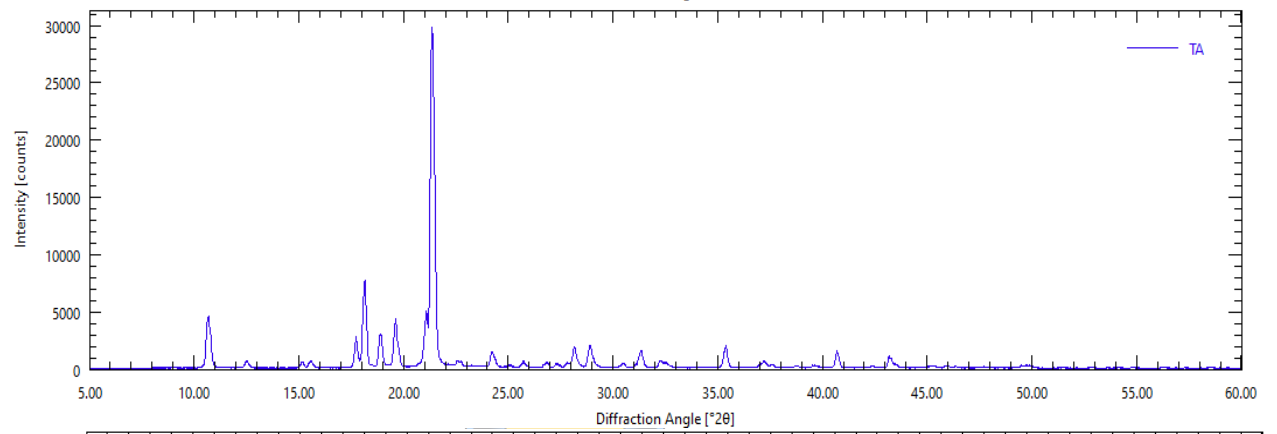
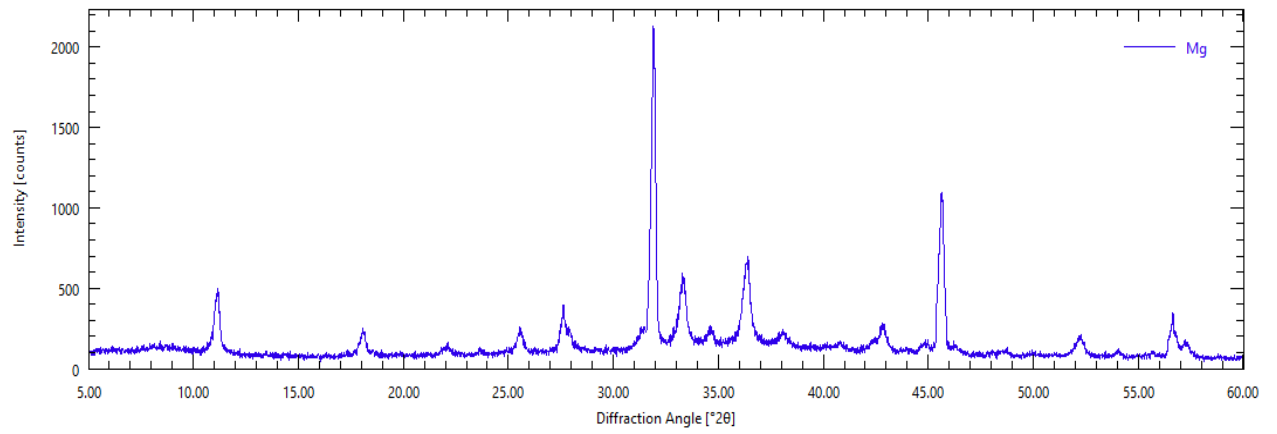
Fourier-Transform Infrared Spectroscopy



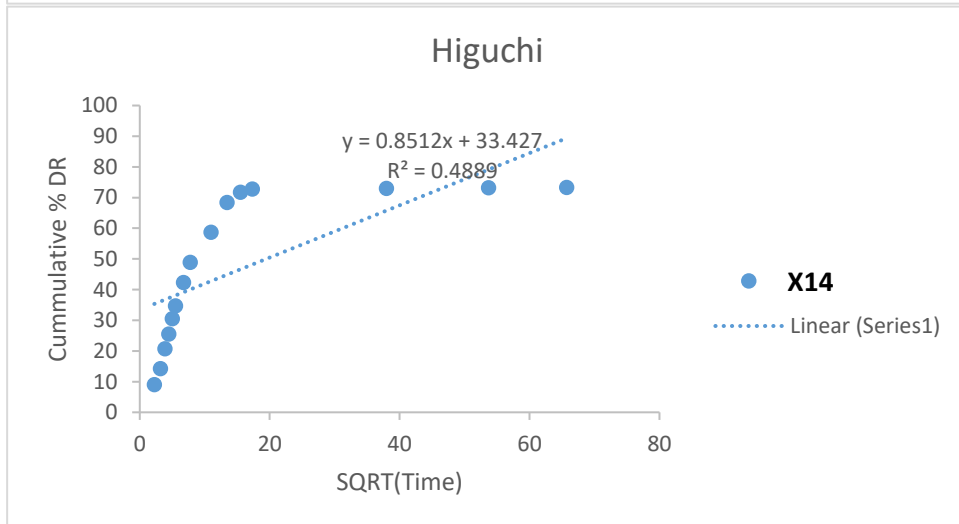
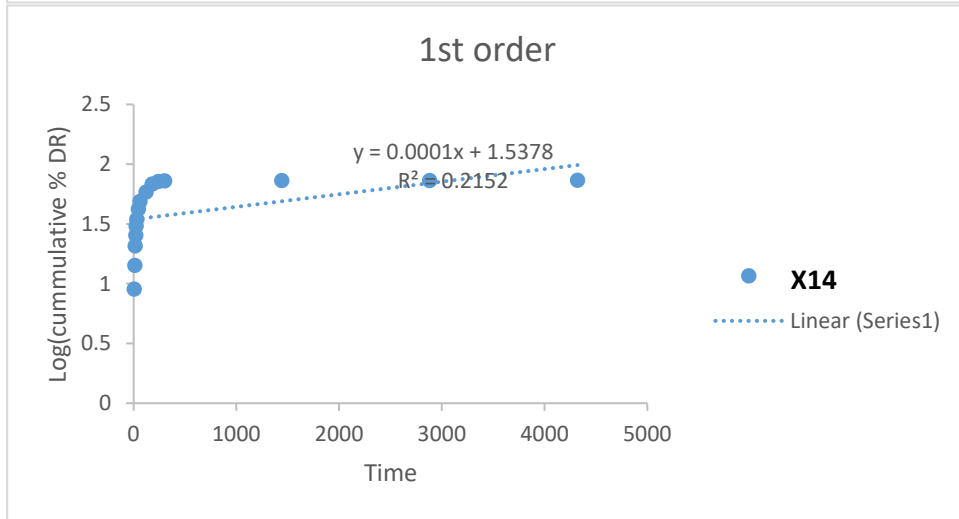
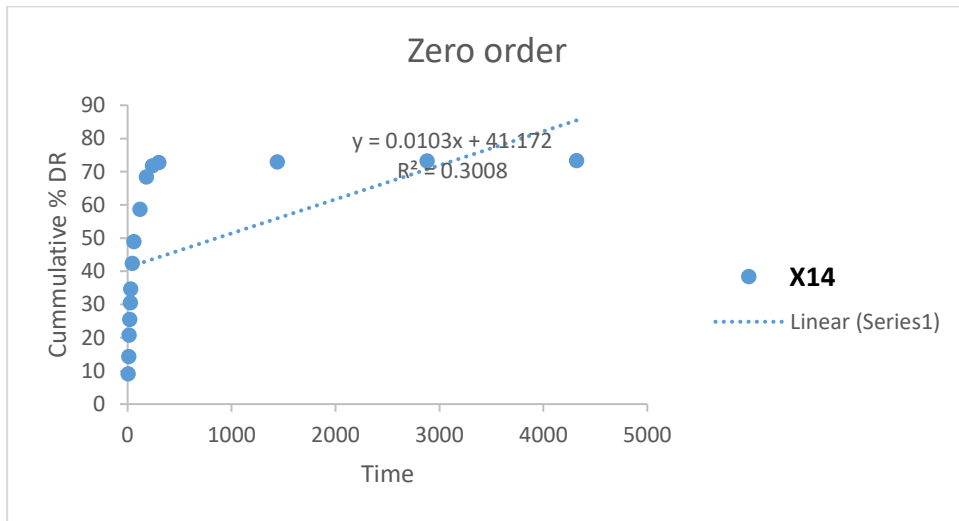


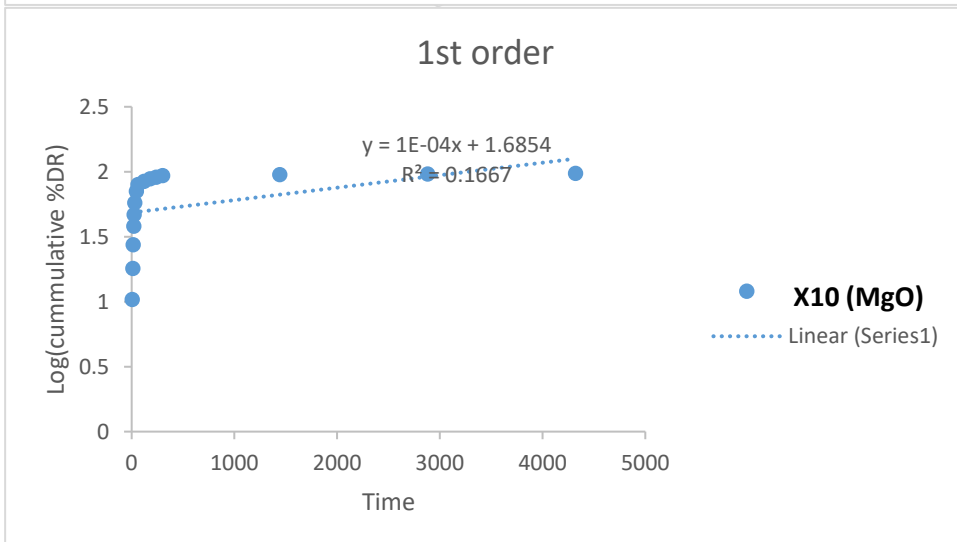
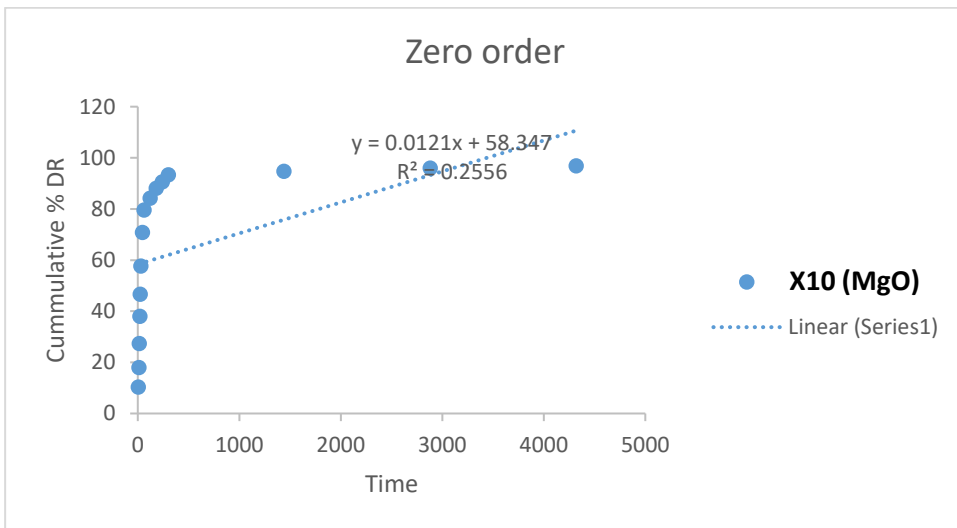
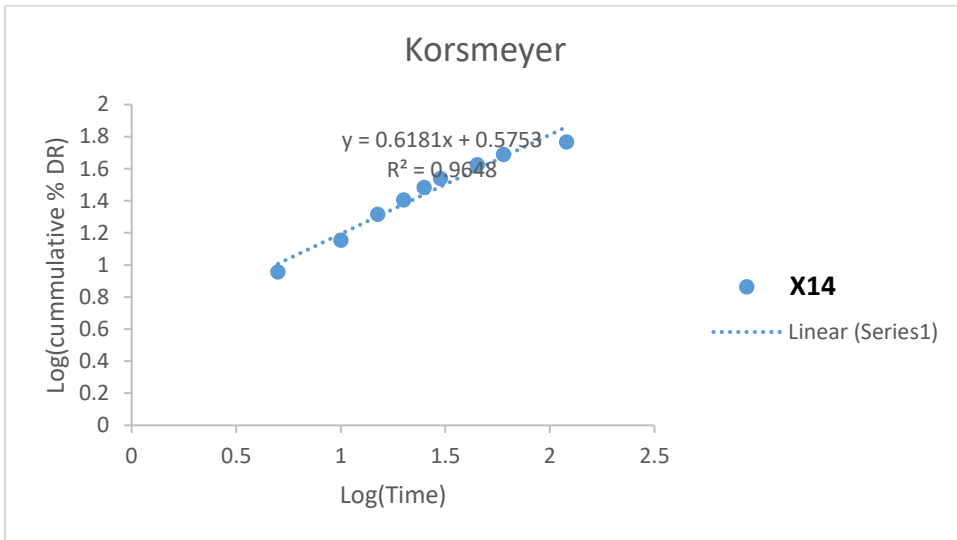
X-Ray Diffraction of Nanoparticles

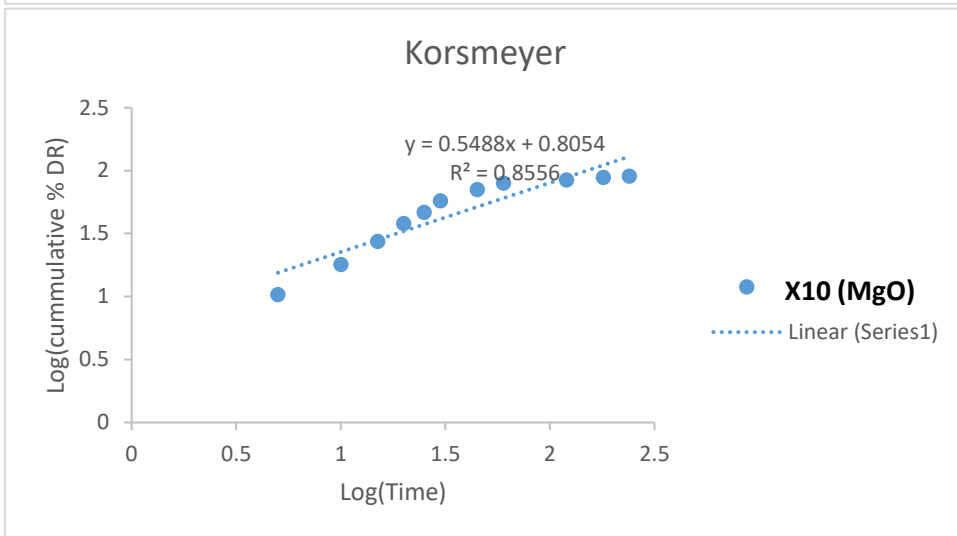
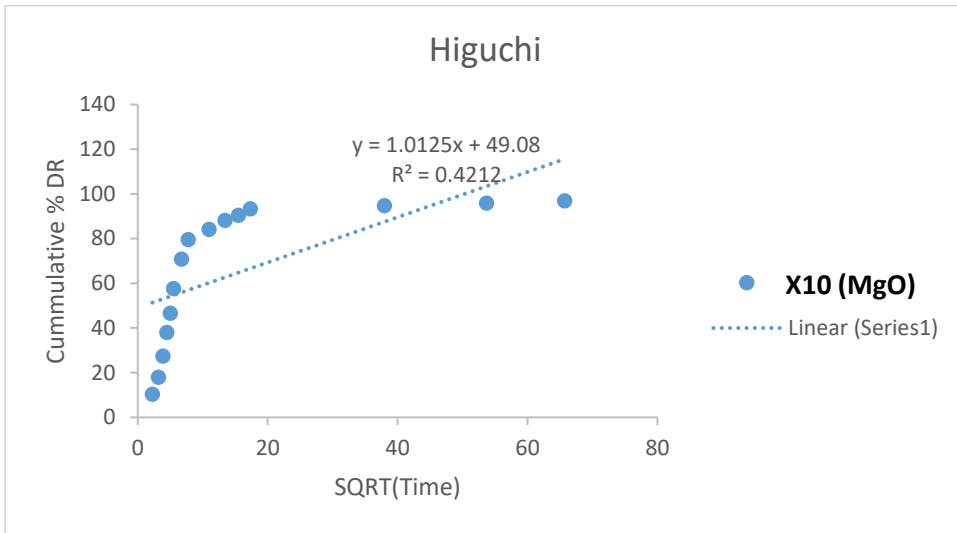




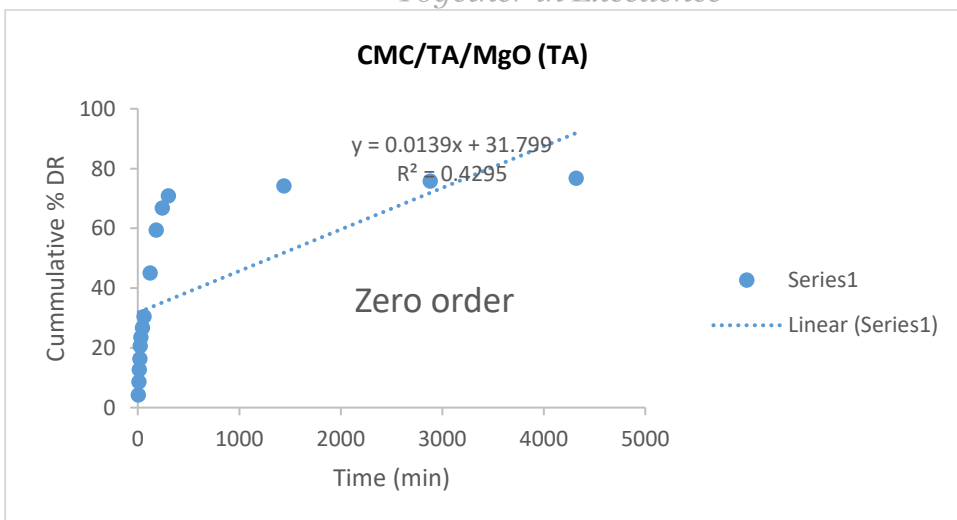
Linear plots for the four mathematical models used

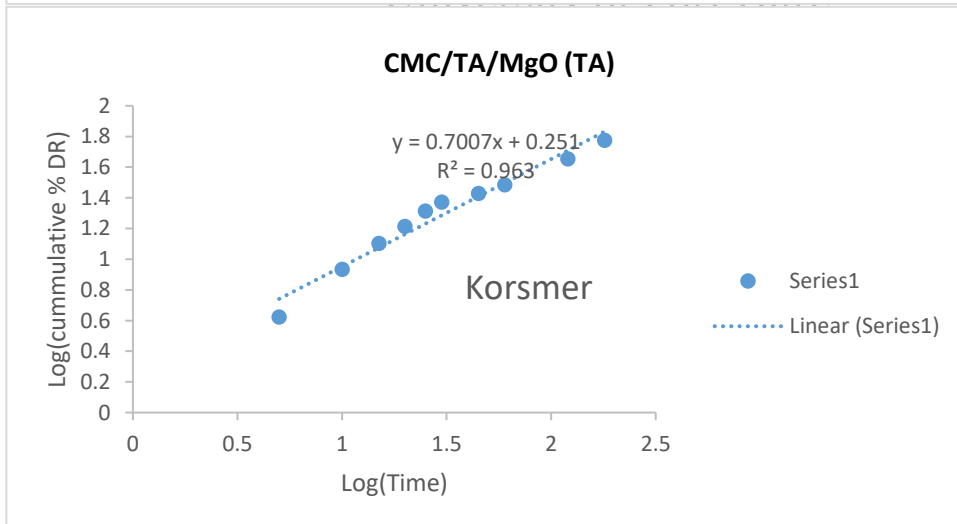
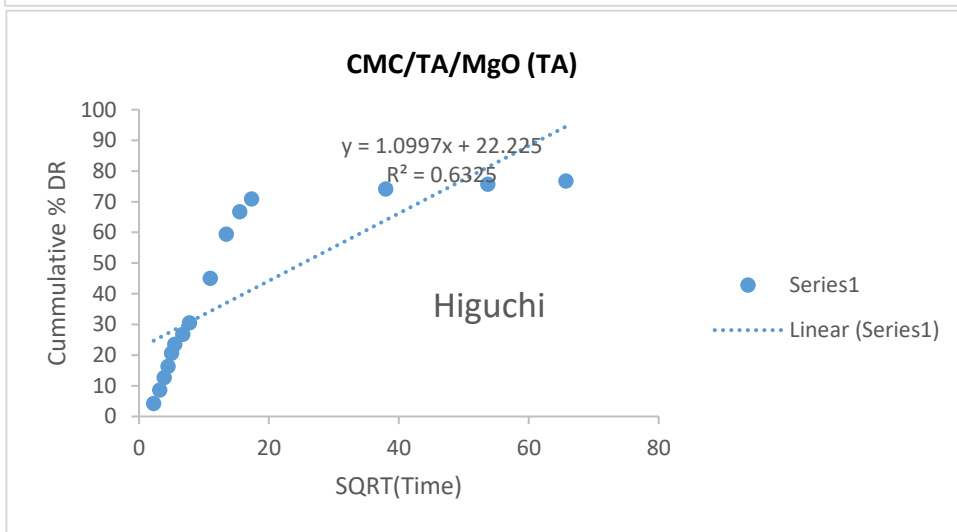
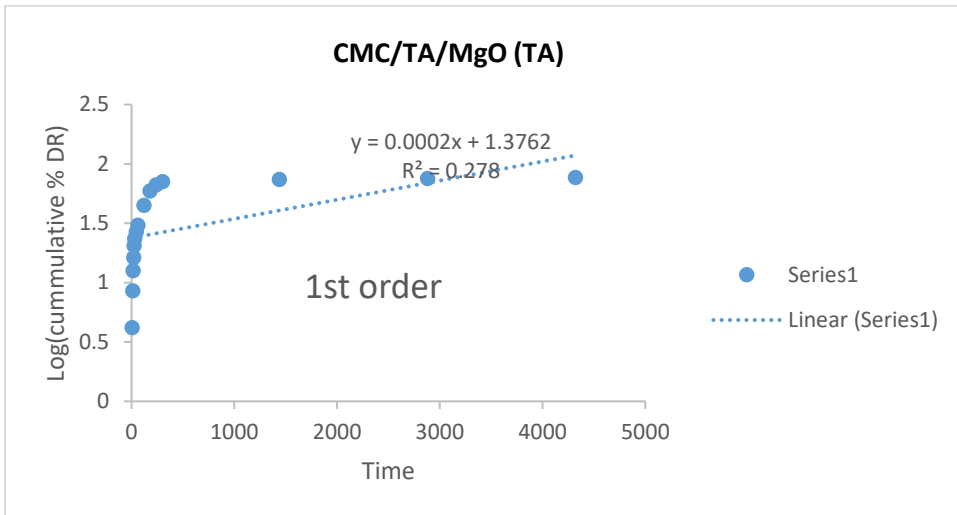


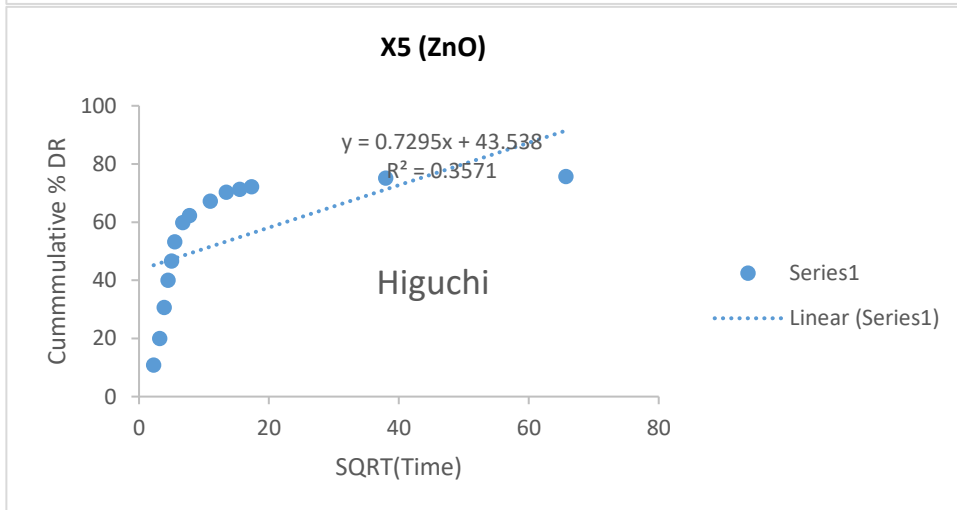
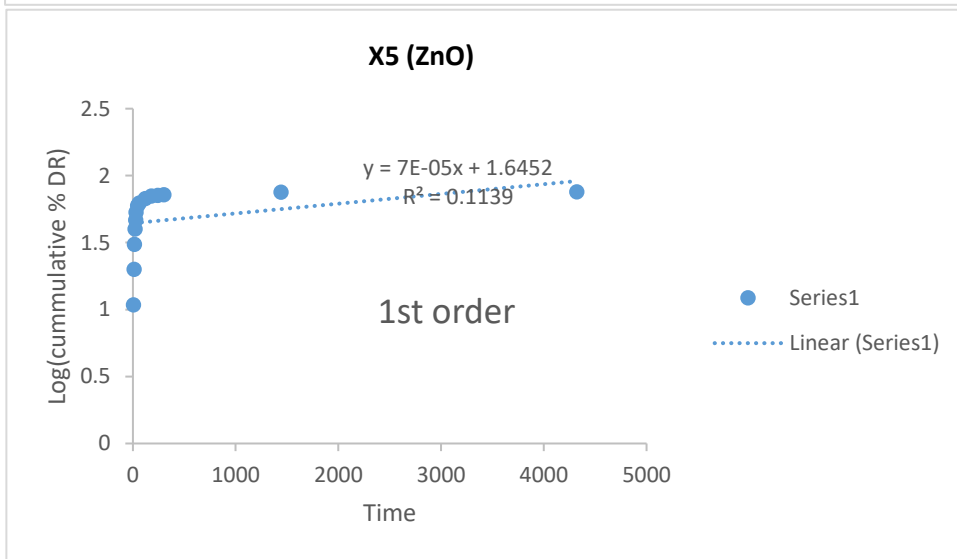
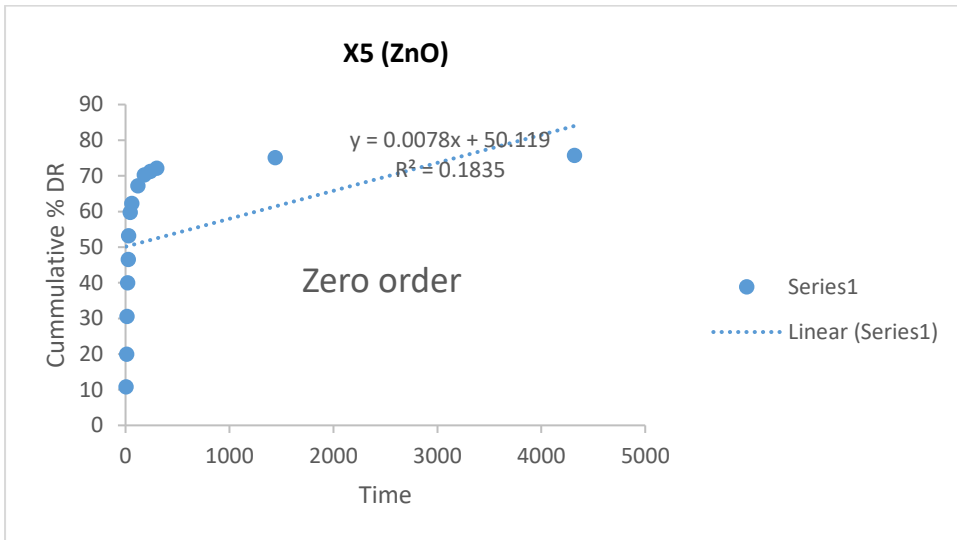


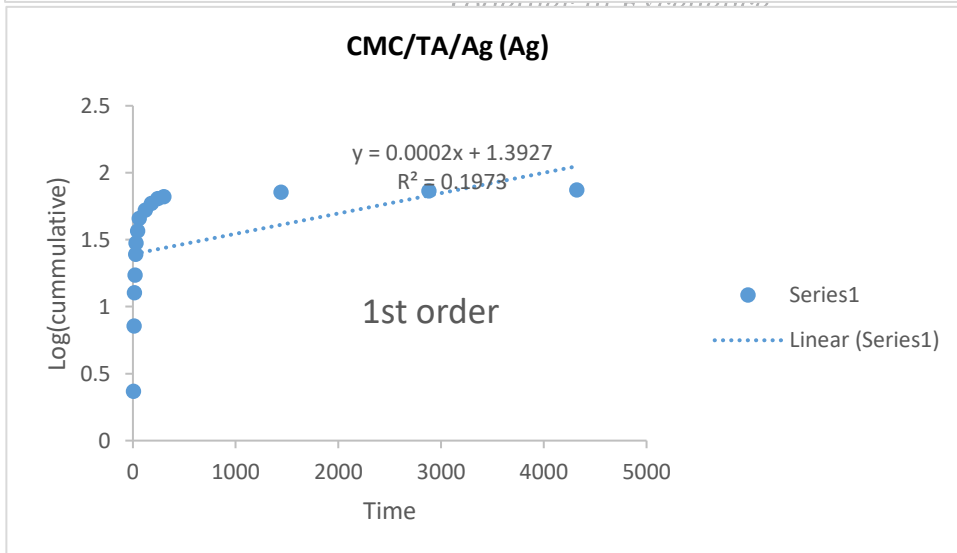
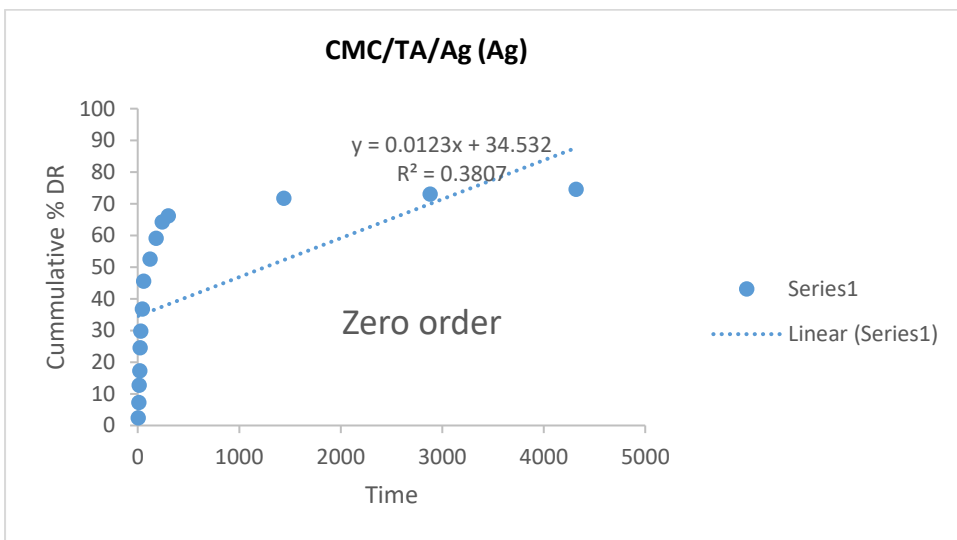
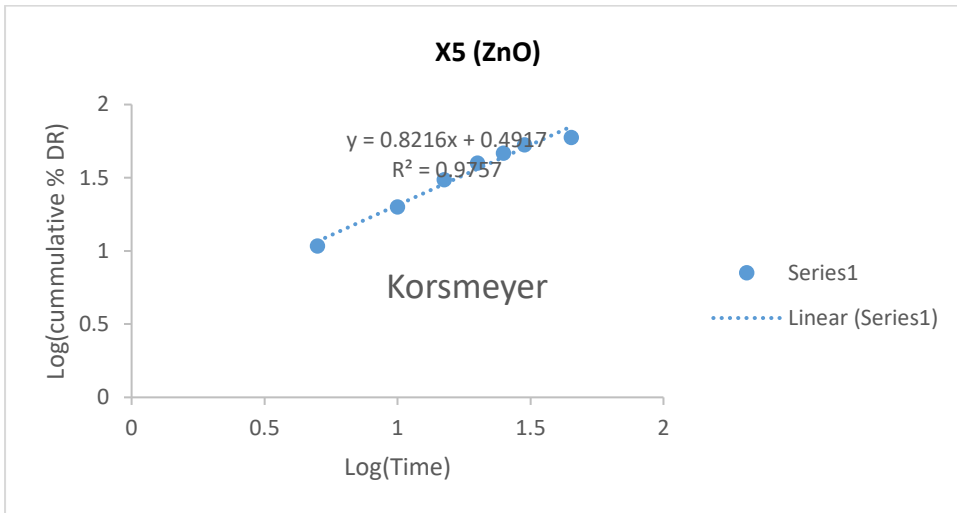


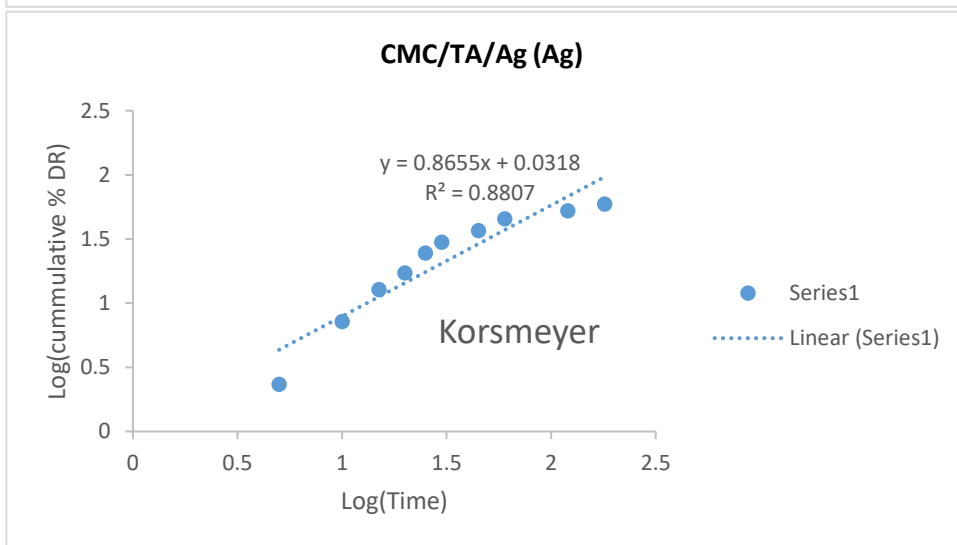
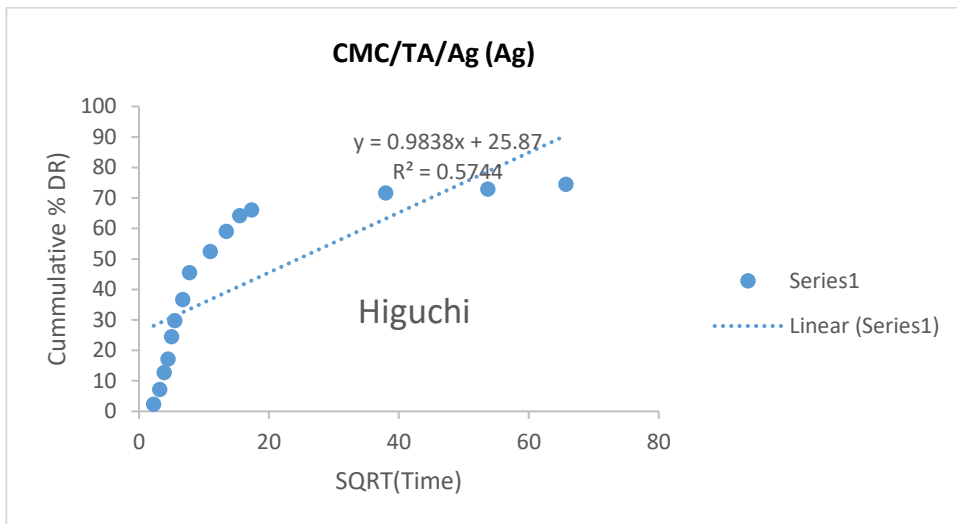
Together in Excellence



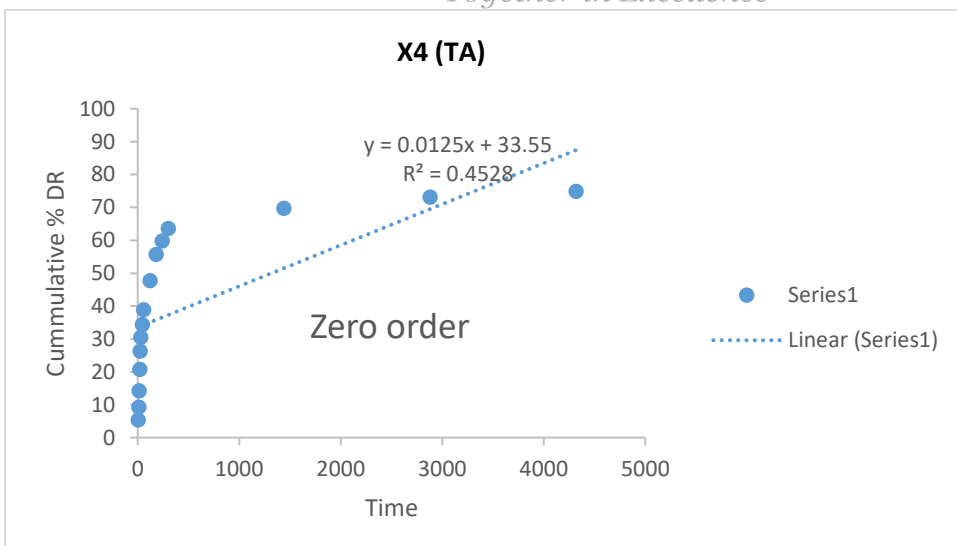


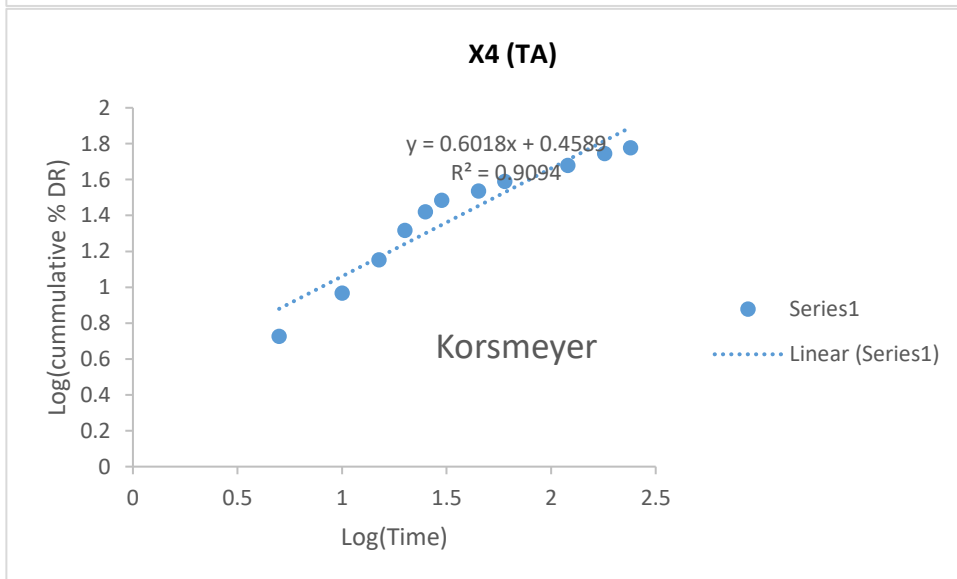
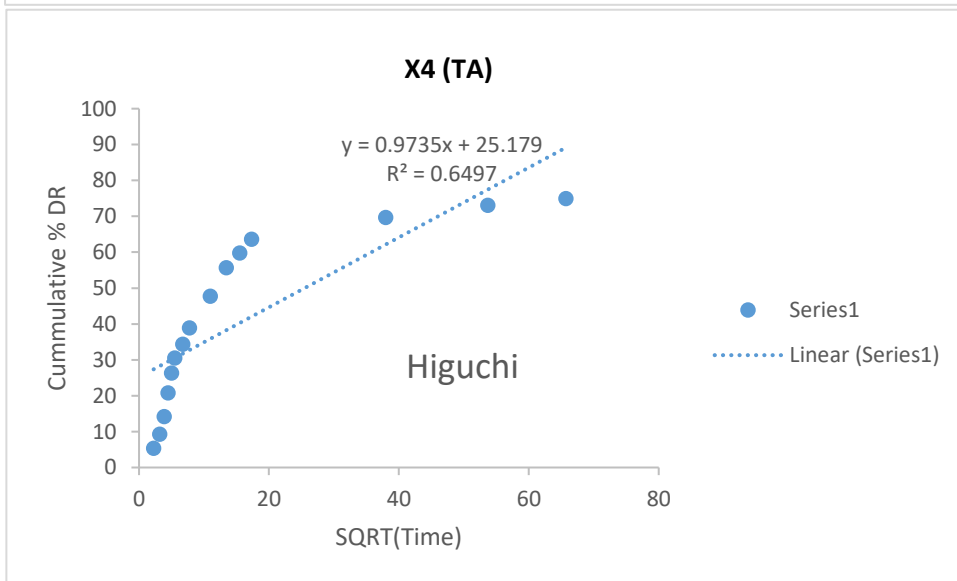
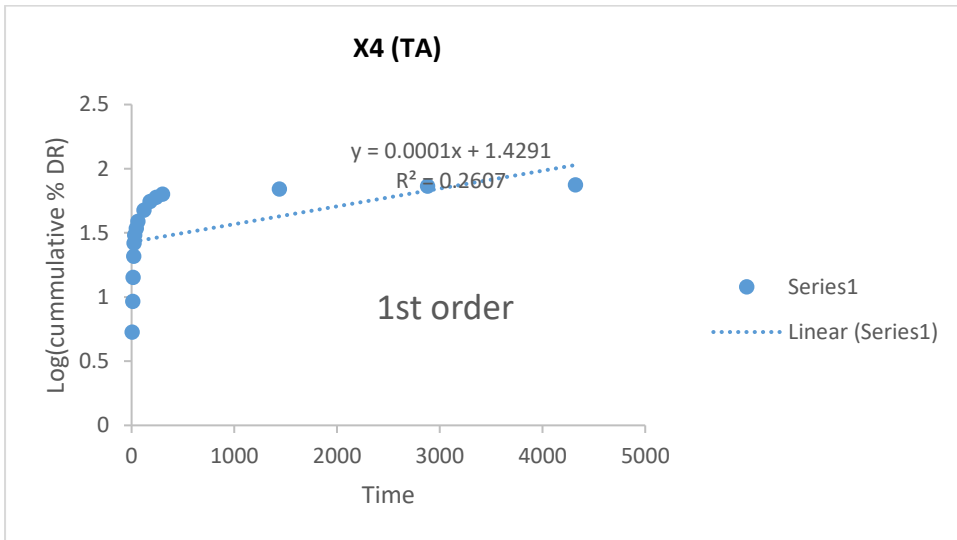


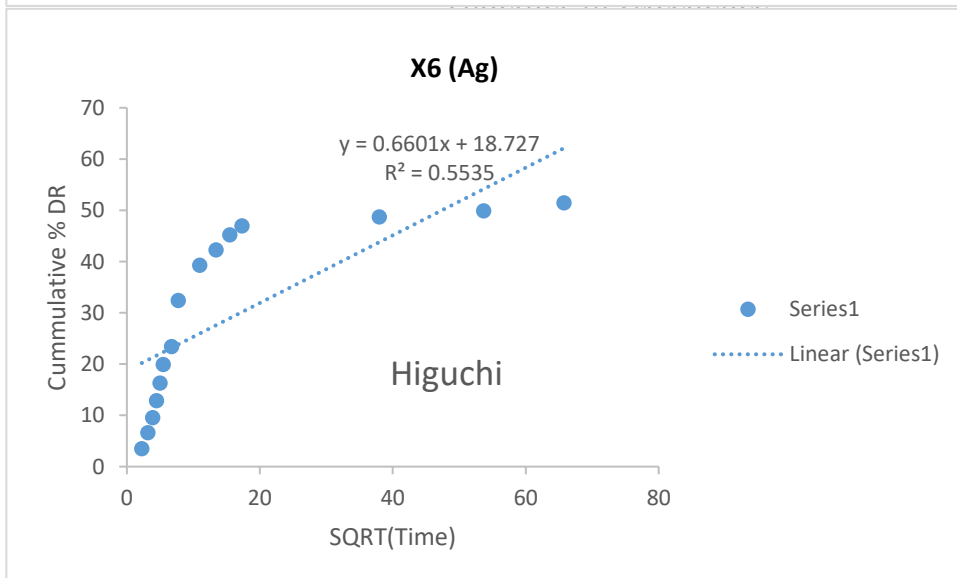
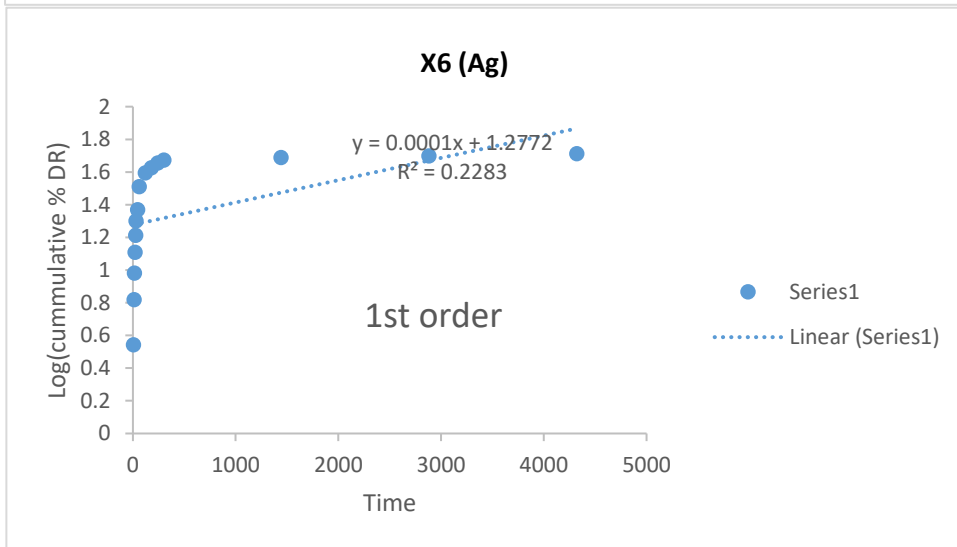
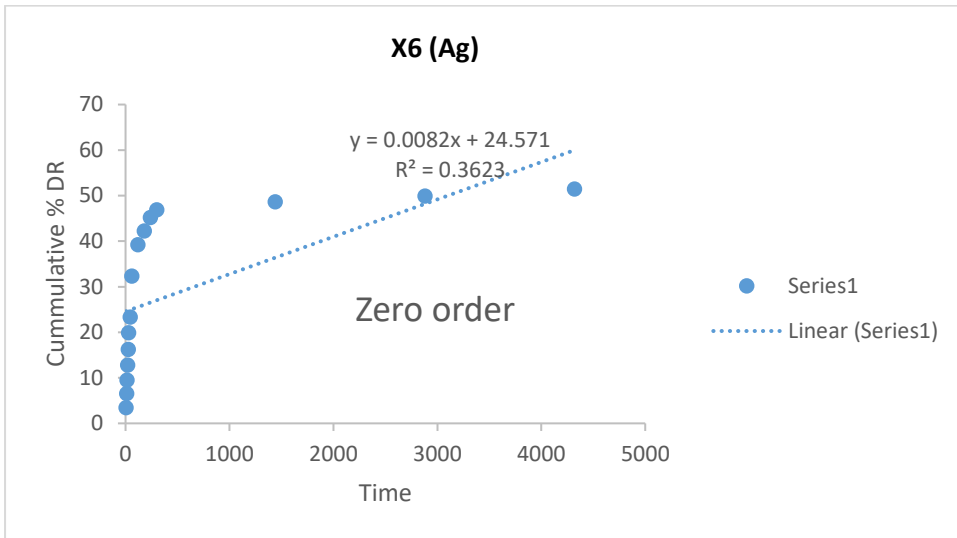


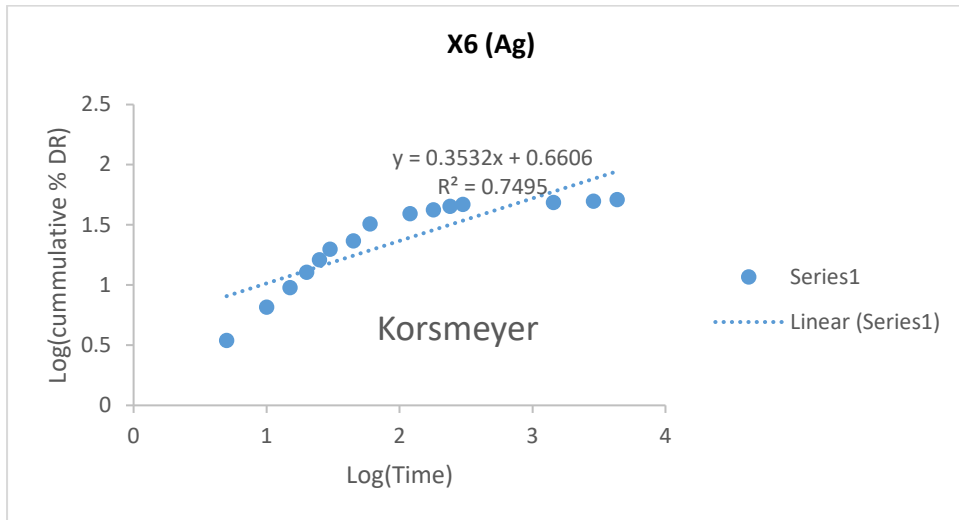


Together in Excellence









University of Fort Hare
Together in Excellence